



HAL
open science

Suivi par sonar de la dynamique des dépôts en réseau d'assainissement

Iacopo Carnacina

► **To cite this version:**

Iacopo Carnacina. Suivi par sonar de la dynamique des dépôts en réseau d'assainissement. [Research Report] IFSTTAR - Institut Français des Sciences et Technologies des Transports, de l'Aménagement et des Réseaux. 2011, 135p. hal-01712037

HAL Id: hal-01712037

<https://hal.science/hal-01712037>

Submitted on 19 Feb 2018

HAL is a multi-disciplinary open access archive for the deposit and dissemination of scientific research documents, whether they are published or not. The documents may come from teaching and research institutions in France or abroad, or from public or private research centers.

L'archive ouverte pluridisciplinaire **HAL**, est destinée au dépôt et à la diffusion de documents scientifiques de niveau recherche, publiés ou non, émanant des établissements d'enseignement et de recherche français ou étrangers, des laboratoires publics ou privés.

IFSTTAR

Projet VITRES 2009

CONVENTION POUR LE SOUTIEN FINANCIER DE
L'INSTITUT CARNOT VITRES - N° 07 CARN 013 01

SUIVI PAR SONAR DE LA DYNAMIQUE DES
DEPOTS EN RESEAU D'ASSAINISSEMENT

Author: Iacopo Carnacina

Final report : 30/07/2011

SOMMAIRE

LIST OF FIGURES	2
LIST OF TABLES	5
LIST OF SYMBOLS	6
1 INTRODUCTION.....	8
2 LITTERATURE REVIEW	9
2.1 <i>Generic back ground and definitions</i>	9
2.2 <i>Sediment interface in combined sewer deposits</i>	16
3 SONAR THEORETIAL BACKGROUND	18
4 EXPERIMENTAL APPARATUS	20
4.1 <i>Marine Electrics 1512 SONAR</i>	21
4.2 <i>Sontek 10 Mhz side looking ADV</i>	28
4.3 <i>In-situ setup</i>	30
5 EXPERIMENTAL SITES, EXPERIMENTAL SETUP AND MEASUREMENTS PROCEDURE.....	33
5.1 <i>Experimental sites</i>	33
5.2 <i>Measurement execution</i>	38
5.3 <i>Data elaboration</i>	39
5.3.1 <i>Profiler.m</i>	40
5.3.2 <i>ADVDATAELABORATION.M</i>	47
6 RESULTS.....	51
6.2 <i>Duchesse Anne (DA) tests</i>	51
6.2.1 <i>Morphological characteristics Test DA-S1 (2010-10-20)</i>	51
6.2.2 <i>Morphological characteristics Test DA-S5 (2011-05-11)</i>	54
6.2.3 <i>Temporal evolution Test DA-S4 (2011-05-11)</i>	58
6.2.4 <i>Flow filed Test DA-S2 (2011-01-21)</i>	60
6.2.5 <i>Flow filed Test DA-S3 (2011-02-04)</i>	66
6.3 <i>Allée de l'Erdre tests (AE)</i>	73
6.3.1 <i>Morphological characteristics Test AE-S6 (2011 03 10)</i>	73
6.3.2 <i>Morphological characteristics Test AE-S7 (2011 03 24)</i>	77
6.3.3 <i>Morphological characteristics Test AE-S8 (2011 05 04)</i>	81
6.3.4 <i>Temporal evolution Test AE-S5 (2011 02 09)</i>	85
6.3.5 <i>Temporal evolution Test AE-S9 (2011-06-16)</i>	87
6.3.6 <i>Flow field Test AE-S2 (2010-11-26)</i>	95
6.3.7 <i>Flow field Test AE-S3 (2010-12-15)</i>	102
6.3.8 <i>Flow field Test AE-S4 (2011-02-02)</i>	115
6.4 <i>Acoustic backscatter correlation with TSS</i>	123
6.5 <i>Comparison between velocity profiles</i>	124
CONCLUSIONS	127
REFERENCES	128
RESUME.....	131

LIST OF FIGURES

Figure 1 lutocline definition 9

Figure 2 Green et al 1999 definition 12

Figure 3 Sediment point gauge. The disc has a thickness of 2 cm and a diameter of 25 cm... 20

Figure 4 SONAR Marine Electronics model 1512. 22

Figure 5 pipe profiler SONAR output for $P_L=4$ us 24

Figure 6 pipe profiler system control panel. 25

Figure 7 detection algorithms proposed in the Marine Electronics Pipe Profiler software 28

Figure 8 ADV and SONAR fastening (same as in-situ conditions)..... 31

Figure 9 Reference system definition..... 32

Figure 10 catchments basins with pipes, quotes (in m) and working section locations ().
Note: tick black lines are the combined sewer networks. 34

Figure 11 catchments basins invert sketch with notation (a) AE (b) DA (dimensions in meters)..... 35

Figure 12 Experimental in situ set-up 37

Figure 13 definition sketch of the ADV control volume position..... 39

Figure 14 Sonar output from laboratory experiences and insitu conditions. 41

Figure 15 section $y=0$, corresponding to $\theta=180^\circ$ and $j=200$ 42

Figure 16 Sonar output before and after application of the filter 44

Figure 17 Matlab script example, data before filtration..... 45

Figure 18 Matlab script example, data filter analysis, blue line represents the median, red and green line represents the confidence bound of width σ 46

Figure 19 Matlab script example, data after filtration..... 46

Figure 20 3D surface bottom surface generation after filter application; data have been displayed from the new reference system relative to the invert z_{BED} 47

Figure 21 quadrant analysis classification 49

Figure 22 Test DA-S1 in situ suspended solids concentrations and particle size distributions 51

Figure 23 Test DA- S1 output 54

Figure 24 Suspended solids concentration test DA-S5 with the free surface (solid line)..... 55

Figure 25 DA-S5 sediment morphology measured with the sonar, flow from left, the scale represents the z_{BED} elevation in mm..... 56

Figure 26 DA-S5 sediment morphology measured with the sonar from the average plane, flow from left, gray scale represents the z_{PLANE} elevation in mm. 56

Figure 27 DA-S5 longitudinal profile for $y=0$ m 57

Figure 28 DA-S5 Sonar output at section $x=-3.20$ m..... 58

Figure 29 Test DA-S4 in situ suspended solids concentrations and particle size distributions 59

Figure 30 Sediment interface temporal evolution detected for tests DA-S4..... 60

Figure 31 Test DA-S2 in situ suspended solids concentrations and particle size distributions 60

Figure 32 (a) DA-S2 transverse profile at $x=-0.5$ m, and (b) amplitude profile at $y=0$ m 61

Figure 33 (a) DA-S2 transverse profile at $x=-1.9$ m, and (b) amplitude profile at $y=0$ m 61

Figure 34 Longitudinal survey referred from the channel sonar centre 62

Figure 35 centreline longitudinal profiles from the interpolating plane z_{PLANE} 62

Figure 36 DA ADV data sect. 1 ($x=-0.5$ m) 63

Figure 37 DA ADV turbulence data sect. 1 ($x=-0.5$) 64

Figure 38 DA ADV data sect. 2 ($x=-1.9$ m)..... 65

Figure 39 DA ADV turbulence data sect. 2 ($x=-1.4$ m)..... 66

Figure 40 Test DA-S3 in situ suspended solids concentrations and particle size distributions 67

Figure 41 DA-S3 Bottom morphology..... 67

Figure 42 DA-S3 centerline longitudinal profile ($y=0$), where the regression line represents the regression trough the z_{BED} points.....	67
Figure 43 DA-S3 ADV data sect. 1 ($x=-0.5$ m)	68
Figure 44 DA-S3 ADV turbulence data sect. 1 ($x=-0.5$ m).....	69
Figure 45 DA-S3 ADV data sect. 2 ($x=-1.9$ m)	70
Figure 46 DA-S3 ADV turbulence data sect. 2 ($x=-1.9$ m).....	71
Figure 47 DA-S3 ADV data sect. 2 ($x=-3.3$ m)	72
Figure 48 DA-S3 ADV turbulence data sect. 2 ($x=-3.3$ m).....	73
Figure 49 TSS, VSS and particle size distribution conditions of test AE-S6	74
Figure 50 AE-S6 sonar output at $x=0$ mm.....	75
Figure 51 AE-S6 Bottom morphology measured with the sonar profiler, from the invert z_{BED} in [mm].....	76
Figure 52 AE-S6 Bottom morphology measured with the sonar profiler, from the interpolating plane z_{plane} in [mm].....	77
Figure 53 AE-S6 longitudinal profile for $y=0$ m.....	77
Figure 54 TSS, VSS and particle size distribution conditions of test AE-S7 at $x=0$ mm	78
Figure 55 AE-S7 sonar output at $x=0$ mm.....	79
Figure 56 AE-S7 Bottom morphology measured with the sonar profiler, z_{BED} in [mm]	80
Figure 57 AE-S7 Bottom morphology measured with the sonar profiler, z_{PLANE} in [mm]	81
Figure 58 AE-S7 longitudinal section $y=0$ m.....	81
Figure 59 TSS, VSS and particle size distribution conditions of test AE-S8	82
Figure 60 Sediment deposits surveyed with a clear Perspex cylinder of 7 cm of internal diameter.	82
Figure 61 AE-S8 sonar output at $x=-0.30$ mm	83
Figure 62 AE-S8 Bottom morphology measured with the sonar profiler from the invert bottom z_{BED} in [mm].....	84
Figure 63 AE-S8 Bottom morphology measured with the sonar profiler, z_{plane} in [mm].....	85
Figure 64 AE-S8 longitudinal section at $y=0$ mm.....	85
Figure 65 TSS, VSS and particle size distribution conditions of test AE-S4 (2010-02-02)	86
Figure 66 AE-S5 Sonar output	86
Figure 67 AE-S5 Bottom morphology measured with the sonar profiler from the invert bottom z_{BED} in [mm].....	87
Figure 68 Flow depth, longitudinal flow velocity and rain intensity for the survey period.....	88
Figure 69 TSS, VSS and particle size distribution conditions of test AE-S7	88
Figure 70 Test S9, Morphological survey, at 2:00, 7:00 and 10:00. Colour shading represents the z elevation in mm from the invert bottom	89
Figure 71 AE S9 sonar output at $t=4:35$ at $x=-9900$ mm, referred toward the SONAR center	90
Figure 72 AE S9 sonar output at $t=10:00$ at $x=-9900$ mm, referred toward the SONAR center	91
Figure 73 Test AE S9. Bottom morphology temporal survey interpolation (blue dots represent the actual surveyed data). Colour shading represents the z elevation in mm from the invert bottom.....	92
Figure 74 Instantaneous longitudinal flow velocity and turbulences recorded during the morphological survey at section $x=0$ m.	95
Figure 75 TSS, VSS and particle size distribution conditions of test AE-S2	96
Figure 76 AE S2 model set-up pipe profiler output.	96
Figure 77 AE-S2 data.output; the contour lines represent the 8 bit signal amplitude (coloured scale from 0 to 256 counts) observed by the sonar, () gauge position.	97
Figure 78 section $y=0$ m, AE S2 data for pulse length of 4 μ s, 8 μ s, 12 μ s, 16 μ s and 20 μ s (legend represents the range and pulse length).	98

Figure 79 AE S2 model results from the filtered ADV readings (of which generally more than 95 % were considered good): (a-c) V= velocity cm/s, (d-f) COR= signal correlation %, (g-i) SNR= sound to noise ratio, db, (l-n) AMP= backscattered signal amplitude of the control volume, counts. Note: 0=beam 0, 1=beam 1, 2=beam 2.....	99
Figure 80 AE S2 model results from the filtered ADV readings (of which generally more than 95 % were considered good): test over field sediments; variation toward the water column of the Reynolds stress.	100
Figure 81 AE S2 unfiltered data normalized turbulence characteristics	101
Figure 82 AE S2 filtered data (Whal 2003 algorithm) normalized turbulence characteristics $u^*=0.99$ cm/s and $\delta=0.88$ m.	102
Figure 83 TSS, VSS and particle size distribution conditions of test AE-S3 (2010-12-15) ..	103
Figure 84 AE transverse profile sonar output	104
Figure 85 Test AE-S3 bottom morphology.....	105
Figure 86 AE longitudinal profile at $x=0$ m, sonar output, flow from the right.....	106
Figure 87 (a) AE transverse profile at $x=-0.5$ m, () gauge position, (x) TSS sampler positions, (b) vertical amplitude profile at $x=-0.5$ m.	106
Figure 88 AE sect.1 averaged ADV data.	108
Figure 89 AE sect.1 Reynolds stress	109
Figure 90 AE sect.1 normalised stresses.....	110
Figure 91 AE transverse profile at section 3 ($x=-2.5$ m),.....	110
Figure 92 AE $x=-2.5$ m averaged ADV data.....	112
Figure 93 AE sect.3 Reynolds stresses.....	113
Figure 94 AE transverse profile at section 5 ($x=-4.5$ m), and amplitude profile at $x=0$ m	113
Figure 95 AE sect. 5 averaged ADV data	114
Figure 96 AE sect.5 Reynolds stresses.....	115
Figure 97 TSS, VSS and particle size distribution conditions of test AE-S4 (2010-02-02) ..	115
Figure 98 Sonar output for $x=-0.5$ (white spot) sediment interface detected with the gauge	116
Figure 99 Sonar output for $x=-1.5$, (white spot) sediment interface detected with the gauge	117
Figure 100 Sonar output for $x=-2.5$ (white spot) sediment interface detected with the gauge	118
Figure 101 sediment surface referred to the invert test AE-S4	119
Figure 102 AE-S4 ADV data sect. 1 ($x=-0.5$ m).....	120
Figure 103 AE-S4 ADV turbulence data sect. 1 ($x=-0.5$ m).....	121
Figure 104 AE-S4 ADV data sect. 3 ($x=-2.5$ m).....	122
Figure 105 AE-S4 ADV turbulence data sect. 3 ($x=-2.5$ m).....	123
Figure 106 Correlation between TSS<2 mm and amplitude in counts	124
Figure 107 DA-S3 Normalised velocity profiles and shear stress profiles	125
Figure 108 AE-S2 Normalised velocity profiles and shear stress profiles	125
Figure 109 AE-S3 Normalised velocity profiles and shear stress profiles	126
Figure 110 AE-S4 Normalised velocity profiles and shear stress profiles	126

LIST OF TABLES

Table 1 Definitions of sediment bed elevation from literature.	13
Table 2 script tasks (see also the annexes for the script layout)	44
Table 3 ADVDATAELABORATION output	49
Table 4 Flow velocity recorded before the morphological survey at the section $x=0$ m	54
Table 5 Flow velocities measured at section $x=0$ m.....	74
Table 6 AE-S7 longitudinal flow velocities	78
Table 7 Test AE-S8 measured velocities	83
Table 8 Suspended solids concentrations measured at different times	88
Table 9 Particle size distribution summary in [μm]	103

LIST OF SYMBOLS

The following symbols have been used in this work:

$\langle u'_i u'_j \rangle$	Reynolds stress	$[m^2/s^2]$
AMP	signal amplitude	[counts]
a_s	the diameter of the particles,	[m]
B_s	constant	[-]
C	particle weight concentration	[mg/l]
c	speed of sound in the water	[m/s]
C_1	constant	[dB]
C_b	reference concentration	[mg/l]
COR	correlation	[-]
D^*	non dimensional diameter	[m]
D_{xx}	diameter for which xx% in weight of settled material is finer	[m]
E	received strength	[counts]
e	the relative elasticity of the material	[-]
E_r	received noise respectively	[counts]
f_0	emitted frequency	[Hz]
f_s	sampling frequency	[Hz]
g	the gravitational acceleration	$[m/s^2]$
h	distance from the sediment interface	[m]
H	quadrant analysis hole size	[m/s]
k	acoustic wave number	$[m^{-1}]$
K_c	acoustic signal conversion factor	[dB/counts]
k_s	roughness height	[m]
k_w	total kinetic energy	$[m^2/s^2]$
M	particle volume concentration	[l/l]
n_b	number of backscatters	[-]
P_L	transmit pulse length	[m],
P_T	transmit power	[W],
R	range along the beam axis	[m],
s	specific density	[-]
S	energy slope	[-]
SNR	signal to noise ratio	[dB]
S_v	scattered signal in decibel	[dB]
$S_{i,H}$	single burst event contribution	[-]
t	time	[s]
T	the transport stage parameter	[-]
TSS	total suspended solids concentration	[mg/l]
T_T	transducer temperature	[°C],
U	depth averaged flow velocity	[m/s]
u	average longitudinal flow velocity	[m/s]
\mathbf{u}	instantaneous longitudinal flow velocity	[m/s]
u^*	critical shear velocity	[m/s]
u^*	shear velocity	[m/s]
u'	instantaneous longitudinal flow fluctuation	[m/s]
u^+	normalised longitudinal velocity	[-]
uv^+	normalised Reynolds shear stress	[-]

v	average transverse flow velocity	[m/s]
\mathbf{v}	instantaneous transverse flow velocity	[m/s]
v'	instantaneous transverse flow fluctuation	[m/s]
V_i	ADV velocity on i th direction	[m]
VSS	volatile suspended solids concentration	[mg/l]
w	average vertical flow velocity	[m/s]
\mathbf{w}	instantaneous vertical flow velocity	[m/s]
w'	instantaneous vertical flow fluctuation	[m/s]
x	longitudinal axis	[m]
y	transverse axis	[m]
y_b	vertical distance from which the reference concentration was measured	[m]
z	vertical axis	[m]
z_{BED}	position of the interface from the invert	[m]
z_{PLANE}	position of the interface interpolating plane	[m]
α	roll angle	[°]
α_s	sediment attenuation coefficient	[dB/m]
α_t	attenuation coefficient	[dB/m],
α_w	water attenuation coefficient	[dB/m]
β	pitch angle	[°]
δ	water depth	[m]
Δf	Doppler shift frequency	[Hz]
δ_v	vertical precision	[m]
θ	material parameter	[-]
$\lambda_{i,H}$	quadrant analysis discriminator	[-]
ν	water viscosity,	[m/s ²]
ρ	water density	[kg/m ³]
ρ_d	dry sediment density	[kg/m ⁴]
ρ_s	particle density	[kg/m ³]
σ_{bs}	acoustical scattering cross section of a single spherical particle	[m]

subscripts

0,1,2	ADV beam tag
ADV	relative to the sonar
i, j	according to the x , y , and z direction
max	maximum value
SONAR	relative to the sonar

1 INTRODUCTION

The present study aims at understanding the morphological characteristics of sediment deposits inside the combined sewer networks of the city of Nantes, also in connection with the flow characteristics measured during the morphological survey. The present study has been supported by the project VITRES 2009, under a collaboration between the French institute IFSTTAR , department GER-HA, and the LEESU, under the guidance of Dr. Frédérique Larrarte (IFSTTAR), Claude Joannis (IFSTTAR) and Prof. Ghassan Chebbo (LEESU).

This report aims at:

- 1) Presenting the results of preliminary tests carried out with a SONAR profiler “Pipeprof 1512,” manufactured by MARINE ELECTRONICS ltd.
- 2) Describing a procedure to use the SONAR, analyse the data and display the results.
- 3) Describing the results obtained from laboratory and sewer applications

The knowledge of both the flow field and the sediment features give them importance due to the fact that both features are strongly related. Indeed, the flow field and its turbulence characteristics are affected by the presence of suspended solids and strong concentration layer referred to as mud flow. The later could participate to the momentum transport toward the stream and substantially modify the boundary conditions. As well, the sediment transport, quantity of sediment carried by the flow and the thickness, viscosity and concentration of the mud flow are strongly dependent on the flow field features and in particular on the interaction between outer and inner layer .

In this context, measures in environment heavily constrained, such as combined sewer network, need to be accurately planed and carried out in short time, in order to reduce the lost of information while going from one measurements to another (the mud flow can change its characteristics during the measurements), and to reduce and prevent large disturbances of the flow. As it will be shown in the next section, the mud flow is easily removable and the simple passage of one intruding probe can compromise the successful survey of the second probe.

The next sections will contain:

- A literature review;
- A brief summary of the experimental installation, the site and the measurement execution;
- Preliminary results relative to the firsts in sewer tests carried out with the sonar profiler;
- Preliminary results and contemporary measurements carried out with both the sonar and the ADV;
- A discussion of the results obtained from the different sites.

2 LITTERATURE REVIEW

2.1 Generic back ground and definitions

Hydraulic conditions, i.e., hydraulic radius, velocity, discharge, shear stress, friction, sediment transport, pollutant fluxes; need the correct assessment of both water surface and sediment bottom surface. This task could be relatively easily achieved under proper environments and controlled conditions, i.e., clear water condition and gradually varied flow condition, where a net separation (interface) between sediment and water phase and water and air phase can be observed.

The simultaneous presence of: (a) the bed load transport and suspended load transport; (b) transport of particles in a thin layer of $O(0.01\text{m})$ (van Rijn, 2007) close to the bed and (c) the transport of particles above the bed-load layer or the presence of “mud flow” (McAnally, Friedrichs, Hamilton, Hayter, Shrestha, Rodriguez, Sheremet, Teeter and Flu, 2007), may reduce the net separation between sediment and water phases. In these conditions, a different definition of sediment-water interfaces has been proposed, i.e., the interface corresponds to a step like sediment concentration profile, also known in literature as lutocline (Figure 1).

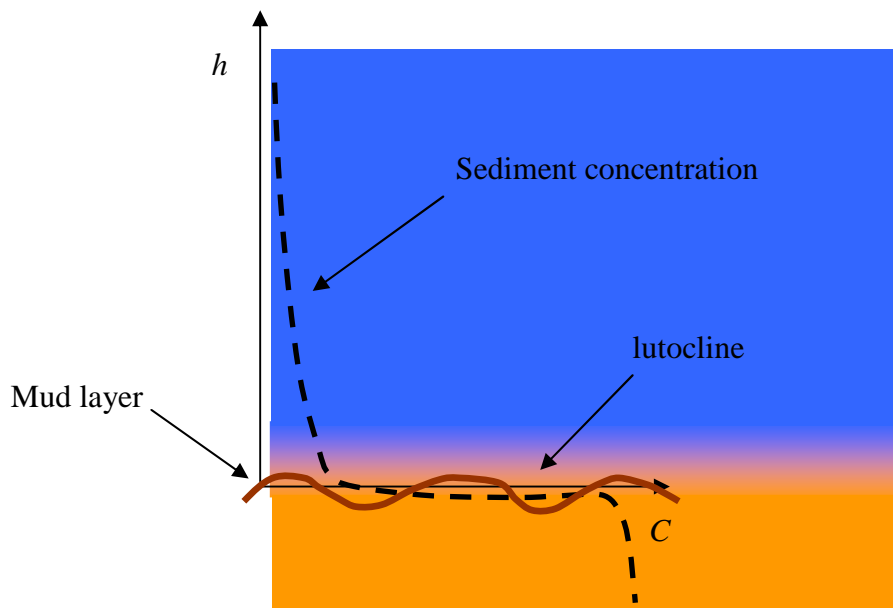


Figure 1 lutocline definition

Kaolin is generally used in laboratory tests on cohesive sediment. (van Rijn and Louisse, 1987), hence, proposes a classification in four different status of kaolin suspension of $D_{50}= 4 \mu\text{m}$, $D_{90}= 15 \mu\text{m}$, and $460 \text{ kg/m}^3 < \rho_d < 640 \text{ kg/m}^3$ where ρ_d is the mean dry density and D_{xx} the diameter for which xx% in weight of settled material is finer, suspended by wave forcing and based on the weight concentration of solid per unit of volume C

- consolidated mud layer ($C > 500 \text{ gr/l}$);
- fluid mud layer ($100 \text{ gr/l} < C < 500 \text{ gr/l}$);
- hindered settling mud layer ($10 \text{ gr/l} < C < 100 \text{ gr/l}$); and
- flocculating mud layer ($C < 10 \text{ gr/l}$).

Since the early '50s and Rouse's work, tremendous amount of methodologies have been developed to measure the sand bottom level and bed forms. (van Rijn and Klaassen, 1981)

used a profiler indicator mounted on a carriage and automatically recorded the bottom at regular intervals. In Kennedy according to (Karim and J.F., 1981) approach, defined y as the vertical elevation above the bed, the water depth h as the distance between the free surface and the bed surface and the bed thickness y_b at which the reference concentration was measured as:

$$y_b = D_{50} u_*' / u_{*c}' \quad (1)$$

where u_*' is the shear velocity, but little information on the definition of the sediment surface level was presented.

A more complicated expression of the reference concentration C_b based on laboratory flume and natural river data was proposed (see also (Karim and Kennedy, 1987)):

$$\begin{aligned} \log(C_b) = & -4.44 + 3.57V_1 + 1.23V_2 - 2.87V_3 + \\ & 1.58V_5 \cdot V_6 - 1.40V_1V_4 + 0.41V_4V_6 - 0.85V_2V_3V_4 \\ & + 0.65V_2V_5V_6 - 5.43V_1V_3V_5 + 2.19V_3V_5V_6 - 1.27V_1V_5V_6 \end{aligned} \quad (2)$$

where $V_1 = \log[U / \sqrt{g(\rho_s / \rho - 1)D_{50}}]$, $V_2 = \log(S10^3)$, $V_3 = \log(u_*' / w)$, $V_4 = \log(wD_{50}/\nu)$, $V_5 = \log[u_*' - u_{*c}' / \sqrt{g(\rho_s / \rho - 1)D_{50}}]$, $V_6 = \log(d/D_{50})$

The relation was based on the nature of sediment (ρ_d , D_{50} , w is the particle fall velocity, u_*'), flow condition (U the average velocity, S the energy slope, u_*'), and water properties (ν is the viscosity, ρ the water density, g the gravitational acceleration).

In case of bed load transport, (van Rijn, 1984) the bed bottom is defined at $0.25d_{50}$ below the top of the particles, methodology which has been validated for particle of $200 \mu\text{m} < D_{50} < 2000 \mu\text{m}$, where d_{50} is the average particle size. In (van Rijn, 1984), the water depth h was defined as the difference between the water surface and the average bed level, but still little information on how to measure the average bed level in presence of suspended load transport was provided. However, interesting insight arouses when the author analyses the effect of the position of the reference level, i.e., the elevation where the reference concentration (the concentration measured at the saltation layer) was measured, on the suspended load concentration profiles, for small variation of reference level could lead to drastic changes on the concentration profile. Consequently, the author concluded, it is not suitable to use the bed-load concentration as the reference concentration, for the large errors that could occur. Hence, in presence of bed forms, the reference level a (formerly y_b) was fixed by (van Rijn, 1984) at the salvation level, i.e., at half the bed forms height Δ or half the sand roughness height k_s (calculated in (van Rijn, 1984)) and in any case with a minimum value of 0.01 m, and propose and equation to calculated the reference concentration C_b :

$$C_b = 0.015(D_{50}/a)(T^{0.15}/D_*^{0.3}) \quad (3)$$

where $T = (u_*'^2 - u_{*c}'^2) / u_{*c}'^2$ is the transport stage parameter and $D_* = D_{50}(g'/\nu^2)^{0.3}$, $g' = g(s-1)$ and $s = \rho_s / \rho_s$ specific density.

(Voogt, Vanrijn and Vandenberg, 1991), carried out a series of large flume experiment on the sediment transport properties of high velocity flow. The Authors studied the sediment transport properties of fine sand in presence of a self eroding flow ($D_{50} = 200 \mu\text{m}$), i.e., a

condition for which no sediments were introduced from the inlet section. Both water depth and sediment surface were measured sounding the bed with a gauge of 0.02 m of accuracy.

In (Abouseida, Muralidhar and Lo, 1992), the reference level of the concentration profile was again defined as the crest of the bottom ripples. Again, no information on how the sediment bottom has been measured was provided.

Recent development of optical and acoustical backscatter probes for marine applications leads to a definition of the sediment bottom that is related with indirect measurements. (Gallagher, Boyd, Elgar, Guza and Woodward, 1996), defined the distance at which the seafloor was detected using a threshold criterion by means of 1 MHz sonar altimeter, i.e., fixing a voltage immediately below the automatic adjusted maximum gain level. After laboratory and field experiences, they defined an automatic gain adjustment algorithm, which included signal normalization and a threshold voltage employed to individuate the time at which the bottom-echo was detected. By means of the automatic gain adjustment algorithm, the authors were able to measure the seafloor with a precision of 0.03 m.

Differently, (Bell and Thorne, 1997), located the sediment bottom on the base of the maximum correlation calculated between the backscatter profile measured with a 2 MHz rotating head sonar and a model bed echo which reflects an ideal approximation of what is the actual bed echo. It is worth observing that, the modelled bed echo has been calibrated to effectively work in marine environment, but little information are available on the backscatter signal in environment where organic sediment maybe present. According to (Bell and Thorne, 1997) and (Thorne and Hanes, 2002) the use of the algorithm improves the localisation of the sediment bottom if compared to threshold methodologies. Moreover, the authors provide a full review of acoustic measurements technique and methodologies to determine the sediment concentration from the backscatter profile.

(Webb and Vincent, 1999), based on three frequency transducer experiments, defined the bed as the place where the strongest backscatter signal is measured.

Differently, (Green and Black, 1999) define the base range as the range of the bin (i.e. one of the volume in which the water column is divided in the sonar image) immediately above the break of slope in the temporal burst-averaged concentration profile (Figure 2).

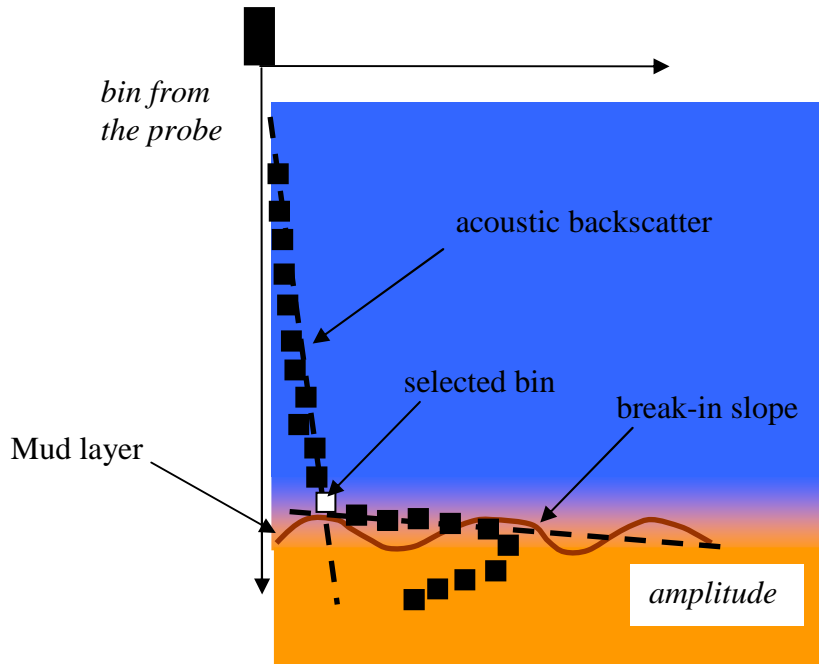


Figure 2 Green et al 1999 definition

The burst-average concentration profile was thus determined on the basis of the averaged root-mean-square backscattered pressure profiles. Hence, according to the nature of the surveyed bed, they located the sediment bottom namely at 0.01 m below the base range for rippled bed, and at 0.02 cm below the base range for transitional and “hummocky” beds (i.e., a stratification in which mounds of sand occur).

(Lee, Dade, Friedrichs and Vincent, 2004) observed the lack of a general consensus on defining an appropriate reference level, also emphasizing the necessity to identify the bed level. Hence the authors adopted the methodology developed by (Green and Black, 1999).

Later on, (Hoitink and Hoekstra, 2005), compared the suspend concentration profiles obtained from acoustic Doppler current profiler (ADCP) acoustic backscatter signal and optical backscatter signal. OBS signals were calibrated over concentrations measured by means of in situ water samples, whilst a formulation valid for $ka_s \ll 1$ has been used to calculate the volume mass concentration M from the acoustic backscatter, i.e., $M \propto 10^{(S_v/25)}$, where k is the acoustic wave number and a_s the diameter of the particles, S_v = scattered signal in decibel. The product ka_s takes into account for the acoustical scattering cross-section rather than the geometrical particle cross-section.

It is worth observing that, again, those relationships have been calibrated, in case of marine application, mainly on sand sediments, whilst the nature of sediments dramatically differs from in sewer deposits nature (shape, cohesive properties, degree of uniformity, flocculation), which are principally composed by organic material (from 30% to 89% of volatile solids) and less homogeneous in particle distribution (Ashley, Bertrand-Krajewski, Hvitved-Jacobsen and Verbanck, 2004). Indeed, the acoustic backscatter of organic sediment is rather different from that observed of mineral sediment as resulted from a survey carried out by (Lewis, Mayer, Mukhopadhyay, Kruge, Coakley and Smith, 2000), in which sediments were characterised by a total organic carbon content up to 4% for the upper 3 cm of the clay-silt mud layer.

(McAnally, Teeter, Schoellhamer, Friedrichs, Hamilton, Hayter, Shrestha, Rodriguez, Sheremet, Kirby and Fl, 2007) and (McAnally, Friedrichs, Hamilton, Hayter, Shrestha, Rodriguez, Sheremet, Teeter and Flu, 2007) described the mechanics of formation of fluid mud in estuarine environment together with the associate mechanisms of formation accumulation and erosion. In general, mud flow can be observed in environment characterised by the presence of low velocity and fine sediments. Hence a fluid mud is associated with a lutocline, i.e. a sudden increase in sediment concentration and they described the fluid mud as high concentrated fine-sediment suspensions, which maintain the potential for mobility. It is worth observing that the authors also included in the definition of fluid mud a mixture of fine grained mineral and organic sediments. In this context, two definitions of the top layer have been provided. Hydraulically, the bed elevation correspond to the plane of zero flows, whilst density criteria are adopted to preserve the navigability, i.e., density between 1151-1347 kg/m³ are employed to define the navigable depth. Hence, base on (Alexander, Teeter and Banks, 1997) results, they observed that acoustic instruments, such as fathometers, have different degree of penetration inside fluid mud according to the signal frequency at which the backscatter is collected. Generally, 200 kHz signal is able to detect the top of the mud layer, corresponding to roughly 1050 kg/m³, but the reflected signal is more properly associated to a gradient of concentration rather than to a specific density. Differently, lower signal of 20-40 kHz are able to penetrate the fluid mud reaching a more consolidated layer. However, in terms of dredging volume definitions, none of the previous elevations seemed suitable and a more appropriate layer definition comes from intrusive instrumentations, such as sled transducer, which has been designed to travel along a physical horizon of constant density and viscosity (Alexander, Teeter and Banks, 1997)

More recently, (Dolphin and Vincent, 2009), adopted again the methodology proposed by (Green and Black, 1999) and locate the sediment bottom as the level at which the “break-in-slope” of the sediment concentration curve was observed from ABS measurements.

Table 1 Definitions of sediment bed elevation from literature.

Authors	Definition	Motivation of the study, domain of application	Measurement technique	Note
[-]	[-]	[-]	[-]	[-]
van Rijn (1984c)	h =distance between the water depth and the averaged bed level, reference level at $a= \Delta$ (bed-form height)/2 or $a=ks/2$ from the averaged bed level with $a(\text{min}=0.01 \text{ m})$	River applications Predicts the suspended sediment concentration in presence of bed forms. Based on the bed shear velocity.	Experimental test Data from Barton and Lin (1951) and Anderson (1942), How they measure it is unknown Hydraulic radius defined as in Vanoni and Brooks (1957) which use a point gauge of 0.1 mm of precision in flume experiments	This definition has been given in presence of bed-forms and suspended sediments, but no information on how they measure the bed level in presence of bed forms is given. Data from Barton and Lin (1951) and Anderson (1942), $90 \mu\text{m} < d < 480 \mu\text{m}$
Karim and Kennedy (1987)	$y_b = D_{50} u_* / u_{*c}$	River applications Development of concentration	Comparison with several datasets, but no definition of sediment bed	Thikness of the bed layer y_b at which the reference concentration has been measured, data based on the Vanoni and Brooks (1957)

		profile laws	measurement has been provided.	
Voogt and van Rijn (1991)	Sand bottom measured after the tests end	River applications. High speed flow over sand bottom $100 \mu\text{m} < d < 400 \mu\text{m}$	Echo sounder.	Self eroded bed tests.
Abou-seida et al. (1992)	reference level = crest of the bottom ripples (how do they measure it?)	Laboratory analysis of the concentration profile in weak currents and wave in shallow waters. sand $d_{50}=0.11 \text{ mm}$, $h=0.35 \text{ m}$.	Reference concentration was extrapolated from the spatial and time averaged concentration profile up to the reference level. No information on how the ripple surface has been measured is given	They mainly concentrate on the concentration profile, a definitions of the reference concentration has been adopted by Bosman and Steetzel 1986 and they defined the thickness of the high concentration layer from the analysis of their data. Mainly they observed a concentration profile characterised by two different gradients, owing the presence of both weak current and waves.
Gallagher et al. (1996)	Bottom distance (range) from the transducer individuated in by the threshold on the acoustic signal	Marine application , measurement and individuation of the seafloor	1 Mhz sonar with automatic gain control (AGC)	Degradation of signal in case of suspended sediments, bubbles, and rough and sloped surfaces.
Bell and Thorne (1997)	Correlation between backscatter and modelled near bed time series echo..	Marine applications	2 Mhz sonar profiler,	They use a similar sonar profiler, manufactured by marine electrics and with similar features. A sinc function has been used to model the signal, whose width depends upon the pulse length and the slope of the reflector (the bed), but the procedure have not been included in the paper, maybe some other.
Webb and Vincent (1999)	Maximum intensity backscatter signal	Marine environemtn	Three frequency (2 MHz, 4 MHz and 5.6 MHz) ABS	
Green and Black (1999)	For ripple of 10 cm of wave lengths: $r_{\text{base}} + 1 \text{ cm} = r_{\text{bed}}$ and for hummocky and transitional beds: $r_{\text{base}} + 2 \text{ cm} = r_{\text{bed}}$ where r_{base} is the distance from the sonar corresponding to the "bin" immediately above the break-in-	Application in zone of wave shoaling , $d_{50}=0.23 \text{ mm}$ and $\rho_s=2650 \text{ kg/m}^3$	Three frequency acoustic backscatter sensor	they evaluate the sediment concentration from an acoustic backscatter sonar (ABS) and then arbitrarily defined the bed 1 cm underneath the base range.

	slope.			
Thorne and Hanes (2002)	Time lag at which the maximum correlation between the measured and the modelled near bed time series echo	Marine application under currents and waves conditions	Acoustic profilers, transducer arrays, pencil bin transducer translation	See the references, are quite useful, A straightforward analysis of the ABS and possible calibration in terms of suspended solids are present IMPORTANT: Some how it can be inferred that the bed is the portion which reflects the strongest echo.
Oms (2003)	Definition of an interface between organic sediments and water	Sewer application, organic layer of $2 \text{ mm} < d_{50} < 5 \text{ mm}$ and $1050 \text{ kg/m}^3 < \rho_b < 1300 \text{ kg/m}^3$	Direct in situ observation via endoscope and automatic image recording system inside an observation box	Observation of a creamy layer of 15 cm of thickness (max observed) not detected with the stick and of unknown nature
McAnally et al. (2007)	Hydrodynamic definition: plane of zero flow, Navigable depth: density between 1150-1200 kg/m^3	Marine application, mud fluid prone environment (law velocity and fine sediments)	Acoustic detection (fathometer 200 kHz-20kHz), electrical conductivity, nuclear detection, optical, vibrating fork	Mud fluid can have similar characteristics as that observed in sewer, especially a high gradient concentration in the mud fluid layer and similar mobilization and deposition patterns
van Rijn (2007)	I) Again the bed load transport is defined as the bed load which occurs inside a thin layer of thickness $\delta=0.01 \text{ m}$. In case of fluid mud layer as that observed by Vinzon and Mehta (2003) it refers to the an immobile layer II) Reference concentration as in Van Rijn 1984 a,b,c, in case of sheet flow the reference level is related to the sheet flow layer roughness 20	River and costal sediment tranporst assessment $60\mu\text{m} < d_{50} < 2300 \mu\text{m}$ mostly mineral	Theoretical study Several data sets and concentration profiles are reported. Comparison with literature data, example Van den Berg and Van Gelder (1993)	He observed that very fine sediments maybe eroded as chunks flocks rather than as single particles. Moreover, he observed that the presence of organic materials and biological effects may considerably reduce the near-bed concentration. In this paper (II, pag 677) it is indirectly referred to near bed layer or sheet flow

	d_{50} .			
Dolphin and Vincent (2009)	The location of the seabed is defined as the location of the "break-in-slope" of the acoustic profile.	Marine application under currents and waves	Acoustic backscatter signal recorded averaged over 20 signal collected in 17 minutes each our.	The C profiles where used to determine the position of the seabed. Following Green et al. (1999).

2.2 Sediment interface in combined sewer deposits

Organic matter transported in proximity of the sediment interface and biological process in sewer network may affect the sediment concentration value at the interface (van Rijn, 2007). The exact definition of the sediment bottom or the interface thus becomes more complicate.

Indeed, owing to the large variability of sediment conveyed in sewer networks, different sediment transport patterns can be observed.

(Crabtree, 1989) defined different typologies of sediments deposits according to they nature. Between those individuated by the Authors, two typologies primarily interested the present study:

- Type A deposits: coarse, granular bed material-widespread;
- Type C deposit: Mobile, fine grained found in slack zones in isolation and overlaying Type A;

Accordingly, type C deposits are characterised by larger fraction of organic material and a weak shear resistance. Different techniques have been employed to define the sediment-water interface, most of theme always biased by environmental and security constraints.

(Laplace, Sanchez, Dartus and Bachoc, 1990) indirectly measured the sediment bottom in the combined sewer network of Marseille by means of a rod referred to the invert ceiling over a total of 48 section and a fixing point survey carried out by means of an ultrasonic sensor fasten into a floating device. However no information on comparison between manual and acoustic measurements is provided.

Later on (Arthur, Ashley and Nalluri, 1996) studied the characteristics of what has been defined as "organic near bed transport" in the Dundee combined sewage system. Sediment was caught by means of sediment traps located at different locations. Organic near bed fluid sediments were characterised by large volatile contents (up to 87.6%), $0.09\text{mm} < d_{50} < 11\text{ mm}$ and bulk density ρ_b from 1000 kg/m^3 to 1998 kg/m^3 . Generally, a reduction of ρ_b , of d_{50} and an increase of the volatile contents were observed with the reduction of the sewer slope (from 1:22 to 1:1750 m/m), most likely connected to larger quantity of organic sediment which remains in contact with the bed at milder slopes.

Observation in the combined sewer system of Paris (Ahyerre, Chebbo and Saad, 2001), both visual and with suctions systems, revealed the existence of high concentrated (up to $C=2\text{ g/l}$) layer toward the water column, in correspondence with what has been considered the organic layer. However, further direct visual observation of the sediment water interface seems to suggest that high concentrations are linked to the survey methodology rather than to the presence of a sediment fluid, owing to the existence of a clear interface between water and

organic layer in dry water period and observation of few particle moving over the top of the organic layer.

(Ashley, Bertrand-Krajewski, Hvitved-Jacobsen and Verbanck, 2004) introduced two different definitions based on sampling technique, namely, near bed solids and dense undercurrent. Near bed organic solids were generally detected by means of sediment traps. Sediment traps allowed observing the presence of larger particles which interacted with the sewer sediment. Near bed organic solids were characterised by the presence, during dry weather flow, of organic material (organic content greater than 90%) of $30 \text{ mm} < d_{50} < 50 \text{ mm}$ transported over the settled bed. Generally, it is found that transport patterns is a combination of bed load over the settled bed and inner suspension, characterised by discrete organic particle in transitory contact with the boundary. When sediment are collected toward the depth column with siphon or pipes samplers, results suggested the presence of an inner suspension, defined as dense undercurrent, characterised by particle not in contact with the bed and of larger dimensions compared to that found in the flow. In dry weather, a weak layer (type C layer) of large organic content (>90% and of $d_{50}=0.5 \text{ mm}$) is observed over the coarser sediment (type A layer). This weak layer is also characterised by a strong re-entrainment potential in presence of flows with shear stress larger than $0.5\text{-}1 \text{ N/m}^2$. A similar pattern is confirmed by direct interface observation carried out by (Oms, 2003). In her work, two visual methodologies for direct sewer observation were developed, i.e., by means of an endoscope and an automatic image recorder installed laterally inside the sewer bench. Endoscope observation revealed the presence of coarser deposits toward the bottom covered by a layer of finer organic material of (bulk density) of $1046 \text{ kg/m}^3 < \rho_b < 1315 \text{ kg/m}^3$. A muddy creamy layer was observed above the organic layer in presence of strong flow deceleration, with observed thickness up to 15 cm. However, little information is available on the granulometry and other characteristics of the creamy layer, owing the problematic connected with the sampling operations. The observation box, installed toward 1 m of length, revealed a rather distinguishable interface between the organic and the coarser layers. The latter was characterised by sediment dimensions between 5mm and 20 mm enclosed into a matrix of finer sediment.

Acoustic measurements of sediment interface and sediment concentrations seems to be recently developed by (Bertrand-Krajewski and Gibello, 2008) and (Le Barbu and Larrarte, 2010). Although limited information has been provided, results seems encouraging the use of acoustic technologies in sewer environments.

3 SONAR THEORETIAL BACKGROUND

The sonar is an acoustic device which generates a pulse and receives the backscatter echo. A backscatter echo can be due to any inclusion having an other acoustic impedance than water. It means any bubble, particle or solid present in the water which reflects, adsorbs or refracts the acoustic pulse generated by the sonar. The acoustic backscatter strength (ABS) per unit of volume S_v [dB] is, hence, based on the well known sonar equation (Hoitink and Hoekstra, 2005)

$$S_v = 2\alpha_i R + K_c (E - E_r) + 10 \log \left(\frac{T_T R^2}{P_L P_T} \right) + C_1; \quad (4)$$

where R is the range along the beam axis [m], α_i the attenuation coefficient [dB/m], E and E_r are the received strength and received noise respectively [counts], K_c the conversion factor [dB/counts], T_T the transducer temperature (°C), P_L the transmit pulse length [m], P_T the transmit power [W], and C_1 is a constant. Accordingly, the values of K_c and E_r depend on the probe and need to be determined from calibration. Further details on the equation derivation can be found in (Deines, 1999).

Accordingly, S_v is generally a function of the density of scatters within a control volume n_b (number of scatters by the control volume) and the mean square scattering cross section of the particle contained in the cross section as:

$$S_v = 10 \log(n_b \langle \sigma_{bs} \rangle) \quad (5)$$

where $\langle \rangle$ denoted the mean square operator,

$$\sigma_{bs} = 4\pi\theta k^4 a^6 \quad (6)$$

is the acoustical scattering cross section of a single spherical particle of diameter a and material parameter θ (i.e. a parameter which takes into account for the particle's elasticity and relative density) in the Rayleigh regime ($ka \ll 1$). The wave number k is equal to $2\pi/\lambda$, where $\lambda = c/f_0$ is the frontal wave length, c is the wave propagation and f_0 is the emitted frequency. The material parameter depends on the relative elasticity of the material $e = E_s/E$ (E_s and E sediment and water elasticity respectively) and the relative density of the material $\rho' = \rho_s/\rho$ (ρ_s and ρ sediment and water density respectively) as:

$$\theta = \left(\frac{e-1}{3e} \right)^2 + 1/3 \left(\frac{\rho'-1}{2\rho'} \right)^2 \quad (7)$$

The material parameter latter might have its importance when considering organic particles, for which both e and ρ' differs from the mineral particles usually analyzed in coastal and river application [for sand grains of quartz $e=39$ and $g=2.65$, while for organic sediment $1.3 < g < 1.6$ (Ashley, Bertrand-Krajewski, Hvitved-Jacobsen and Verbanck, 2004)].

Hence, knowing that the volume mass concentration

$$M = n_b \rho_s 4/3\pi \langle a \rangle^3 \quad (8)$$

S_v can be expressed as a function of the volume mass concentration as

$$S_v = 10 \log \left(3\theta \cdot k^4 \langle a \rangle^3 M / \rho_s \right) \quad (9)$$

The sound attenuation is linked to the water attenuation (molecular) α_w and the sediment attenuation α_s as:

$$\alpha_t = \alpha_w + \alpha_s \quad (10)$$

in which both α_w and α_s can be derived from the literature (Hoitink and Hoekstra, 2005). From the latter, α_w is a function of the temperature, salinity and ph. For $ka \ll 1$, α_s increased with the volume concentration M and also depends on k , the emitted frequency f_0 , e and g (Thorne and Meral, 2008). Differently, (Larrarte and François, 2008), evaluated the attenuation properties of waste water for a TSS (total suspended solid concentration) of 500 mg/l.

Alternatively, the mass volume concentration M can be derived from the received intensity E_r , after operating a calibration in which the coefficient C_k of a system (also including the transmitted power P_T) can be obtained from Eq.9 (Deines, 1999):

$$C_k = 10 \log(M/\rho_s) - 20 \log(R) - 2 \alpha R - 10 \log(P_L) \quad (11)$$

In which M is the volume concentration measured at the distance R .

Hence, to calculate $C_v = 10 \log(M/\rho_s)$ from the acoustic profile, it can be used the following:

$$C_v = C_k + 20 \log(R) - 10 \log(P_L) + 2 \alpha R + K_c(E - E_r) \quad (12)$$

The distance R is evaluated from the traveling time the emitted echo needs to hit the particles contained in the control volume and travel back to the receiver (Wunderlich, Wendt and Muller, 2005):

$$R = ct/2 \quad (13)$$

(Apelt, 1988), derived an expression to relate the temperature T , water depth z and salinity s to c :

$$c = c(s, T, z) = c_o + a_o(T - 10) + \beta_o (T - 10)^2 + \gamma_o(T - 18)^2 + \delta_o (s - 35) + \varepsilon_o(T - 18)(s - 35) + \zeta_o |z| \text{ [m/s]} \quad (14)$$

where $c_o = 1493$; $a_o = 3$, $\beta_o = -0.006$, $\gamma_o = -0.04$, $\delta_o = 1.2$, $\varepsilon_o = -0.01$, $\zeta_o = 0.0164$.

4 EXPERIMENTAL APPARATUS

According to the literature, several methods can be used to measure the characteristics of the bedform (thickness of the deposits, wavelength, wave height, slopes). Owing to the high sediment concentration, optical probes, i.e., laser altimeters, cannot be successfully used and, generally, Optical Backscatter (OBS) probes are used to characterise the sediment concentration. When soft sediments, i.e., the organic layer of sewer deposits, are presents, the introduction of a sediment gauge might interfere with the sediments destroying the organic layer. A point sediment gauge with a large disc of 25 cm of diameter has been used in the present tests (Figure 3).

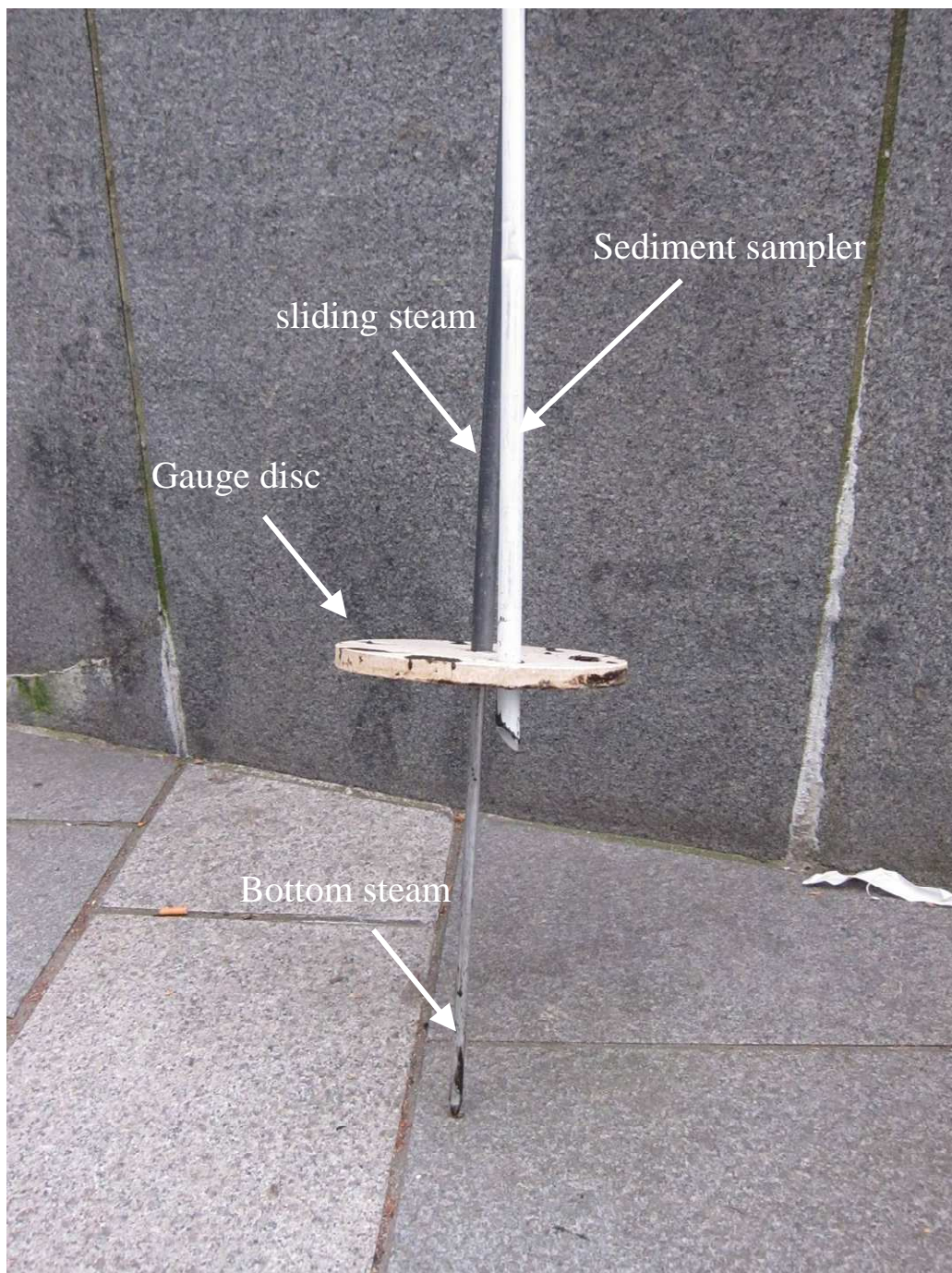


Figure 3 Sediment point gauge. The disc has a thickness of 2 cm and a diameter of 25 cm.

When operating with a sediment gauge, the sensibility of the operator might further represent a source of incertitude of the measure. Accordingly, the point gauge should be introduced without exerting any pressure on the disc, in order to reach the top of the organic layer without entering this latter. However, the disc can stop at different height, according to the capacity of the mud layer to support the weight of the disc. Water has been sampled using a suspended solid sampler device, made of four pipes of 10 mm of diameter, placed at different heights from the bottom. Each pipe is connected to a 2.5 l bottle in which a pressure of about - 0.07 MPa was realised. Once the pipes were connected to the bottles, the device was immersed in the water and the connectors opened for around 15 second. However, in presence of a mud layer, the pipes were eventually clogged by large sediment or the pressure wasn't reduced enough to collect the sediments.

Hence, acoustical measurement may represent an adequate solution in terms of installation feasibility (small dimensions and light < 5 kg, no needs of special equipments, correspondence with ATEX and TBTS standards, water proof) and the ability of detecting the interface.

Two different acoustic probes have been used:

- A sonar profiler (thereafter mentioned SONAR), manufactured by Marine Electronics Ltd., model pipe profiler 1512, of working frequency of 2 MHz, used to measure the bottom transverse and longitudinal acoustic response of the sediment bed;
- A Sontek side looking Acoustic Doppler Velocimeter (ADV), of 10 Mhz of working frequency, used to measure the three components of the flow velocity u , v , w along the Cartesian coordinates (x , y and z , longitudinal, transverse and vertical velocity respectively) and to measure the acoustic response of the flow.

4.1 Marine Electrics 1512 SONAR

The profiler consisted in an emitter and an acoustic receiver which rotates inside the probe case, which has been made by means of an alloy cylinder of about 70 mm of diameter and about 445 mm of length. The sonar profiler (Figure 4) is provided with a rotating head that measure the acoustic backscatter along 400 beams of 0.9° each and for 250 control volume, or bin, from the centre of the probe to the maximal measured distance or range R_{\max} , with a frequency of 1 Hz (i.e., a section each second).

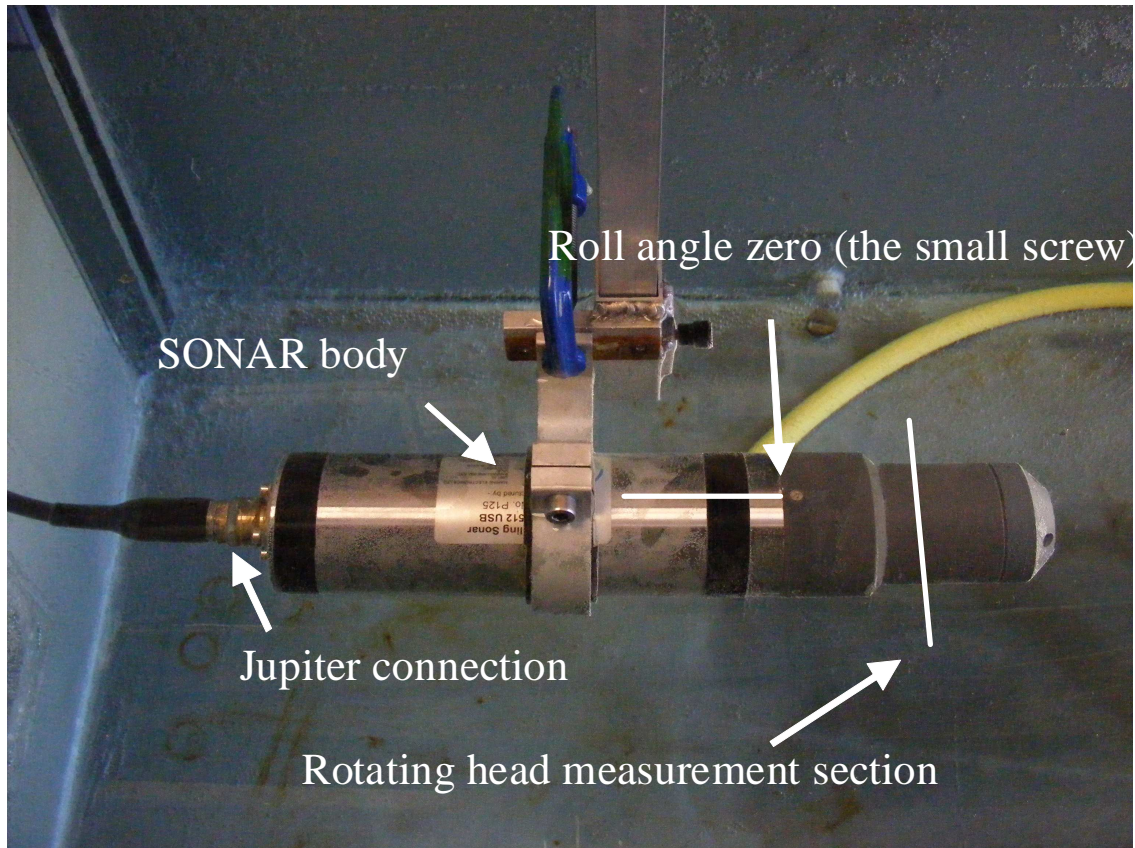
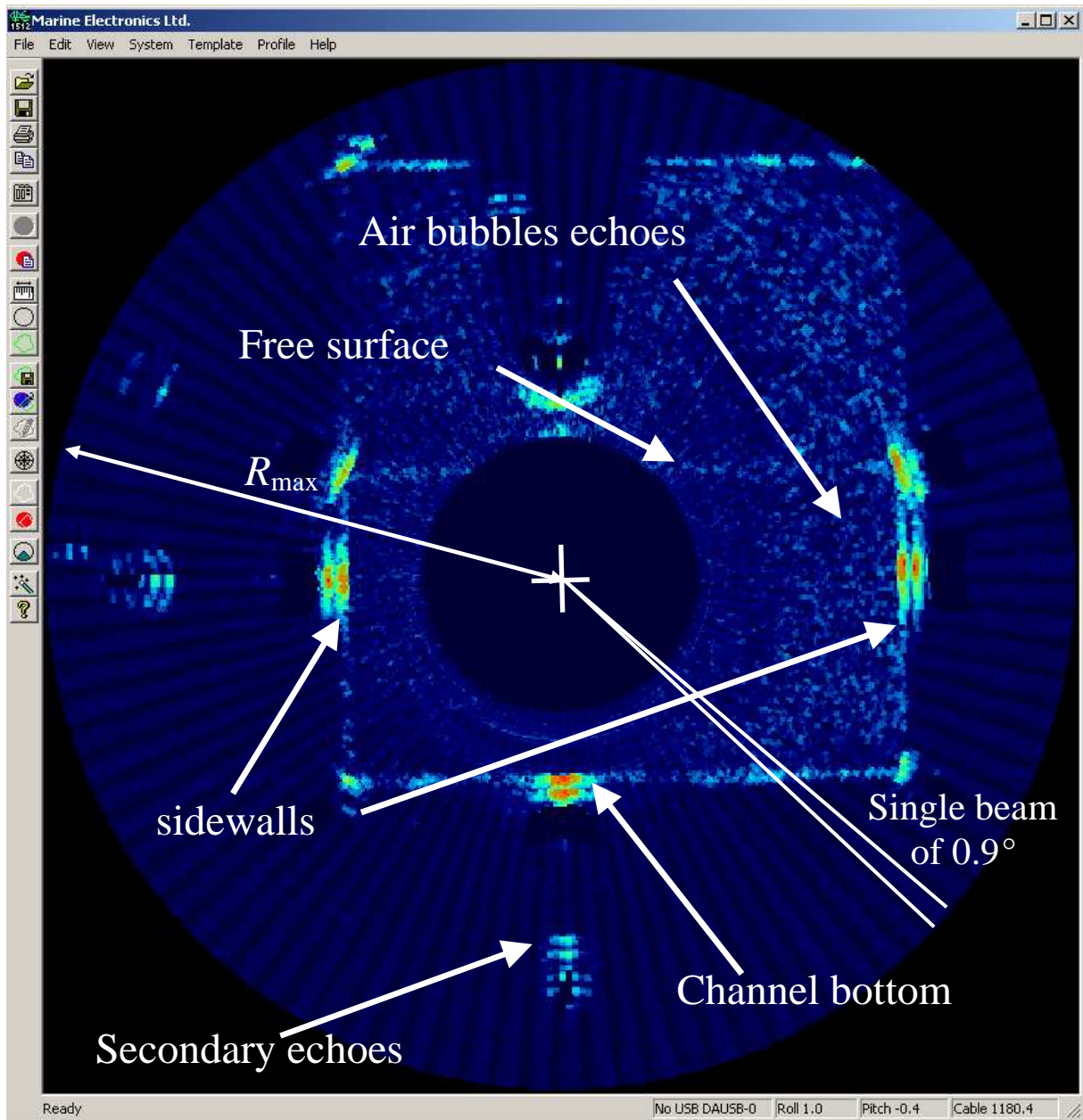


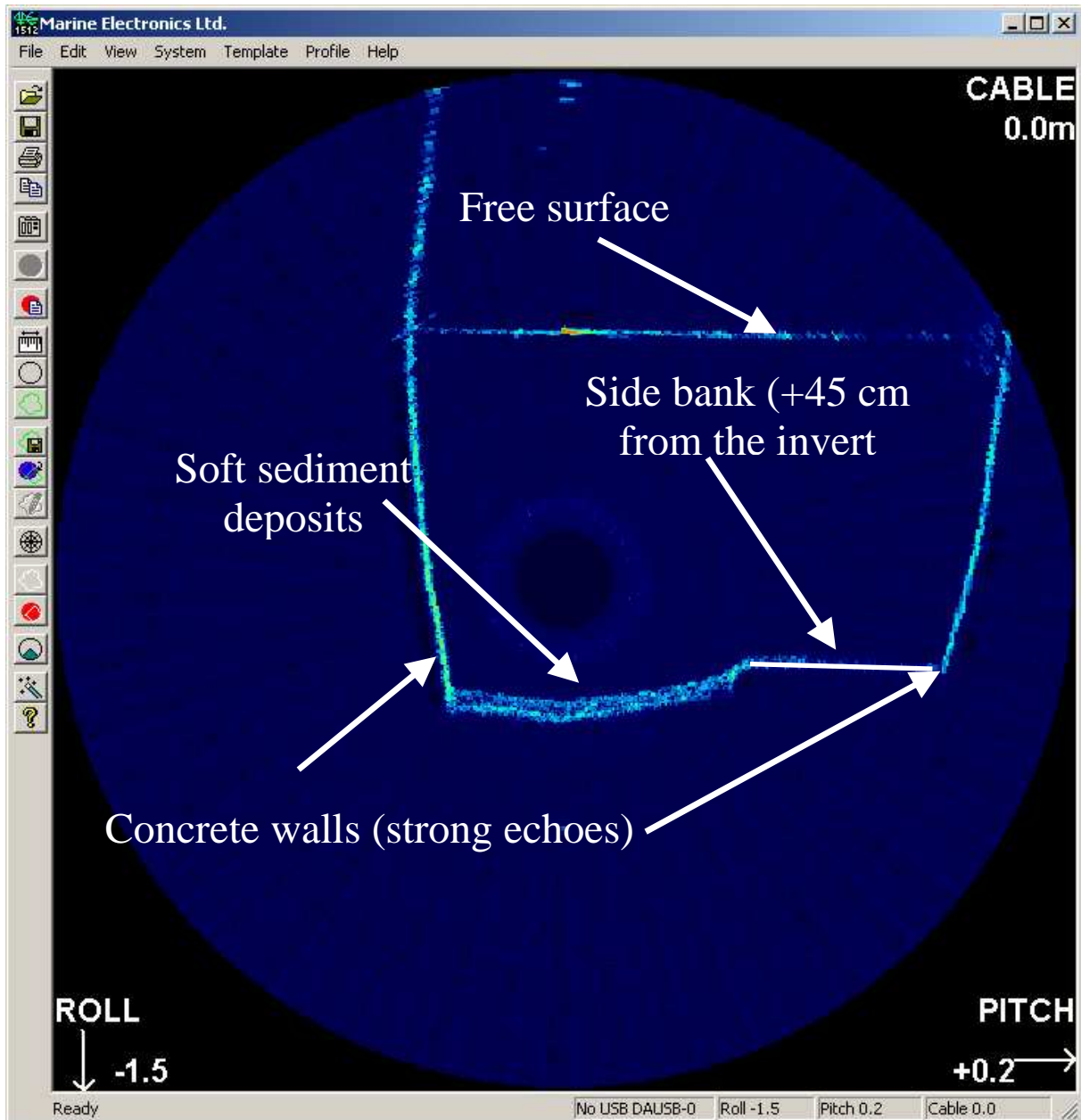
Figure 4 SONAR Marine Electronics model 1512.

The plane of rotation is located at around 4.5 cm from the edge of the PVC boot. The working frequency of the profiler is of 2 MHz. The probe can detect the acoustic backscatter (ABS) with maximum distances (subscript “max”) ranging between $0.125 \text{ m} < R_{\text{max}} < 6 \text{ m}$, where R is the generic position of the control volume or bin from the SONAR center. The probe is able to detect both pitch and roll angle (right bottom of the frame), with a precision of $\pm 0.1^\circ$.

Figure 5a-b show the ABS output recorded with the software “pipe profiler” in laboratory conditions and in situ conditions respectively. The black centre is automatically blanked by the software, as the zone of 20 cm of diameter is perturbed by the transducer noise. The image shows the bottom and the side walls of the channel. Generally, when the signal hit perpendicularly a surface, a large part of the signal is reflected by the walls (the red spot in the image). Vice versa, the larger is the reflection angle toward the normal direction, the smaller will be the signal intensity (see the bottom reflection in the laboratory channel figure). Further, the free surface acts as a mirror, as shown in the figure in the upper part of the image. The sonar also detects the air bubbles present in the flow which are represented as the clear spot inside the channel. As it is possible to observe from the in situ conditions, sediment deposits generally shows a different ABS compared to the concrete sidewalls, owing to the different nature of the soft deposits.



(a) SONAR output, laboratory conditions, $R_{max}=500$ mm, the + represent the sonar center



(a) SONAR output, insitu conditions, $R_{\max} = 1000$ mm

Figure 5 pipe profiler SONAR output for $P_L = 4$ μ s

The main parameters that can be regulated from the system control software are (Figure 6):

- The “range” or maximum detectable distance ($0.125 < R_{\max} < 6$ m); the probe hence presents a geometrical resolution of $1/250$ of the maximum range, since each radial beam is divided in 250 control volume between $0 < R < R_{\max}$.
- The “pulse length” ($4 \mu\text{s} < P_L < 20 \mu\text{s}$), which represent the duration of the pulse generated by the sonar; the vertical resolution δ_v is connected to P_L by $\delta_v = cP_L / 2$.

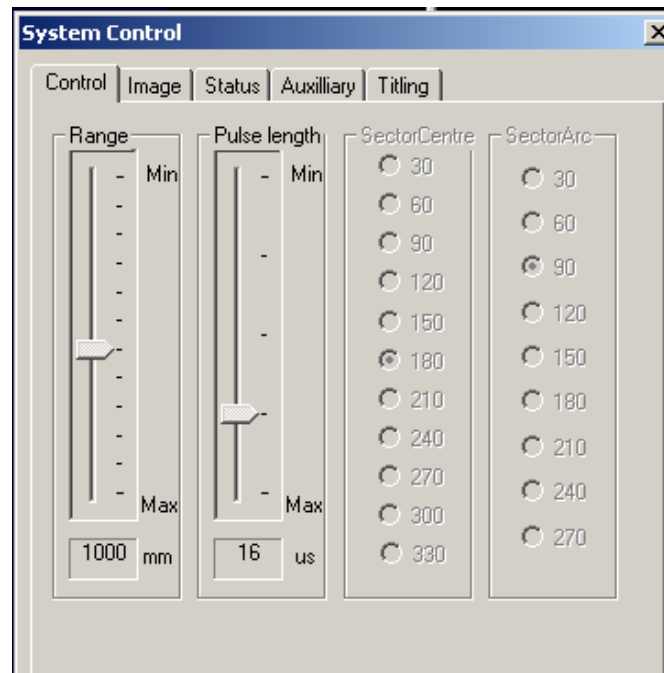


Figure 6 pipe profiler system control panel.

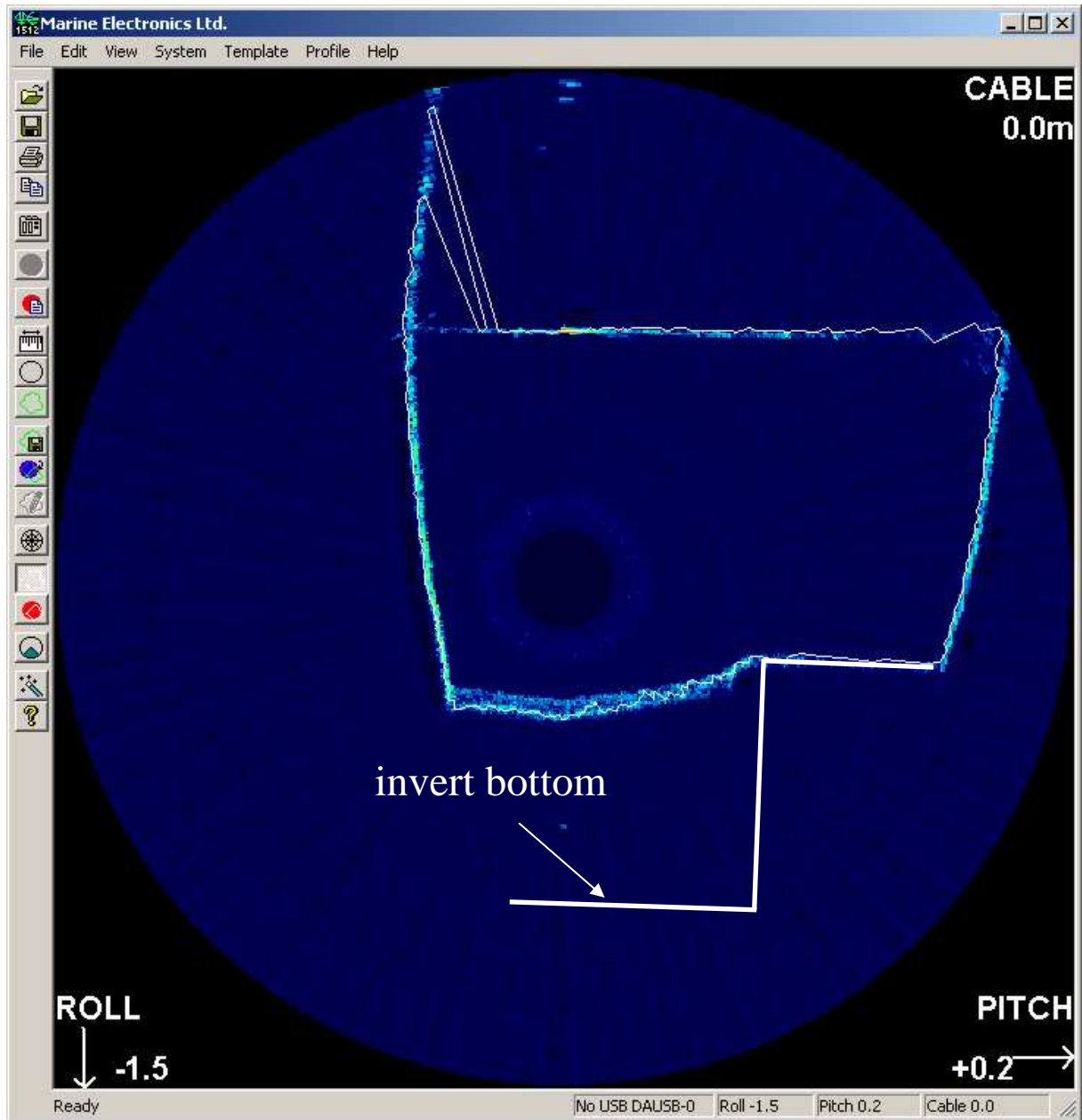
The output generated by the software is given in counts using an 8-bit scale. The SONAR is equipped with a 70 dB logarithmic receiver, in which the output voltage (the voltage post-processed by the probe and which is latter converted in counts) produced by the probe is proportional to the logarithm of the input voltage (the row signal recorded by the piezoelectric transducer of the SONAR). The software automatically adjusts the gain to the largest detected backscatter. However, the row image also gives the gain used for the automatic adjustment (see appendix for more details).

The software also allows the regulation of the maximal intensity and the threshold, which, however, doesn't modify the accuracy of the measure. The temperature needs to be manually adjusted, as the probe has not been equipped with a thermometer.

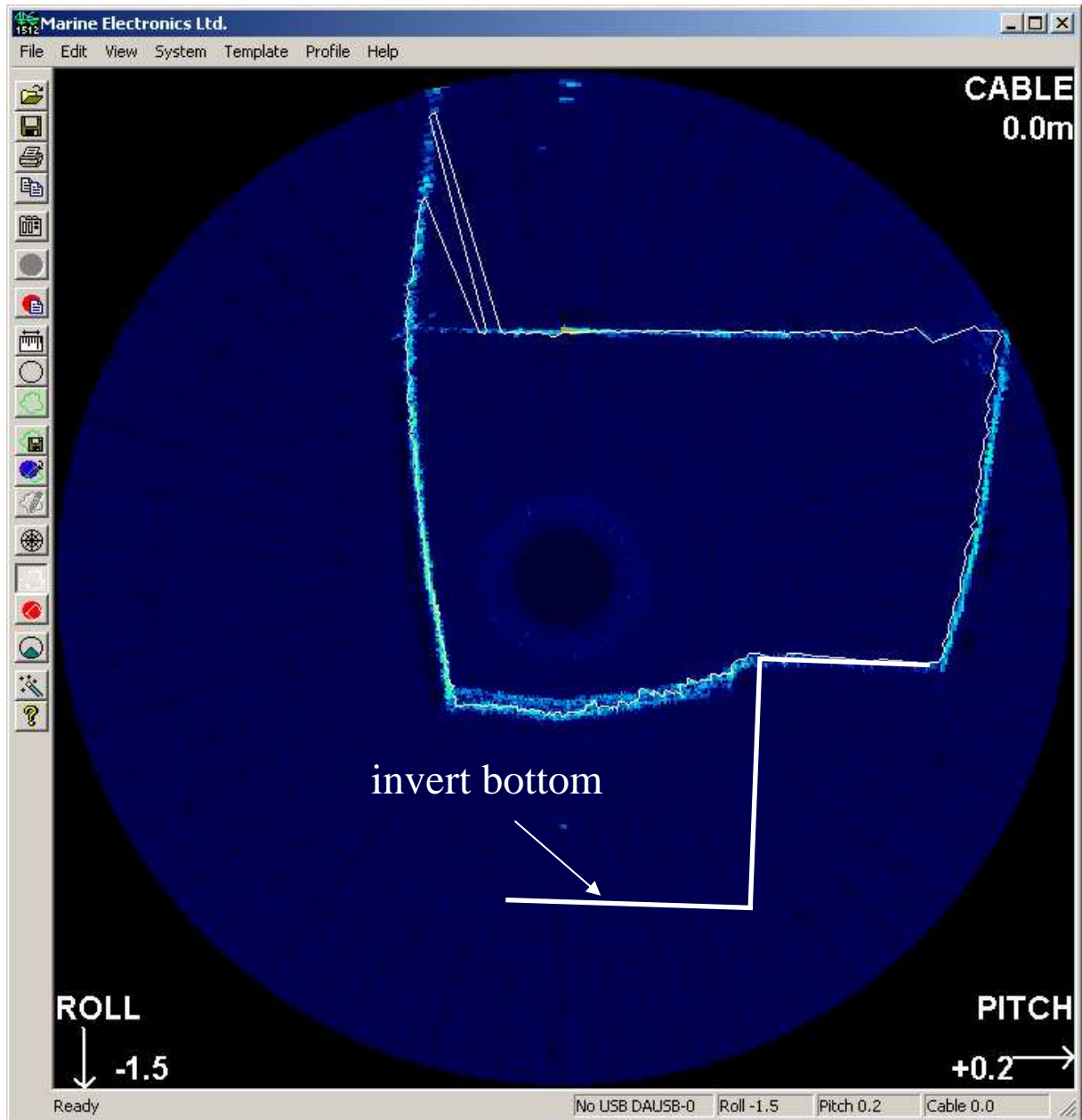
A profile of the bottom can be obtained by the recorded image using three different algorithms via software. The software elaborates separately each beam or sector of 0.9° :

- “Max”, the profile is obtained from the points were the maximum ABS is detected;
- “3/4”, the profile is obtained from the point were $\frac{3}{4}$ of the maximum ABS is detected;
- “Areal”, the profile is obtained from the point were the largest energy is detected

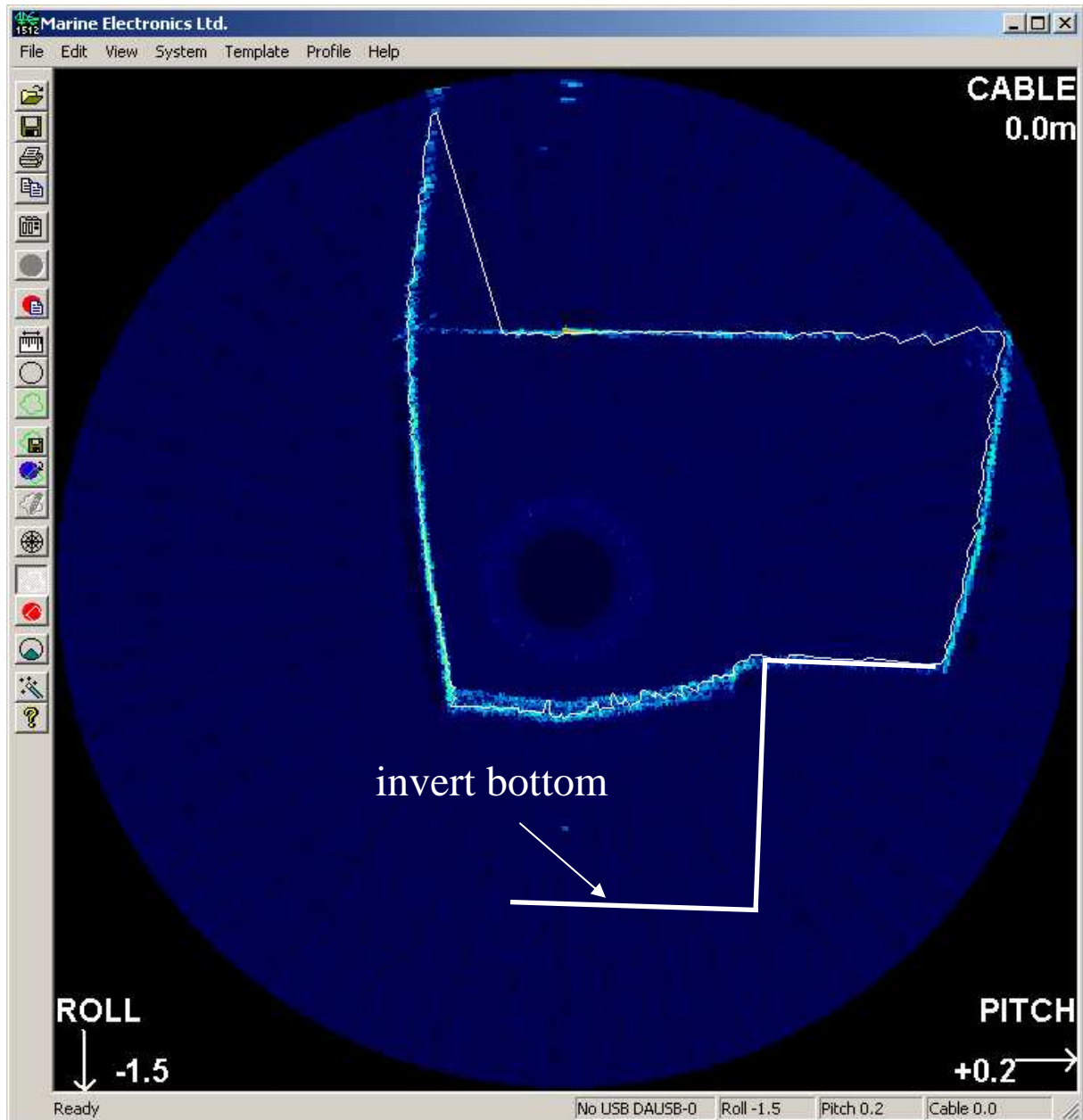
Figure 7 shows an example of the profile individuated by the SONAR outputs using the algorithms proposed in the pipe profiler software. The white lines in the figures show the profile individuated by the algorithms. In general, “max” shows a profiler which is more extended compared to the other two. However, slight differences occurs between them, generally less than 1 cm, whilst the profile individuated over the bottom sediment is quite scattered and shows even slighter differences amongst the three proposed algorithm.



(a) "max" algorithm insitu conditions, $R_{\max} = 1000$ mm



(b) "3/4" algorithm insitu conditions, $R_{\max} = 1000$ mm



(c) “AREA1” algorithm insitu conditions, $R_{\max} = 1000$ mm

Figure 7 detection algorithms proposed in the Marine Electronics Pipe Profiler software

Further details on the working operation are included in the appendix

4.2 Sontek 10 Mhz, side looking ADV

The ADV is an acoustic device which measures the three components of the instantaneous velocity u , v and w (longitudinal, transverse and vertical components respectively) according to the axis orientation shown in Figure 8. The coherent pulse ADV works with a maximum frequency of 25 Hz, allowing for the characterisation of the flow turbulence. The ADV has an operative frequency of $f_0=10$ Mhz, owing to the shorter distance of the control volume compared to that measured by the SONAR. The ADV has one emitter at the centre of the probe and three receivers (Beam “0”, Beam “1” and Beam “2”). The receivers are focused at about 10 cm from the emitter in order to reduce the flow disturbance.

The ADV velocity measurement is based on the frequency shift of the backscattered signal:

$$V_i = c \Delta f / f_0 \quad (15)$$

where V_i is the velocity measured along the half bisector beam

Hence, the ADV measure the average velocity of the particles inside the control volume (about 1 cm^3 and function of the geometry and the directivity of the emitter/receiver). Several parameters can be regulated when measuring the data, amongst which the most important are:

- Sample frequency f_s : ranging from $1 \text{ Hz} < f_s < 25 \text{ Hz}$; corresponding to the frequency used to record the instantaneous velocity;
- Velocity range V_{\max} : $0.03 \text{ m/s} < V_{\max} < 250 \text{ m/s}$; corresponding to the Nyquist velocity, or the maximum instantaneous velocity which can be measured without aliasing.

According to the principle of pulse coherent Doppler velocity measurement, there are no limits for the lowest velocity which can be measured with the probe. However, according to the manufacturer, the precision of the measurement is about 1% of V_{\max} .

The half-bisector velocity from each beam is then rotated according to geometrical transformations, in order to obtain the velocity in the Cartesian system. The measure of each velocity along the half bisector of the angle beam/transmitter might be affected by an error in the estimation of the velocity, which further reduce the accuracy of the final velocity measurement in Cartesian coordinates. As example, the presence of particles larger than the control volume or high turbulence near the walls (which however is the quantity to measure) might produce a spike or peak in the velocity time-series. Hence data need to be post-processed, in order to eliminate the spike. Several criteria to assess the quality of ADV measure have been proposed. In particular two main parameters measured by the probe are of main importance:

- Signal to noise ratio (SNR): this parameter gives the ratio in dB scale of the ABS strength to the floor noise (either acoustical or electrical); generally the quality requirements need this value to be larger than 15 dB; this parameters also reflects the quantity of scatters present in the water, the larger the n_b is the larger will be the SNR,
- Correlation: this parameters assess the correlation between the transmitted pulse and the received pulse; generally if the signal received comes from the scatters present in the control volume the correlation is high while in case of large turbulence the sudden changes of the particle may reduce the correlation; a good signal has a correlation larger than 70%.

Hence a first screening might be based on the analysis of those parameters. A first attempt has been done by (Wahl, 2003) based on the consideration that the acceleration of a particle cannot be larger than the gravity acceleration, otherwise the particle would escape from the flow. A second attempt has been proposed by (Goring and Nikora, 2002) and (Wahl, 2003) introduced a different algorithm to remove the spike and filter bad samples from the signal. This algorithm called “phase space threshold”, considered not only the variance of the velocity fluctuation but also the variance of the first and second derivatives. According to the (Wahl, 2003) correction, an elliptic space can be created using the three variances evaluated

for each derivate. The axis of the space can be multiplied by a level of significance, in order to improve or reduce the number of data removed. Hence all the samples outside from the space are removed. In order to evaluate other properties connected to the turbulence and the energy dissipation (such as auto and cross-correlation spectra), the filtered signal needs to be continuous, i.e., the holes left by the application of any filtering procedure needs to be fitted. In this work we adopted the technique suggested by (Wahl, 2003), in which a cubic regression is obtained for the first 7 sample after the filtered samples and the last 7 samples before the filtered one. It is worth observing that the filtering procedure is used for the three components of the velocity. Hence, if one of the component has shown a “bad” sample, the samples at the same index in the other two components of the velocity are automatically removed, owing to the fact that if one of the components contained a bad sample, the error of the measure might have propagated also to the other two components.

4.3 In-situ setup

In order to achieve contemporary measurement of both sediments morphology and velocity fields, the two probes have been used in the mean time fastened together (Figure 8). The ADV has been fastened below the SONAR, in order to quickly locate its position, based on the sonar results and therefore to locate the control volume position in time effective fashion. Indeed, this specific application allows at reducing the measurements time and to improve the precision, as no need in device change is required, as well as it improves the operator's safety, as the number of operation to carry out inside the sewer is optimised. Moreover, the measurement condition are better defined, as for each vertical, the measurements are carried out within few minutes between the first and the last survey. It is worth observing that the ADV has been fastened looking downstream, although the original configuration considered by the manufacturers is a lateral configuration. This means that velocity components need to be reoriented toward the 3 principal axes. The sketch shows the standard configuration used by the manufacturer. It is important observing that the data analysis has been carried out to ascertain whether there is any influence on the average velocity and turbulence characteristics linked to the probe orientation, although (Strom and Papanicolaou, 2007) observed that no theoretical criterion required the flow to be 2D, i.e., with zero mean transverse component.



Figure 8 ADV and SONAR fastening (same as in-situ conditions)

In the figure x_{ADV} , y_{ADV} , and z_{ADV} are coordinate referred to the sonar centre, over which the velocity component are referred, namely, u , v , and w , while x_{SONAR} , y_{SONAR} , and z_{SONAR} are the system of coordinate relative to the sonar centre of rotation, which is at about 4.7mm from the probe head. The particular configuration assumed in the present test was chosen in order to:

- 1) allowing measurement of near interface velocity reducing the bottom interaction;
- 2) determining the position of the ADV control volume based on the SONAR position toward the bottom detected by the sonar;
- 3) facilitating the transport and the installation of the two probes.

However, the two probes can be separated to accomplish specific tasks as further shown in the note. Velocity measurements have been carried out installing the probe in the flow orienting x_{SONAR} axis (and than the z_{ADV} axis) toward the x axis of the flow, and hence in the flow direction, as defined later in the text. Hence the offset between the SONAR centre and the centre of ADV control volume was fixed at 186 mm. In this configuration, the SONAR head is oriented toward the flow direction in order to reduce the disturbance effect on the flow velocity measured with the ADV.

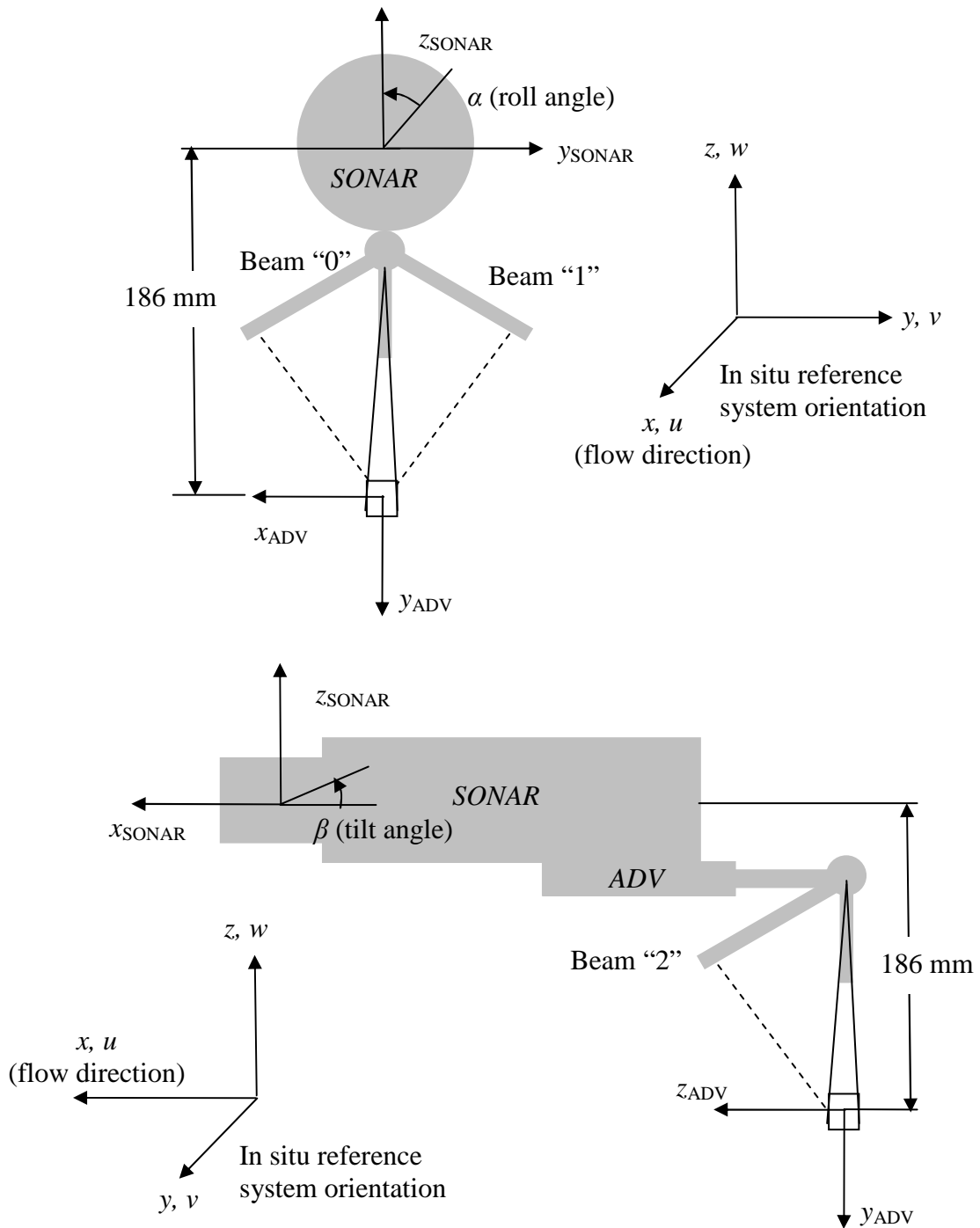


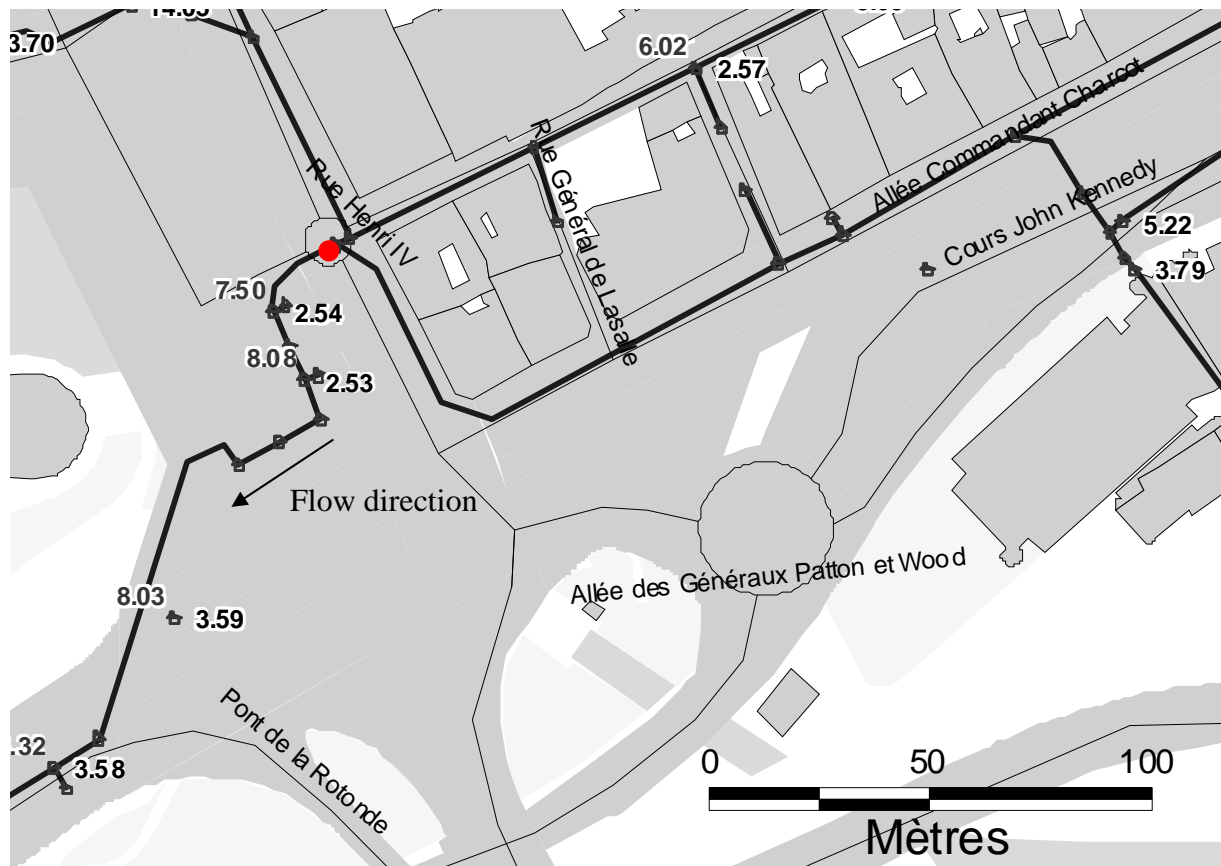
Figure 9 Reference system definition

5 EXPERIMENTAL SITES, EXPERIMENTAL SETUP AND MEASUREMENTS PROCEDURE.

5.1 Experimental sites

Two experimental sites have been selected, namely the “Duchesse Anne” combined sewer (DA) and the “Allée de l’Erdre” combined sewer (AE), based on the different characteristic of the flow and of both bottom and suspended sediments.

In the working section, the DA site is characterised by a slope of $S=0.3\%$ (Figure 10a), a catchments area of 4.11 km^2 , connected into a network of 21 km of length, while the AE site has a slope of $S=1.2 \%$ (Figure 10b), a catchments area of 1.41 km^2 ha and a network length of about 60 km.



(a) Duchesse Anne (DA) experimental site



(b) Allée d'Erdre (AE) expertement site

Figure 10 catchments basins with pipes, quotes (in m) and working section locations (●).

Note: tick black lines are the combined sewer networks.

During the dry weather period, the DA sewer deposits are generally characterised by rather mineral sediments (type A, according to (Crabtree, 1989)) and most likely a second type C deposit, whose presence has not been directly measured.

The AE site generally shows, from the bottom, a first layer of relatively mineral sediments (type A), most likely a second type C deposit, which again has not been directly measured, and generally a highly concentrated layer whose thickness can broadly vary toward the channel longitudinal direction. Hence, it is expected that the response of the sonar profiler on different sites should, as well as the turbulence intensity measured at various location, be affected by the different suspended sediment concentration and typology.

Both sewer pipes are characterised by an egg shaped transverse section with one lateral bank, which allows the passage of the operators, therefore reducing the sediment disturbance. The sketch in Figure 11 shows sites dimensions and the notations, in which y =distance between the ADV and the free surface, h =distance between the sediment bottom shown by the

SONAR and the ADV, δ = total water depth between the sediment bottom shown by the sonar and the free surface.

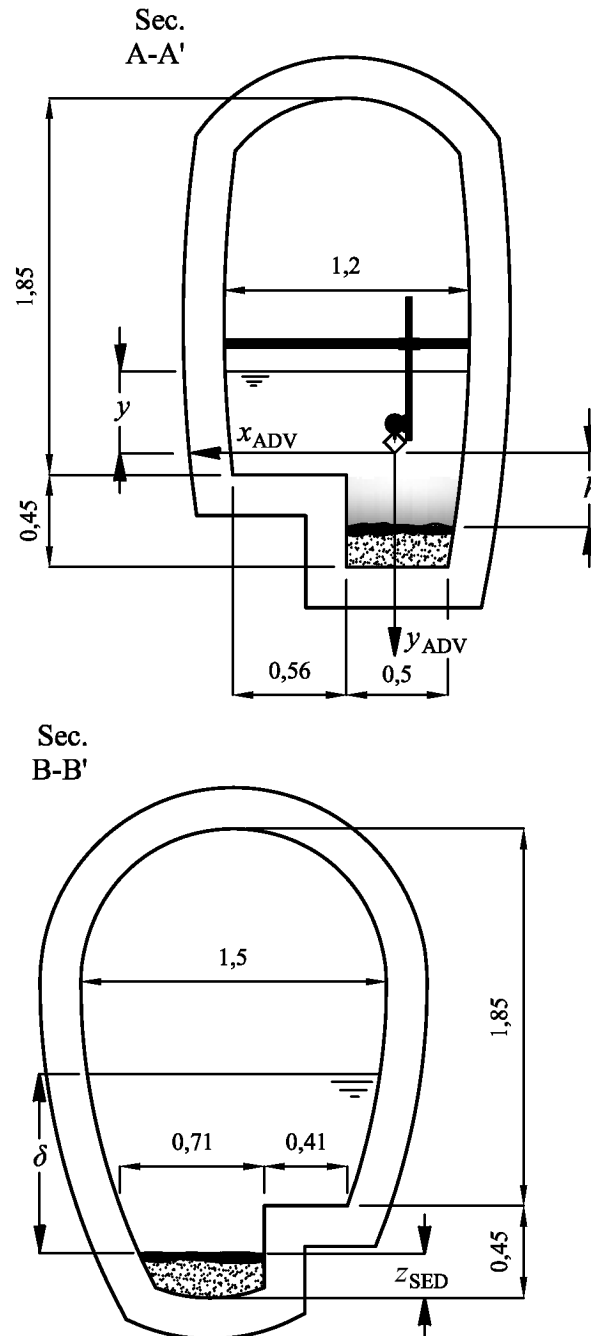
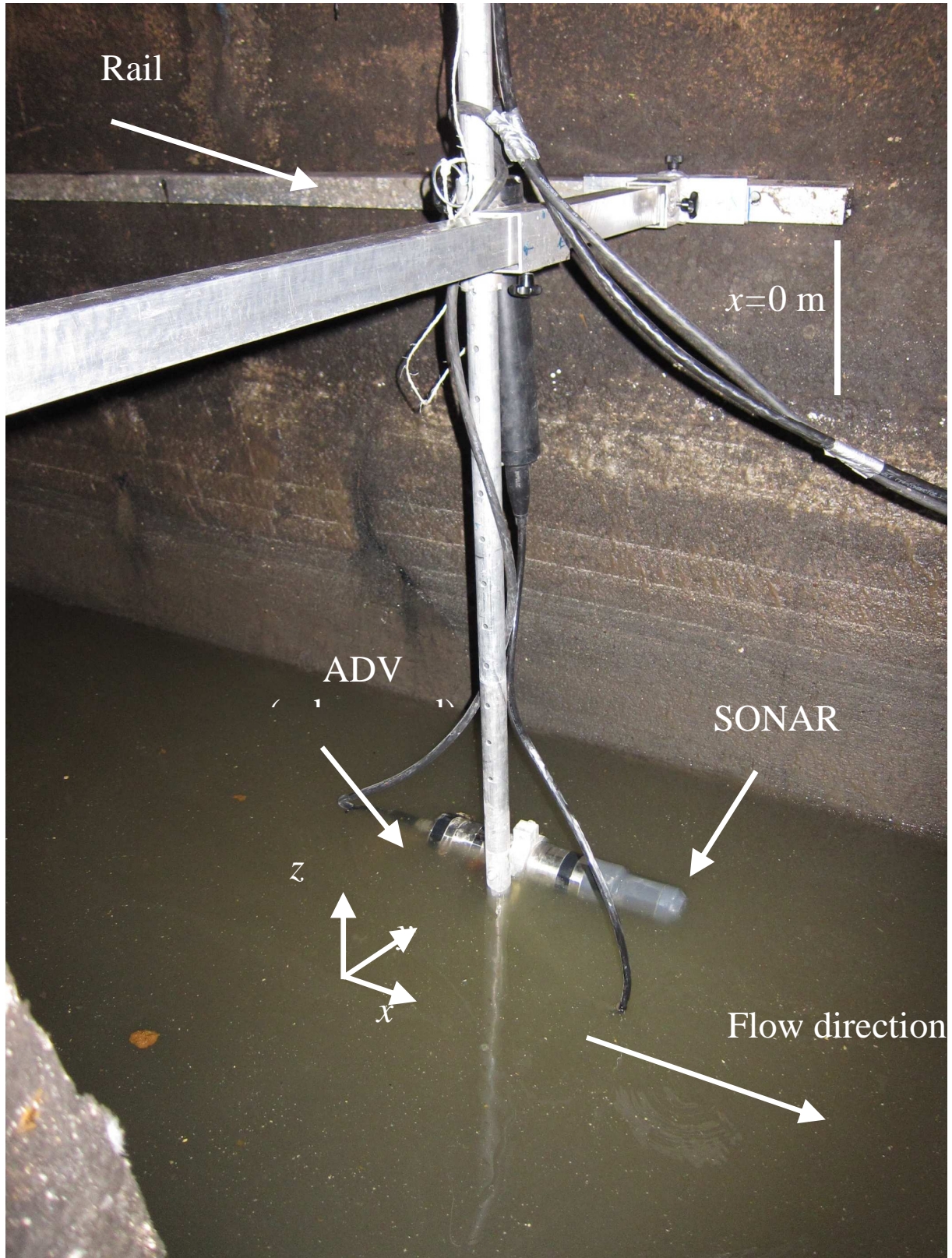


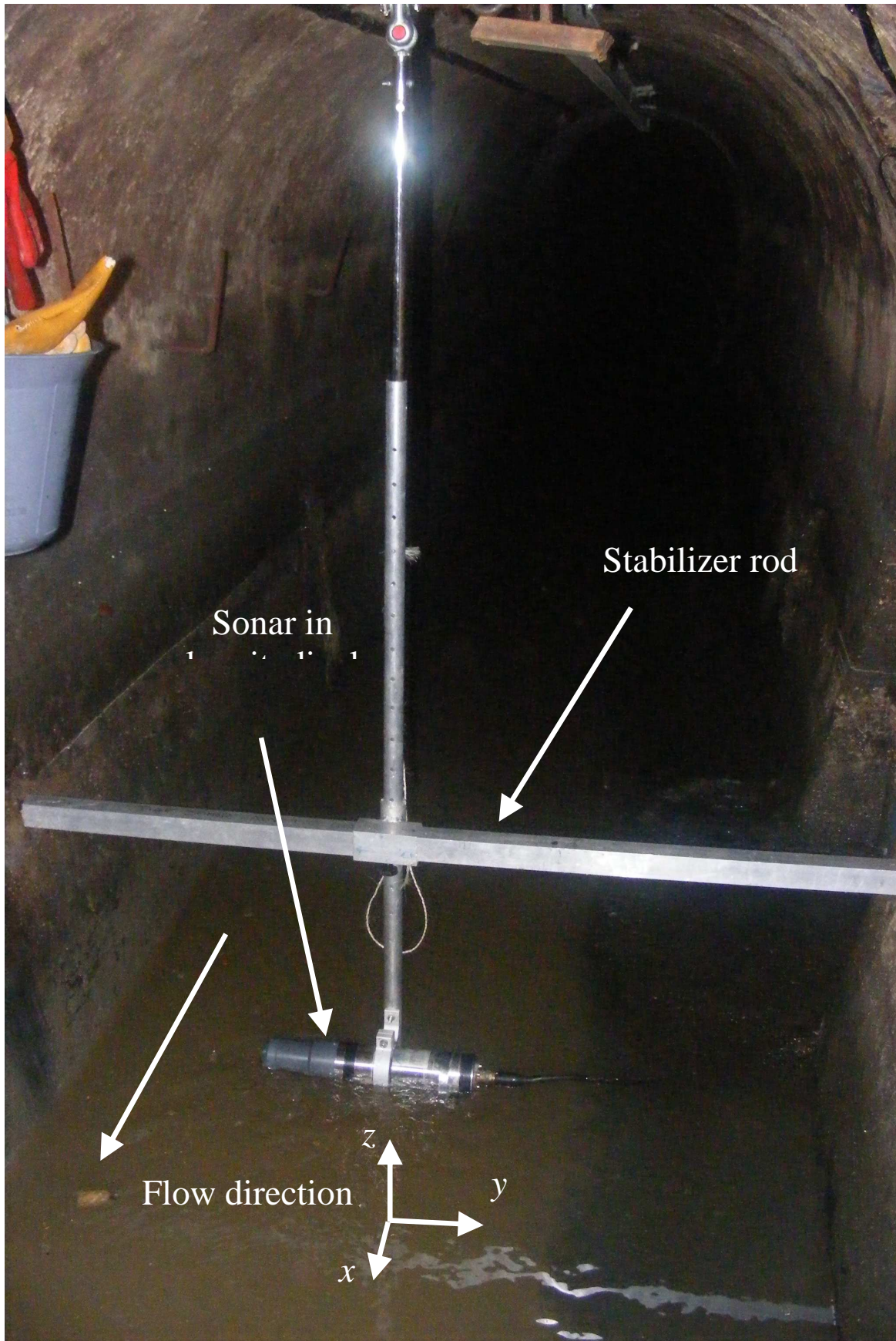
Figure 11 catchments basins invert sketch with notation (a) AE (b) DA (dimensions in meters).

Two different carriage systems have been installed inside the sewer in order to shift the probes both longitudinally and transversally. At the DA site two rails have been installed longitudinally at the invert sides toward 10 m of length at about 1.2 m from the bottom, in order to reduce their inundation likelihood. The rails have been fixed starting from the

manhole toward the upstream direction (Figure 12a), and consisted of 4 cm width squared alloy bars.



(a) AE, SONAR in transverse position and ADV in down looking position (submerged, flow from left)



(b) DA, SONAR during a longitudinal survey (submerged, flow from the top of the image)
Figure 12 Experimental in situ set-up

A 1.08 m alloy bar of the same dimensions and section of that used for the rail has been fixed transversally over the rails and a mobile support, which can to slide along all the channel width, held the vertical bars. In order to adjust the probe orientation, the latter bar consisted of a cylindrical section that completely rotates in both directions. All the material composing the carriage system has been made in alloy both to warrant lightness and prevent corrosion problems. Longitudinal and transverse distances have been measured by means of 0.5 cm precise meters, glued over the rails and over the bar. Five longitudinal section at distance of 1 m each other (i.e., $x=-0.5\text{m}$, $x=-1.5\text{m}$, $x=-2.5\text{m}$, $x=-3.5\text{m}$, and $x=-4.5\text{m}$) have been then preliminary taken into consideration in order to survey both the flow velocity and the morphology of the sediments.

Differently, the experimental installation of DA site (Figure 12) consisted of a single rail fixed at the ceiling of the invert, over which a carriage has been arranged, allowing for longitudinal movements. Vertically, the position of the probes is regulated by means of a cylindrical bar, directly hanging from the small carriage, which again can be rotated in order to adjust the probe orientation. However, only small transverse regulations are possible to fix the probe at the dry weather channel centre. The longitudinal position of the probe is measured by means of a 1 cm precise scale fixed over the rail. Moreover, a transverse bar has been used to stabilise the whole system, hence preventing and reducing lateral probe oscillations and tilting.

5.2 Measurement execution

For each transverse section, the probe centre has been fixed at the invert centre, in order to minimize side walls and asymmetry effect toward the velocity measurements, although it is known that the flow is strongly 3D (Bonakdari, Larrarte, Joannis and Levacher, 2008). For each sampled section, signals were sampled from both the probe at several vertical points, generally at 5 cm apart vertically, although possible refinements were possible when desired. Hence, a first SONAR image is recorded and the sewer profile extracted. As aforementioned the image included also information on the backscatter intensity. The image is thus made by the backscatter intensity detected for each sector of 0.9 rad. In real time conditions and based on the 8-bit backscatter intensity, the software shows the bottom profile using the max algorithms (Figure 14), which is defined as the line connecting the point in which the maximum backscatter intensity is detected for each sector. The operation for the image record took about 10 second after the probe is placed at the wished height. Successively, the SONAR is turned off in order to reduce the acoustic noise and the ADV operations start. In general, ADV sampling duration are carried out for 300 seconds (Sarkar and Dey, 2010) in order to obtain a time independent sample. However, due to operational constraints the velocity measurements were lasted only 60 seconds, with a sampling rate of 25 Hz. The vertical position of the ADV is derived from the sonar position either toward the sediment bottom (h) or toward the free surface (y), with a precision of about 0.5 cm vertically (Figure 13).

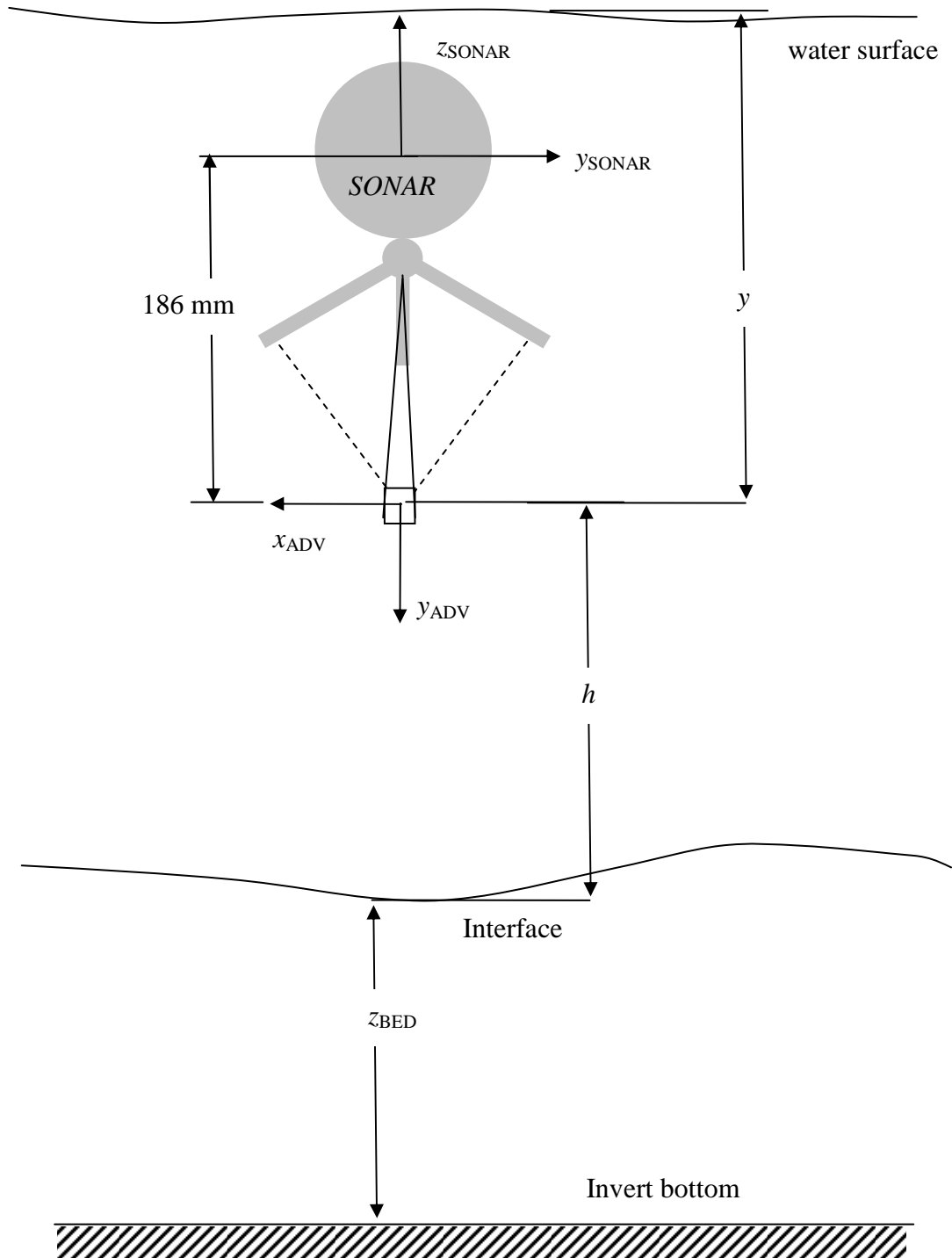


Figure 13 definition sketch of the ADV control volume position

The whole operation lasted about 15 minutes each measured vertical.

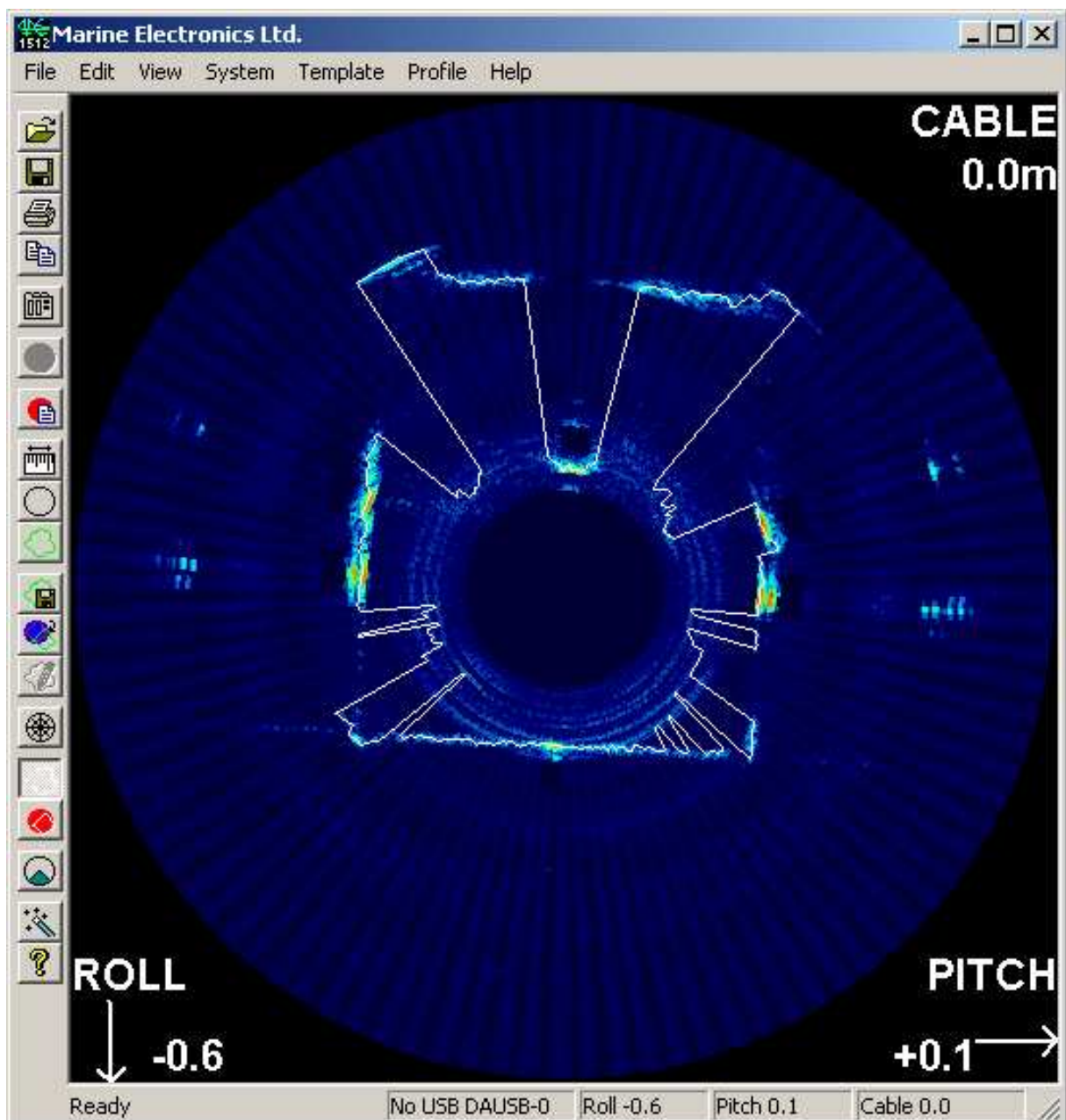
5.3 Data elaboration

Based on preliminary tests, observation and different literature approaches, scripts have been created using the software Matlab 7.1, in order to elaborate the data:

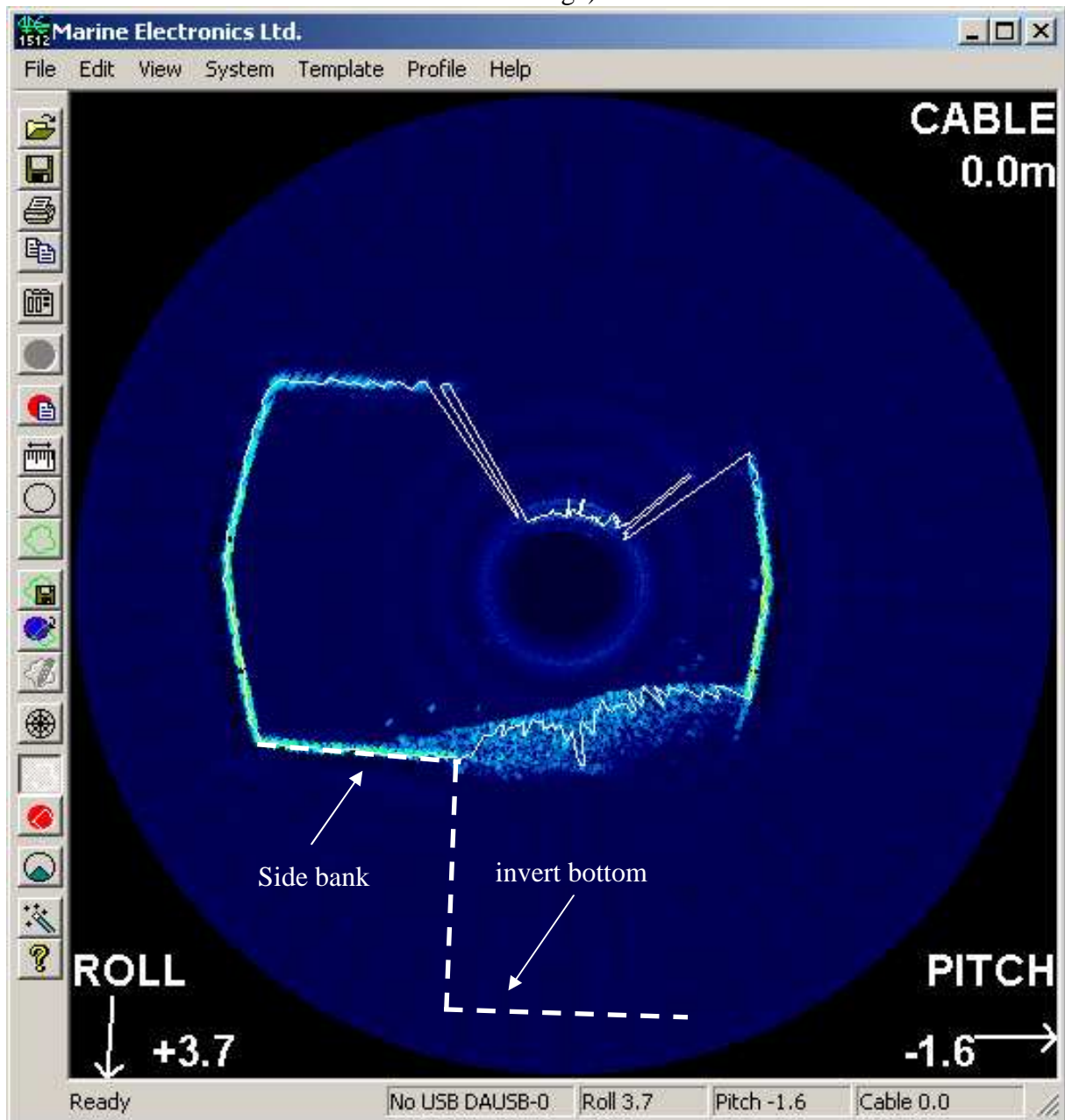
- “Profiler”
- “ADVDATAELABORATION”

5.3.1 Profiler.m

A first methodology to describe the characteristics of the deposits has been defined on the base of the survey realized with the sonar. Two different analysis can be done: a static morphological survey, in which the sonar is shifted over the rails to measure the spatial characteristics of the interface; and a temporal analysis of the morphological features, in which the sonar is left in the same section while the survey is done at different times. Accordingly, the acoustic interface can be defined as the distance from the probe where the backscatter signal shows the largest gradient. The algorithms developed by Marine Electronics shows a good correspondence with the observed geometry in laboratory conditions (see appendix and figure) and, more in general with compacted material (concrete, sand, Figure 14a) as represented by the white line in the image.



(a) SONAR output in laboratory condition using AREA1 detection algorithm (white line on the image)



(b) Example of in situ condition with soft sediment at the AE site (test AE-S9 x=-9.9 m); note that it is possible to observe the side bank underneath the soft sediment for thin sediment deposits.

Figure 14 Sonar output from laboratory experiences and insitu conditions.

However, the algorithm developed was not able to detect the interface of soft deposits (Figure 14b). Hence, it has been necessary to include the new algorithm elaborating the ".img" signal output. Knowing the structure of the file it has been possible to obtain:

- the pitch angle;
- the roll angle;
- the actual range;
- the amplitude signal for each cell.

A Gaussian filter of 5 mm of variance (equal to the instrumental variance) and of 10 cell of extension has been used for each beam.

$$f'(R) = f * g(R) = \int_{r=0}^{r=R} f(R) \cdot g(\zeta - R) dR \quad (16)$$

This digital filtration aims at removing the spikes in the original signal.

$$R_{\text{int}}^j = \max [f'(R^j)] \text{ for } 0 < j < 400 \quad (17)$$

in which j represents the j^{th} beam of 0.9° detected by the SONAR.

Figure 15 shows an example of the application of eq.18 on the row signal (the red dashed line). The row signal clearly shows its maximum value at $R=300$ mm, whilst eq.19 distinguishes the interface at around $R=255$ mm.

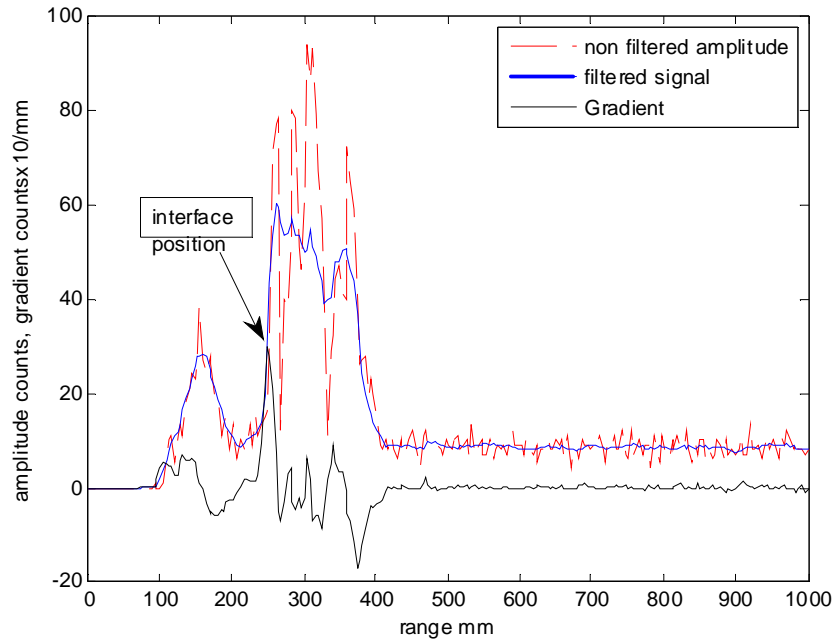
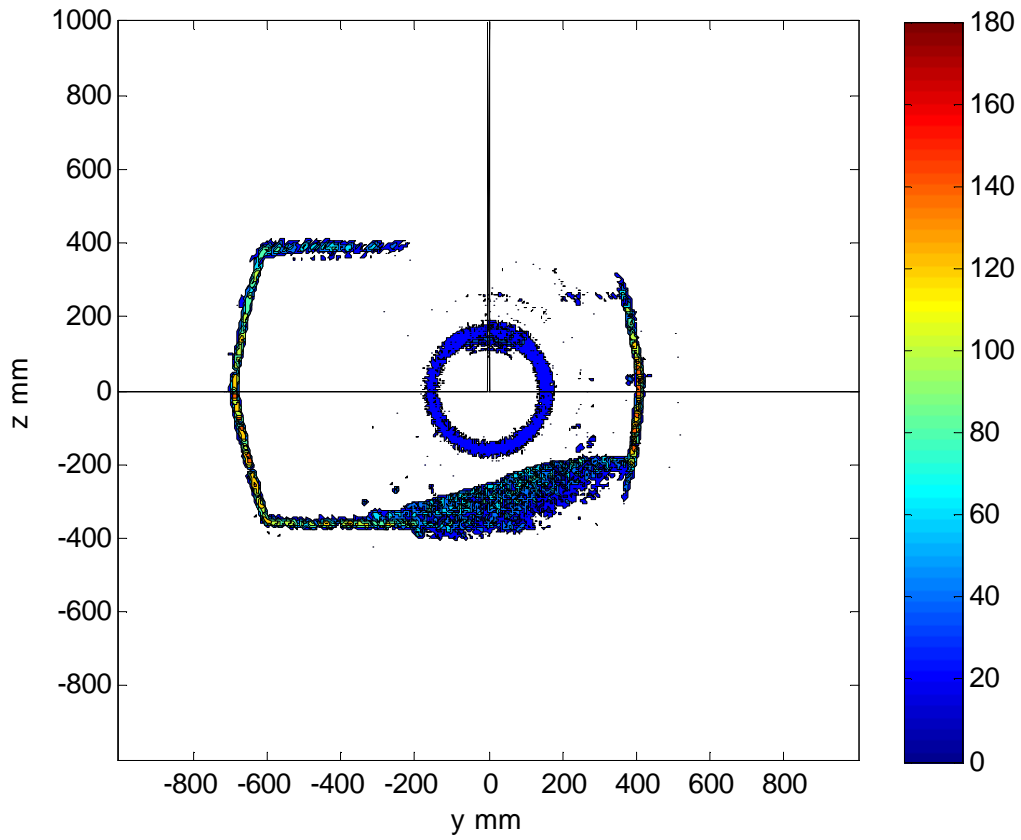
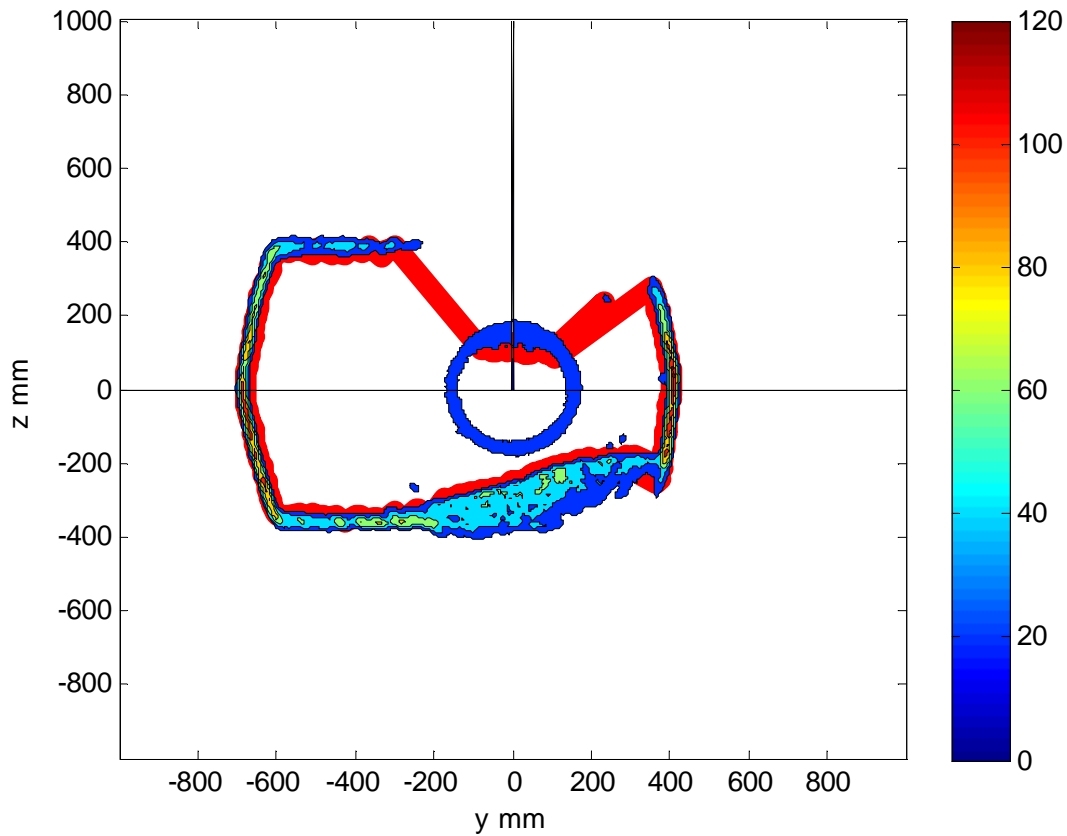


Figure 15 section $y=0$, corresponding to $\theta=180^\circ$ and $j=200$

The final result of the digital filtration is shown by the comparison of the two sonar output of Figure 16. The red line, hence, shows the interface contour detected by the eq. 19, which hence corresponds to the transition between the flow and the soft sediment deposits.



(a) sonar output before filtration (test AE-S9 x=-9.9 m)



(b) sonar output after filtration (test AE-S9 $x=-9.9$ m), the red line represents the interface detected by the new algorithm.

Figure 16 Sonar output before and after application of the filter

In order to quickly analyse the SONAR image, an automated script have been developed in MATLAB. The script has been developed in order to achieve the following tasks (Table 2):

Table 2 script tasks (see also the annexes for the script layout)

Task ID	What	NOTE
1	read both the txt file and img file from the folder	the name of the file must be either a distance in cm or a time in seconds ex. “-090.txt” corresponds to the section $x=090$ or $t=90$ seconds, according to the use the operator has done of the sonar
2	Automatic pitch and roll correction	This correction is based on the sonar pitch and roll output. On insitu conditions fine adjustment of the SONAR position might not be easily achieved
3	filter the data	This task will ask the operator to remove the bed points or validate the automatic filtration task.
4	Define the reference centre of the figure	In case of movement of the probe a new reference centre can be defined
5	Generate a 3D graph	This task will generate a 3D graph from the filtered data Output: - surfbottom.fig - clinebottom.fig - cnointbottom.fig
6	Generate the contour line surface referred to the average plane	In order to compare different survey, a regression plane is let pass trough the interface.
7	Create a section	This task will generate both longitudinal and transverse section of the surface Output: sectionxz(yz)XXmm.fig
8	Store the filtered data into an excel sheet or a txt sheet	the output file XYZ.xls is generated from the filtered data
9	Evaluate the statistical characteristics for each section and the height h of the ADV (when necessary) as output (bottom variable)	This task will give as output the average characteristics of each section in terms of wavelength, half height, position of the ADV toward the bottom (to use with ADV) Output: stats.fig

The following pictures shows an example of the manual filtering that can be done with the script, using the “max” algorithm. The filter is based on both manual and automated procedure. The manual procedure allows to the user to select the points to be eliminated using a rectangular box selection. The points included in the rectangular selection will be eliminated from the section. The automated procedure is based on a mobile median and standard deviation obtained from the z_{i-5} and z_{i+5} data, where z_i is the i -th point of the vertical component of the interface. Hence, the space of acceptable values is defined as the median value \pm the standard deviation obtained from the 10 points. If the value of z_i is outside the threshold is rejected, otherwise is retained. This procedure is done for all the points of the profile detected by the sonar. The algorithm is repeated until the differences between the n -step standard deviation and the $n-1$ -step is zero.

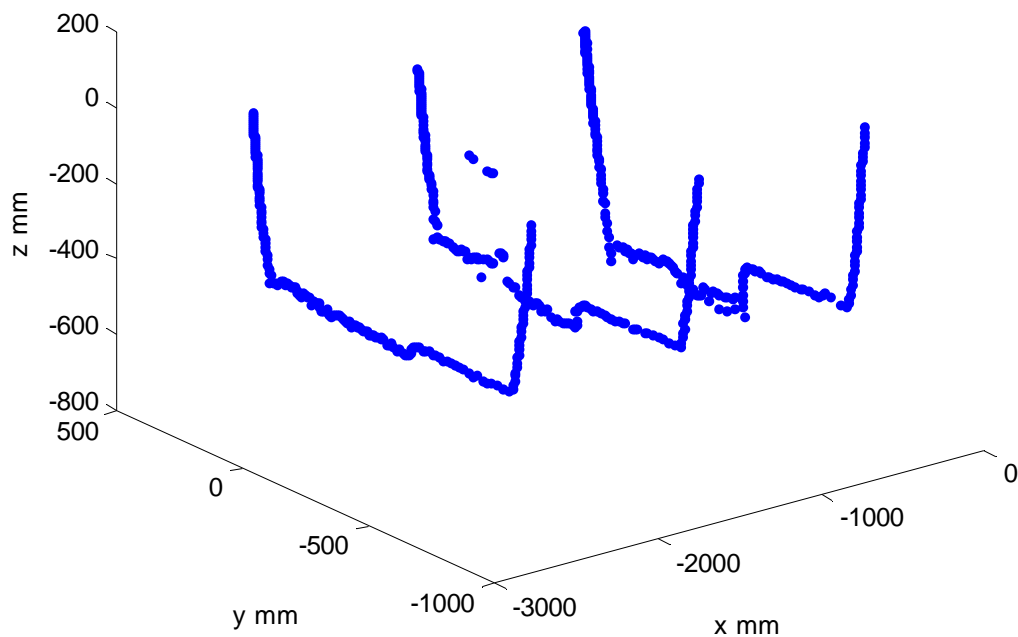


Figure 17 Matlab script example, data before filtration

In the Figure 18, the black points are the automatically filtered points, while the red one are the point which remains after the analysis. Some point might still be manually eliminated selecting it with the box tool provided in the script.

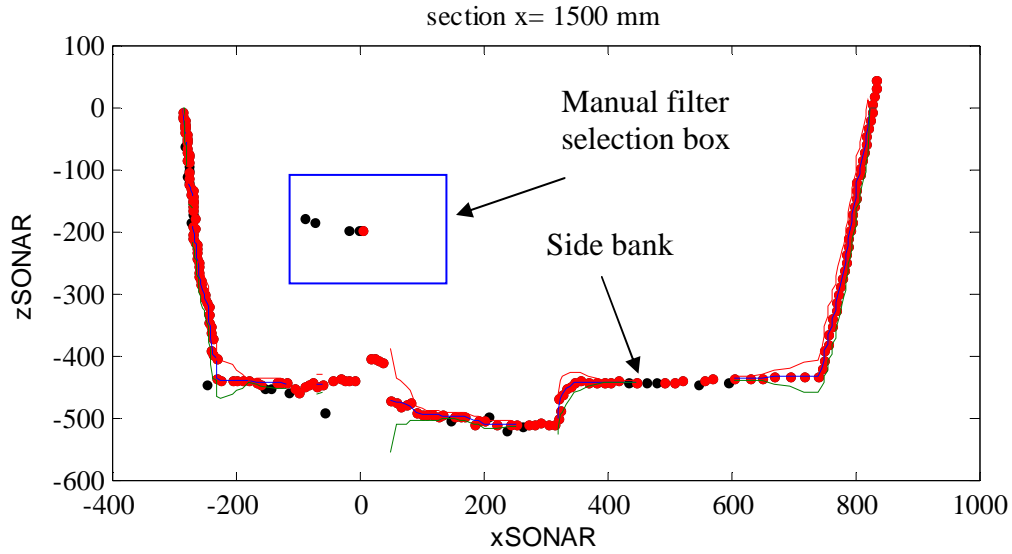


Figure 18 Matlab script example, data filter analysis, blue line represents the median, red and green line represents the confidence bound of width σ .

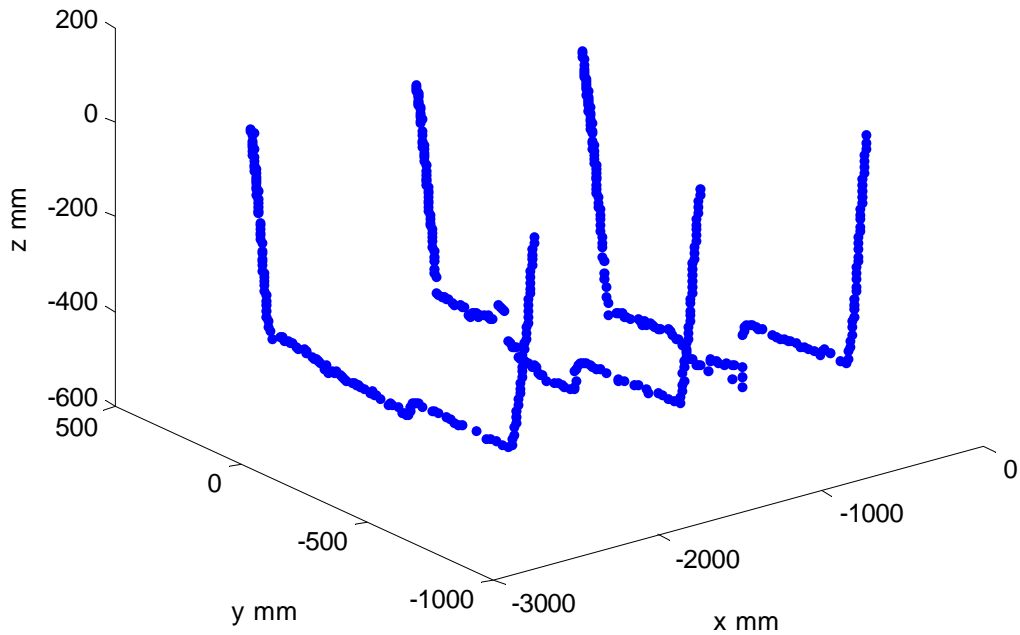


Figure 19 Matlab script example, data after filtration

Figure 20 shows the final results of the elaboration after data filtration. The figure has been obtained from one of the channel tests. The blue dots in the figure represent the row data after filtration, while the surface represents the interpolated surface using matlab.

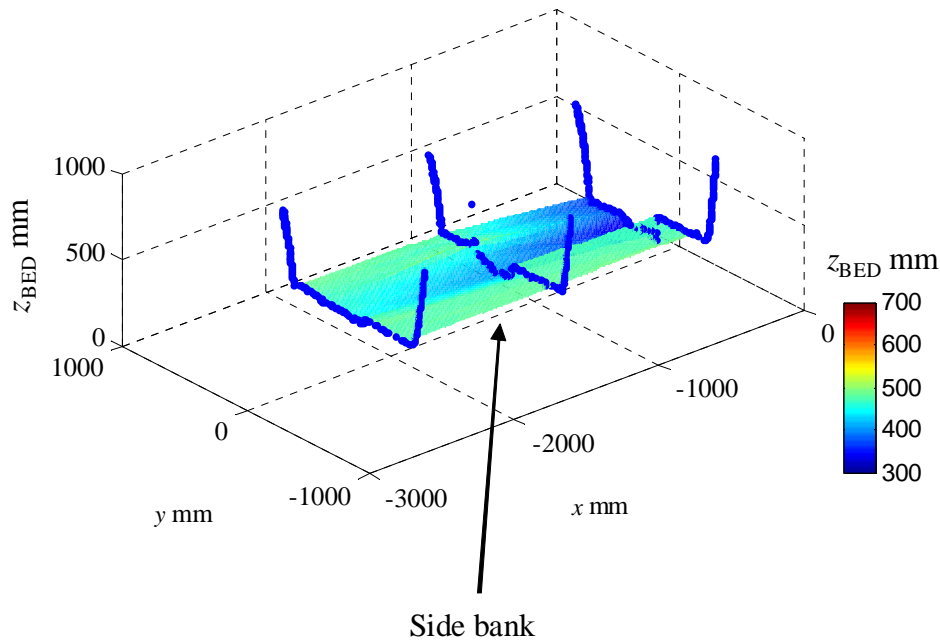


Figure 20 3D surface bottom surface generation after filter application; data have been displayed from the new reference system relative to the invert z_{BED} .

5.3.2 ADVDATAELABORATION.M

The ADV raw data are contained in the .adv file. This file can then be elaborated with the WinADV software. This software included several post processing tools which can be used to reduce the noise (generally referred to as spikes) from the measured velocity. Accordingly, a first criteria might be based on the analysis of the SNR and the correlations. Those should be greater than 15 db and 70% respectively. Hence, in first approximations, all the samples outside this range might be excluded from the data set. A second criteria is based on the phase space threshold algorithm introduced by (Goring and Nikora, 2002) and modified by (Wahl, 2003). This option is also available in the WinADV software. Hence, the software allows obtaining the time series of:

- the three instantaneous velocity components in the ADV reference system V_{x_0} , V_{y_0} and V_{z_0} , corresponding to \mathbf{u}_{ADV} , \mathbf{v}_{ADV} and \mathbf{w}_{ADV} ;
- the three SNR values for each beam $SNR0_0$, $SNR1_0$, $SNR2_0$ in [dB];
- the correlation values for each beam $COR0_0$, $COR1_0$, $COR2_0$ in [%];
- the signal amplitude for each beam $AMP0_0$, $AMP1_0$, $AMP2_0$ in [counts] (1 counts = 0.43 dB);
- the recorded temperature in [°C];
- and the values of SNR, correlation and amplitude averaged from the three beams

The suffix “_0” indicates the number of the probe, as the software allows for multiple probes elaborations.

Hence the WinADV software consisted in an output (.vu or .vf, i.e., unfiltered and filtered according to the previous criterion, SNR, correlation and space threshold).

The data are taken by the script from the vu or vf files, according to the choice of the operator. Applying the Reynolds decomposition for the 3D velocity field, i.e., $\mathbf{u}=\mathbf{u}+\mathbf{u}'$, $\mathbf{v}=\mathbf{v}+\mathbf{v}'$, $\mathbf{w}=\mathbf{w}+\mathbf{w}'$, for each point it is possible to define the first order or averaged components of the velocity on the three axes, u , v , w , the time series of the velocity fluctuation u' , v' , w' and the higher

momentum components, like variances $\langle u'^2 \rangle$, $\langle v'^2 \rangle$, $\langle w'^2 \rangle$, covariance, $\langle u'v' \rangle$, $\langle v'w' \rangle$, $\langle u'w' \rangle$, and the total kinetic energy $k_w = (\langle u'^2 \rangle + \langle v'^2 \rangle + \langle w'^2 \rangle) / 2$. Practically, the variance and the covariance have been calculated as:

$$\langle u_i' u_j' \rangle = \frac{1}{N} \sum_{t=1}^{t=N} (u_i' u_j')_t \quad (18)$$

in which $i, j = 1, 2, 3$ corresponding to x, y and z direction respectively, and N is the number of sample for each series).

It is worth observing that the ADV signal and the turbulence characteristics which can be deduced from the ADV measurements are biased by scattered noise in presence of suspended solids, and calculated shear stress or shear velocity from ADV data should be considered with care (Kim, Friedrichs, Maa and Wright, 2000).

The ADV is connected to the SONAR and, hence, have the same orientation of the sonar, which generally does not correspond with that of the flow. Hence it is necessary to transform the component of the flow velocity from the rotated reference system to the new one. Since the sonar profiler measures with an accuracy of 1 degree both the tilt and the rolling angles, a correction for the wrong ADV orientation has been made based on first correcting the rotation and successively the tilting angle based on the following application:

$$\begin{bmatrix} u_{SONAR(rot)} \\ v_{SONAR(rot)} \\ w_{SONAR(rot)} \end{bmatrix} = \begin{bmatrix} \cos(-\alpha) & -\sin(-\alpha) & 0 \\ \sin(-\alpha) & \cos(-\alpha) & 0 \\ 0 & 0 & 1 \end{bmatrix} \begin{bmatrix} u_{SONAR} \\ v_{SONAR} \\ w_{SONAR} \end{bmatrix} \quad (19)$$

$$\begin{bmatrix} u_{SONAR(tilt)} \\ v_{SONAR(tilt)} \\ w_{SONAR(tilt)} \end{bmatrix} = \begin{bmatrix} 1 & 0 & 0 \\ 0 & \cos(-\beta) & -\sin(-\beta) \\ 0 & \sin(-\beta) & \cos(-\beta) \end{bmatrix} \begin{bmatrix} u_{SONAR(rot)} \\ v_{SONAR(rot)} \\ w_{SONAR(rot)} \end{bmatrix} \quad (20)$$

where α and β are the roll and the tilt angle registered by the sonar respectively (Figure 9), positive if CW (clockwise) oriented toward the SONAR axis. Successively, the ADV axis have been reoriented in order to provide more readable velocities, i.e., rotating the ADV axis on the SONAR axis, and thus with the u directed toward the flow and w vertically. An extract of the output generated by the script is shown in Table 3, in which the height corresponds to the height h from the interface at which the velocity has been measured.

Table 3 ADVDATAELABORATION output

height mm	"Vx_0"	"Vy_0"	"Vz_0"	"COR0_0"	"COR1_0"	"COR2_0"	"SNR0_0"	"SNR1_0"	"SNR2_0"	"AMPO_0"
65	0.92	0	20.39	97	97	95	35.7	35.3	38.7	125
62	1.225	0.03	20.28	96	96	94	33.5	33.5	37	120
58	0.43	0.4	20.425	96	96	95	31.8	31.4	35.7	116
52	0.93	0.11	19.94	96	96	94	31	30.1	34.4	114
44	1.17	0.28	19.92	96	95	94	32.3	29.7	34	116
34	0.21	0.365	18.775	95	94	93	28.8	26.7	31	109
24	0.23	0.35	17.56	94	92	93	27.5	24.9	30.1	106
18	0.17	0.25	11.925	95	95	88	34	35.7	34.8	121
14	0.035	0.02	6.17	97	98	88	49.9	55.5	53.8	158
12	0	-0.02	0.13	98	98	98	58.9	60.6	62.3	179

continued

height mm	"SNRAvg_0"	"AmpAvg_0"	"Pressure_0"	"Temperature_0"	u' 2 cm2/s2	v' 2 cm2/s2	w' 2 cm2/s2	<u'v'> cm2/s2	<u'w'> cm2/s2	<v'w'> cm2/s2
65	36.5	127	0	16.04	1.89	1.09	2.20	0.19	-0.24	0.72
62	34.7	122.33	0	16.06	2.32	1.58	2.80	0.36	-0.04	0.94
58	33	118.67	0	16.06	1.93	1.20	2.61	0.11	-0.11	0.89
52	32	116.33	0	16.09	2.01	0.94	3.12	0.34	0.05	0.90
44	32	115.67	0	16.11	2.46	0.94	2.96	0.56	0.17	0.72
34	28.8	109	0	16.13	3.00	0.97	3.73	0.29	0.35	0.60
24	27.5	106	0	16.13	2.45	0.95	5.10	0.49	0.15	0.40
18	34.7	122.67	0	16.15	1.57	0.50	16.05	0.44	-0.02	-1.10
14	53.2	165.67	0	16.17	0.68	0.26	38.49	0.35	-0.03	-1.83
12	60.8	183.33	0	16.19	0.47	0.23	75.96	0.49	-0.03	-2.54

The ADVDATAELABORATION script also allows for the quadrant analysis of the data (according to (Nezu and Nakagawa, 1993)). Hence, each u' and w' couple of the velocity measurements is subdivided in quadrant according to their signs and associated to a different event typology.

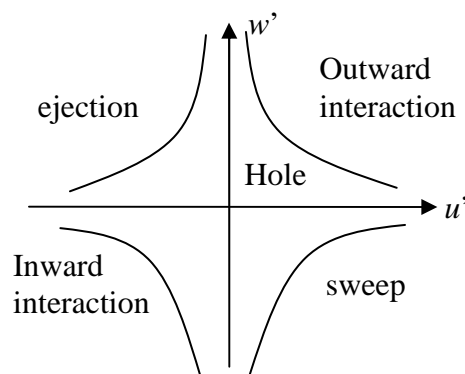


Figure 21 quadrant analysis classification

Moreover, the software also evaluate the contribution of single events $S_{i,H}$, in which i is the i th quadrant and H is the hole size, according to the following equation (Sarkar and Dey, 2010):

$$\langle u'w' \rangle_{i,H} = \lim_{T \rightarrow \infty} 1/T \int_0^T u'(t)v'(t)\lambda_{i,H}(h,t) \quad (21)$$

and

$$S_{i,H} = \langle u'w' \rangle_{i,H} / \langle u'w' \rangle \quad (22)$$

were $\lambda_{i,H}=1$ if the couple u',w' are in the i th quadrant and $|u'w'| > H[(u'^2)^{0.5}(w'^2)^{0.5}]$.

However, in order to accelerate the data elaboration process this last graph is not regularly plotted by the script, but it can be added in any moment for specific data analysis.

Finally, according to (Ha, Hsu, Maa, Shao and Holland, 2009), a correlation between acoustic impedance and bulk density exist in cohesive sediments when the sound velocity inside these latter equals that of the water. Bulk density is defined as $\rho_b = M_s/V_t + \rho_w (1 - \phi_s) = \rho_w + \phi_s (\rho_s - \rho_w)$. Assuming a uniform spherical sand of $\rho_s=2650 \text{ kg/m}^3$ and of fraction of sediments on the total volume of $\phi_s=0.65$, $\rho_b= 2072.5 \text{ kg/m}^3$.

6 RESULTS

6.1 Introduction to results

Before installing the sonar on in-situ conditions, several parameters have been tested, in order to assess the sonar precision and accuracy on the measure. A summary of the different variables and materials tested to reproduce in situ conditions is presented in the annexes.

Each survey will be separated in order to frame the results in terms of total suspended solid (TSS) concentration measured for each survey, particle size distribution characteristics of the solids, velocity measurements, morphological measurements, and temporal evolution measurements. The results will be compared and further discussed in terms of flow characteristics, morphologies and temporal evolution.

6.2 Duchesse Anne (DA) tests

6.2.1 Morphological characteristics Test DA-S1 (2010-10-20)

The first test has been, hence, carried out at the DA site, in which a temporary support, slightly different from that presented in chapter 2, has been used.

During the experiences a water depth of about $\delta=0.41$ m from the sediment interface has been measured with the gauge (Figure 23), while a sediment thickness z_{sed} equal to 0.1 m has been gauged at around 9:00 am. Sediment concentrations in terms of TSS and VSS (volatile suspended solids) for two different sieve sizes (0.125 mm and 2 mm) are shown in Figure 22a, while Figure 22b shows the sediment bottom particle size distribution, in which D is the diameter for which the percent P in weight of sediment is finer. The particle size distribution has been evaluated manually sieving the fraction $D>0.560$ mm and by a laser granulometer for the fraction $D<0.560$ mm.

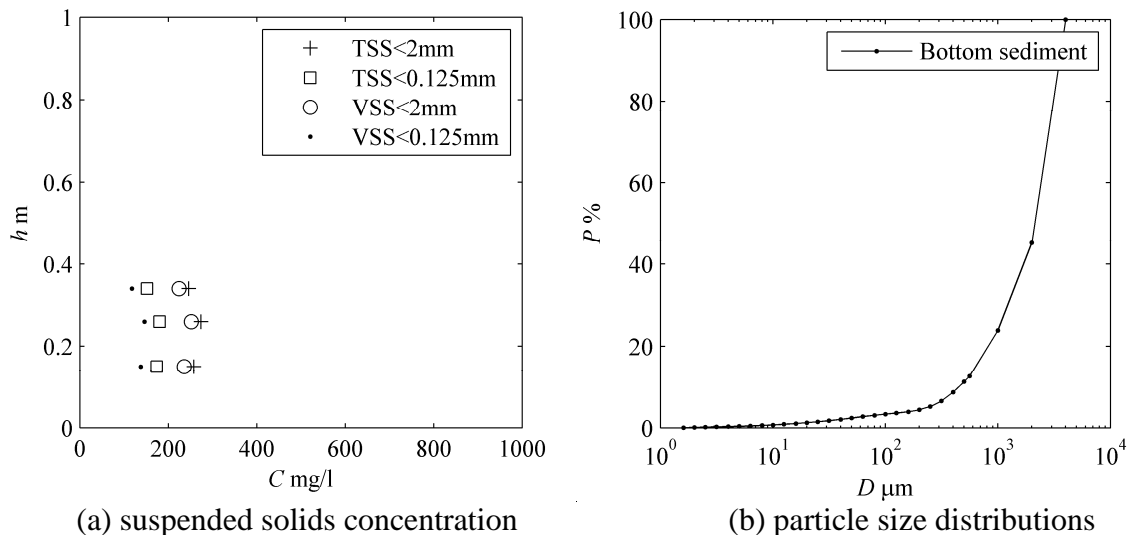
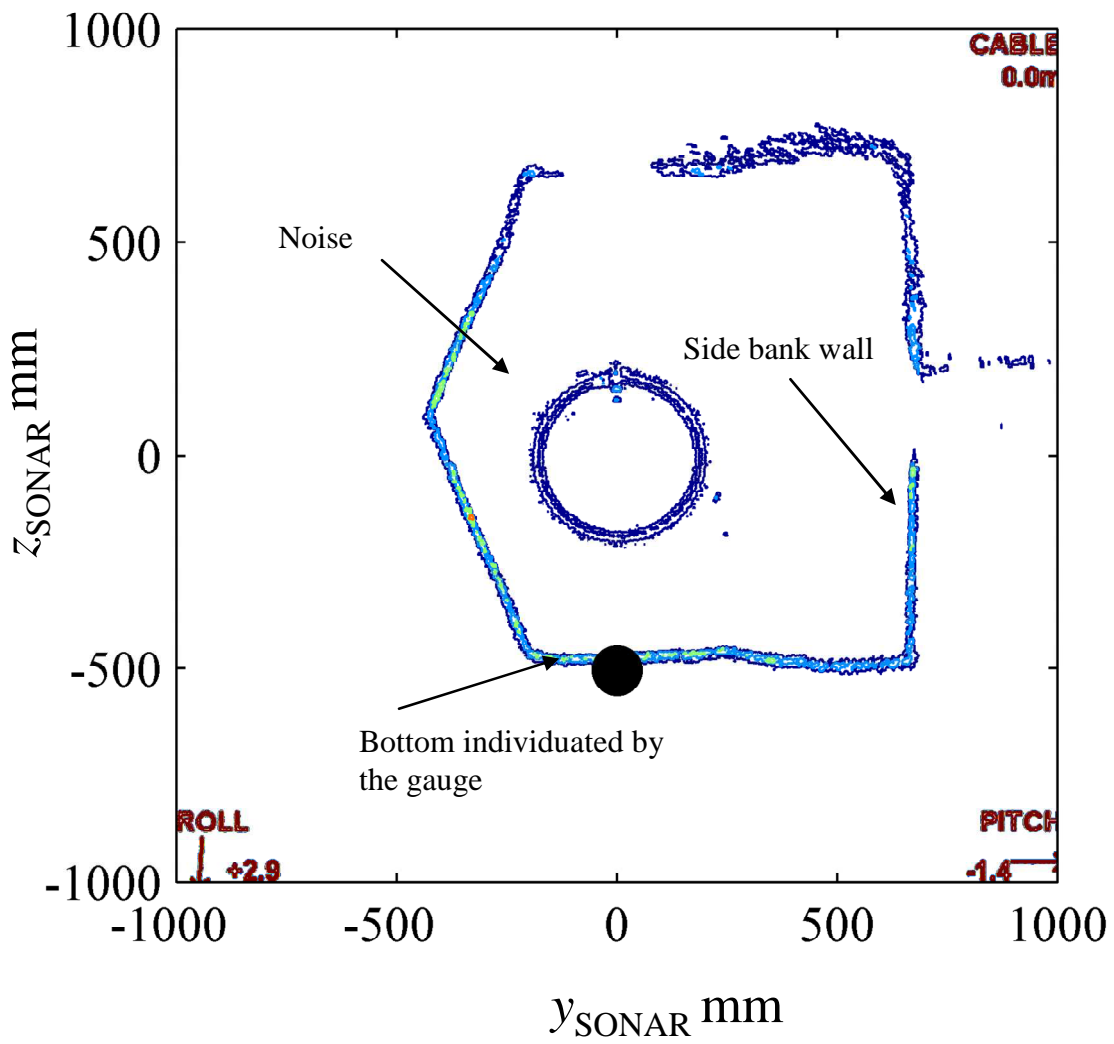


Figure 22 Test DA-S1 in situ suspended solids concentrations and particle size distributions

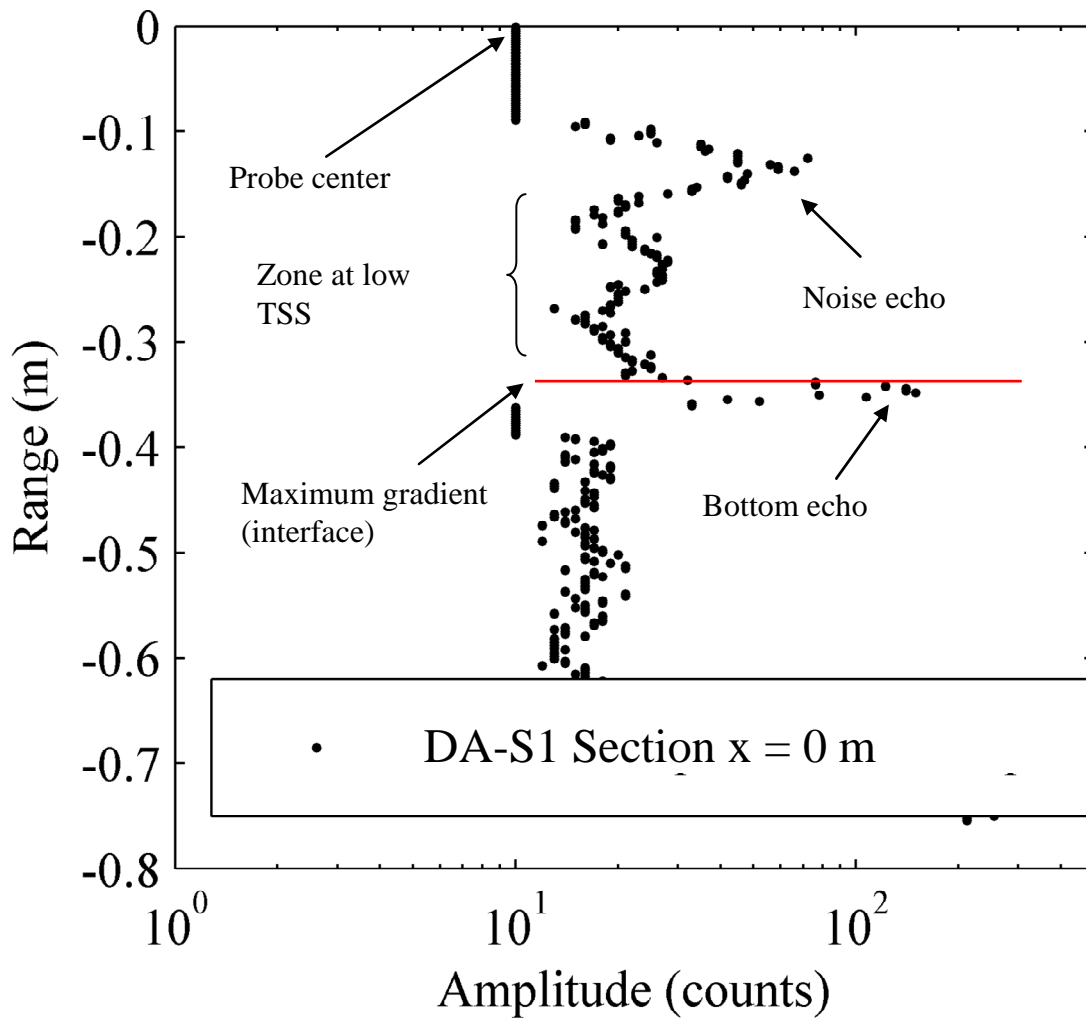
TSS and VSS concentration show a rather constant distribution, with a maximum concentration of $C_{TSS2}=270$ mg/l (total suspended solids inferior of 2 mm, subscript 'TSS2').

Altogether, the fraction of VSS for the same sieve size shows rather high values of about 92%.

The SONAR rotating head has been stream wise oriented so that a transverse image of the sewer trunk can be collected (Figure 23). The figure shows the backscatter contour lines obtained from the SONAR image. The image has been obtained with a pulse length of 4 μ s and a range of 750 mm. According to the 8-bit backscatter amplitude, the larger the backscattered signal is, the larger the amplitude registered by the SONAR is. The image clearly shows the lateral walls of the trunk, of which one is the bank vertical wall. Accordingly, since the sonar was immersed deeper if compared to the bank surface, it has not been possible to directly measure the side bank. The change in the sidewall shape ($y < 0$) is due to the water surface, which acted like a mirror and symmetrically reflected the sidewall. At the right hand side, above the line of the image reflection, it is possible to infer the presence of the lateral bank surface. From this image it has been possible to obtain a 8-bit backscattered vertical profile from the centre of the probe (Figure 23b). In the plot, the range has been fixed at the centre of the probe. The centre of the probe relates to the probe dead zone, which is automatically filtered by the software and automatically set to 0. The first peak observed at about 15 cm from the centre related to a noise detected by the probe and not filtered. Downward, the backscatter shows an almost constant value of about 20 counts. When the signal approaches the sediment bottom, the signal amplitude drops at about 181 counts and then reduced due to the presence of sediment bottom, showing a marked peak at the zone where the sediment have been detected by the gauge. The image clearly shows that the sediment bottom is not perfectly flat, most likely connected to secondary current which could modify the shear stress and the sediment accumulation. In particular, it seems that the larger deposits are present near the left sidewall, while at the bank wall, less sediment seems to accumulate. According to gauge measurement, an average $z_{SED} = 10$ cm of sediment has been detected, for a total water depth of $\delta = 41$ cm. SONAR measurement shows $\delta_{SONAR} = 44$ cm and a distance between the average sediment plane and the bank of about 32 cm, while the total bank wall height was 45 cm, therefore showing a sediment depth of $z_{SED} = 12$ cm which seems reasonable, owing the numerous inaccuracies which may occur during gauging operations (the gauge doesn't reach the bottom, the gauge sinks too much in the sediment, the sediment morphology is not constant). Hence it can be inferred that slight difference of the order of 20% occurred, therefore showing satisfactorily results for SONAR measurements.



(a) DA-S1 sonar output referred to the SONAR centre contour lines with gauge measurement (●)



(b) 8 bit signal amplitude at $y=0$ cm, section 12 m upstream the bend.
Figure 23 Test DA- S1 output

6.2.2 Morphological characteristics Test DA-S5 (2011-05-11)

Figure 24 shows the suspended solid conditions and particle size distribution which were observed during the test. Average longitudinal flow velocities measured with a PVMPD are summarized in Table 4.

Table 4 Flow velocity recorded before the morphological survey at the section $x=0$ m

Time	y_{probe}	h	u	z_{BED}	δ
hours	m	m	m/s	m	m
8:00	0.10	0.34	0.41	0.02	0.44
8:00	0.25	0.19	0.46	0.02	0.44

The water depth at the moment of the flow measurement was about $\delta=0.58$ m from the sediment interface, and y_{probe} is the distance between the probe and the free surface.

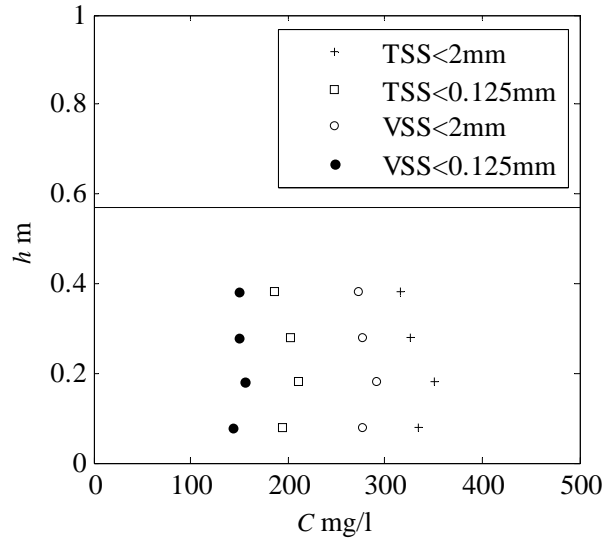
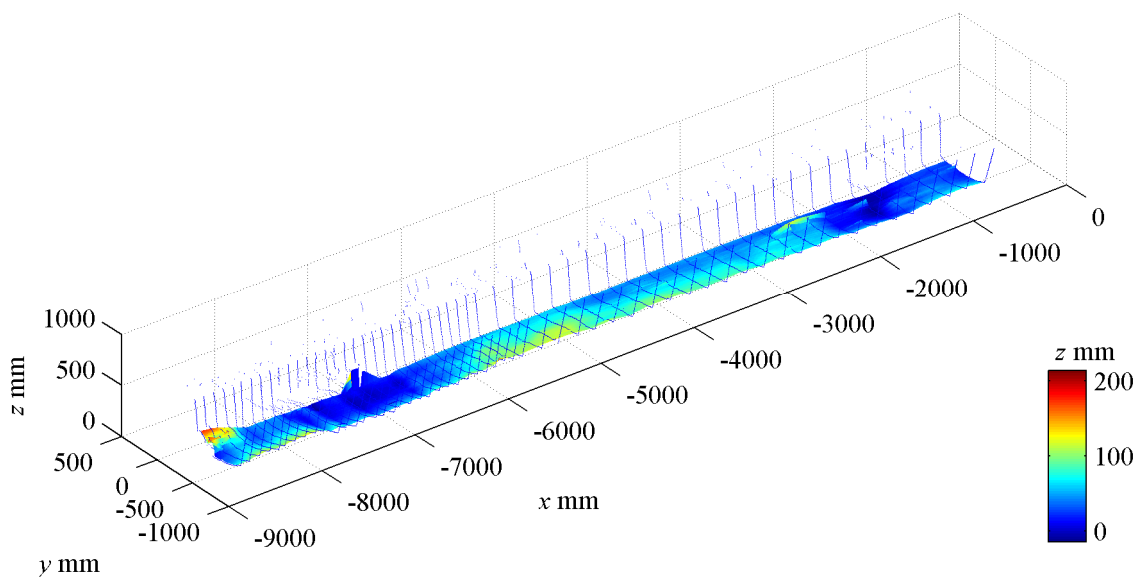


Figure 24 Suspended solids concentration test DA-S5 with the free surface (solid line)

A survey of the morphological characteristics of the sediment bottom at the DA has been carried out with a longitudinal resolution of 20 cm for about 9 m from the rail end ($x=0\text{m}$, positive toward the flow direction). The morphological survey first highlights the presence of a thin sediment deposit, as shows in Figure 25. The figure also highlights the presence of the side bank, which is almost clear of deposit. Although the thickness of the deposit is rather reduced, some important features can be observed. Generally the shape of the deposits is not flat, whit average wave height of 50 mm and wavelength of 1000-1200 mm (Figure 25). A zone of larger sediment deposits is individuated near the side bank at $x= -8500\text{mm}$, whilst this feature is no longer observed along the whole invert. The sediment deposit observed at $x= -7000\text{mm}$ is actually a hole under the side bank which has been used to gauge the trunk. In general, sediment deposits shows a rather three-dimensional pattern, most likely consequence of the strong three dimensional flow field typical of sewer (Larrarte, 2006), also observed from the previous velocity measurements.



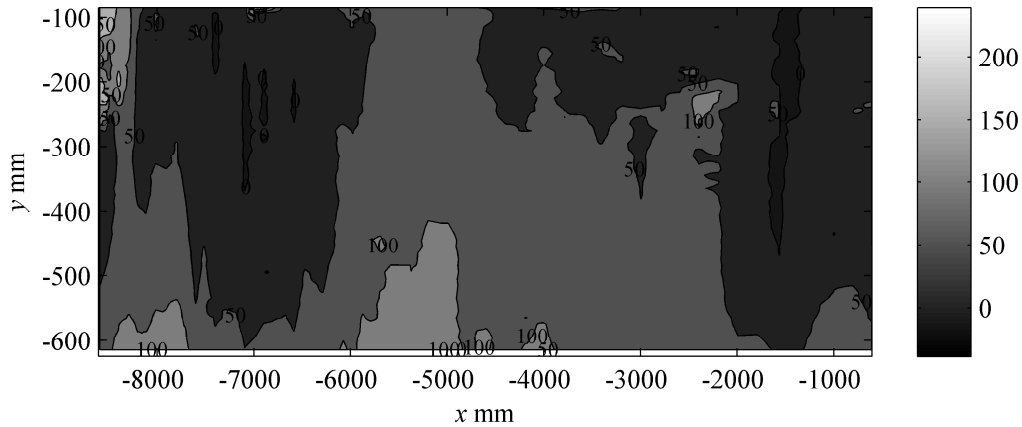


Figure 25 DA-S5 sediment morphology measured with the sonar, flow from left, the scale represents the z_{BED} elevation in mm.

In order to analyze the bed morphology, an average plane has been defined as $z_{average} = a + bx + cy$, in which a and b are the minimum squared error coefficients evaluated on the points z_{BED} obtained from the SONAR output. In the following, the data will be referred to this plane as z_{PLANE} , i.e., the vertical distance from the average plane $z_{BED} - z_{average}$. Figure 26 shows the results of this elaboration. Although the flow is generally three dimensional in narrow channel conditions [$b/\delta < 3$ where b is the width of the free surface at the height δ (van Rijn and Klaassen, 1981)] the sandy deposit shows a morphology referred to the average plane rather two dimensional.

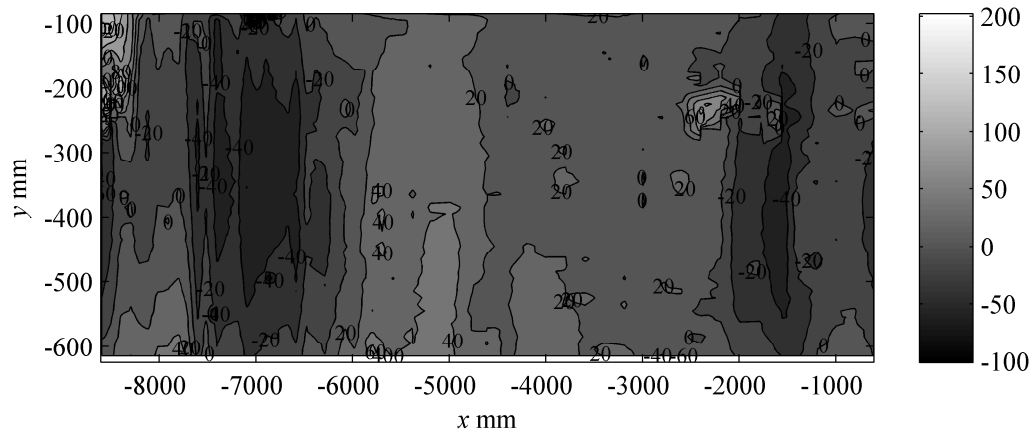


Figure 26 DA-S5 sediment morphology measured with the sonar from the average plane, flow from left, gray scale represents the z_{PLANE} elevation in mm.

The longitudinal profile (Figure 27) shows the centerline longitudinal sediment deposit profile from the invert bottom z_{BED} . The profile shows a maximum deposit wave height of about 100 mm. The deposit is also characterized by the presence of a first big trough, followed by a steep dune deposit. The downstream side of the dune shows a slope milder compared to upstream slope. The dune again ends in a trough that touches the invert bottom.

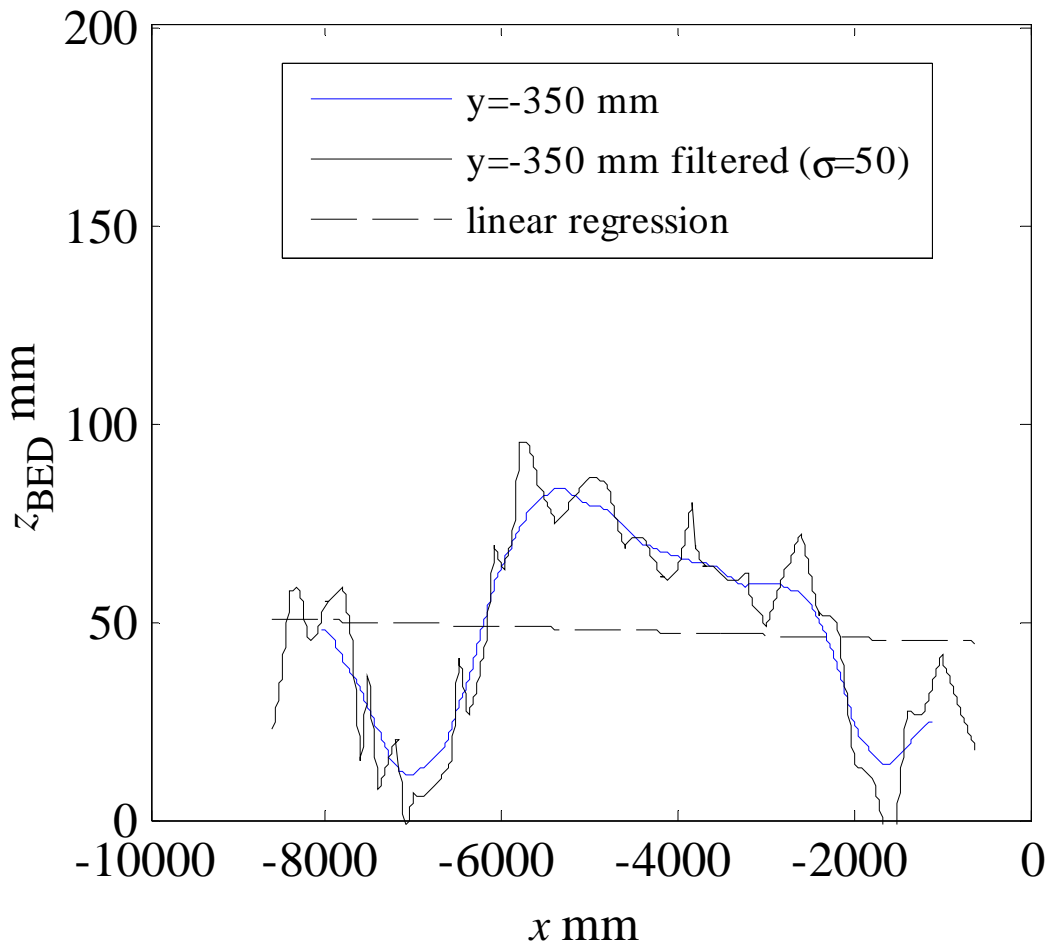


Figure 27 DA-S5 longitudinal profile for $y=0m$

The high velocity, observed in the experimental site, prevent from the accumulation of the mud layer over sand deposit, although reduced quantity of sediments accumulates during dry weather period over the invert Figure 28.

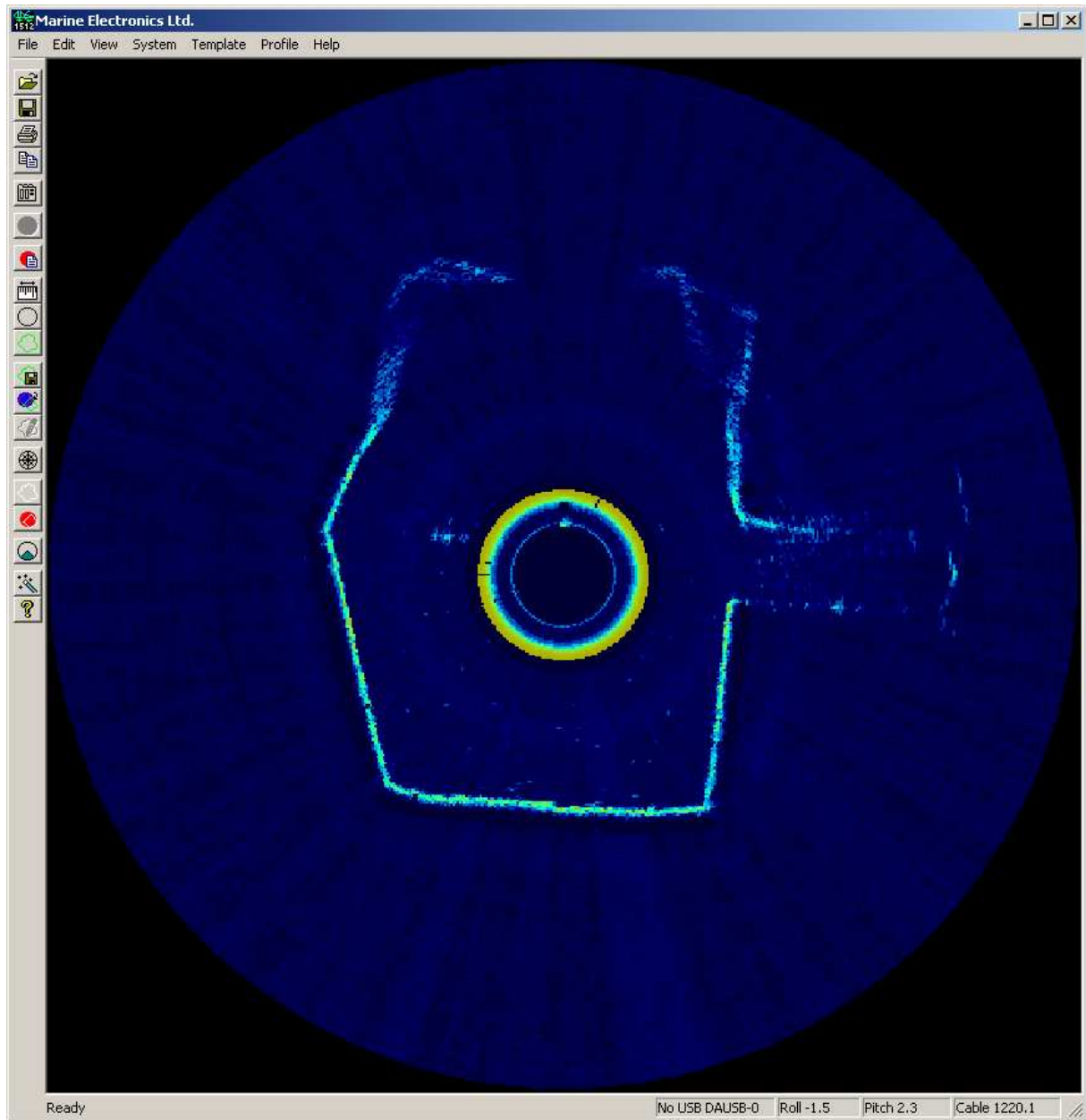
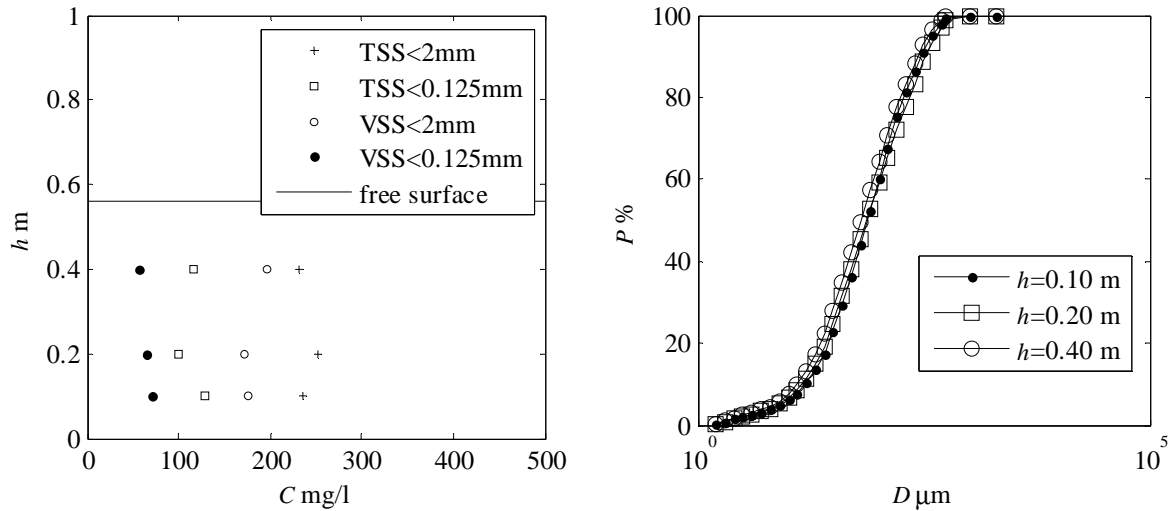


Figure 28 DA-S5 Sonar output at section $x=-3.20$ m

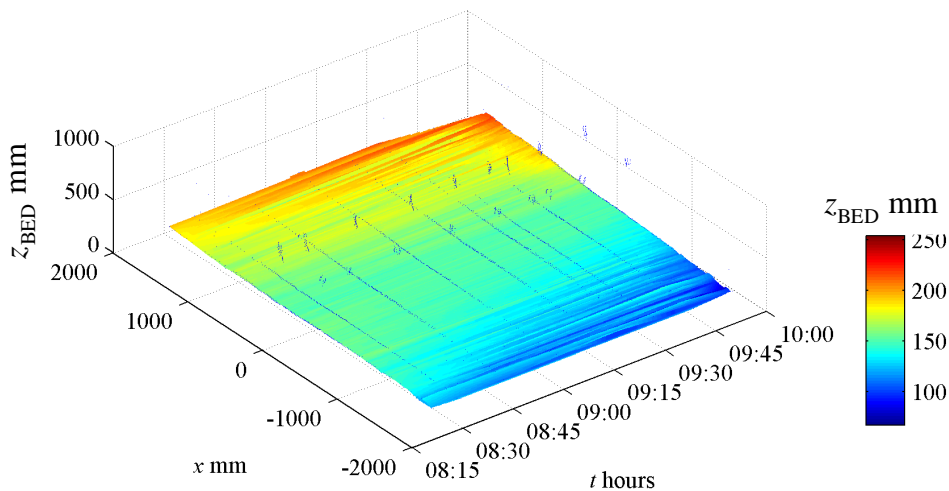
6.2.3 Temporal evolution Test DA-S4 (2011-05-11)

Figure 29 shows the measured suspended solids and particle size distribution. Both TSS and VSS shows almost constant values toward the vertical, as well as the particle size distribution shows similar diameters.

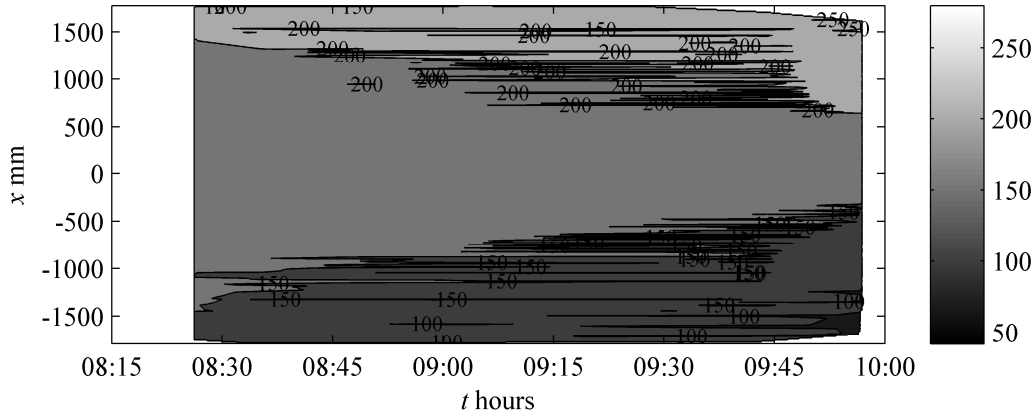


(a) suspended solids concentration (b) particle size distributions for $D < 0.56$ mm
 Figure 29 Test DA-S4 in situ suspended solids concentrations and particle size distributions

Although the survey has been carried out only between 8:15 and 10:00 am, it is possible to observe that the sediments are generally moved from downstream to upstream. Indeed, the contour line at $z_{\text{BED}}=150$ mm advances downstream, whilst that at $z_{\text{BED}} 200$ mm (Figure 30), tends toward the downstream direction, thus indicating that the sediment eroded downstream are accumulated on the upstream dune.



(a) surface output with surveyed section, height from the bottom invert



(b) contour line plot, height from the bottom invert z_{BED} mm.

Figure 30 Sediment interface temporal evolution detected for tests DA-S4

6.2.4 Flow filed Test DA-S2 (2011-01-21)

Measured total suspended solids and volatile suspended solid presented on Figure 31 show slight differences toward the vertical, whilst particle size distributions shows increasing average size toward the vertical. The bottom sediments (B. S.) have an average diameter of $D_{50}=1.2$ mm and a density of 2621 kg/m³, which well falls into the sand sediment category.

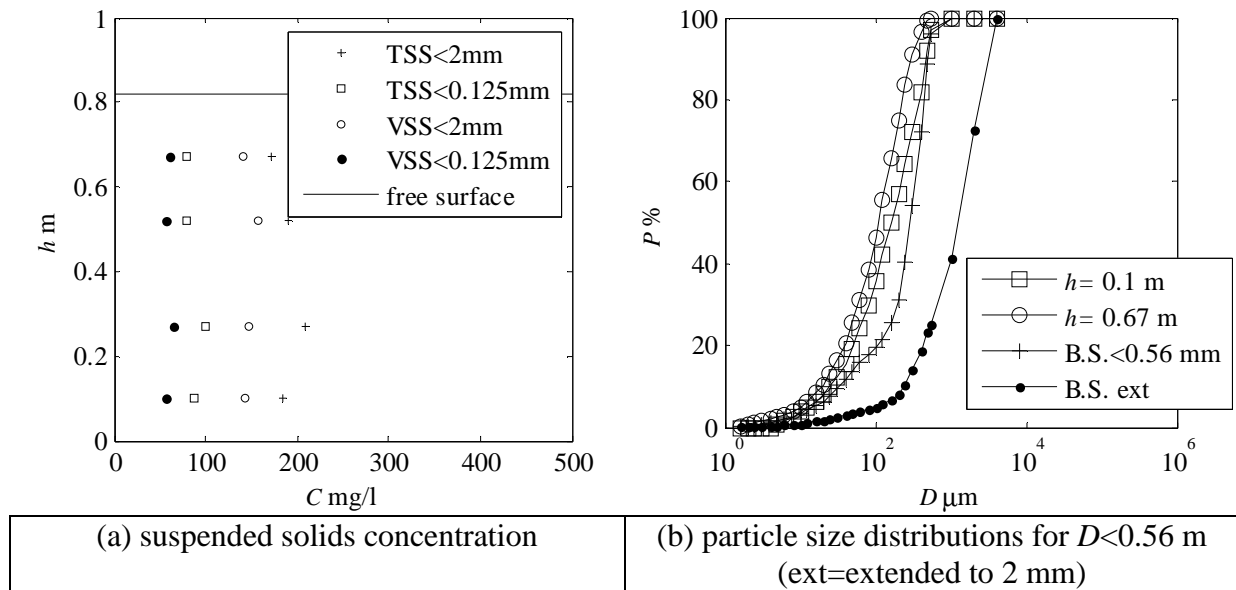


Figure 31 Test DA-S2 in situ suspended solids concentrations and particle size distributions

Figure 32 and Figure 33 shows the bottom profile observed at the section $x=-0.5$ m of the DA site and $x=-1.9$ m, in which it is possible to observe a relatively low level of sediment over the invert. According to the vertical section in Figure 32 and Figure 33, the acoustic backscatter of the bottom sediment shows high ABS values, comparable to the ABS of the concrete walls, suggesting the presence of a harder and compacted layer. The transition between the flow and the sediment is also much more sharpened compared to that observed in presence of a sheet flow. Transverse ripples shows at the $x=-0.5$ m have a wave height of about 1.6 cm, whilst they present a length wave (distance between crests) of about 44 mm.

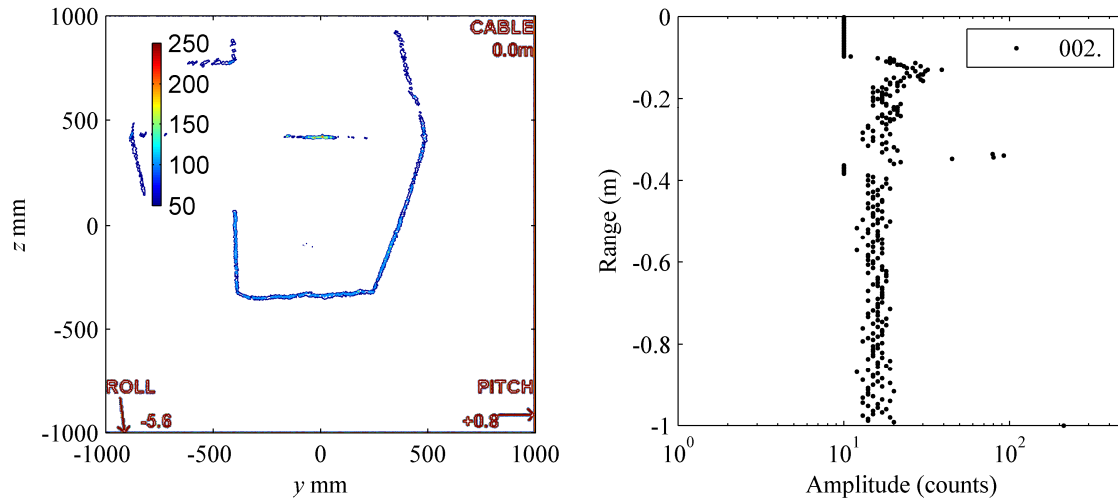


Figure 32 (a) DA-S2 transverse profile at $x=-0.5$ m, and (b) amplitude profile at $y=0$ m

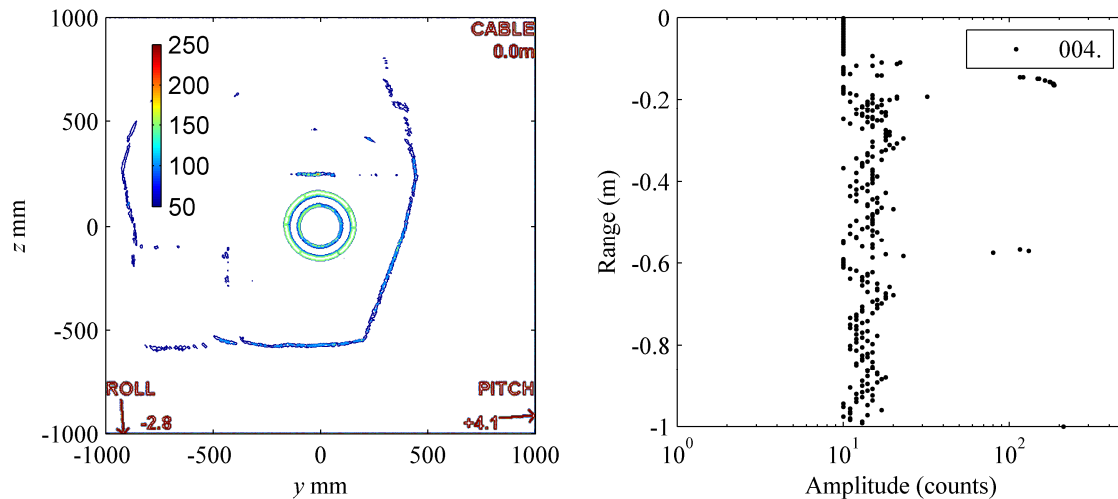


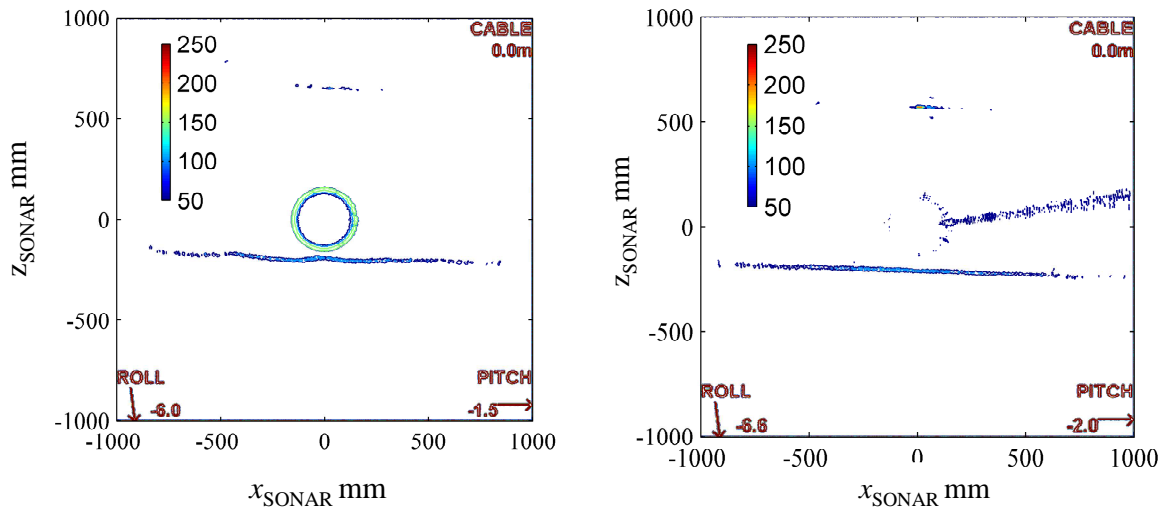
Figure 33 (a) DA-S2 transverse profile at $x=-1.9$ m, and (b) amplitude profile at $y=0$ m

The longitudinal profile of the bottom sediments (Figure 34a and Figure 35a) at $x=-1.9$ m clearly shows the presence of longitudinal dunes over the concrete bottom. This time the bed forms show length larger than that observed transversally, with wave length of about 50 mm and wave height of about 377 cm¹. The small pattern observed over the dunes is most likely connected to detection algorithm errors rather than connected to the presence of ripples over the dunes². Differently, the bed forms at section $x=-0.5$ (Figure 34b and Figure 35b) shows a flatter bottom, over which small features can be detected (about 32 mm of wave height and 60

¹ Note that the bed form pattern have been evaluated trough a regression line and not toward others methodology based on data filtration of larger and smaller patterns (such as after low pass and long pass filtration) or on different shapes.

² It would be probably better to filter the data from the profile small features of less than 5 mm as the maximum sonar resolution with the pulse length of 4 μ s is of about 5 mm.

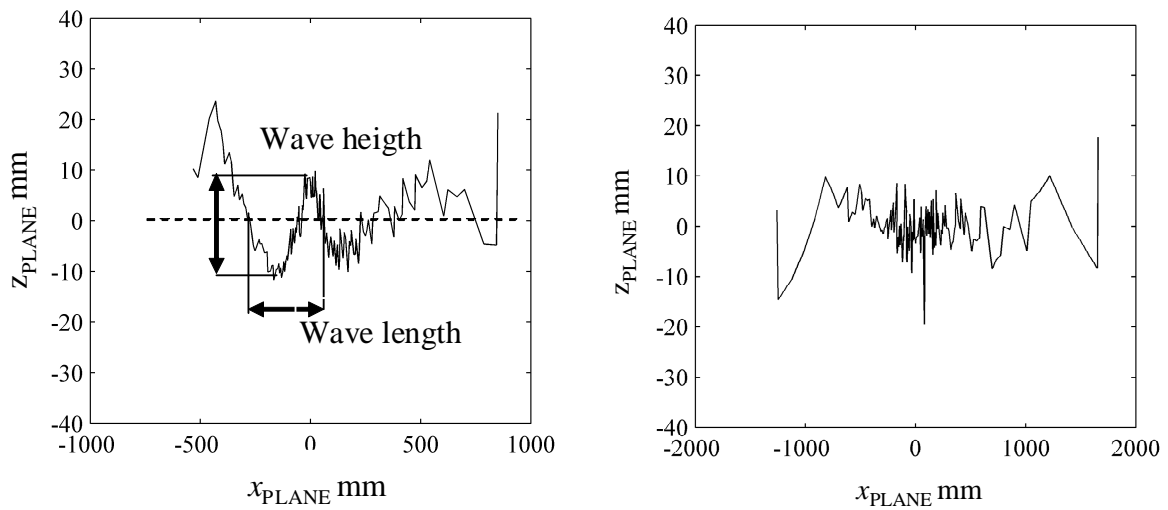
cm of length). In the plot, the data have been referred toward the regression line interpolating the points detect by the probe.



(a) bed-form observed at $x=-1.9$ m, flow from the left.

(b) bed-forms observed at $x=-0.5$ m, flow from the left.

Figure 34 Longitudinal survey referred from the channel sonar centre



(a) bed-form observed at $x=-1.9$ m, flow from the left.

(b) longitudinal bed-form observed at $x=-0.5$ m, flow from the left.

Figure 35 centreline longitudinal profiles from the interpolating plane z_{PLANE}

Velocity profiles at section 1 ($x=-0.5$ m)

The velocity profiles referred toward the sediment bottom (Figure 36) shows a maximum longitudinal velocity of about 40 cm/s. The u velocity profile shows the typical pattern of a fully developed turbulence, while the secondary flows components (v and w) shows important magnitudes due to the presence of secondary flows. Correlation profiles shows values a general reduction of the quality signal toward the vertical, due to the probe clogging which continuously needed to be cleaned.

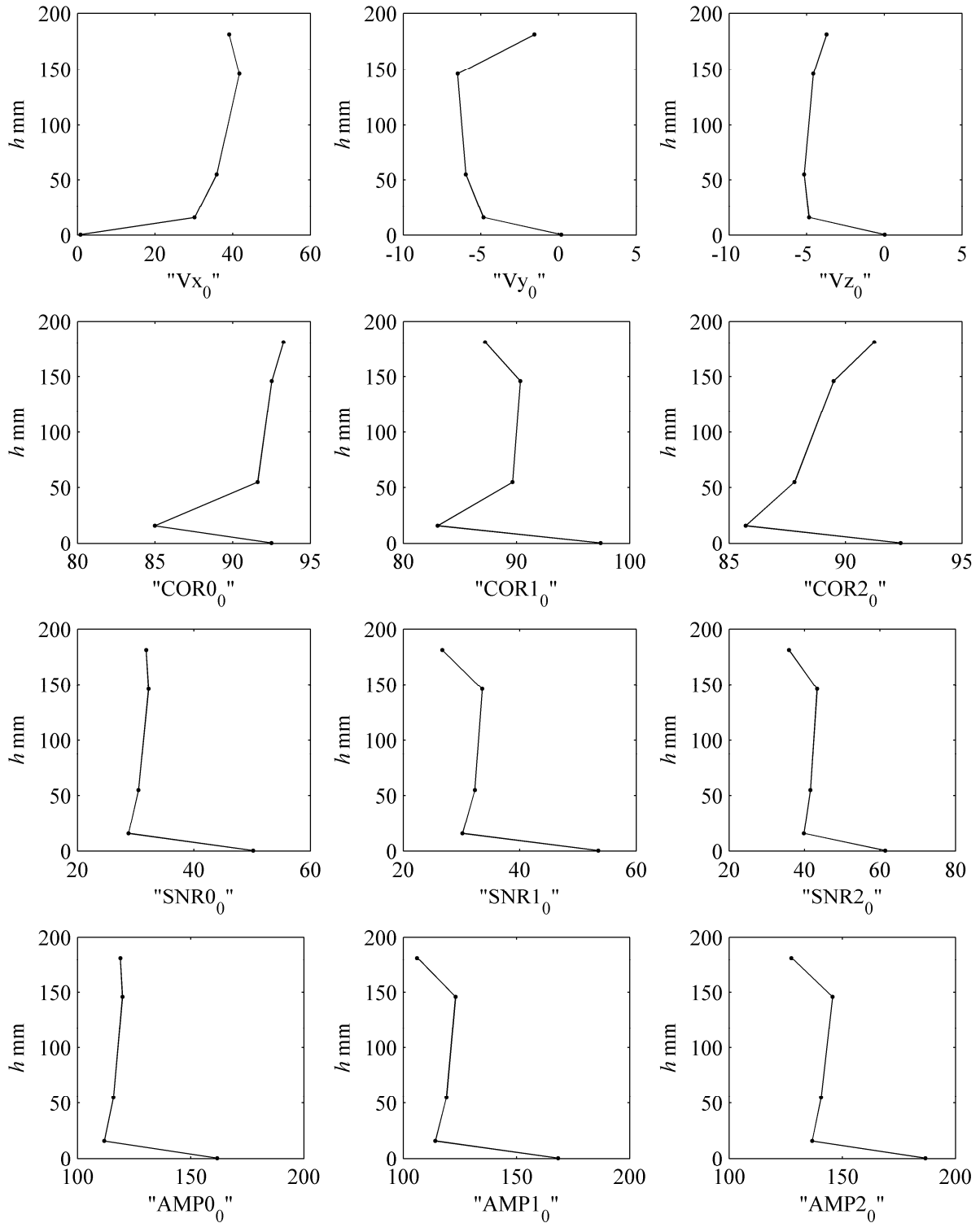


Figure 36 DA ADV data sect. 1 ($x=-0.5$ m)

Although necessary, cleaning operations increased the execution time of several minutes, as, in some case it is necessary to clean the probe several time for 1 vertical. However, since a certain degree of sensibility and experience is necessary when collecting the data (a “bad” signal can be also produced by a reduced number of scatter elements present into the flow). Both SNR and amplitude profiles for the three beams shows a decreasing dependence of the

signal toward the vertical³, whilst when the control volume hit the sediment, the signal clearly increased⁴.

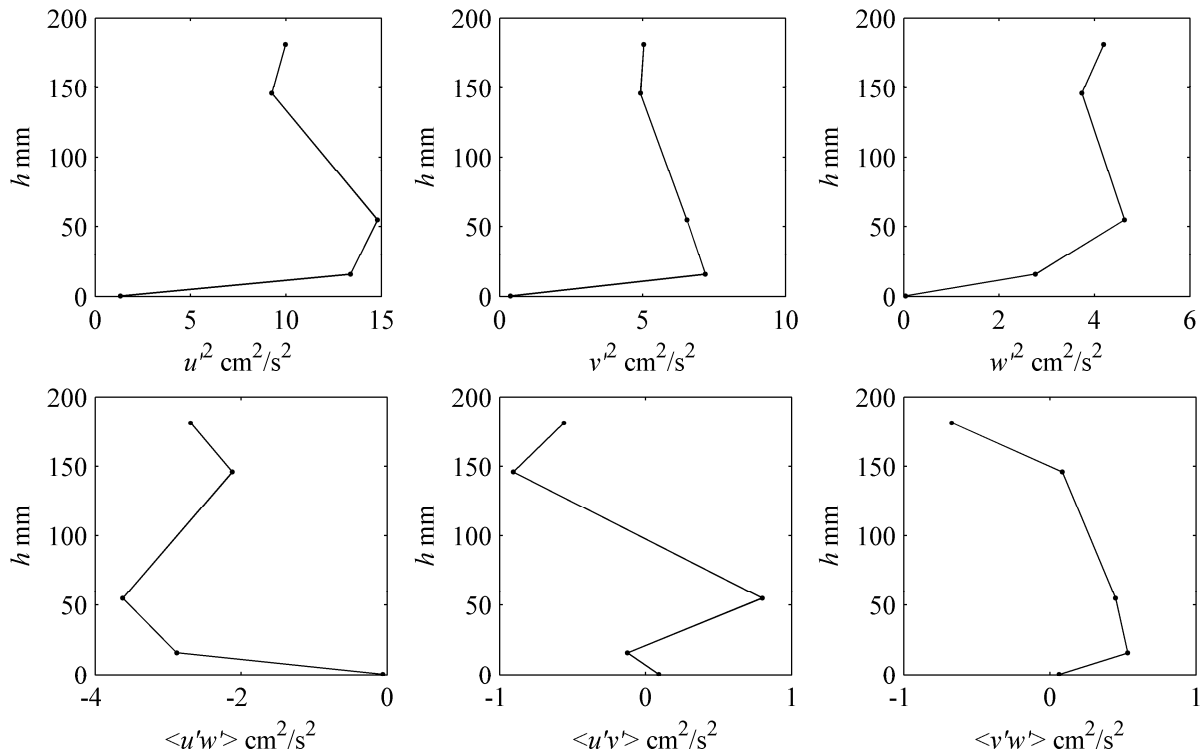


Figure 37 DA ADV turbulence data sect. 1 ($x=-0.5$)

Turbulence profiles (Figure 37) shows the typical pattern of turbulent flows, in which the turbulence intensity reduced toward the vertical in the outer flow, and in which the stream wise intensity u^2 shows the larger intensity values. Similarly, the $\langle u'v' \rangle$ Reynolds increased toward the vertical, apart the last two point which tends to reduce. The data extrapolation of the stress also suggests a value of the shear velocity of about $u^* = 2$ cm/s.

Velocity profiles section 1 ($x=-1.9$ m)

The data for the second section have been collected with the ADV starting from the water surface, i.e., keeping the sonar profiler as close at the water surface as possible. However, a dead zone is still present owing to geometrical constraints. A simple probe rotation of 180 degrees could be performed in order to obtain also the data toward the water surface, if really required. Data have been collected at approximately the channel centre, (see Figure 33a). The longitudinal velocity component u shows again a well developed turbulent profile in which a maximum velocity of $u=47.5$ cm/s is attained at about 420 mm from the sediment bottom. and than decreased toward the water surface (Figure 38). Both transverse and vertical velocities show non negligible components, in which w shows negative values.

Although the velocity profiles didn't revealed the presence of strong anomalies, a part the v at $h=400$, correlation profiles from the three beams shows the most interesting results. Indeed, a cross-check with the amplitude and SNR profiles may explain the contradictory results

³ TSS and particle size distributions need to be analysed.

⁴ It is again important to observe that the probe and the control volume exact positioning depends from the operator sensibility and that the control volume should approach but not enter the sediment to obtain corrected values of the velocity.

obtained from the turbulence profiles. In this case, the cleaning operation have not been performed until the point $h=200$ mm, as shown by the deterioration of the correlation and the SNR signal for $200\text{mm} < h < 400$ mm, as well as from the drop observed successively. However, the correlation signal observed from the beam 2, shows almost constant values, indicating that, most likely, the amplitude profile observed by that beam can be considered the most corrected amongst the three. Indeed, the amplitude profile of the beam 2 shows a certain increase of the amplitude, most likely indicating an increase of the sediment concentration.

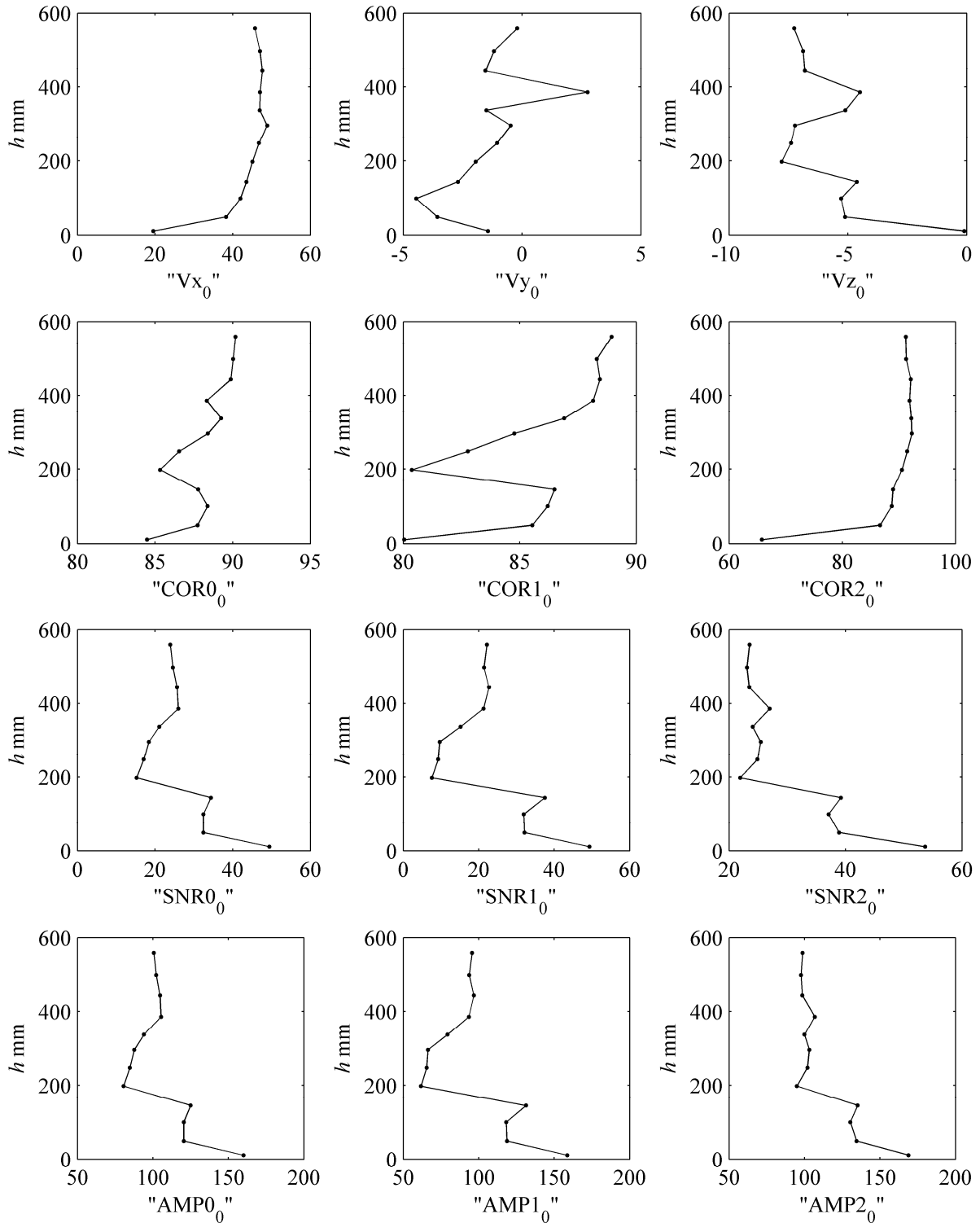


Figure 38 DA ADV data sect. 2 ($x=-1.9$ m)

However, the deterioration of the signal correlation and the probe clogging may have had a certain impact on the measure of the velocity fluctuation and therefore on the turbulence intensities and Reynolds stress shown by Figure 39. In fact, although the u'^2 shows growing values toward the sediment bottom ($h=0$ mm), $\langle u'v' \rangle$ show a maximum value for $h=200$ mm, exactly the point after which the cleaning operations have been performed. After cleaning the probe, $\langle u'v' \rangle$ successively reduced to the next point toward the bottom, and again increased at about $h=50$ mm. However, from the extrapolation of the longitudinal Reynolds stress, a value of the shear velocity of about 2.2 cm /s can be inferred, which is quite similar to the value obtained from the section $x=-0.5$ m.

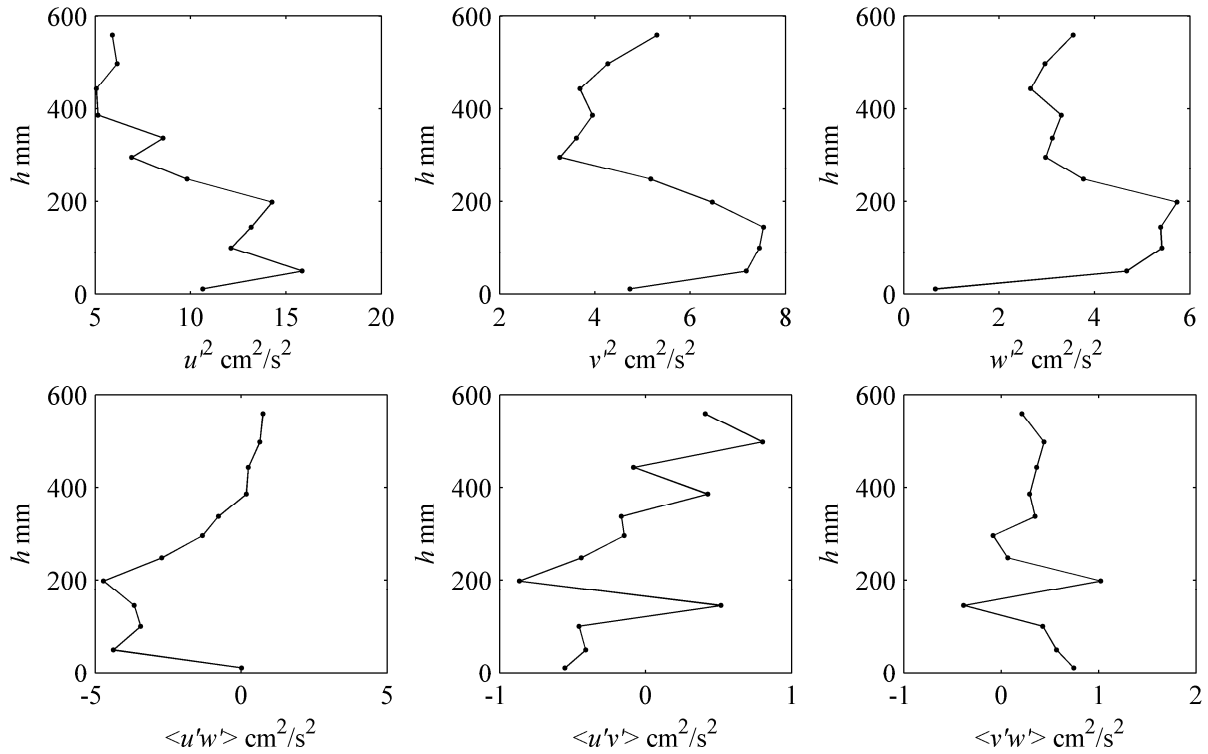
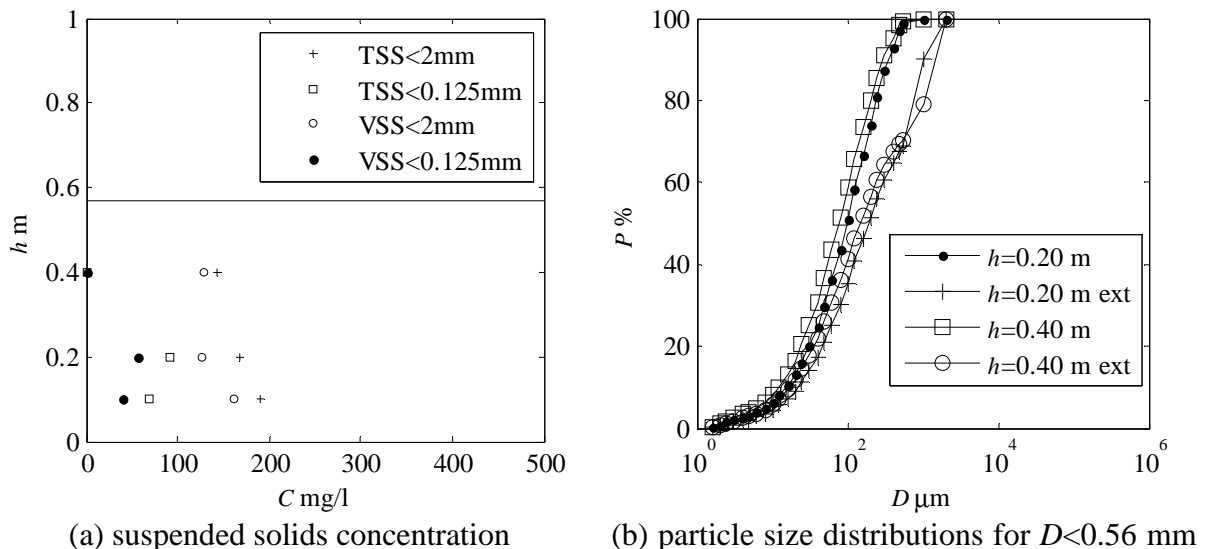


Figure 39 DA ADV turbulence data sect. 2 (x=-1.4 m)

6.2.5 Flow filed Test DA-S3 (2011-02-04)

Figure 40 shows the suspended solids and particle size distribution for the test DA-S3.



(a) suspended solids concentration

(b) particle size distributions for $D < 0.56$ mm

(ext=extended to 2 mm)

Figure 40 Test DA-S3 in situ suspended solids concentrations and particle size distributions

This time, both TSS and VSS increases toward the bottom. The bottom morphology and the longitudinal morphologies (Figure 42 and Figure 43) shows a almost negligible deposit in the centre of the surveyed sections, whilst small deposits ($z_{BED} < 100\text{mm}$) occurred at both ends of the surveyed trunk.

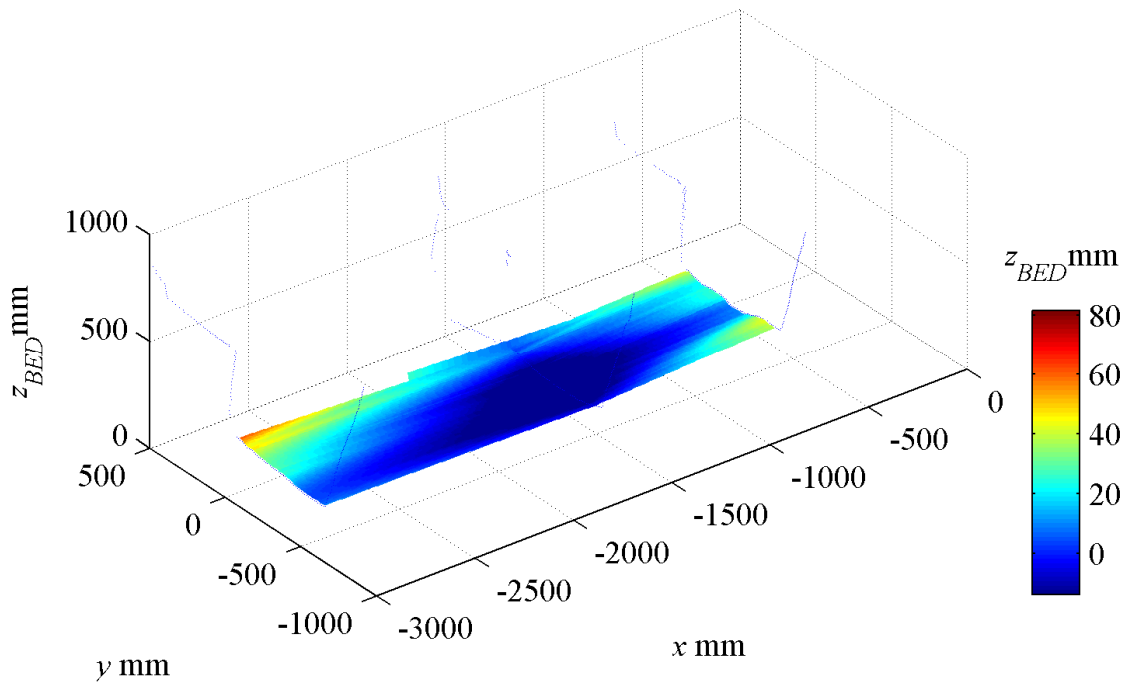


Figure 41 DA-S3 Bottom morphology

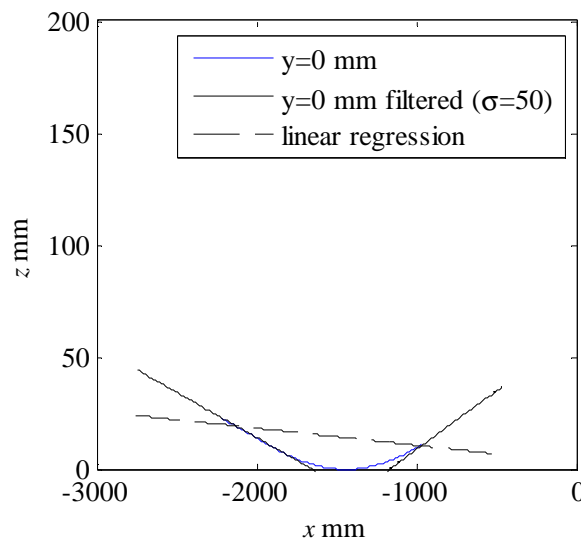


Figure 42 DA-S3 centerline longitudinal profile ($y=0$), where the regression line represents the regression trough the z_{BED} points.

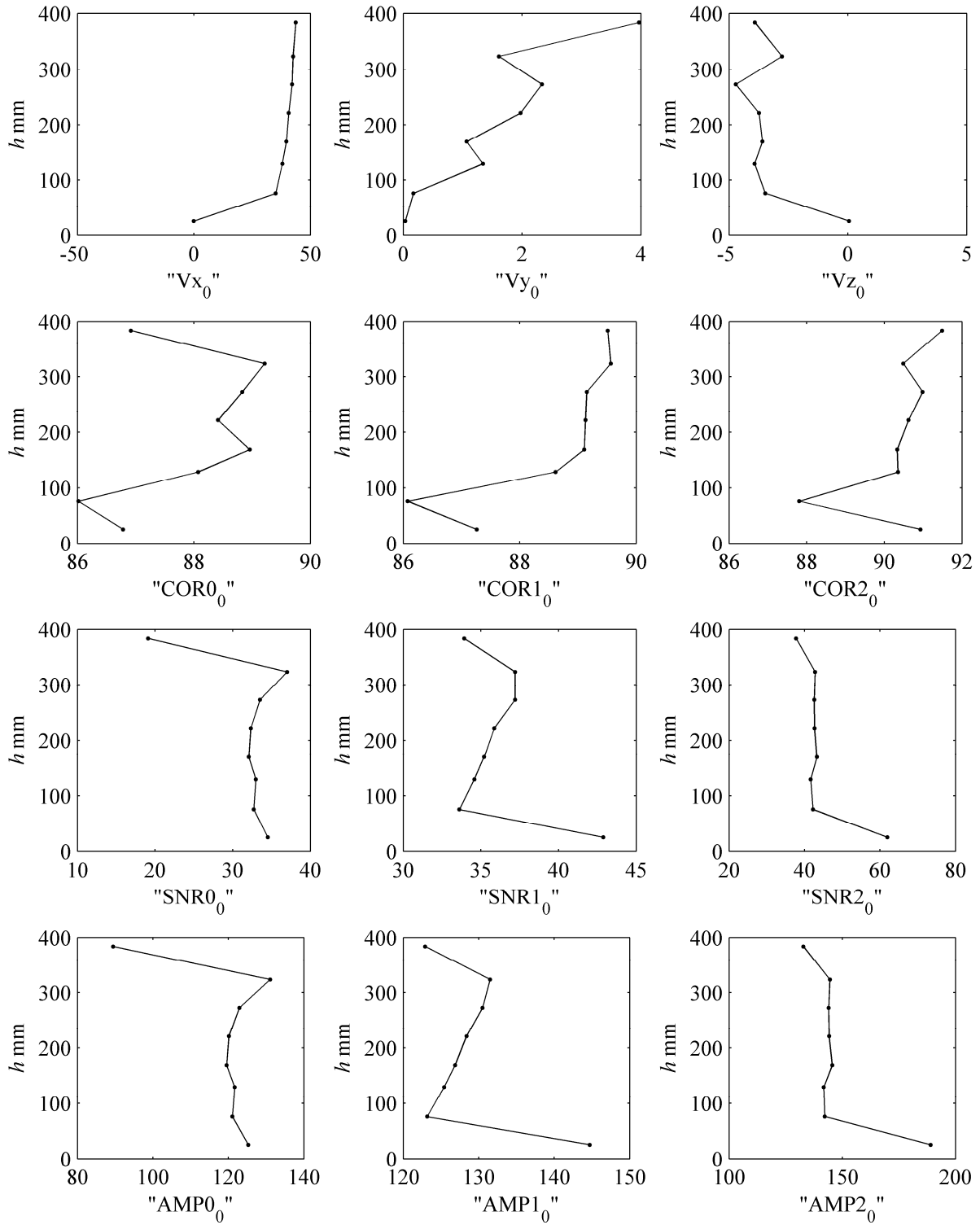


Figure 43 DA-S3 ADV data sect. 1 ($x=-0.5$ m)

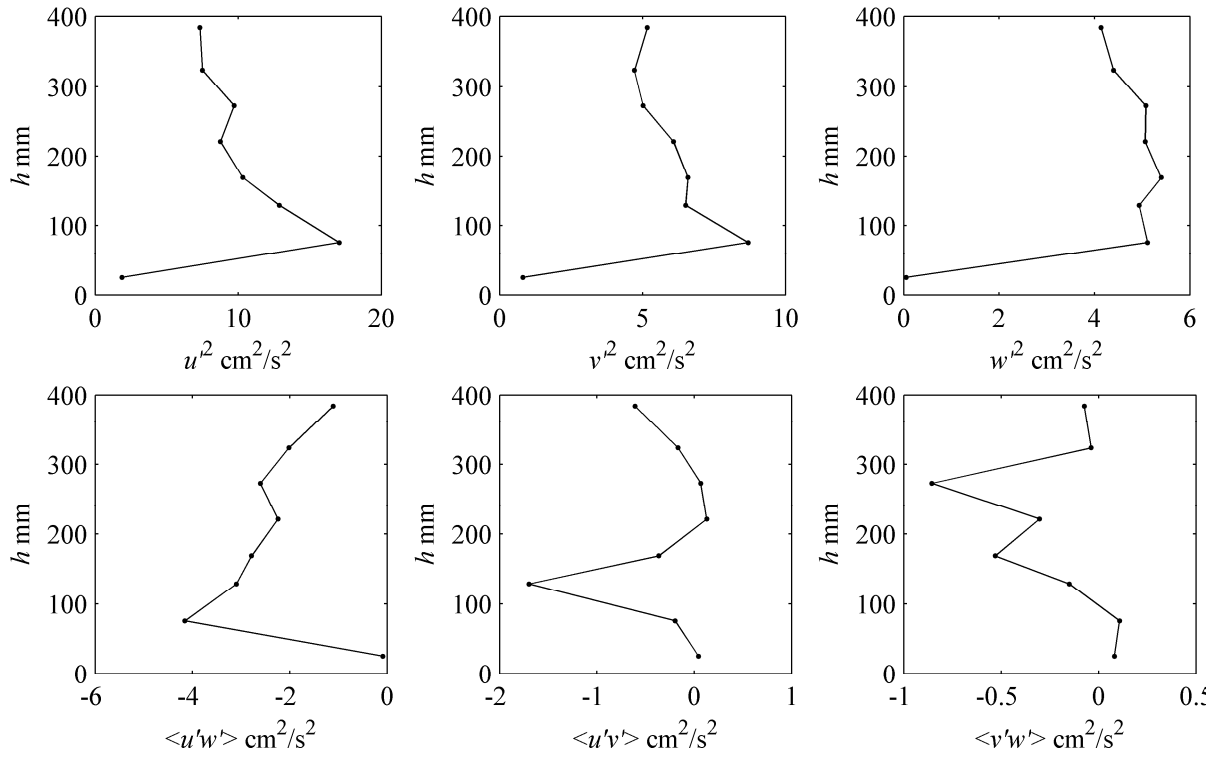


Figure 44 DA-S3 ADV turbulence data sect. 1 ($x=-0.5$ m)

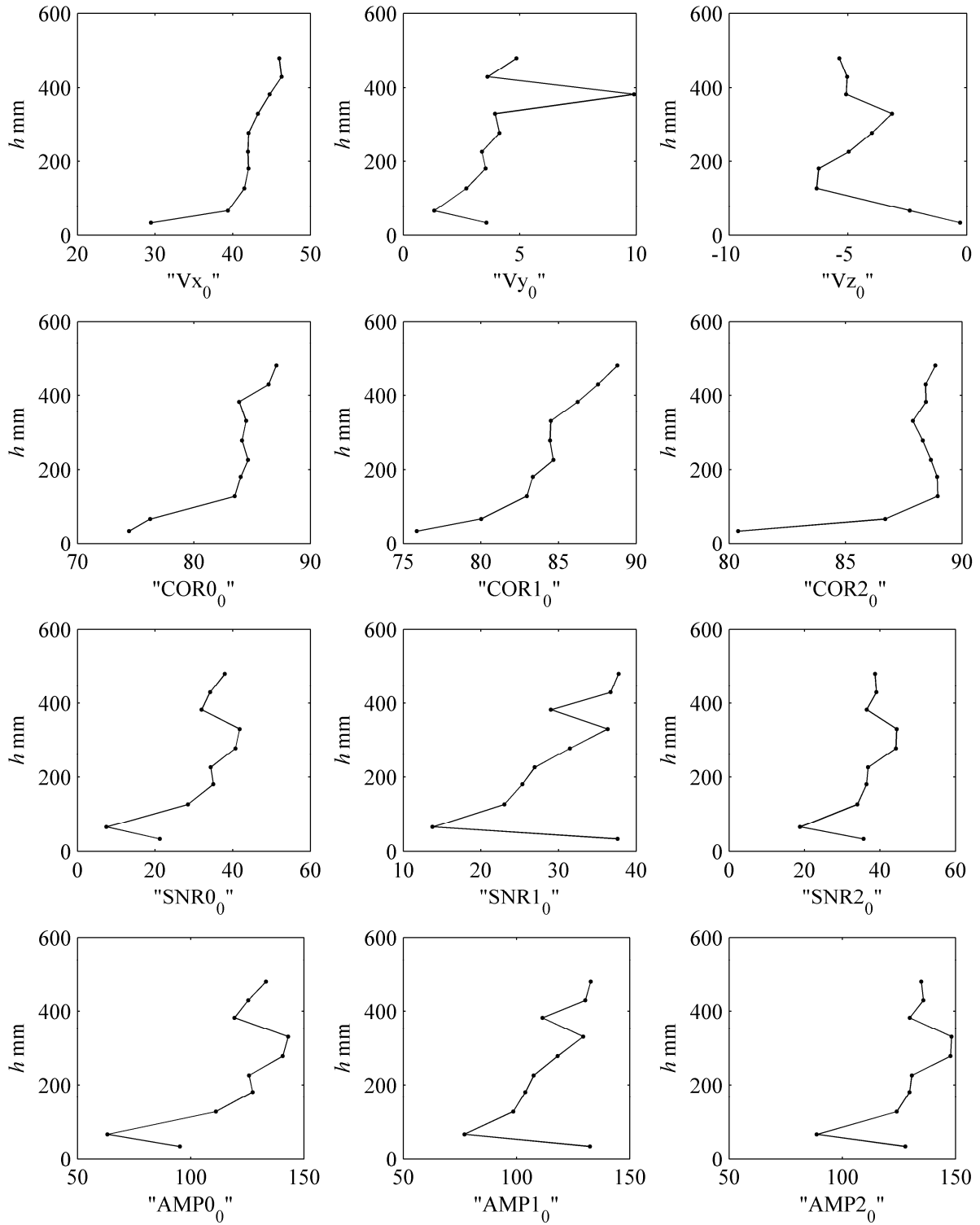


Figure 45 DA-S3 ADV data sect. 2 ($x=-1.9$ m)

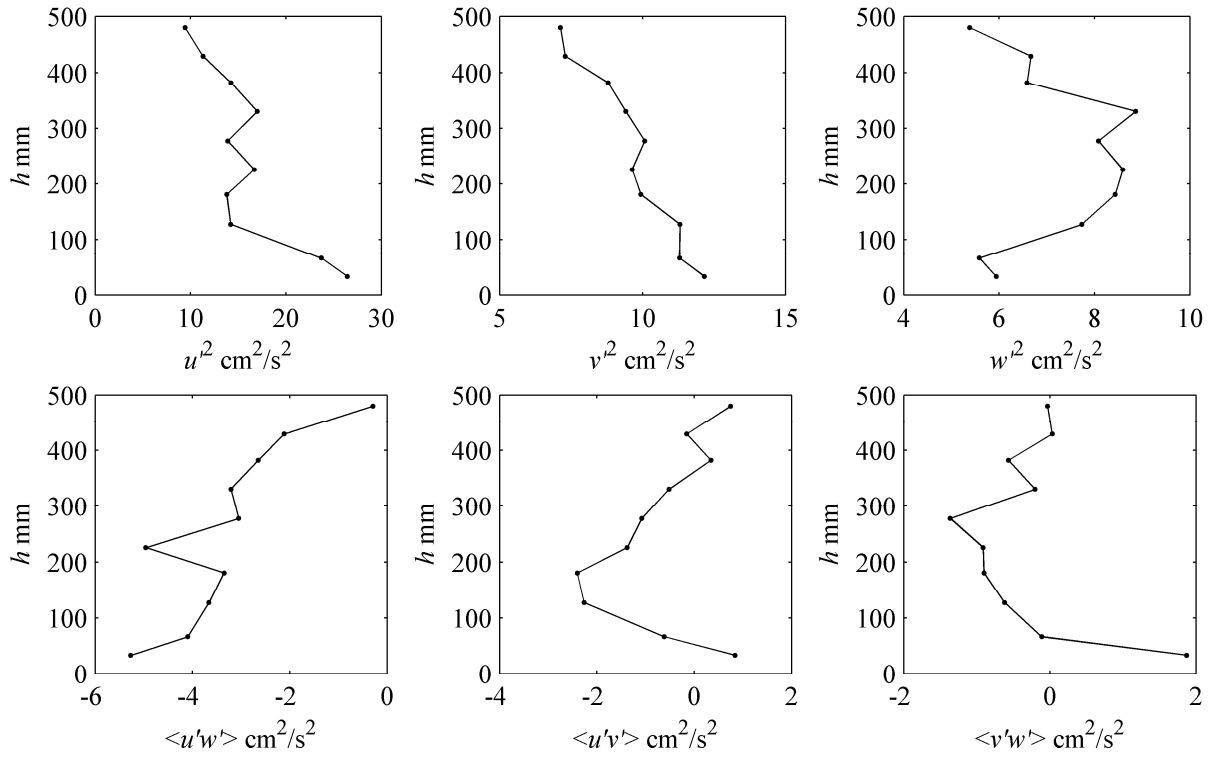


Figure 46 DA-S3 ADV turbulence data sect. 2 ($x=-1.9$ m)

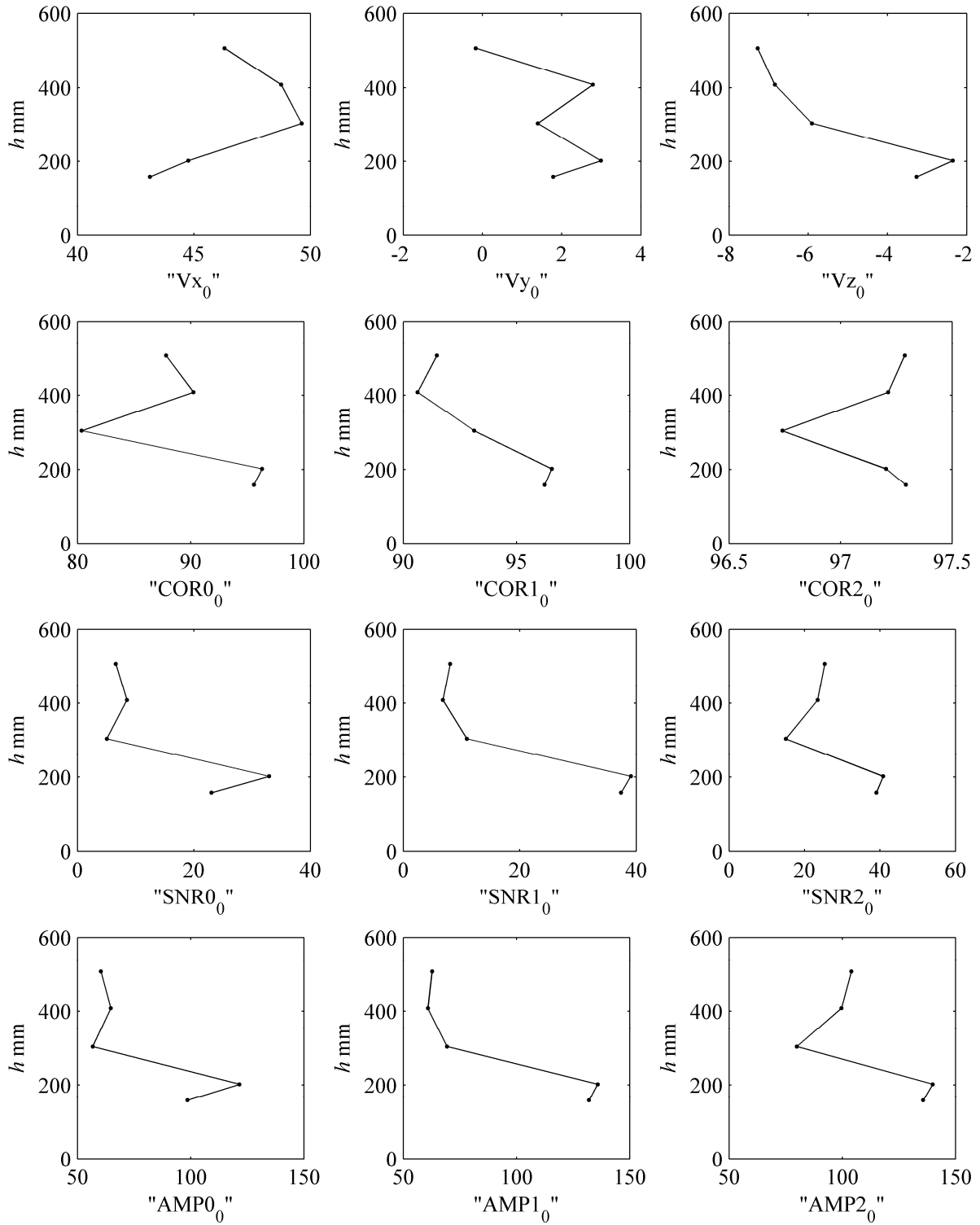


Figure 47 DA-S3 ADV data sect. 2 ($x=-3.3$ m)

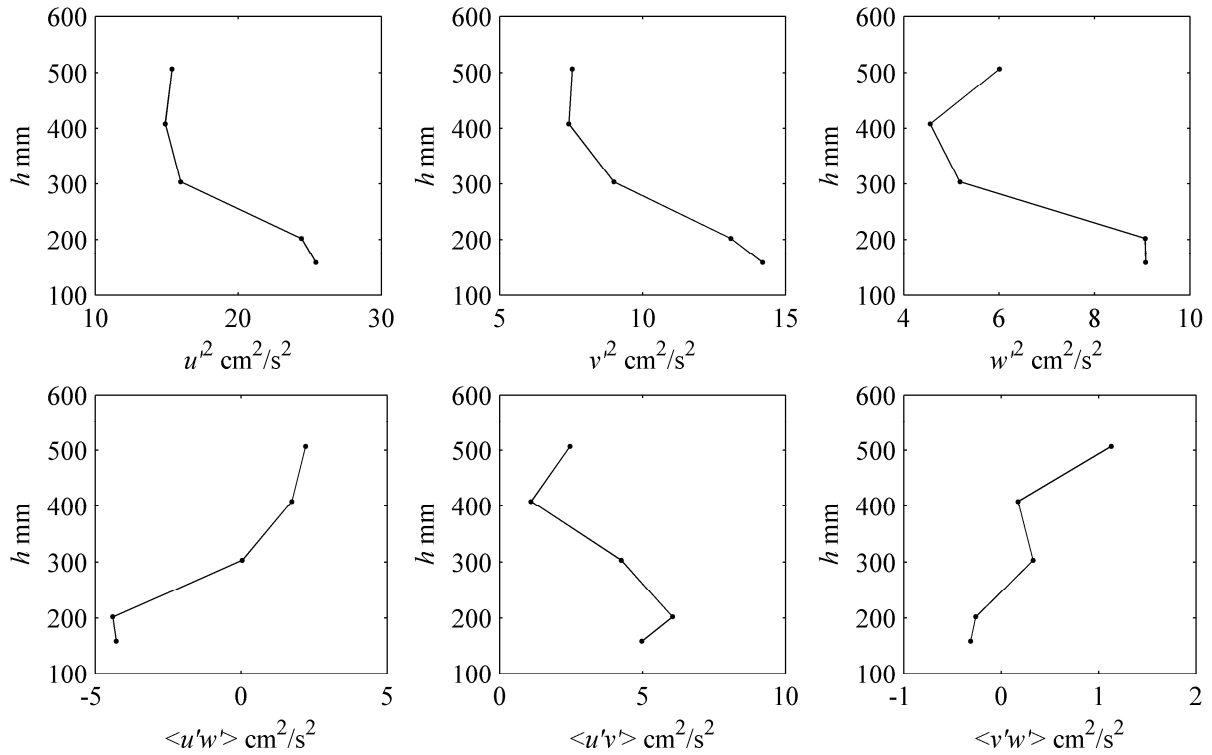


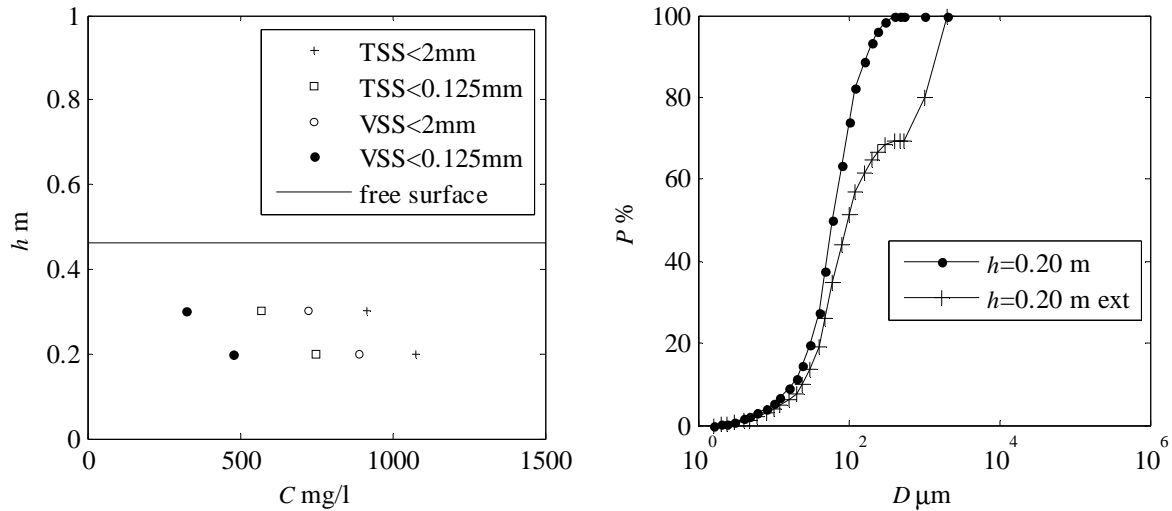
Figure 48 DA-S3 ADV turbulence data sect. 2 ($x=-3.3$ m)

6.3 Allée de l'Erdre tests (AE)

This section shows the results obtained at the second experimental site. This site is characterised, as further discussed, by soft deposits, compared with the previous site, presenting some peculiar characteristics that will be discussed later. The test will again be presented first analysing the morphological characteristics of the sediment deposits and their possible evolution in conjunction with the flow characteristics. Finally a summary of the flow field recorded in different conditions will be analysed.

6.3.1 Morphological characteristics Test AE-S6 (2011 03 10)

Figure 49 shows the conditions under which the measurements have been carried out. Accordingly to the observation, this site shows sediment TSS of the order of 1g/l with percent of organic matter larger than 50%.



(a) Suspended solids concentrations at different eight from the interface

(b) bottom sediment particle size distribution and water sediment particle distribution.

Figure 49 TSS, VSS and particle size distribution conditions of test AE-S6

The sonar output of Figure 50 didn't highlight the presence of a massive mud flow layer, although the TSS indicated rather large concentration. The dune observed in the figure shows a high ABS, indicating the presence of a hard deposit. Surveyed flow velocities are shown in Table 5.

Table 5 Flow velocities measured at section $x=0$ m

Time	y_{probe}	h	u	z_{BED}	δ
hours	m	m	m/s	m	m
7:50	0.10	0.37	0.138	0.35	0.47
7:50	0.10	0.37	0.088	0.35	0.47
7:50	0.10	0.37	0.123	0.35	0.47
7:50	0.20	0.27	0.088	0.35	0.47
7:50	0.20	0.27	0.084	0.35	0.47

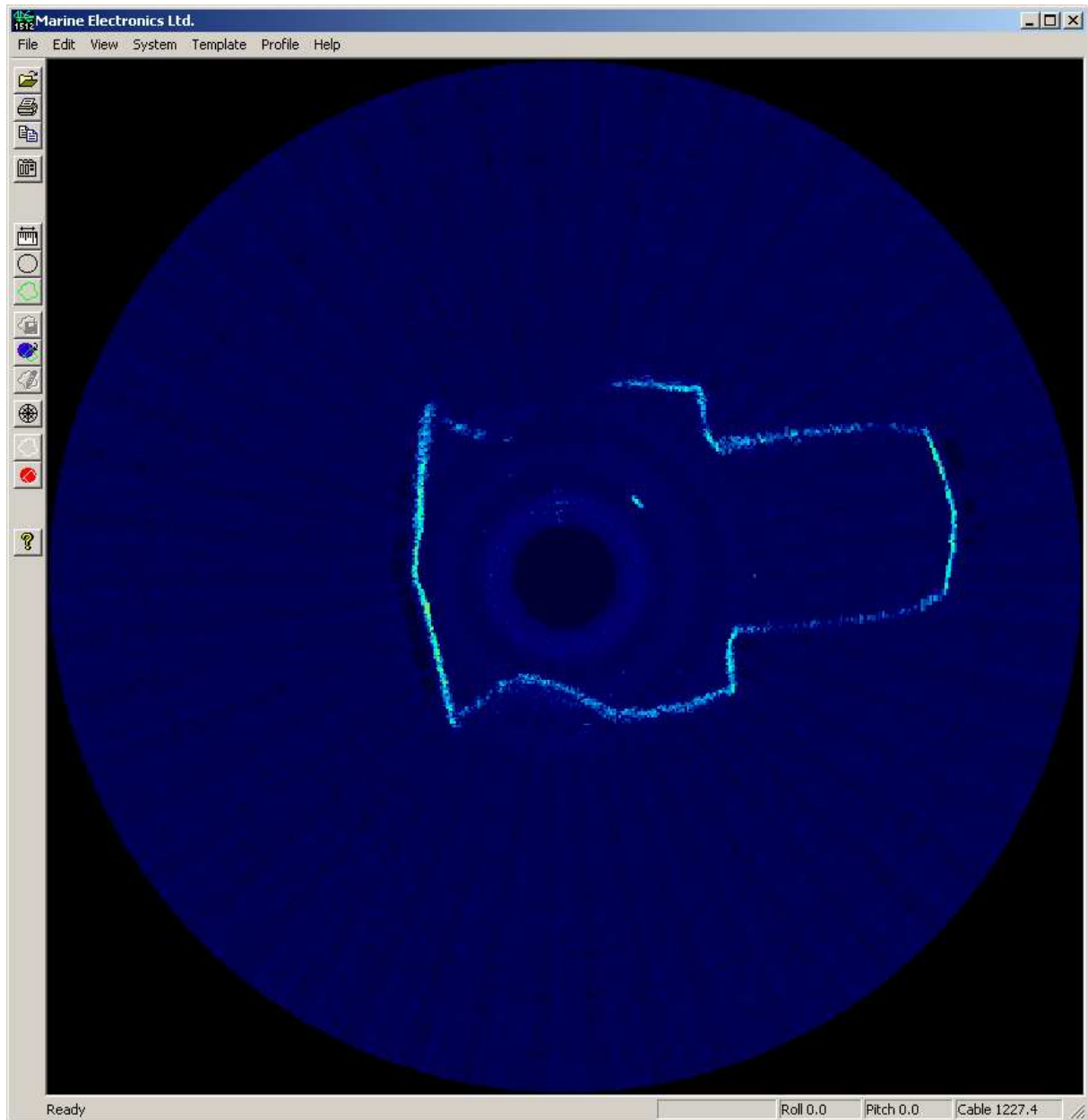
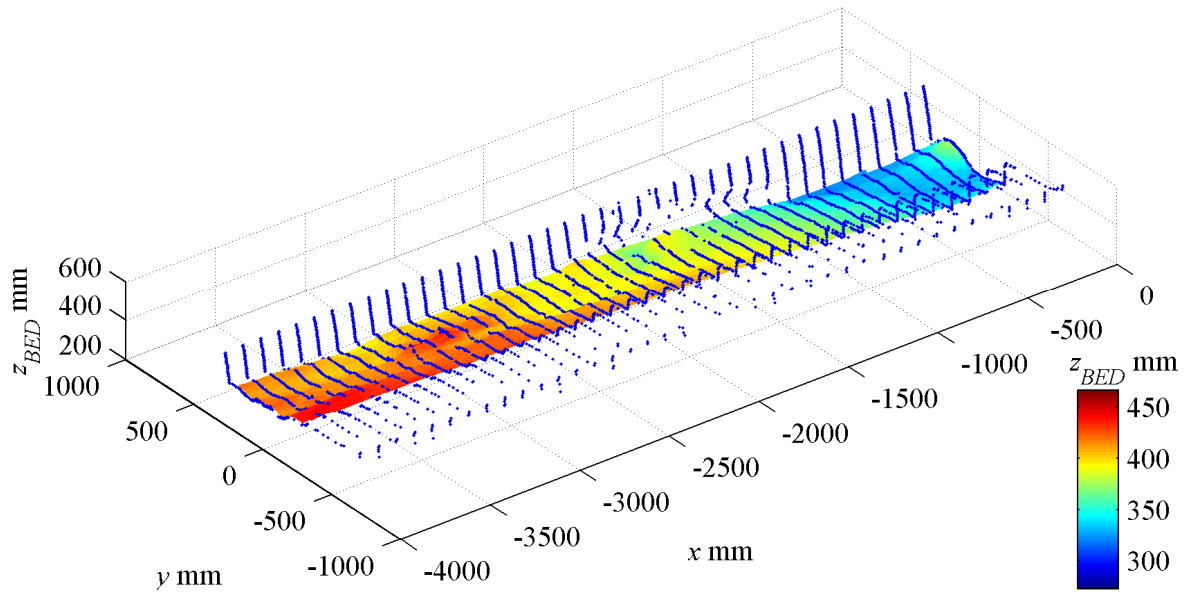
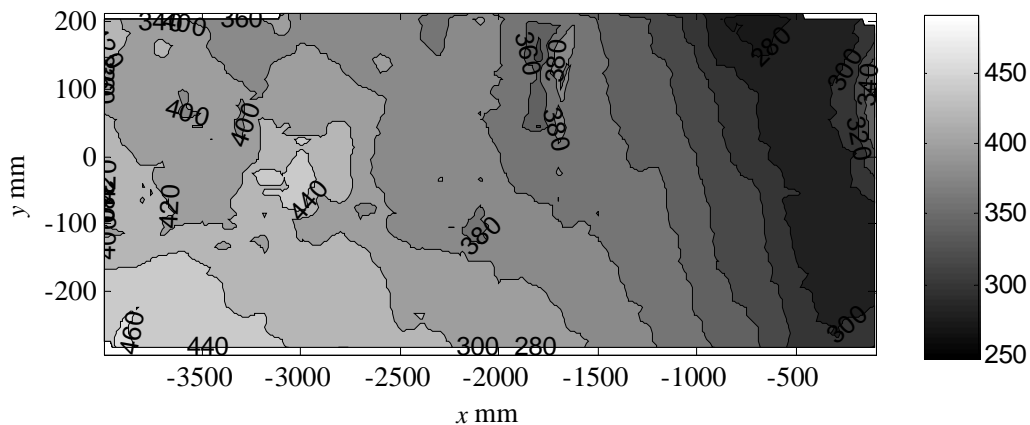


Figure 50 AE-S6 sonar output at $x=0$ mm

The bottom morphology surveyed with the sonar is shown in the Figure 51. The survey shows the interface from the invert bottom. The deposits shows a downstream slope and a through between $-1000 \text{ mm} < x < -500 \text{ mm}$. A dune occurs at about $x=0$ mm. The morphology shows generally smaller z_{BED} in the right side of the channel, probably due to the iteration with the side bank and the secondary flow generated by the upstream bend.



(a) AE-S6 surface morphology



(a) AE-S6 contour line morphology

Figure 51 AE-S6 Bottom morphology measured with the sonar profiler, from the invert z_{BED} in [mm].

Figure 52 shows the morphological survey form the average plane, still showing a complex morphology, in which the highest bed form reach value of about $z_{PLANE}=40$ mm at $x=-3000$ mm, whilst the deepest trough has a $z_{PLANE}=-20$ mm at around $x=-500$ mm. However, the morphology is rather complex and don't present any two dimensional pattern, apart from the end of the survey $-1000 \text{ mm} < x < 0 \text{ mm}$.

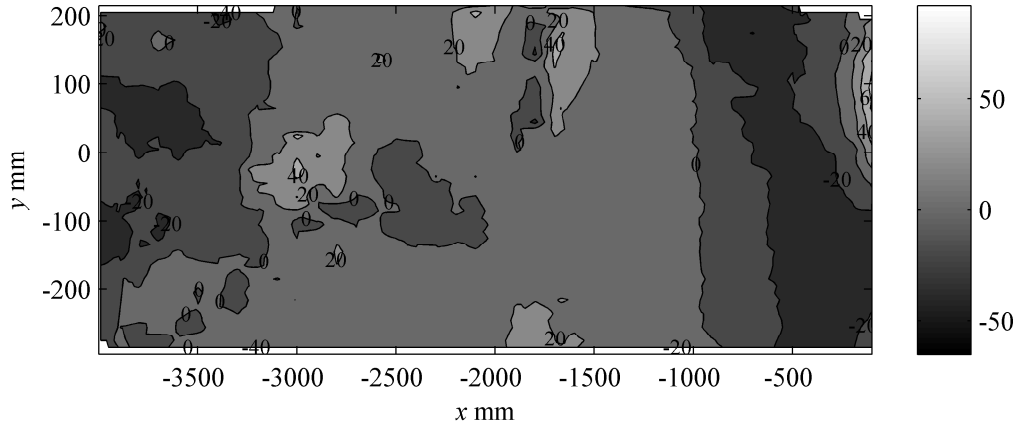


Figure 52 AE-S6 Bottom morphology measured with the sonar profiler, from the interpolating plane z_{plane} in [mm].

The longitudinal profile in Figure 53 well highlights the presence of a dune in the middle of the section which present a rather steep upstream slope, while the downstream dune side shows a milder slope. Again, the second dune observed at the end of the survey is characterised by a steep slope.

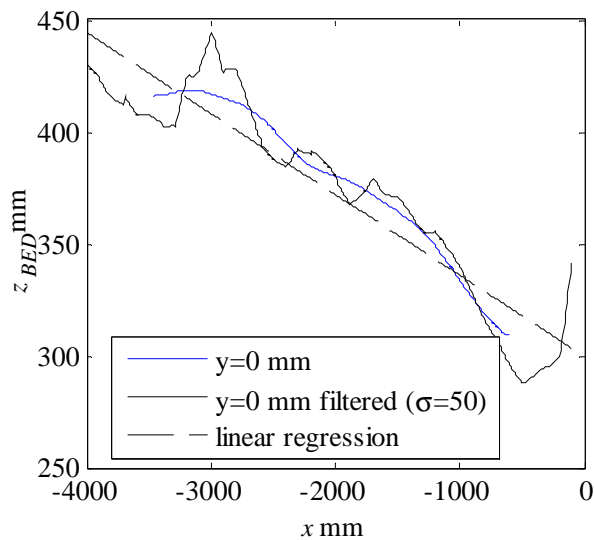
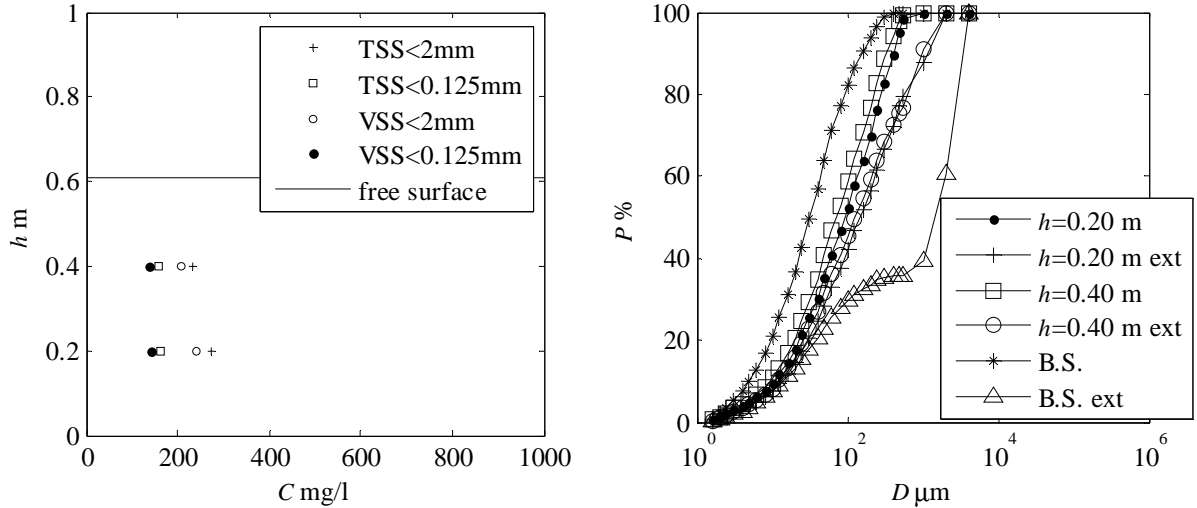


Figure 53 AE-S6 longitudinal profile for $y=0$ m.

6.3.2 Morphological characteristics Test AE-S7 (2011 03 24)

Figure 54 shows the suspended solids concentrations observed during the morphological survey. Suspended solid concentration shows lowest concentration compared to the previous test. Bottom sediments also shows an average diameter of $D_{50}=1.5$ mm, with a specific weight of $\gamma_s=1800$ kg/m³.



(a) Suspended solids concentrations at different eight from the interface

(b) bottom sediment particle size distribution and water sediment particle distribution for $D < 0.56$ mm.(B.S.: bottom sediment, ext: extended to 4 mm)

Figure 54 TSS, VSS and particle size distribution conditions of test AE-S7at $x=0$ mm

Indeed, the sonar output and the bottom ABS is higher compared to the previous survey (compare Figure 55 and Figure 50), thus confirming that mud layer was less important in the present conditions. Indeed, flow velocities were larger compared to that observed in the S6 tests, although measured later in the morning when generally the velocities reduced.

Table 6 AE-S7 longitudinal flow velocities

Time	y_{probe}	h	U	z_{BED}	δ
Hours	m	m	m/s	m	m
10:18	0.50	0.11	0.059	0.12	0.61
10:18	0.50	0.11	0.080	0.12	0.61
10:19	0.40	0.21	0.111	0.12	0.61
10:19	0.40	0.21	0.106	0.12	0.61
	0.30	0.31	0.124	0.12	0.61
	0.30	0.31	0.133	0.12	0.61
10:21	0.20	0.41	0.130	0.12	0.61
	0.20	0.41	0.141	0.12	0.61
	0.10	0.51	0.147	0.12	0.61
	0.10	0.51	0.142	0.12	0.61

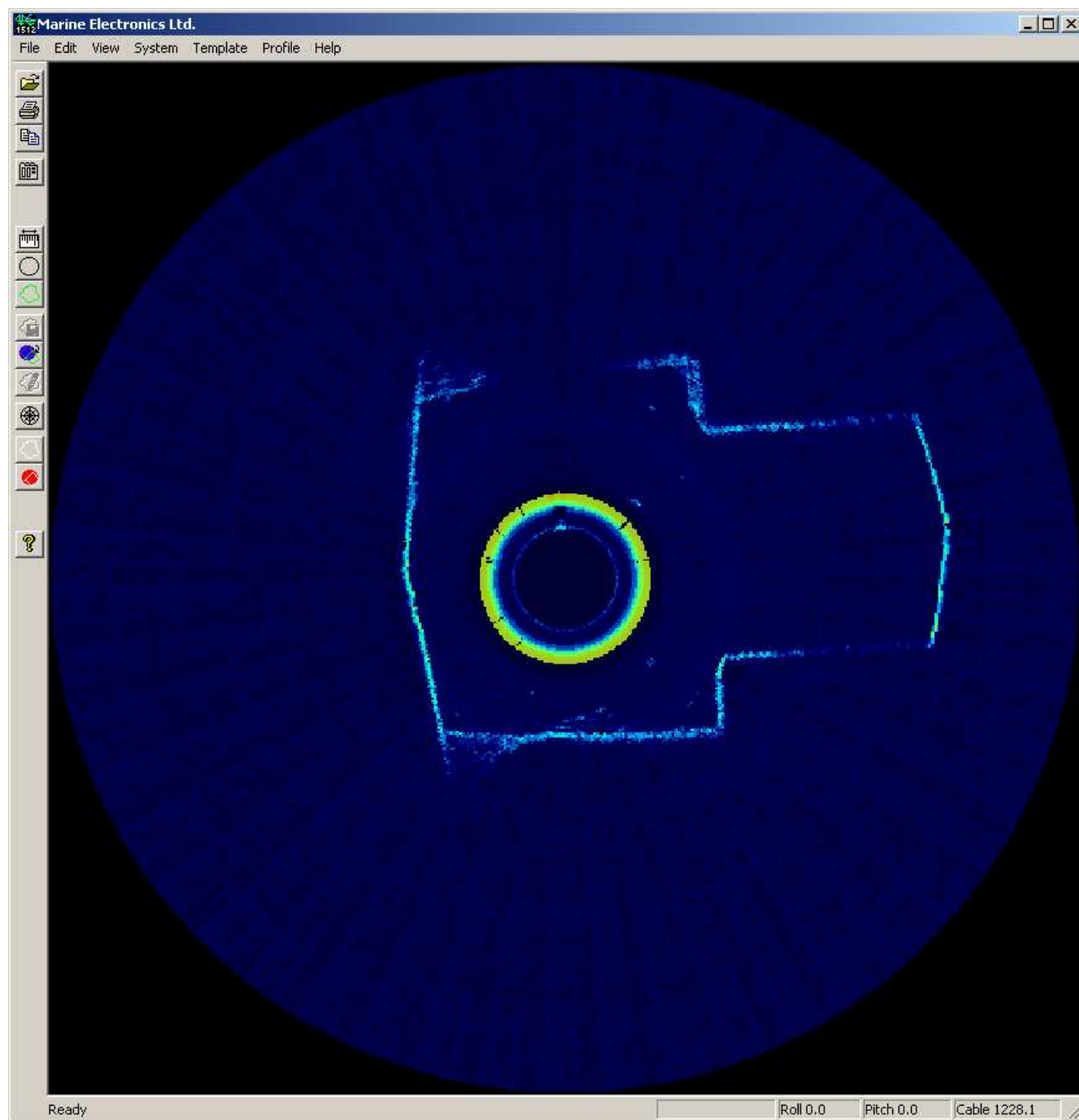


Figure 55 AE-S7 sonar output at $x=0$ mm

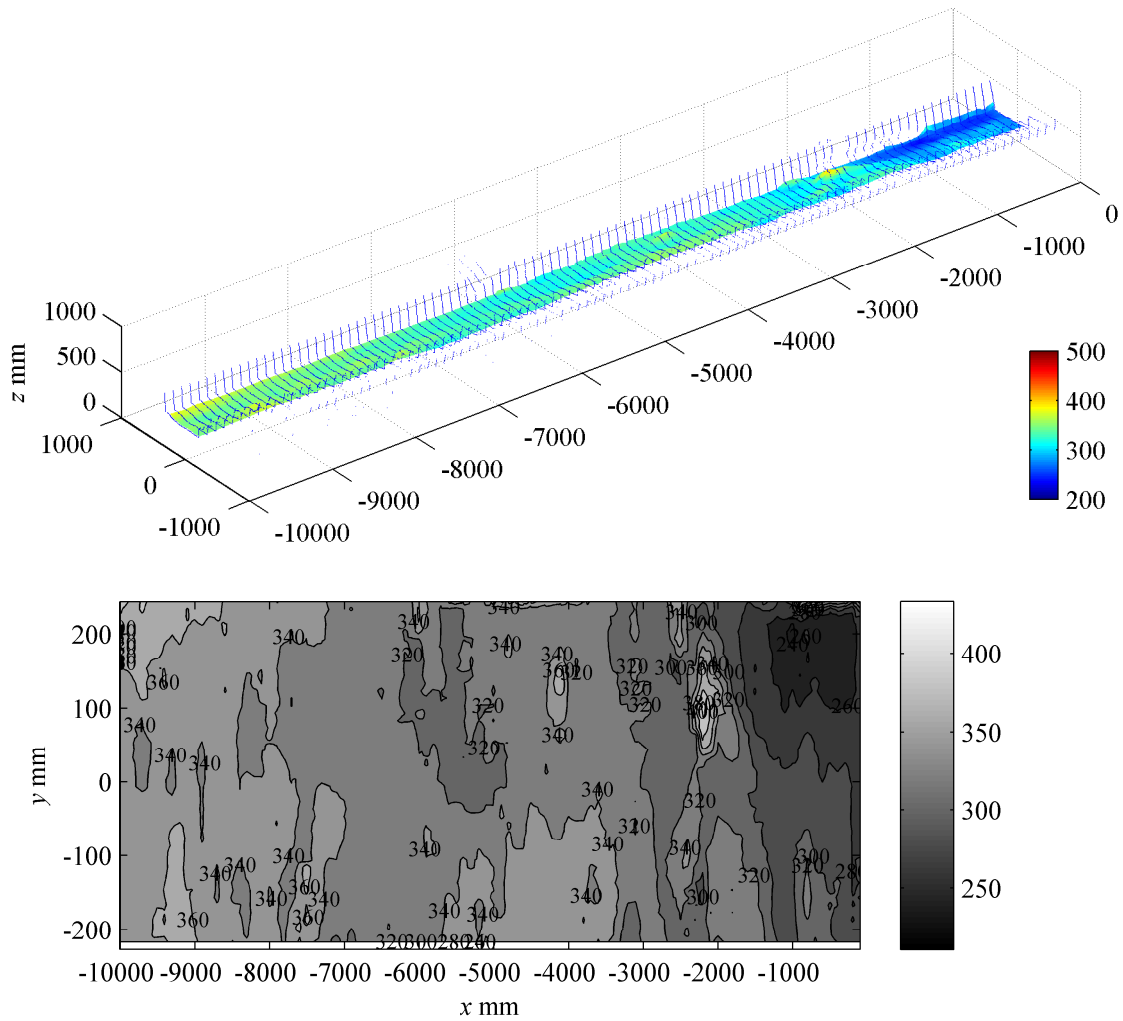


Figure 56 AE-S7 Bottom morphology measured with the sonar profiler, z_{BED} in [mm]

The Figure 57 displays the morphology of the sediments in which the vertical coordinate has been shifted of the value of the plane averaging the surveyed bottom in which $a=-286.34$, $b=-0.006$ and $c=-0.074$ are the plane coefficient, meaning that the average longitudinal slope was of about **0.6 %** and **7% transverse** at the point where the survey has been made.

Indeed, the similar velocities and conditions observed between tests S6 and S7 produced comparably similar bed morphologies (Figure 58, see also the S6 profile in Figure 53), which present a wave length of the order of 4 m, with dune height and of about 20 mm over the average plane (Figure 57 and Figure 52) and troughs of 40 mm.

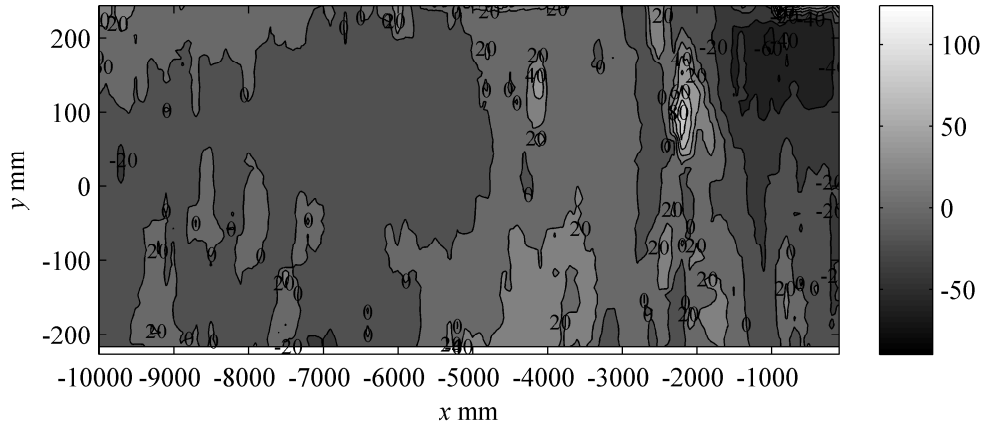


Figure 57 AE-S7 Bottom morphology measured with the sonar profiler, z_{PLANE} in [mm]

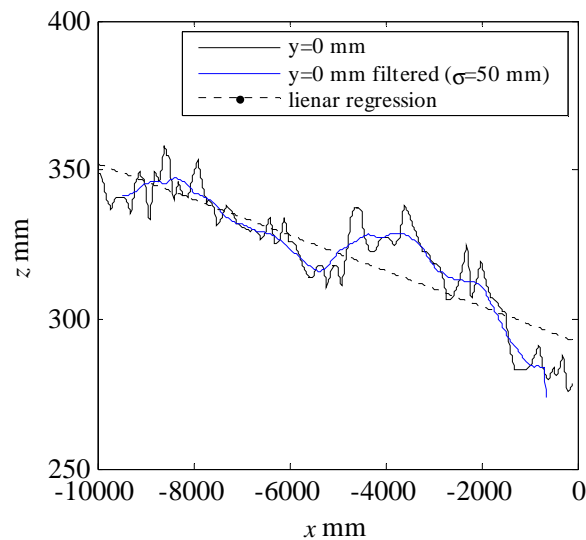
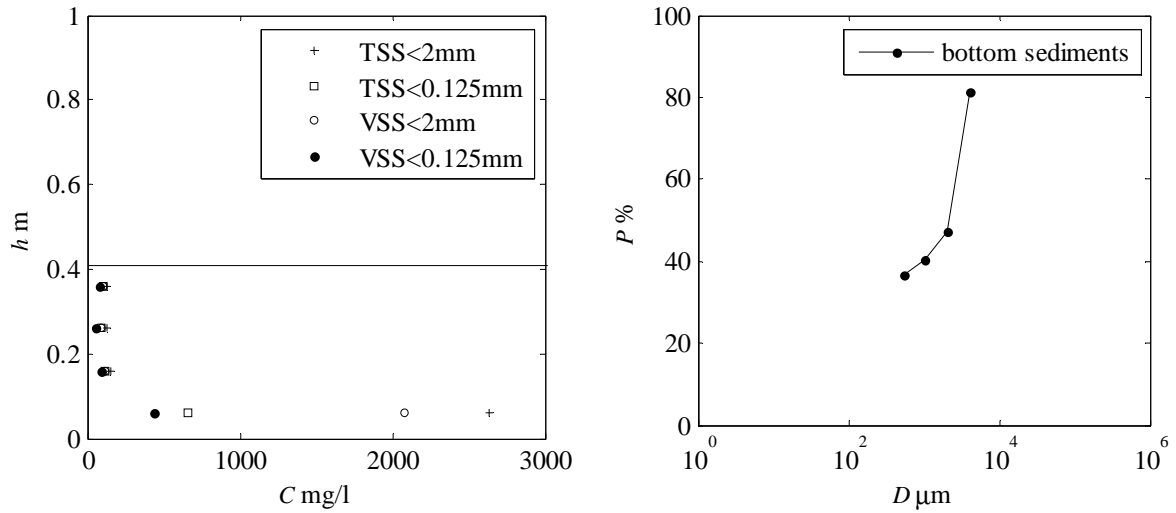


Figure 58 AE-S7 longitudinal section $y=0$ m

6.3.3 Morphological characteristics Test AE-S8 (2011 05 04)

Suspended solids of Figure 59 show almost constant concentration toward the vertical, while the closest sample has been probably measured to close to the interface and has probably interacted with this latter. Bottom sediments presented an average diameter of about $D_{50}=2$ mm and a specific weight $\gamma_s=1800 \text{ kg/m}^3$. Figure 60 shows a sediment column collected in a clear Perspex tube of 7 cm of diameter, showing an almost unique layer of gross sediment, close to type-C deposits. However, it is worth observing that, once the column is extracted from the bottom, the sediments interface may settle of about 7 cm in 10-20 seconds.



(a) Suspended solids concentrations at different eight from the interface

b) bottom sediment particle size distribution for $D < 4$ mm

Figure 59 TSS, VSS and particle size distribution conditions of test AE-S8



Figure 60 Sediment deposits surveyed with a clear Perspex cylinder of 7 cm of internal diameter.

Again, from the sonar output in Figure 61, the mud layer seems unnoticed, although the sediment observed are rather organic.

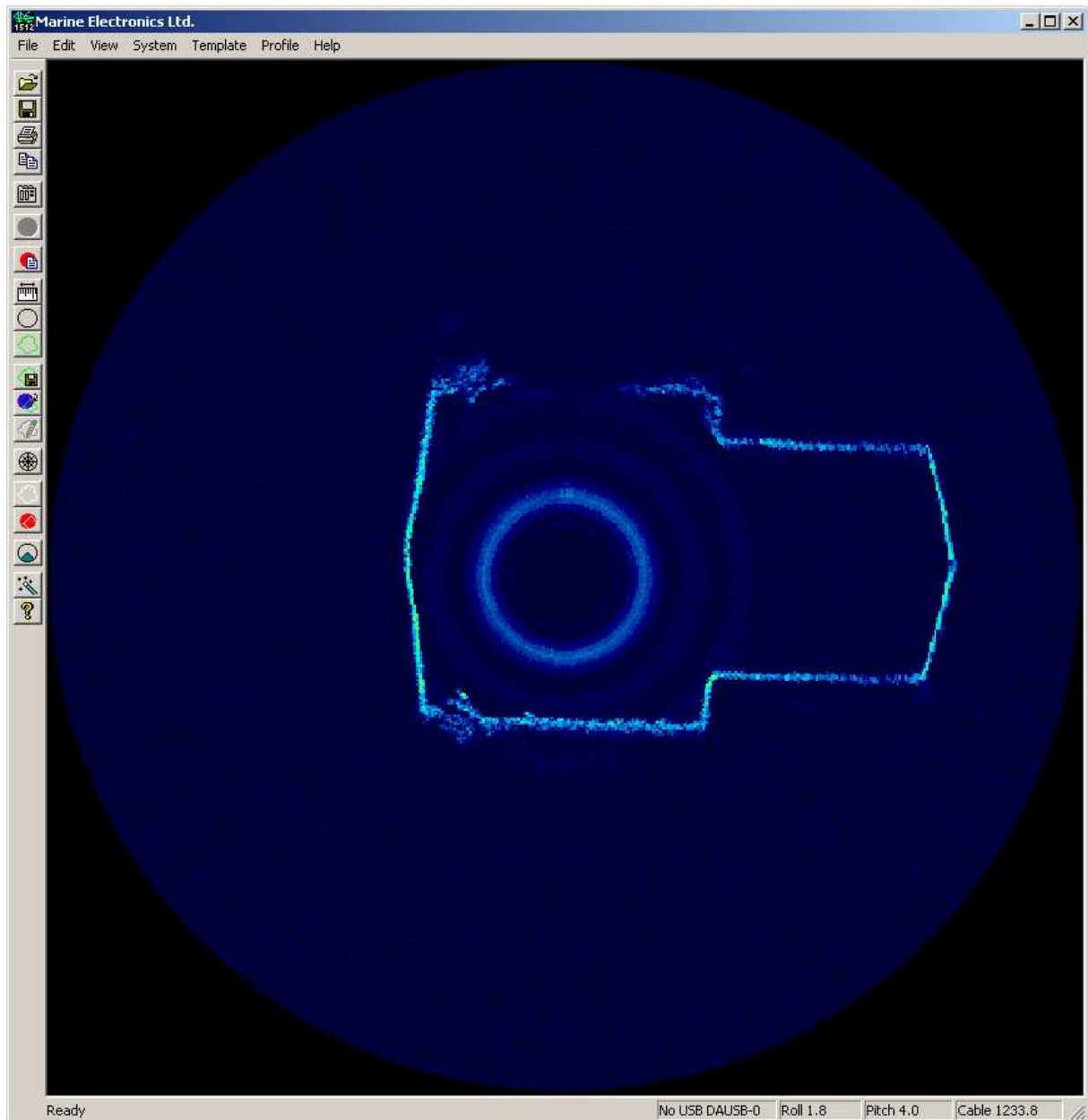


Figure 61AE-S8 sonar output at $x=-0.30$ mm

Flow velocities are summarised in Table 7, showing values slightly reduced compared to the previous tests.

Table 7 Test AE-S8 measured velocities

Time	y_{probe}	h	u	Z_{BED}	δ
hours	m	m	m/s	m	m
10:18	0.20	0.21	0.100	0.35	0.41
10:18	0.20	0.21	0.094	0.35	0.41
10:19	0.30	0.11	0.085	0.35	0.61

The morphological survey of Figure 62 shows a steeper slope compared to the previous two observations of about 2 % of slope. It is worth observing that, owing to the presence of a strong noise in the sonar output, the section between $-5000 \text{ mm} < x < -4500 \text{ mm}$ is rather disturbed and present a trough which actually doesn't exist. However, the sediment deposits is still characterised by a lower sediment deposit near the side bank.

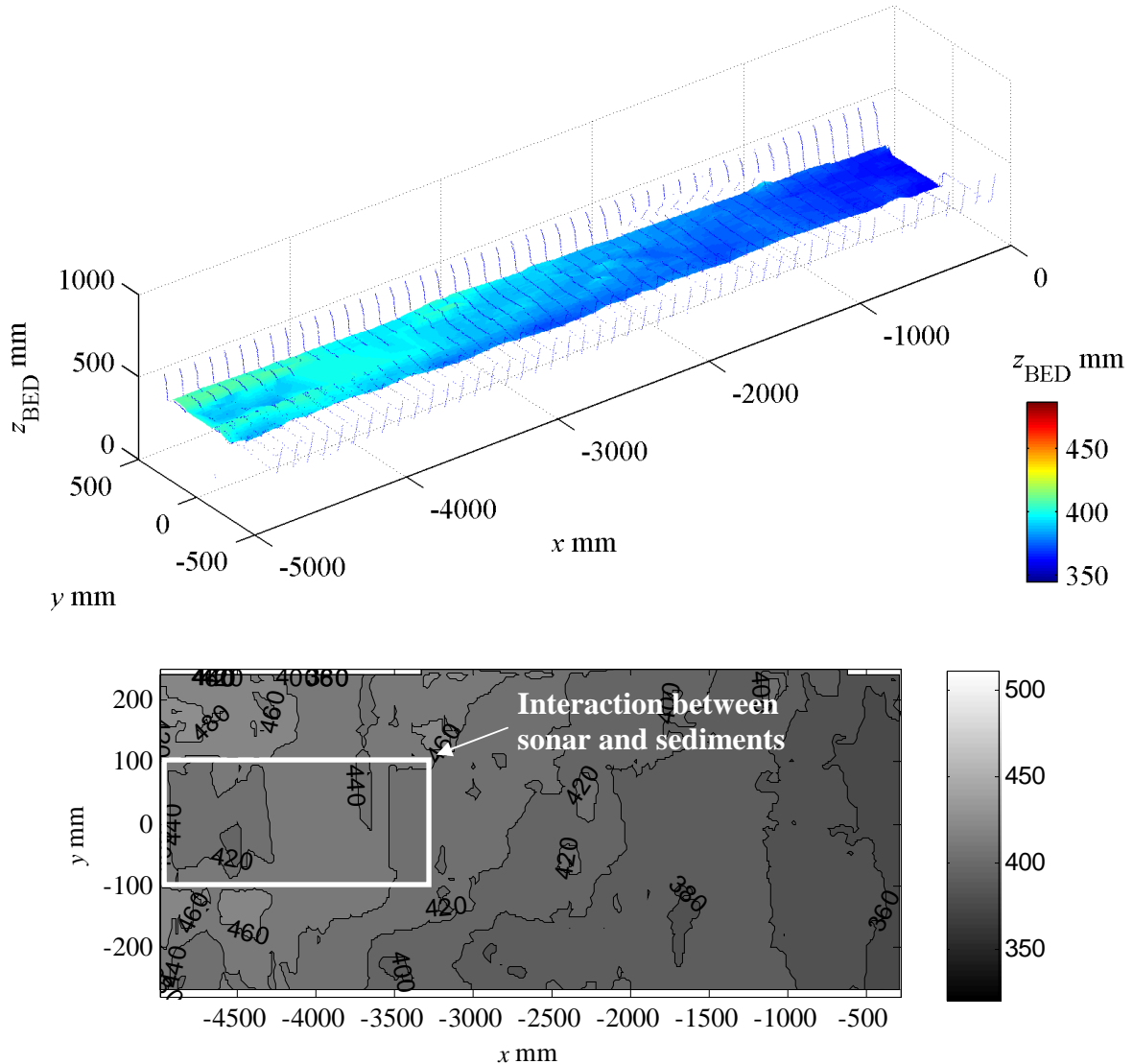


Figure 62 AE-S8 Bottom morphology measured with the sonar profiler from the invert bottom z_{BED} in [mm]

Figure 63 and Figure 64 well shows that, although characterised by a steeper slope, the longitudinal morphology is characterised by smaller ripples of generally 10 mm without any regular two dimensional pattern

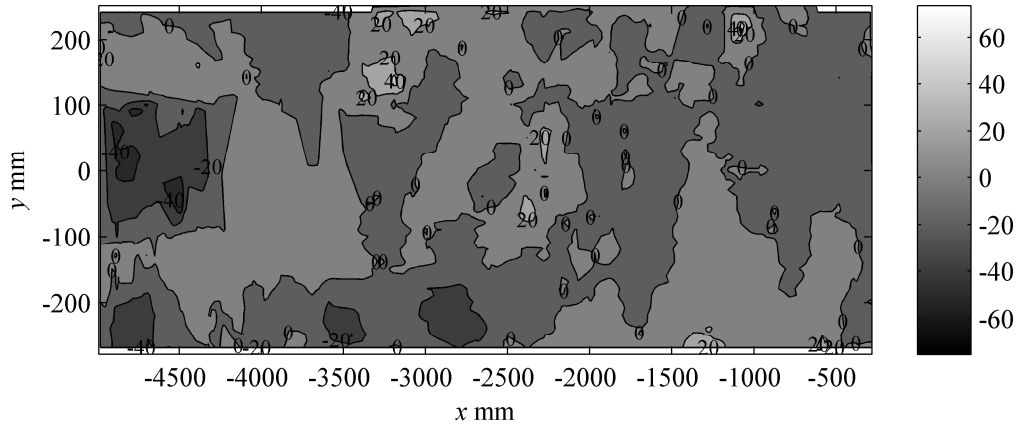


Figure 63 AE-S8 Bottom morphology measured with the sonar profiler, z_{plane} in [mm]

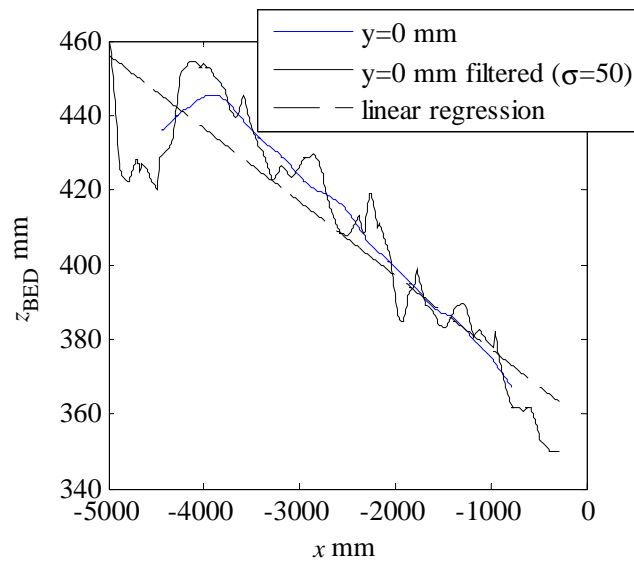


Figure 64 AE-S8 longitudinal section at $y=0$ mm.

6.3.4 Temporal evolution Test AE-S5 (2011 02 09)

In order to understand the temporal pattern of the sediment deposit in a shorter period, the temporal evolution of the sediment deposit interface has also been evaluated at the AE experimental site. Sediment concentrations are reported in Figure 65, together with the particle size distributions of both water sediment and bottom sediments (B.S.).

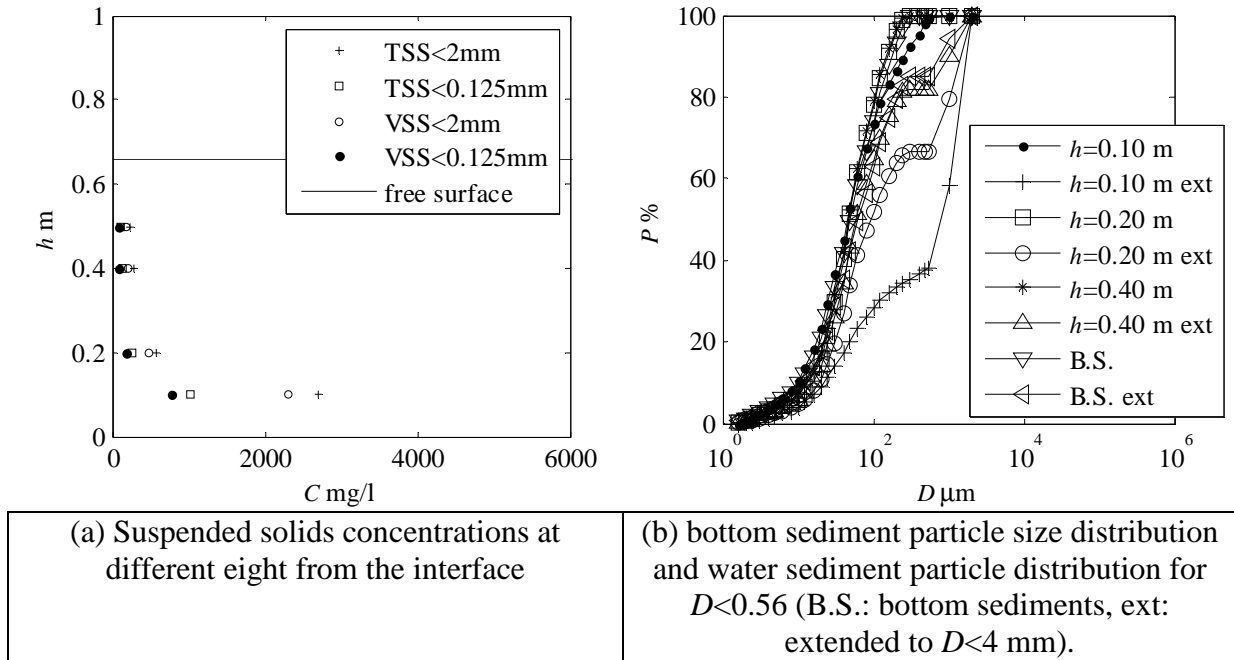


Figure 65 TSS, VSS and particle size distribution conditions of test AE-S4 (2010-02-02)

In this case, the sediment interface has been characterised by the presence of an important mud flow layer over the gross deposit, as can be also observed from the sonar output of Figure 66a, which shows a relatively low ABS with a large depth underneath the sonar. According, the output at $t=12:07$ slight differs in terms of maximum intensity from that observed at $t=8:45$. However, the sediment interface occurs for a larger distance from the sonar centre ($z_{\text{SONAR}}=0$) for $t=12:07$ (Figure 66b).

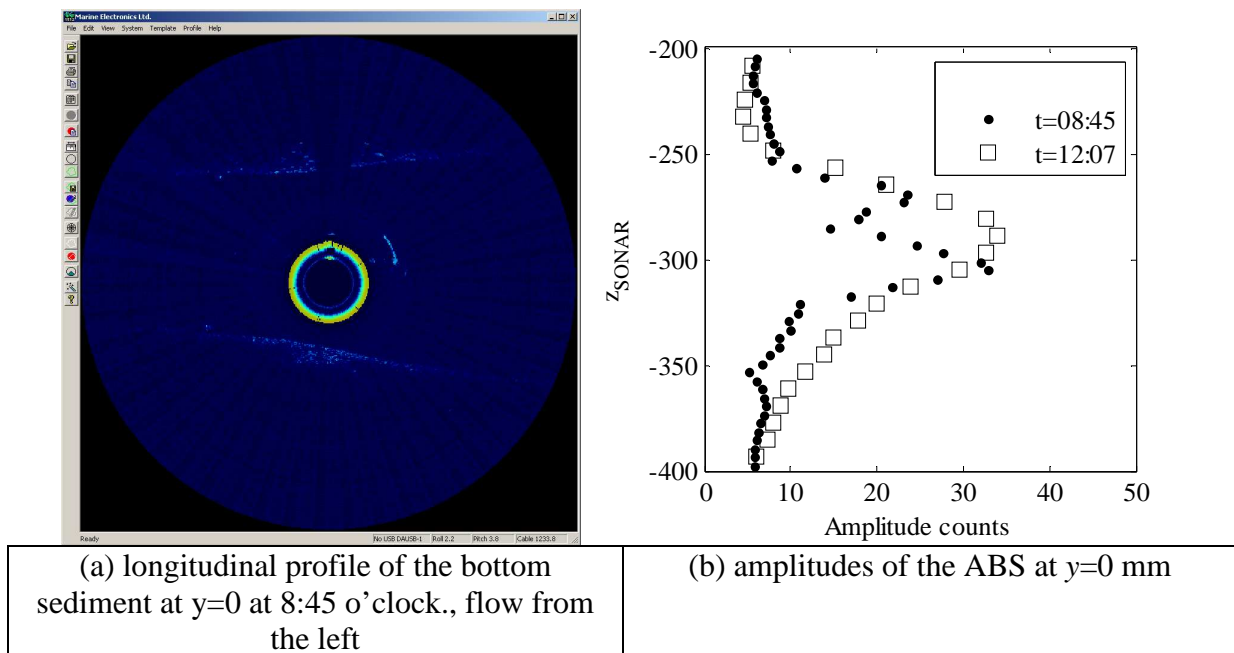


Figure 66 AE-S5 Sonar output

A flow velocity of about 0.056 m/s has been recorder at about 220 mm from the interface. The lower velocity recorder hence seems in connection with the formation of the mud flow layer. Hence, the temporal evolution of the bottom longitudinal profile of Figure 67 gives a first insight of the erosion potential which may occurs during the dry weather day time. Accordingly, sediment are eroded from the through at $x=1000$ mm, while the upstream side of the survey shows constantly the same height.

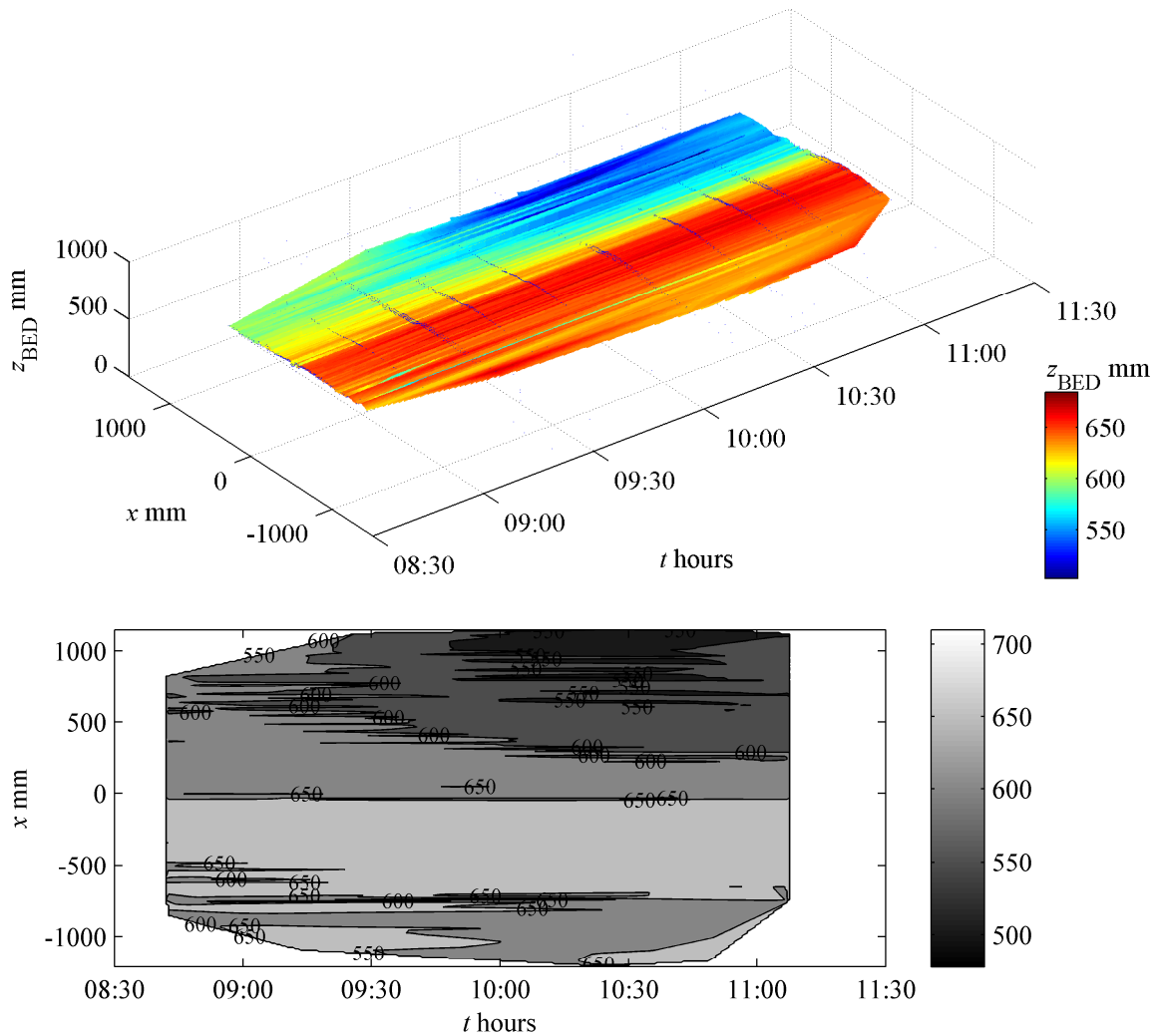


Figure 67 AE-S5 Bottom morphology measured with the sonar profiler from the invert bottom z_{BED} in [mm]

6.3.5 Temporal evolution Test AE-S9 (2011-06-16)

In order to correlated the different flow conditions with the different nature of the sediment interface a survey has been carried out at different moment. These have been chosen in order to observe the sediment deposits early in the night, i.e., 2:00 o'clock, when normally the flow velocity are the lowest which occurs in a combined sewer network, up to 10 o'clock, in order to include the flow velocity peak and the water depth peak.

Figure 68 shows the water depth and the flow velocity recorded with a pressure transducer and flow meter NIVUS which usually gauged the trunk .

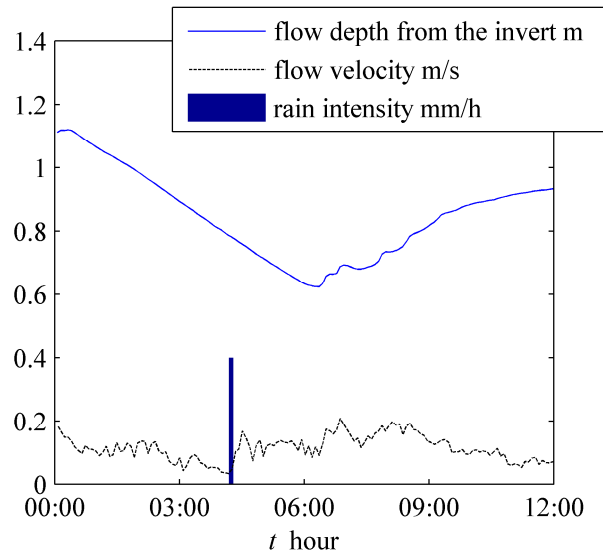
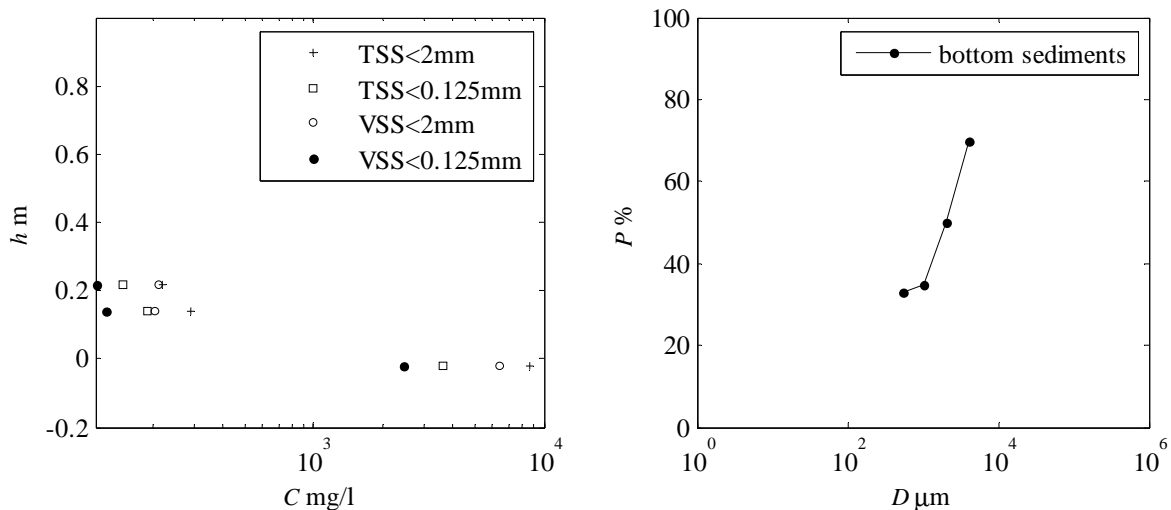


Figure 68 Flow depth, longitudinal flow velocity and rain intensity for the survey period

Figure 69 shows the different conditions in terms of suspended solid concentration observed during the morphological survey (see Table 8).



(a) Suspended solids concentrations at different eight from the interface and for $D < 4$ mm different time (see)

Figure 69 TSS, VSS and particle size distribution conditions of test AE-S7

Table 8 Suspended solids concentrations measured at different times

TSS (mg/L) <2mm	TSS (mg/L) <125 μ m	VSS (mg/L) <2mm	VSS (mg/L) <125 μ m	h (m)	δ (m)	hours
8729	3650	6386	2460	-0.02	0.24	4:35
292	188	204	124	0.14	0.41	8:30
220	146	210	112	0.22	0.49	10:00

Several tests have been carried out in order to analyse the temporal behaviour of the bottom deposits. The analysis of the movement of the sediments during the day time highlights some important features, also regarding the relation between the sediment deposits and the evolution of the velocity and of the turbulence.

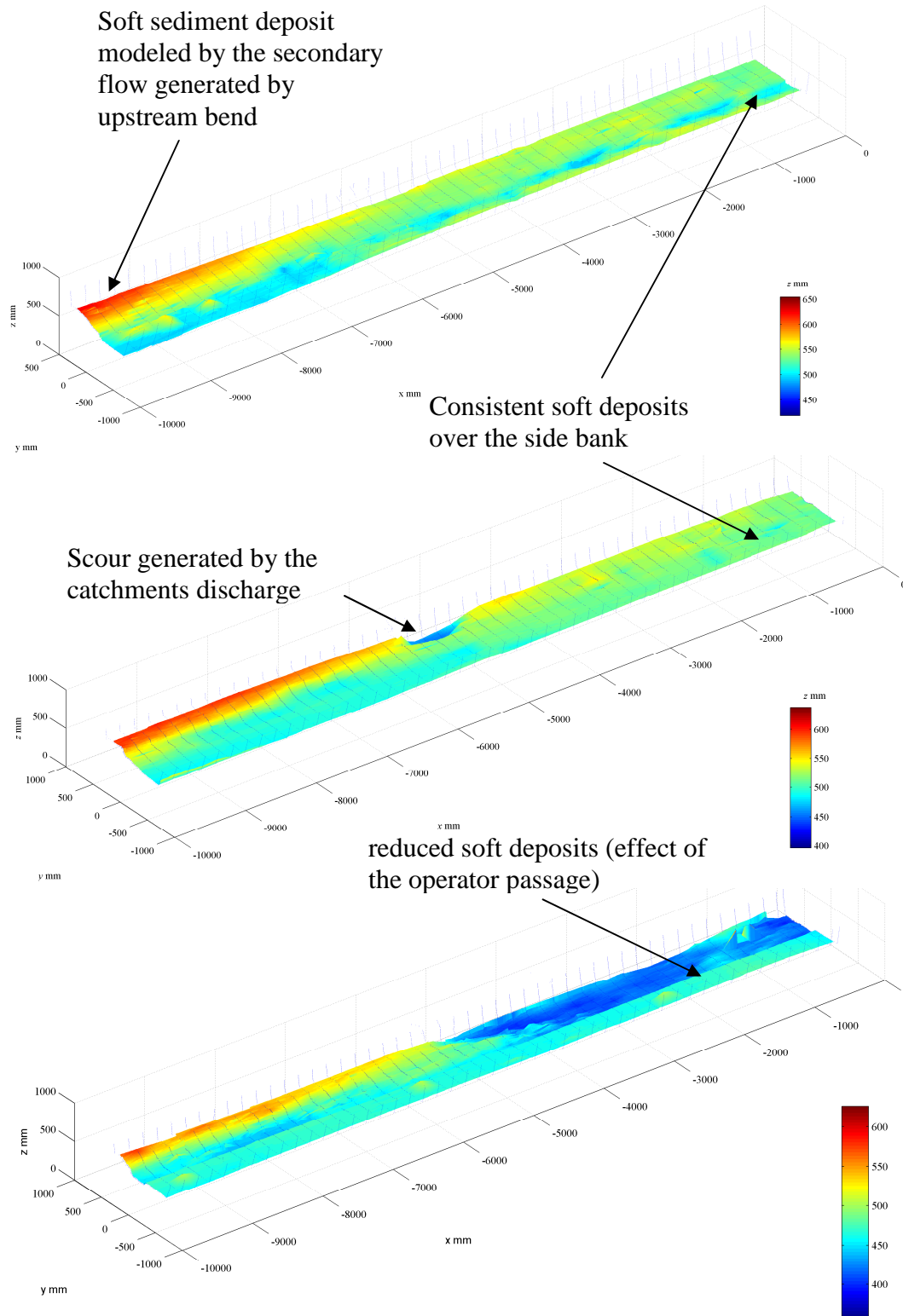


Figure 70 Test S9, Morphological survey, at 2:00, 7:00 and 10:00. Colour shading represents the z elevation in mm from the invert bottom

Figure 70 shows the sediment bottom morphologies measured from the bottom of the invert for three different moments, i.e., at 2:00, 7:00 and 10:00 am. From the image it can clearly possible to observe the differences in the sediments deposits heights. The survey reveals important features:

- 1) A large amount of soft sediments occurs over the side bank, which alter the actual shape of the invert, i.e., the side bank doesn't affect anymore the flow;
- 2) Successively, the sediment and the soft deposits are washed out, resulting in larger erosion near the corner of the side bank;
- 3) The rain event and the concentrated discharge of the gully ($x=-6000$) is responsible of a large erosion, which in the time, further propagates downstream.
- 4) Lower sediment deposits occurred over the side bank.

Previous conclusions are also confirmed by the analysis of the sonar output at two different time (Figure 71 and Figure 72), which show how the mud layer is eroded over both the side bank, and in the central part of the invert, thus leaving only the harder sediment deposits.

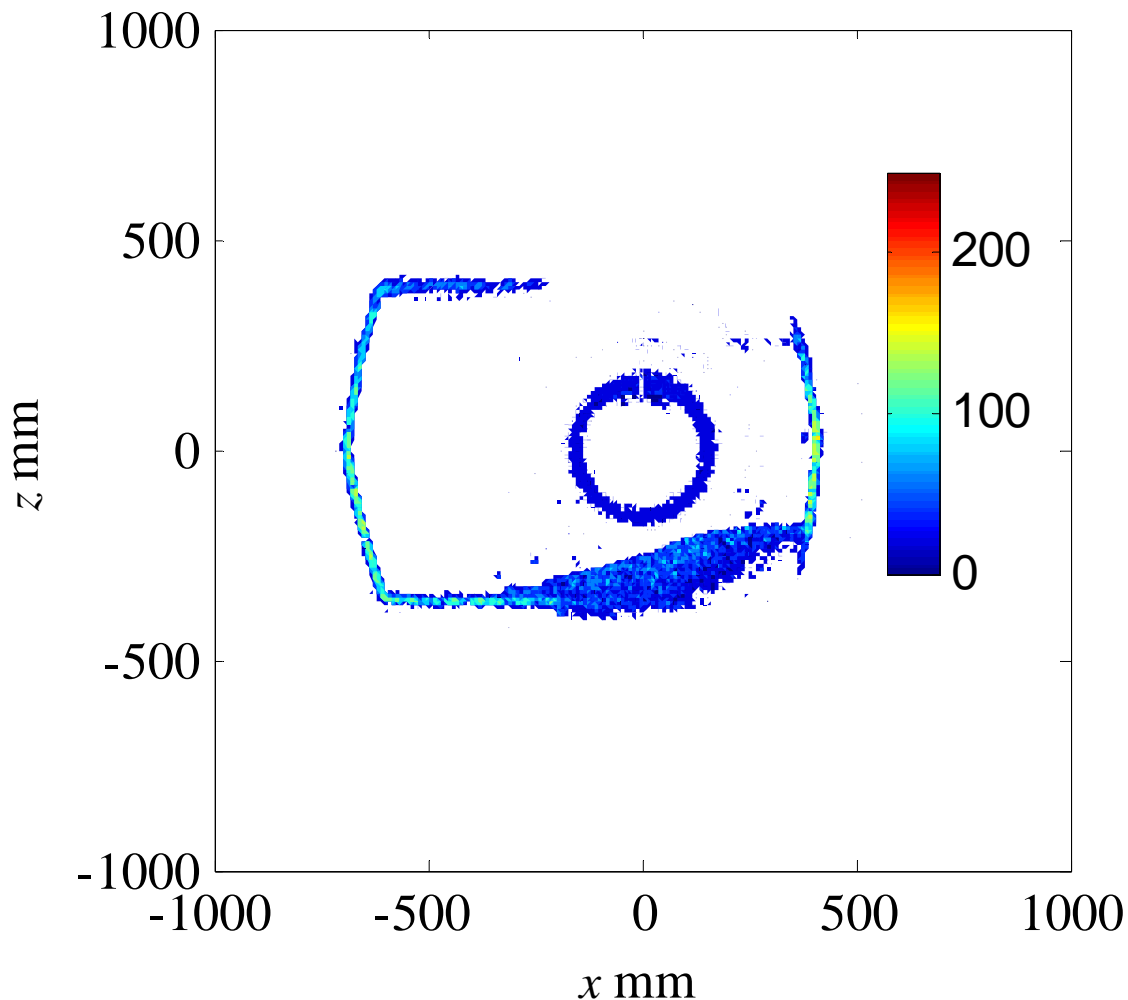


Figure 71 AE S9 sonar output at $t=4:35$ at $x=-9900$ mm, referred toward the SONAR center

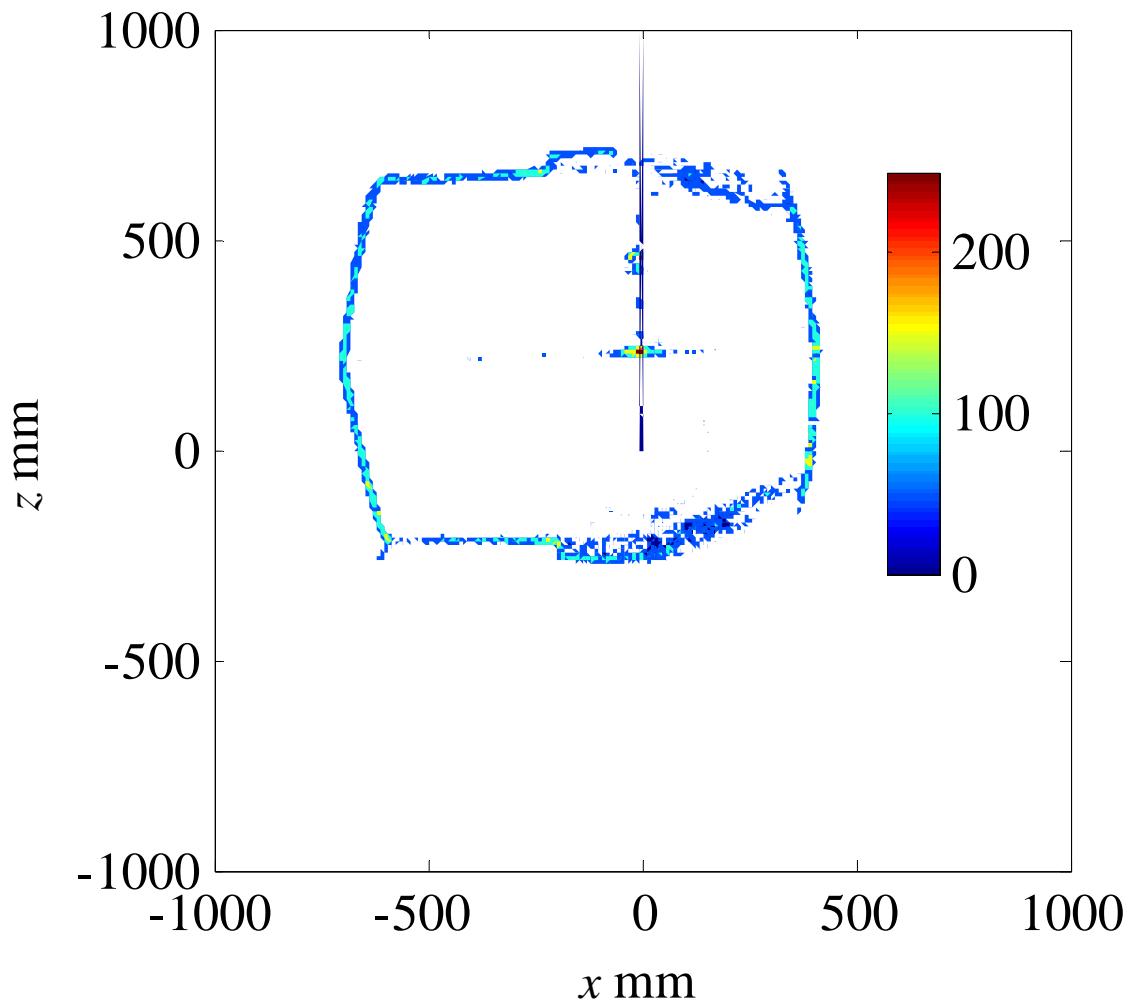


Figure 72 AE S9 sonar output at $t=10:00$ at $x=-9900$ mm, referred toward the SONAR center

The temporal evolution surface and contour line plot in Figure 73 highlights even better the acceleration of the sediment erosion. Indeed, the slope of the contour lines at $z_{BED}=450$ mm, and $z_{BED}=400$ mm represents somehow the sediment erosion rate. As it can be observed, this contour lines (highlighted by the with dashed line) tends toward x negative values, with a slope of the iso-lines which increases with time, revealing a larger erosion potential during the time.

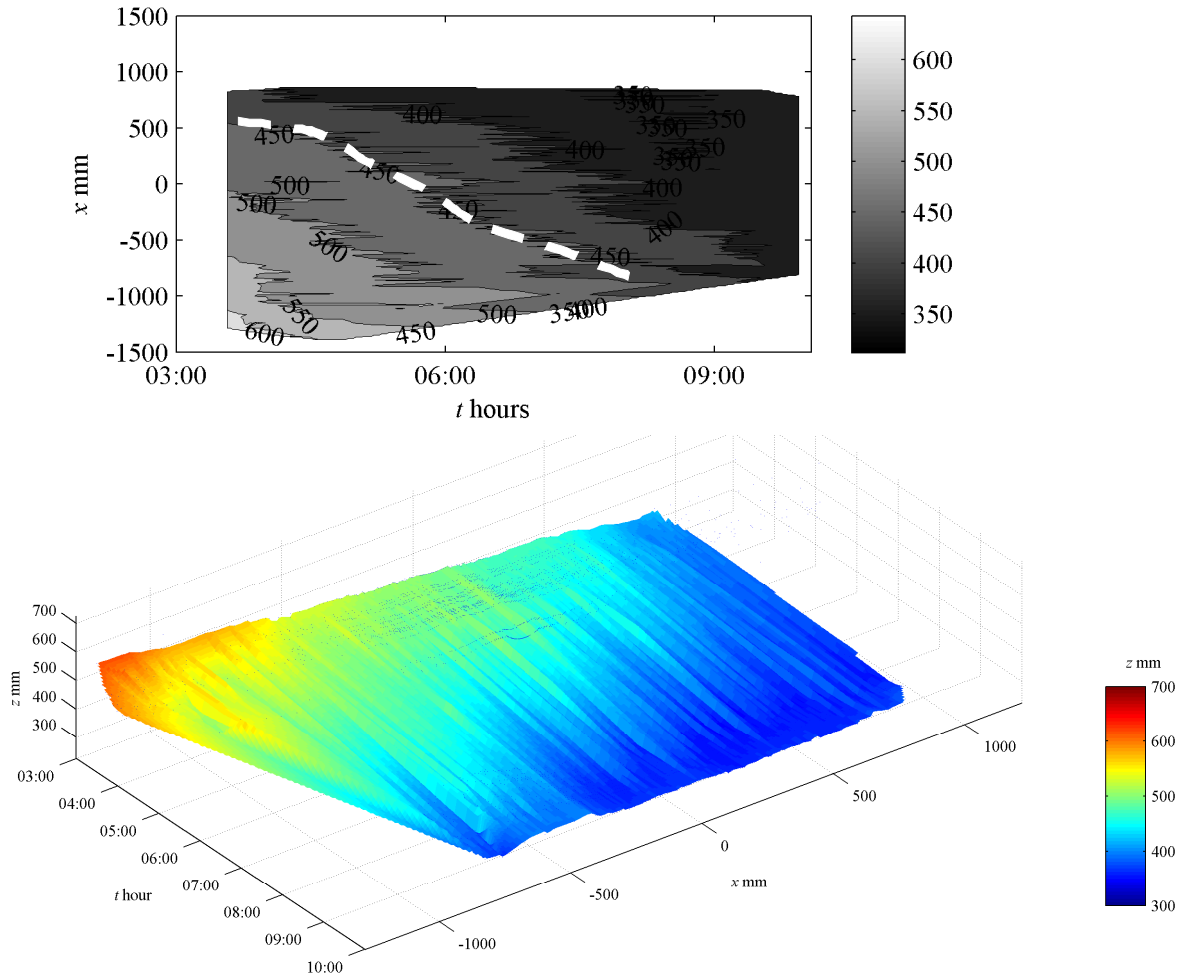
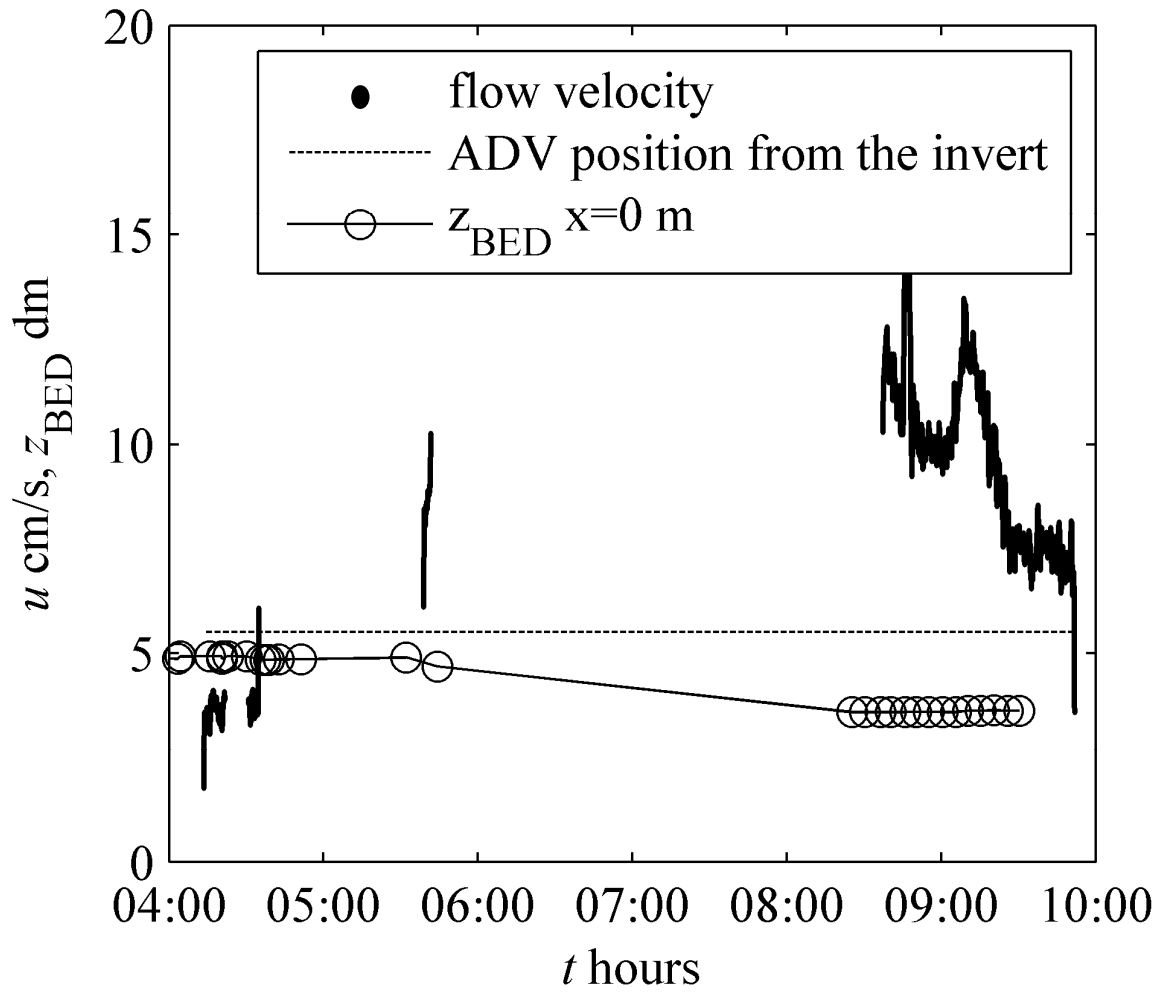
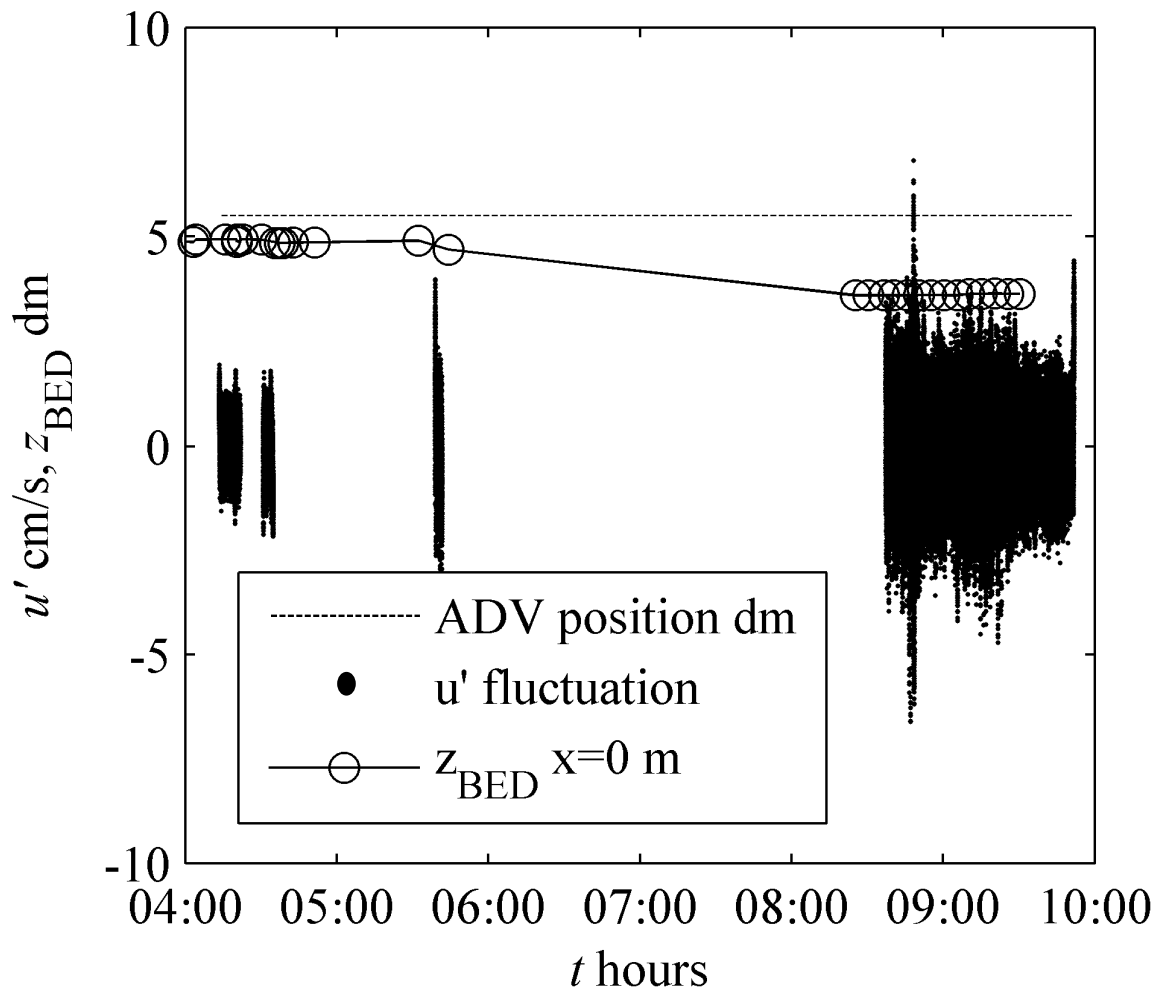


Figure 73 Test AE S9. Bottom morphology temporal survey interpolation (blue dots represent the actual surveyed data). Colour shading represents the z elevation in mm from the invert bottom.

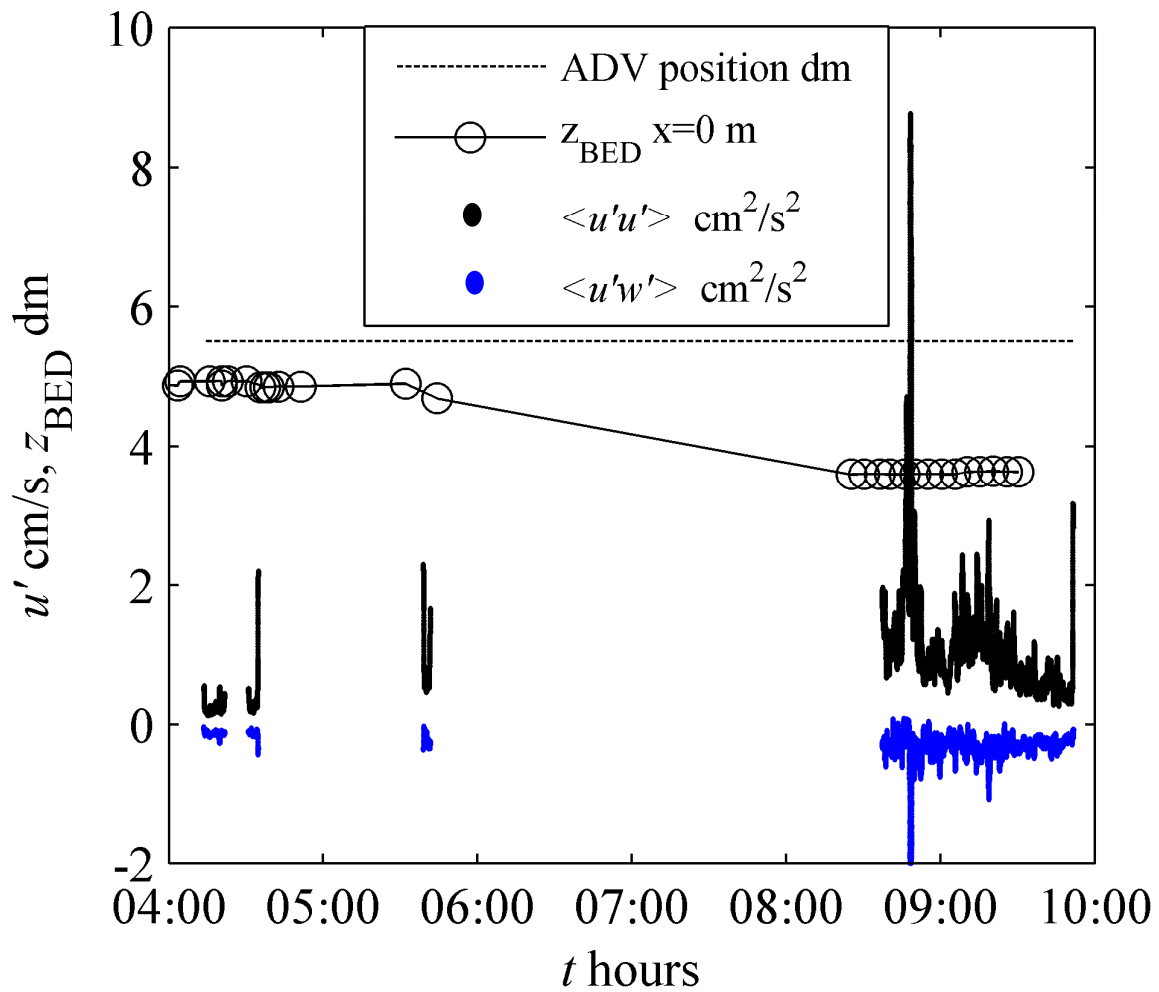
The slope of the sediment erosion and the presence of the mud layer over can, thus, be correlated with the average flow velocity and the turbulence level registered during the survey. Indeed, the velocity measurements of Figure 74, revealed a strong reduction of the sediment bed at around $5:30 < t < 6:00$, in which the flow velocity, flow fluctuations and turbulence intensities increased, compared to the measurements at $4:00 < t < 5:00$. Although starting from $t=8.30$ the flow velocity and the flow turbulence are even larger, the erosion rate seems to reduce, revealing that the mud layer has been previously removed. Thus leaving only deposits characterised by a higher resistance.



(a) average flow velocity (5 minutes average)



(b) flow fluctuation from the average flow velocity (5 minutes average)



(c) turbulent intensity and Reynolds stress from the average flow velocity (5 minutes average)

Figure 74 Instantaneous longitudinal flow velocity and turbulences recorded during the morphological survey at section $x=0 \text{ m}$.

6.3.6 Flow field Test AE-S2 (2010-11-26)

The plot in Figure 75 shows the concentration measured at the $x=0 \text{ m}$. Unfortunately, pipes clogging occurred at the time of measurements and only one point showing a concentration of about $C_{\text{TSS2}}=350 \text{ mg/l}$ has been measured. However the clogging of the pipe may suggest that a hyper concentrated layer above the tough sediment bottom was present (a lutocline).

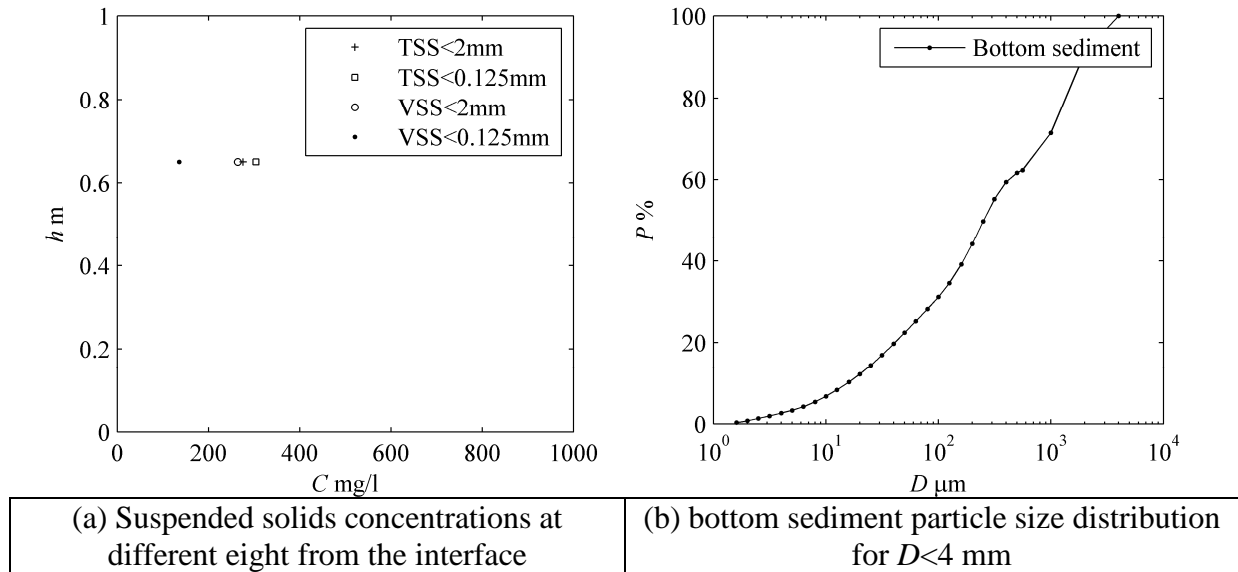


Figure 75 TSS, VSS and particle size distribution conditions of test AE-S2

Sonar measurements finally revealed (Figure 76 and Figure 77) that the mud flow layer can't totally be penetrated by the sonar pulse but a rough estimation of mud flow thickness can be obtained by means of the gauge estimation and sonar evaluation. However, it seems that the solid deposits are "hindered" by the presence of mud flow (see fig. 14), as the black spot (●) lies far underneath the "interface measured by the sonar."

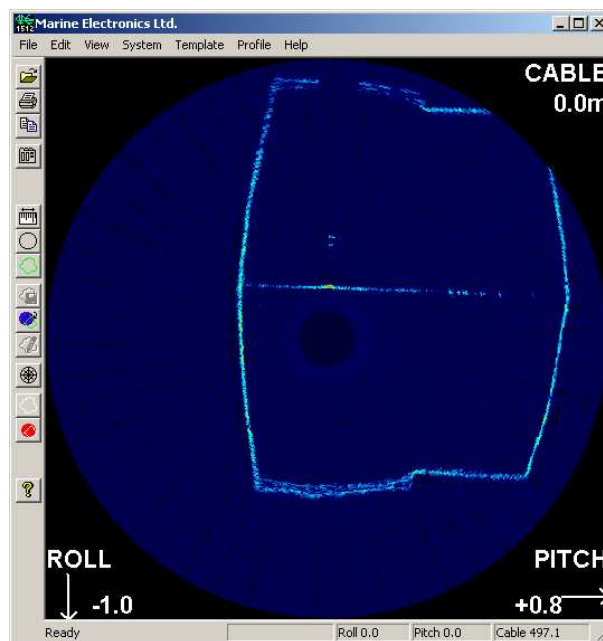


Figure 76 AE S2 model set-up pipe profiler output.

In order to understand the efficiency of the sonar, measurements at constant height but different pulse lengths have been carried out. In the two plots of Figure 77, it can be observed that generally the concentrated flows show a higher backscatter compared to that of the diluted flow. However both plots (pulse length of $4 \mu\text{s}$ and $20 \mu\text{s}$ respectively) show that slight differences occurs in the localisation of the high backscatter portion, and hence in the localisation of the mud flow

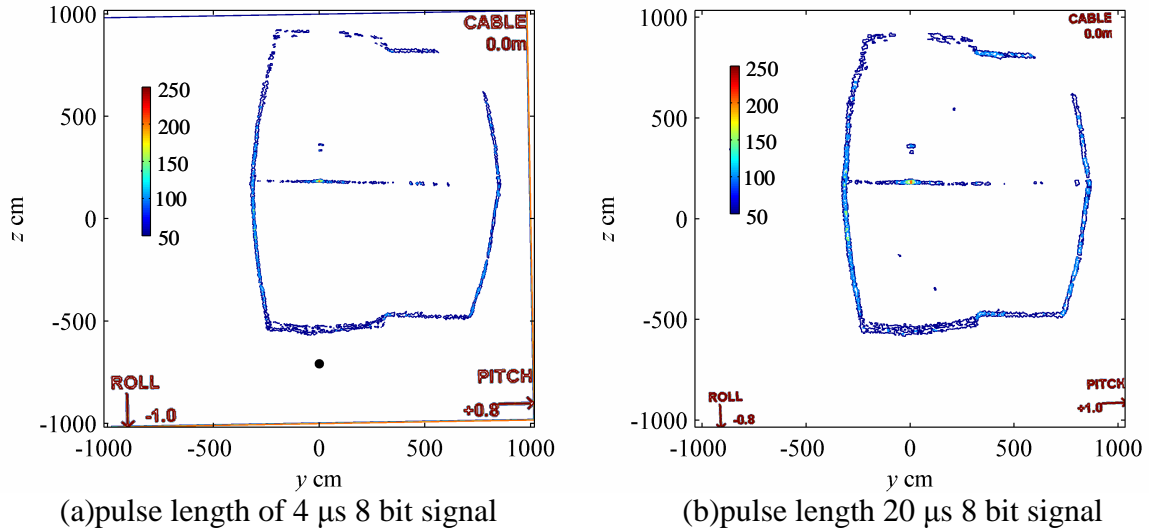
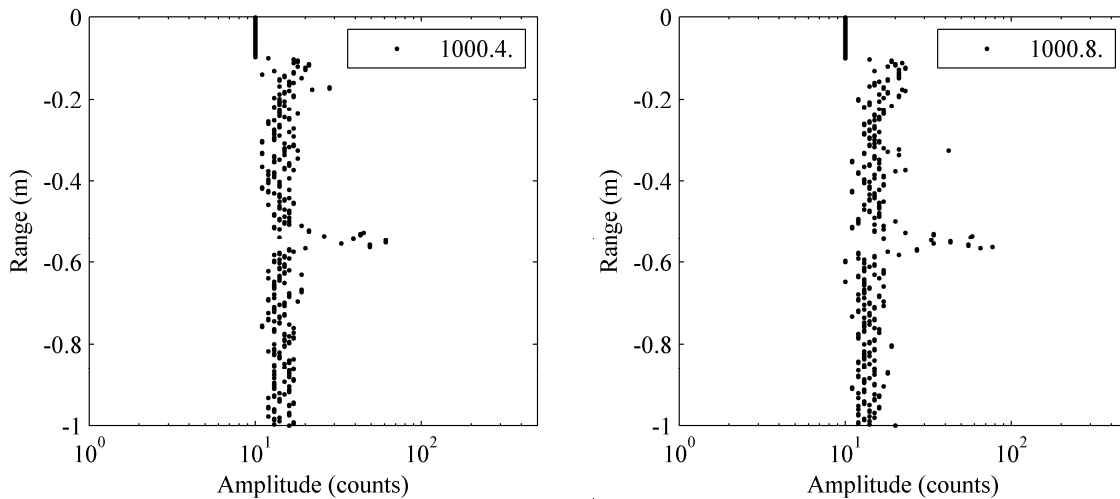


Figure 77 AE-S2 data.output; the contour lines represent the 8 bit signal amplitude (coloured scale from 0 to 256 counts) observed by the sonar, (●) gauge position.

Data have been also plotted for the vertical section below, i.e., $y_{\text{SONAR}}=0$ m to understand the effect of the pulse length on the backscattered amplitude measured with the sonar. Data shows almost the same values both in terms of backscatter in the water column were the sediment concentration was almost constant. It also worth observing the different shape the interface echoes shows compared to that generally observed in DA tests, in which the sharp interface observed in presence of mineral sediments becomes larger and of reduced amplitude.



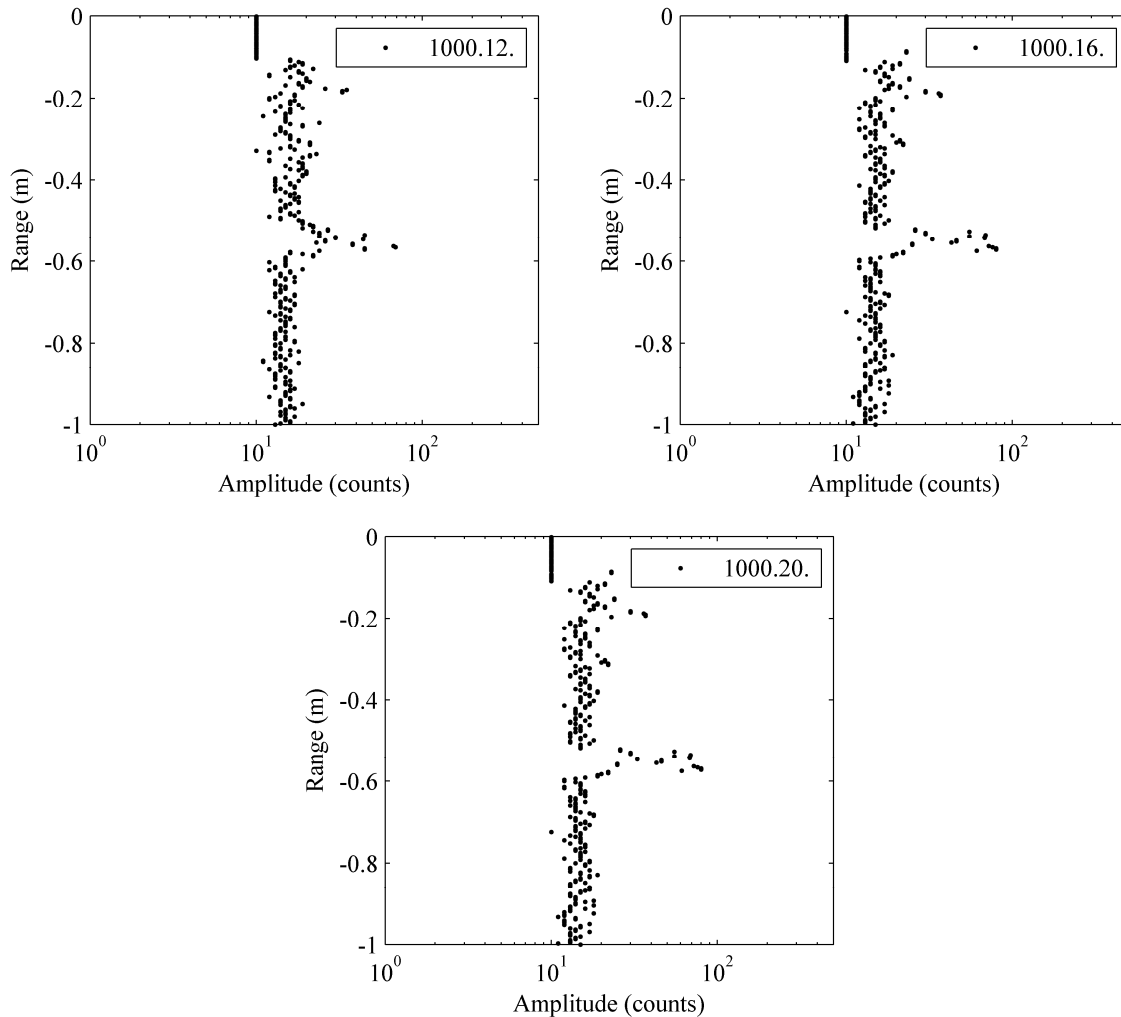


Figure 78 section $y=0$ m, AE S2 data for pulse length of $4 \mu\text{s}$, $8 \mu\text{s}$, $12 \mu\text{s}$, $16 \mu\text{s}$ and $20 \mu\text{s}$ (legend represents the range and pulse length).

Coupling both sonar measurements and ADV, it is possible to refer the ADV measurement both toward the free surface, the bottom of the sediments or the bank. At the time of velocity measurements, the water depth was about 640 mm (over the bank)+ $450 \text{ mm} = 1090 \text{ mm}$ from the concrete bottom and considering a sediment elevation of about $z=0.21 \text{ cm}$ the value from the sediment bottom will be of $\delta=0.88 \text{ m}$.

Data from ADV measurements are plotted in the Figure 79. In this case h has been fixed as the distance between the control volume and the sediment bottom (“mud flow interface”) individuated by the sonar, which, however, does not coincide with the hard sediment bottom as shown in Figure 77. The main purpose of referring h toward this values is to understand immediately wheatear the measurements have been taken underneath the interface individuated by the sonar or close to this interface. Indeed, it can be inferred that, although the mud flow participates to the total discharge, this latter differs from the outer portion of the flow both in terms of fluid (much more viscous, different behaviour in terms of friction, probably not Newtonian) and momentum exchange. Moreover it can be believed that different momentum exchanges can be observed toward the interface as well as the turbulence structure could behave differently in terms of ejection and sweep event probabilities.

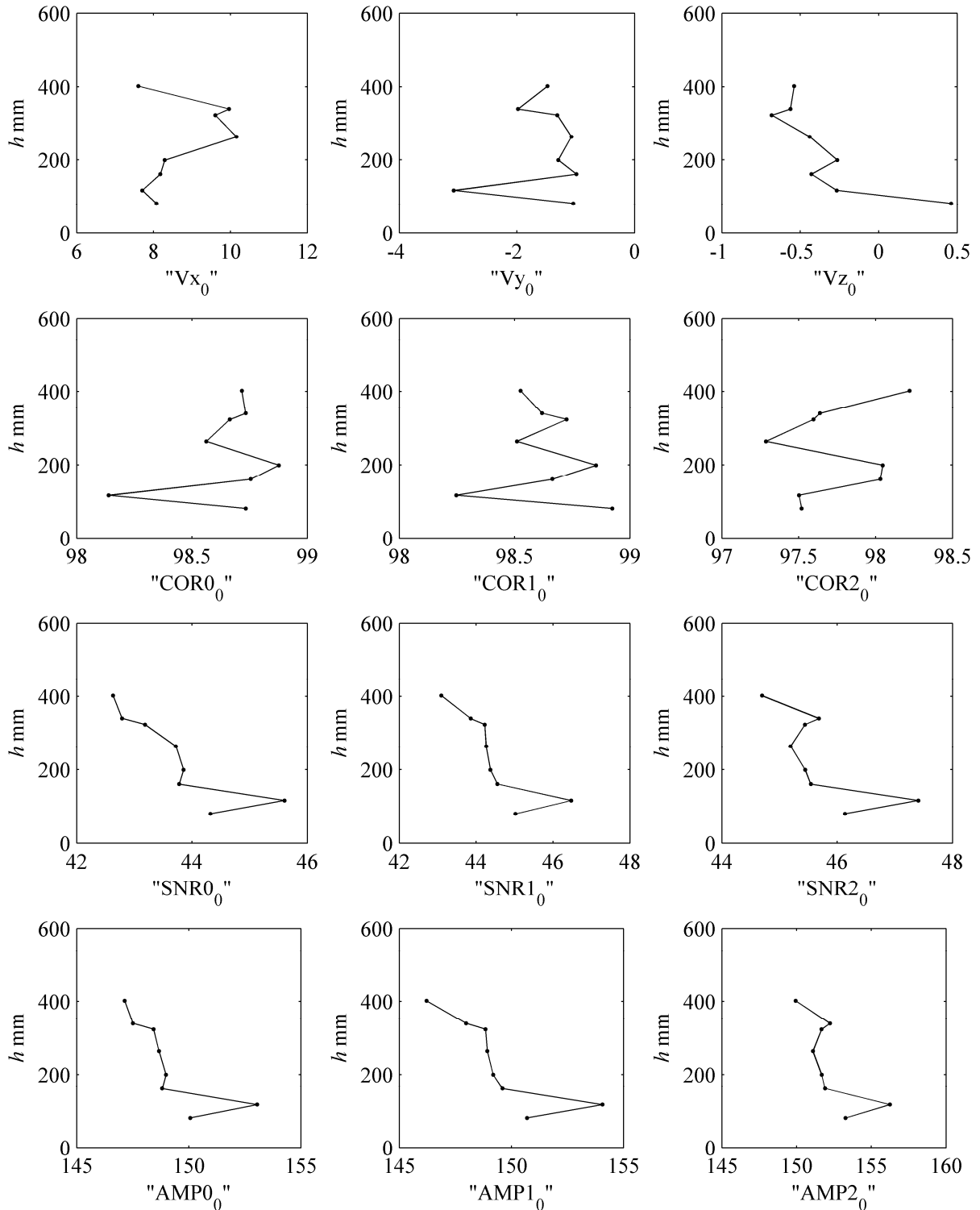


Figure 79 AE S2 model results from the filtered ADV readings (of which generally more than 95 % were considered good): (a-c) V = velocity cm/s, (d-f) COR= signal correlation %, (g-i) SNR= sound to noise ratio, db, (l-n) AMP= backscattered signal amplitude of the control volume, counts. Note: 0=beam 0, 1=beam 1, 2=beam 2

In the figure xx, the u velocity profile shows lower values of the velocity near the free surface ($h=300$ mm, $\delta=880$ mm), while tends to grow irregularly near the centre and than they reduced again toward the sediment bottom. Interestingly, the data shows a constant velocity value between 0 mm $< h < 200$ mm, whilst the velocity profiles shows an unusual convexity

compared to that of the logarithmic law profile, characteristic of free surface flows. However, although the sidewall effect could be strong in the present conditions, some doubt on the velocity profiles are especially linked to the presence of the bars over the profiler, which might have somehow modified the velocity profile⁵. Correlations from the three beams shows rather high values (98%) with small oscillation toward the values. This revealed a strong accuracy of the velocity measurements and that in any case the ADV beams have never been clogged by floating material and remained clean. The analysis of the backscattered amplitude profiles shows a general growth of the amplitude, hence linked to a growth of the sediment concentration toward the bottom. A drop of the amplitude can be observed at about $h=120$ mm, probably indicating a drop in the sediment concentration. However the successive data shows a relatively lower signal. This can be explained into two ways: a) the observed signal was not corrected, b) in presence of a concentrated layer, such in hard bottom, if the control volume is buried too much underneath the interface, the signal is absorbed by the layer above the control volume (as observed in the SONAR signal vertical backscatter profiles)⁶. The Reynolds stresses have been calculated based on the experimental data obtained from the measurements, together with the turbulence intensity (Figure 80).

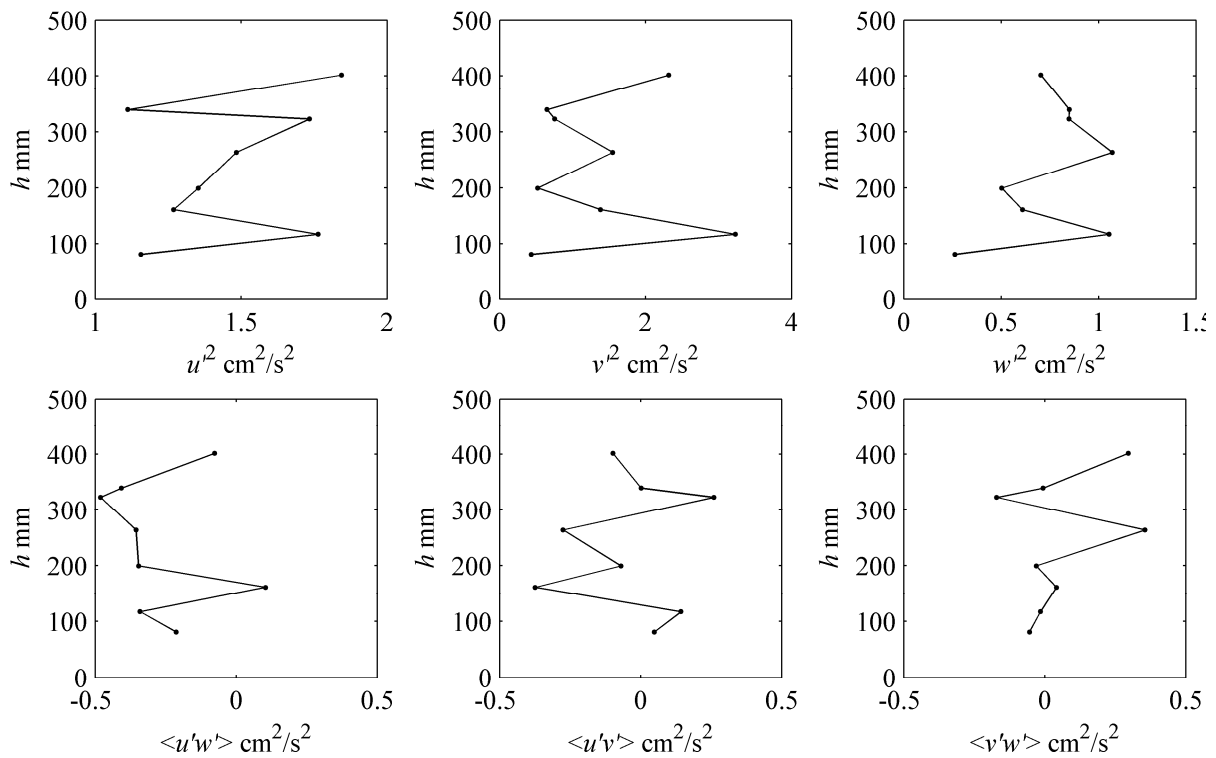


Figure 80 AE S2 model results from the filtered ADV readings (of which generally more than 95 % were considered good): test over field sediments; variation toward the water column of the Reynolds stress.

Vertical exchange of the longitudinal momentum are referred to as $\langle u'w' \rangle$ (Figure 80). Data have been measured only for 60 second. Hence turbulence properties might present some inaccuracy due to the short survey duration. The values observed in the lower portion, apart

⁵ Interestingly, the second series of profile collected at the same place shows a similar results. Is that a consequence of the presence of the sheet flow ?

⁶ The analysis of laboratory data over ground sediment shows a similar pattern when the control volume is deepened inside the layer. It is also worth observing that the ADV and the sonar operated at two different frequency and that the “interface” which can be individuated is rather different (ADD US AMRY REFERENCE ON LUTOCLINE)

from the point at $h=150$ mm, shows almost constant values, up to $h=270$ mm, of about $\langle u'w' \rangle = 0.37$, then the stresses increased toward the free surface and again reduced for $h=400$ mm. Turbulence intensities u' , v' and w' all shows rather contradictory values, and more in general a growing dependence from h . This suggest that in general the measured portion of the flow is governed by viscous forces, rather than from inertial ones, as in general, both turbulence intensity and vertical exchange of the longitudinal momentum decreases in the zone dominated by the gravity force.

Normalized vertical distribution of stress terms are shown in the following Figure 81, were u^{*2} could be defined from the hydraulic radius calculation i.e., $u^{*2} = (gRS)^{0.5}$ or, since the energy slope cannot be deduced only from one section, from the velocity profiles slope in the inner flow. From the previous profiles, excluding the velocity toward the bottom, a value of about $u^{*2} = 0.99$ cm/s can be obtained. Note that $\delta = 880$ mm is the water depth from the sediment bottom measured with the sediment gauge.

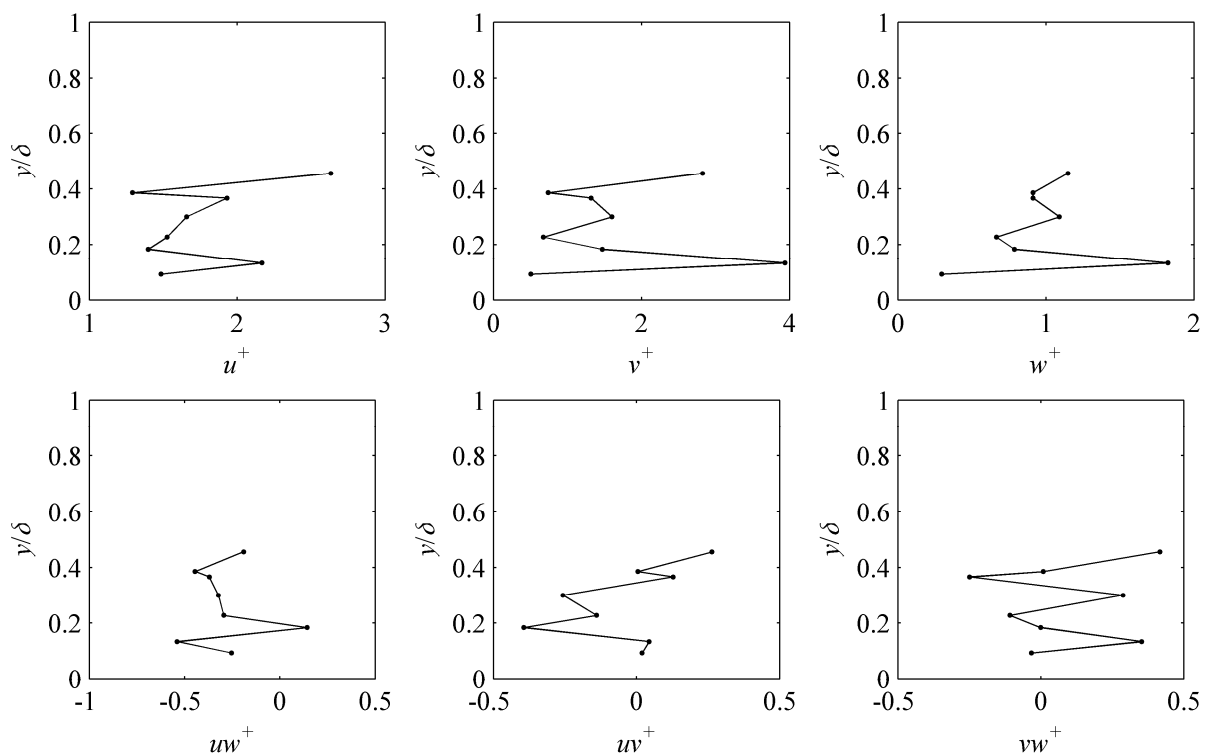


Figure 81 AE S2 unfiltered data normalized turbulence characteristics

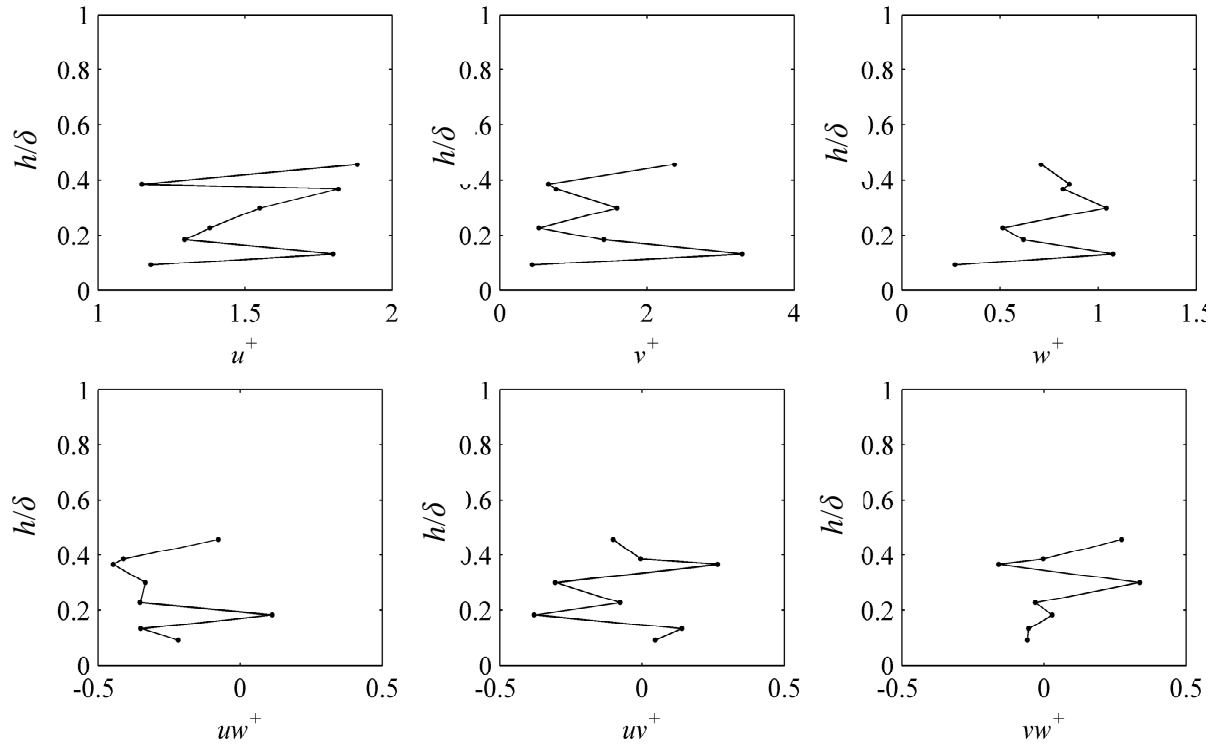


Figure 82 AE S2 filtered data (Whal 2003 algorithm) normalized turbulence characteristics $u^*=0.99$ cm/s and $\delta=0.88$ m.

The comparison between filtered (Figure 81) and unfiltered (Figure 82) data shows that, in general, the unfiltered one are slightly biased by the presence of spikes into the velocity series, as also in general confirmed by the correlation data⁷.

6.3.7 Flow field Test AE-S3 (2010-12-15)

The second test carried out at the AE site with the SON-ADV application (AE-S3), presented a water depth from the sediment bottom of $h=0.61$ m and a sediment height of $z_{SED}=0.34$ m. The TSS and VSS measured at the section $x=0$ m together with the particle size distribution are shown in the Figure 83a-b. Accordingly, the flow was heavily charged, with point of $C_{TSS2}=7500$ mg/l at 20 cm from the bottom. Particle sizes of suspended solids for $D<0.560$ mm perhaps shows similar distributions toward the water column (Table 9).

⁷ However the analysis of the spectre should be carried out to characterised the dissipative properties of the measured data and whether a with noise can bias the data or not.

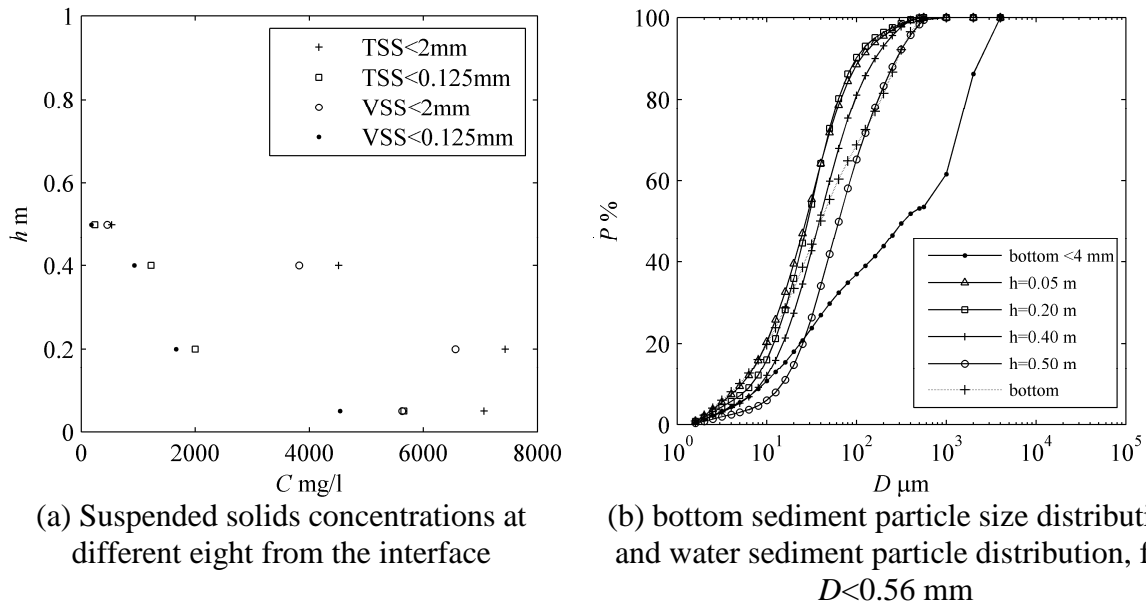


Figure 83 TSS, VSS and particle size distribution conditions of test AE-S3 (2010-12-15)

In general, the particle sizes tend to reduce toward the sediment bottom, while the bottom sediments for $D < 0.560$ mm show averaged particle sizes larger if compared to that of the suspended solids (D_{50} in Table 9).

 Table 9 Particle size distribution summary in [μm]

Sample	D_{10} %	D_{50} %	D_{90} %	D_{95} %
B1 $h=0.05$ m	5.33	27.10	110.66	184.95
B3 $h=0.20$ m	6.86	28.51	98.33	159.12
A3 $h=0.40$ m	8.63	38.35	160.10	236.10
A4 $h=0.50$ m	14.95	63.01	278.02	378.84
Bottom	4.98	39.76	286.76	364.15
Bottom AE < 4mm*	9.27	327.12	2287.49	2894.43

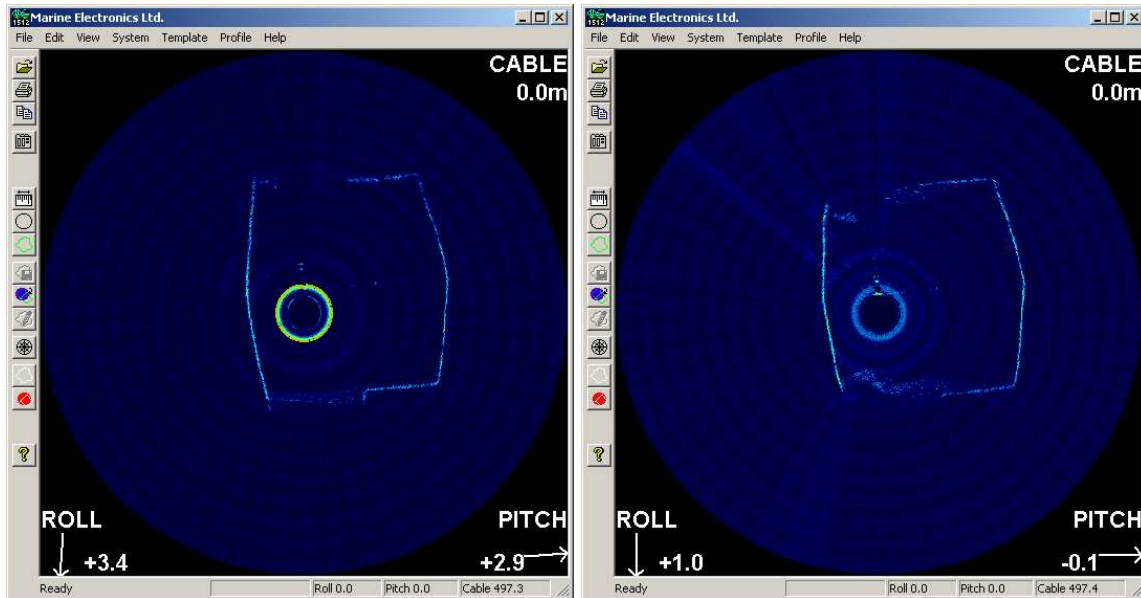
In summary they have been measured:

- 5 sections (transverse profile) with the sonar at $x=-0.5$ m (sec.1 in the folders) m from the sewer access and then each 1 m downstream.
- 3 vertical velocity profiles with the ADV
- 1 longitudinal profile at the section $x=-0.5$ turning the probe 90 degrees clockwise
- Sonar measurements of the sheet flow (mud flow or lutocline) in presence of the sediment gauge .

It is worth observing immediately that, differently from the previous campaign made at the same location, the SONAR profiler shows a strong noise toward the centre of the instrument. This could create strong incertitude when the sediments or the bottom are inside the noise. This problem are generally linked to the power supply. However, the noise presence slightly affects the ABS in the region outside the noise.

The analysis of the “interface” detected by the SONAR at $x=-0.5$ m ((a) section 1 ($x=-0.5$ m)
 (b) section 2 ($x=-1.5$ m)

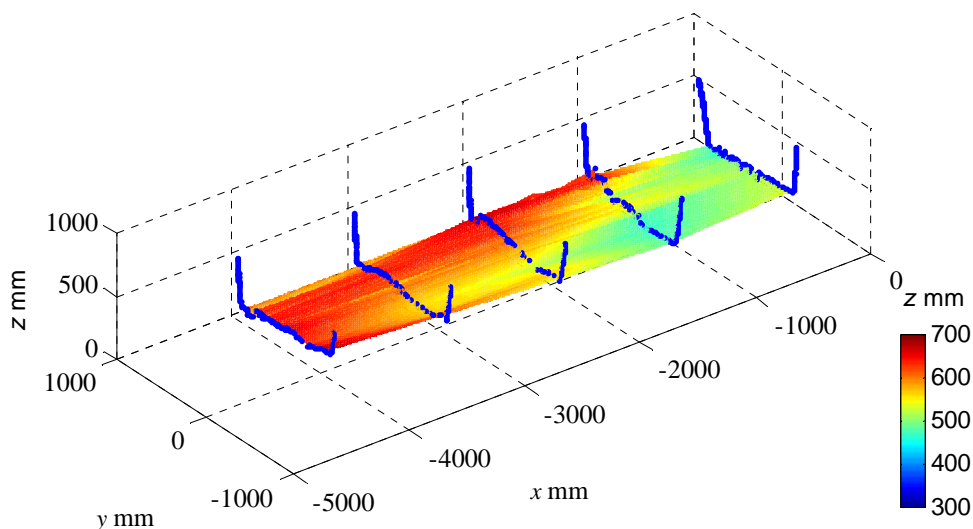
Figure 84) shows a fuzzy interface, in which again the sheet flow seems to hinder the hard sediment bottom. The level detected by the profiler at that section is clearly underneath the side bank, whilst the image at section $x=-1.5$ m the “interface” start to change shape, as if its thickness increased downstream.



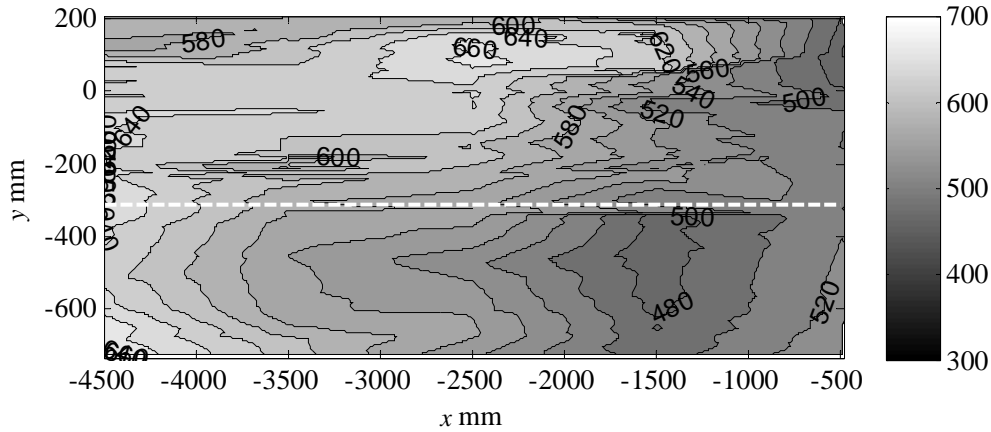
(a) section 1 ($x=-0.5$ m) (b) section 2 ($x=-1.5$ m)

Figure 84 AE transverse profile sonar output

The elaboration of the profiles detected by the sonar is shown in Figure 85. In this plot, the interface has been defined starting from the invert bottom. The profile clearly shows how the interface tends to grow downstream. Indeed part of the sheet flow has been also observed over the side bank ($x=-2.5$ m, $x=-3.5$ m, $x=-4.5$ m).

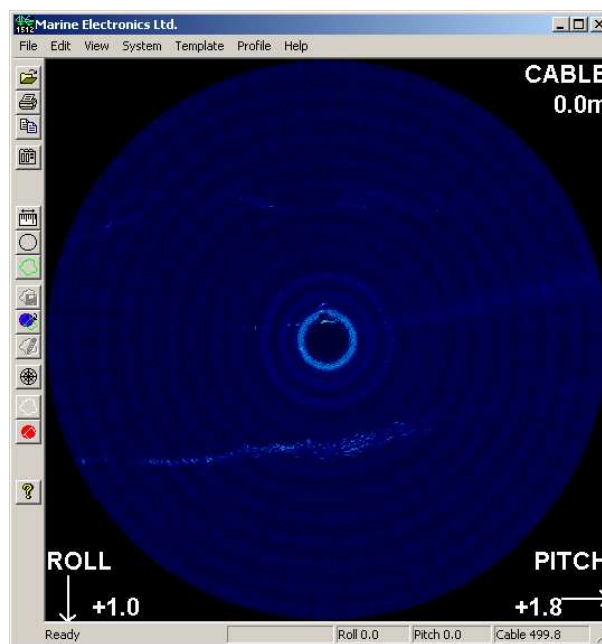


(a) “interface” morphology detected from the SONAR, data from transverse sections (·)

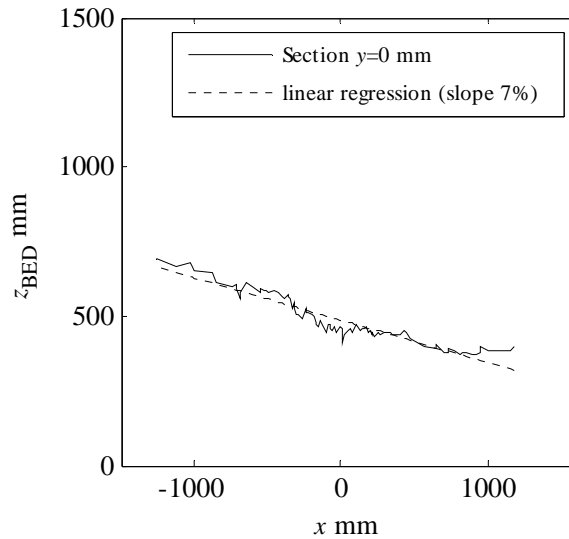


(b) sediment interface contours lines (side bank position,----), grey scale z_{BED} in mm
Figure 85 Test AE-S3 bottom morphology

From the survey it is possible to observe that larger sediments deposits occurs on the left side of the channel, with height which may exceed the side bank height. This phenomena might be consequence of the secondary flow generated by the bend upstream the surveyed section. The longitudinal survey, carried out turning the SONAR head of 90° CW (clockwise) shows the acoustic backscatter for the bottom sediment, in which the flow is directed from the right. The data observed again shows the presence of an interface which presented a faint acoustic backscatter. Indeed, also the sheet flow has its own morphology and variation which might be linked to the hydrodynamic conditions.



(a) AE-S3 original sonar output, longitudinal profile at $x=0$ m (ABS strength quite under 50 counts)



(b) longitudinal profiler from referred from the invert bottom, average slope 7%
Figure 86 AE longitudinal profile at $x=0\text{m}$, sonar output, flow from the right.

Moreover, the sediment deposits show, in the centre line of the dry weather channel, i.e., $y=0$ mm, a slope which is larger compared to that of the invert (about 7%, Figure 86). However, this might be a part of a longer bed forms structure, as the survey has been limited to only 2 m longitudinally for this latter and to 5 m for the former survey. The longitudinal section is characterised by an average bed forms eight of about 50 mm and average wave length of 200 mm.

Sect.1 ($x=-0.5\text{m}$)

Data obtained for the first surveyed section $x=-0.5\text{m}$, shows rather small backscatter amplitude compared to hard bottom (Figure 87), demonstrating the presence of the mud layer or more in general of a drop in the concentration (lutocline). Indeed, since the lutocline is made of soft sediment, this latter is able to absorb the signal but still presents a small backscatter. However, observing the TSS, there is not a clear correspondence between the acoustic backscatter and the TSS of Figure 83, most likely due to the suction of a lower level of sediment operated by the suspended solid sampler.

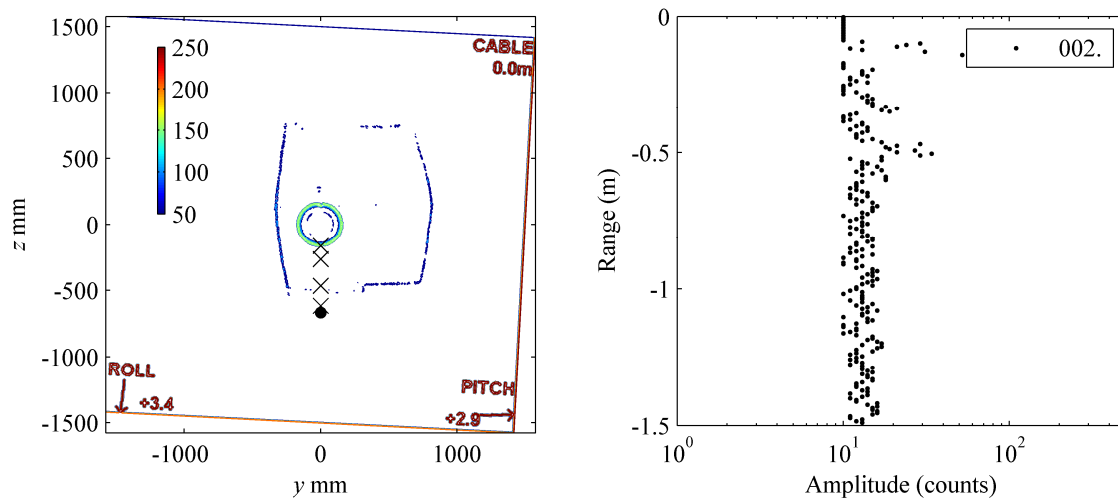


Figure 87 (a) AE transverse profile at $x=-0.5\text{m}$, (●) gauge position, (×) TSS sampler positions, (b) vertical amplitude profile at $x=-0.5\text{ m}$.

In the figure xx the crosses represent the point at which the sampler pipes have been located, while the big black spot represents the location of the gauge (the hard bottom). Hence, it is possible again to observe that the soft deposits hind the hard ones, and that the sampler pipes might fall well underneath the mud layer.

The graphs in Figure 88 show the ADV data for the sect.1. In this case the reference level has been taken as the bottom profile detected from the sonar. This has been done in order to understand how much the ADV was far from the interface measured with the sonar, and in order to understand the acoustic backscatter from the ADV. The distance between the nominal sediment interface and the free surface was about 600 mm. Accordingly the velocity profile shows almost a linear pattern, whit some noise toward the sediment bottom. Interestingly, the acoustic response of the ADV is constant, while, as it approaches the mud flow, the amplitude shows a strong drop, most likely linked to the fact that the water shows high sediment concentration near the bottom⁸. It is worth observing that the probe was always moved from the free surface toward the bottom. However, when the average velocity was about to be zero, the operator was asked to rise the probe of about 2.5 cm. Hence, it might be possible that the drop in the ADV acoustic profile is connected to the fact that the probe has interacted with the sheet flow, leading to the intrusion of less concentrated water into the sheet layer. At the same time, the vertical w velocity the transverse one v shows slight variation toward the zero, indicating that both the influence of the probe on the vertical velocity could be neglected and that the probe was at the centre of the channel. However, small variations could be also connected to the probe orientation. Correlation profiles show rather good results, with values always of 99% for the three beams.

⁸ they still have to be compared with the MES data in the discussion section

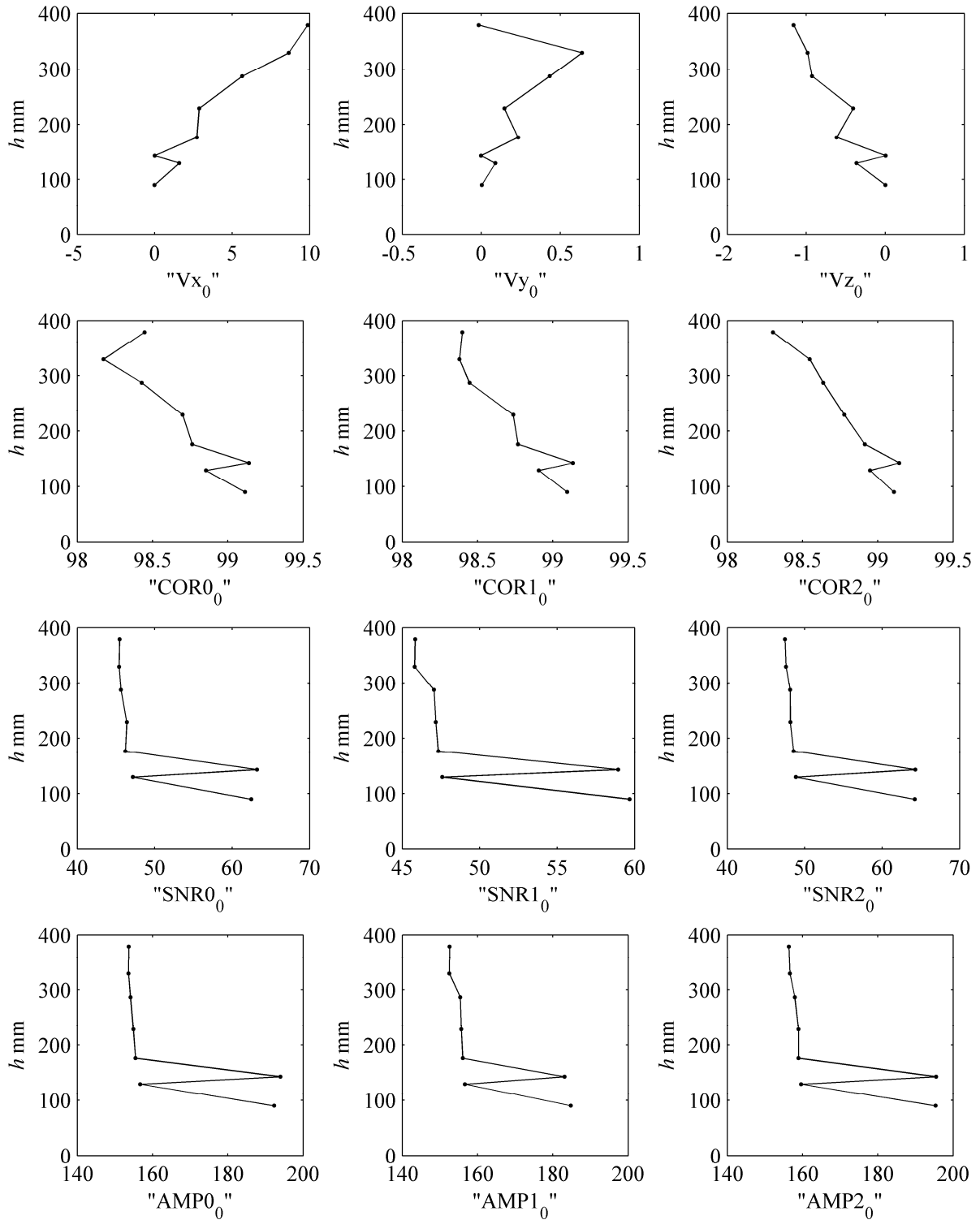


Figure 88 AE sect.1 averaged ADV data.

The longitudinal turbulent intensity shows some interesting results. From theoretical considerations, both the turbulence intensity u' and shear stress $\langle u'w' \rangle$ in the outer layer should be reduced from the free surface toward the sediment surface. The pattern shown by in Figure 89 clearly indicated that in the region near the sediment surface and near the sheet layer is almost in transition conditions rather than turbulent. However, also a dumping effect of the turbulence could be related to the high sediment concentration measured by the sampler.

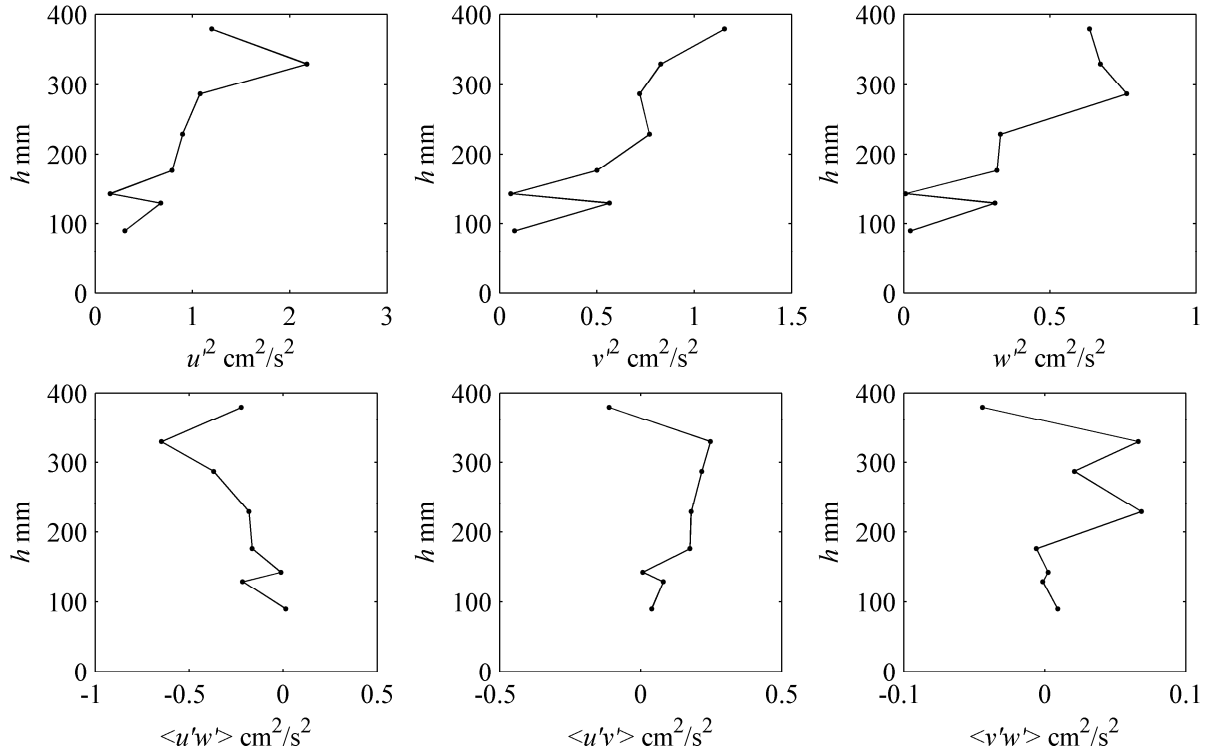


Figure 89 AE sect.1 Reynolds stress

In this case, in order to normalise the Reynolds stresses, since the water depth was $\delta=0.81$ m over the sediment, and taking into account for 0.34 cm of sediment on the bottom measured with the gauge, the hydraulic radius becomes $R=(0.938-0.171)/(3.15-1.17+0.6)=0.30$ m. Hence, from the slope a shear velocity of :

$$u^*=(gRS)^{0.5}=0.02 \text{ m/s} \quad (23)$$

can be evaluated, in which g is the gravitational acceleration and S is the channel slope. Again data should be better normalised taking into account for the value of u^* deduced from the velocity profiles in the inner region or from the Reynolds stress. From the u velocity profile the value of $u^*=0.021$ m/s for the section $x=-0.5$ m. A comparison with the normalised stress indicate perhaps, that in the lower portion the normalised values obtained are quite low and that most likely, the data of the velocity profile over which the u^* has been calculated are relative to a portion of the flow affected by the sheet layer. It is important to remind the fact that the definition of a constant von Karman's constant $k(=0.4$ in the present work) is still not accomplished. Although (Coleman, 1981) shows that k can be considered constant regardless of C , successive re-elaboration of the velocity profiles (a literature review has been detailed in (Gaudio, Miglio and Dey, 2010)) and Coleman's data actually shows that the k reduced with C .

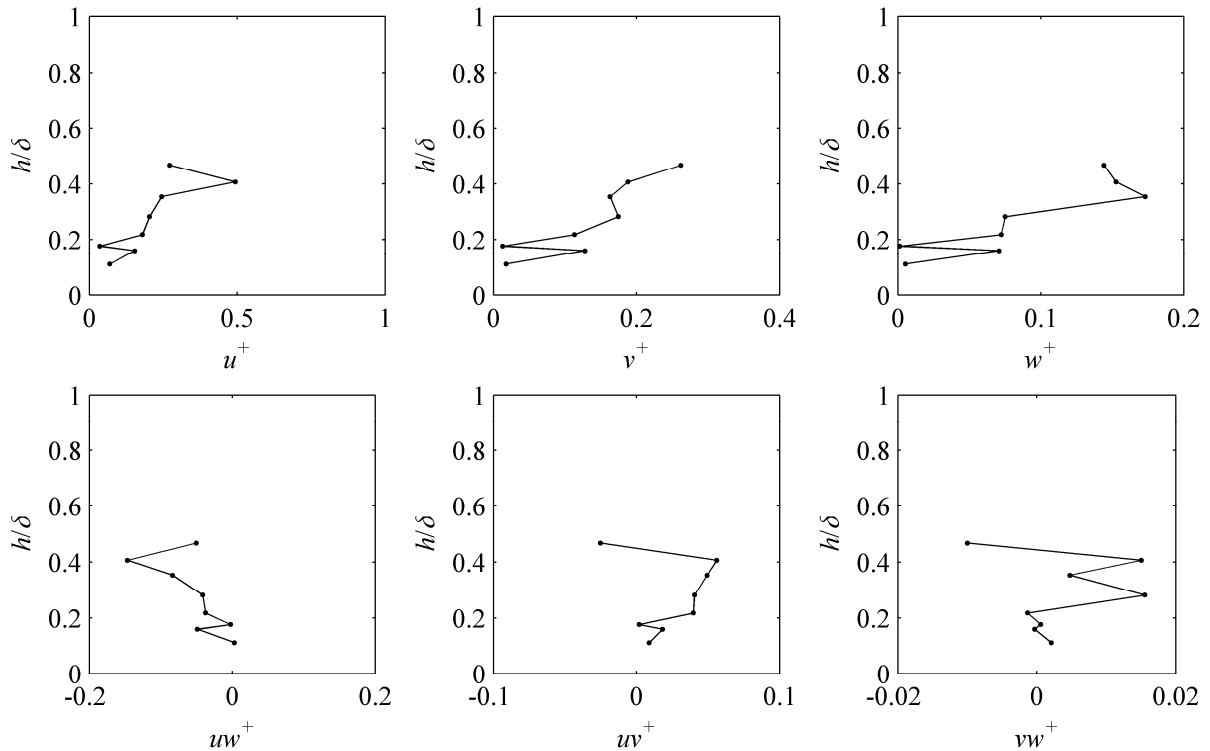


Figure 90 AE sect.1 normalised stresses.

Sect.3 (x=-2.5m)

In this case, the bank seems covered by a layer of stronger concentration (Figure 91) compared to that observed at x=-0.5m, showing an amplitude of about 100 counts at about 0.35 m underneath the probe. Again the first peak observed at Range=-0.15 m is linked to the signal noise produced by the SONAR.

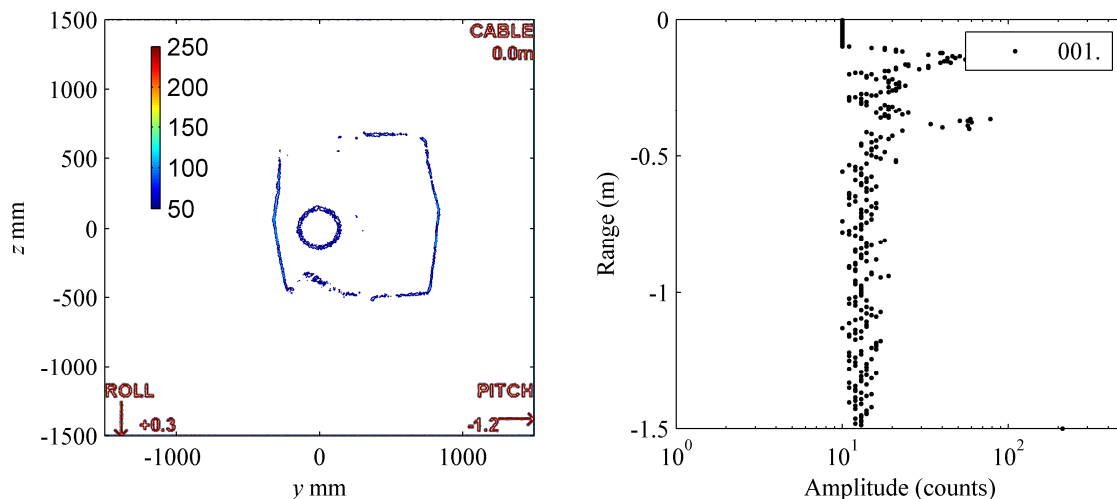


Figure 91 AE transverse profile at section 3 (x=-2.5m),

Indeed part of the velocity profile seems to have been measured underneath the “interface” detected by the SONAR. The ADV backscatter intensity inside the flow seems to be reduced compared to x=-0.5 m, but still shows the grow-up of the intensity toward the sediment interface, this time showing a milder transition compared to that detected at x=-0.5 m.

However, the third beam shows a steep reduction in the amplitude, but in this case not connected to a reduction of correlation or to the sensor clogging. However, the amplitude data observed suggests the presence of an increase in the concentration due to the presence of the sheet flow. The comparison of data showed that toward the “interface” measured at $x=-0.5$ m the ADV amplitude reached a backscatter amplitude up to 195 counts, whilst that observed at $x=-2.5$ m of 160 counts⁹. However, both the velocity and turbulences at $h<0$ mm showed relatively small values (it is important observing that data have been measured only for 5 seconds, because of batteries failure).

⁹ It is indeed true that the signal can be absorbed not only because of a lutocline presence but also due a gradient of concentration, this might create further problems into the individuation of the hard sediment but also of the sheet layer.

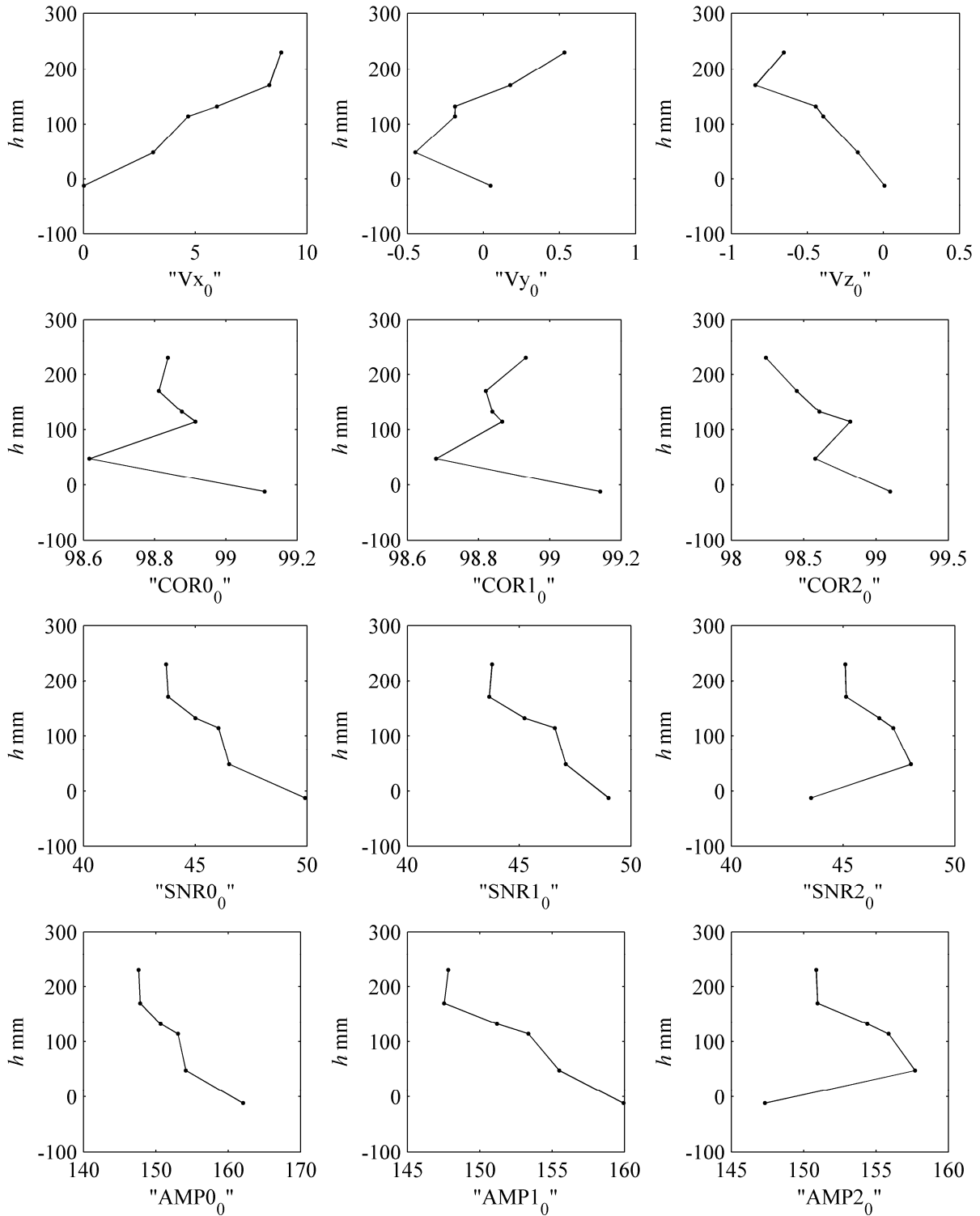


Figure 92 AE $x=-2.5$ m averaged ADV data

The Reynolds stress measured at the base of the profile (Figure 93) seems to suggest values of u^* of the order of $u^*=0.54$ cm/s, whilst a value of $u^*=3.2$ cm/s can be obtained from the analysis of the u velocity profile. However, a comparison with the data observed in section 1 revealed that the Reynolds stress inversion appeared later and, in general, for $x=-2.5$ they show a tendency more common for the inner layer of turbulent flows.

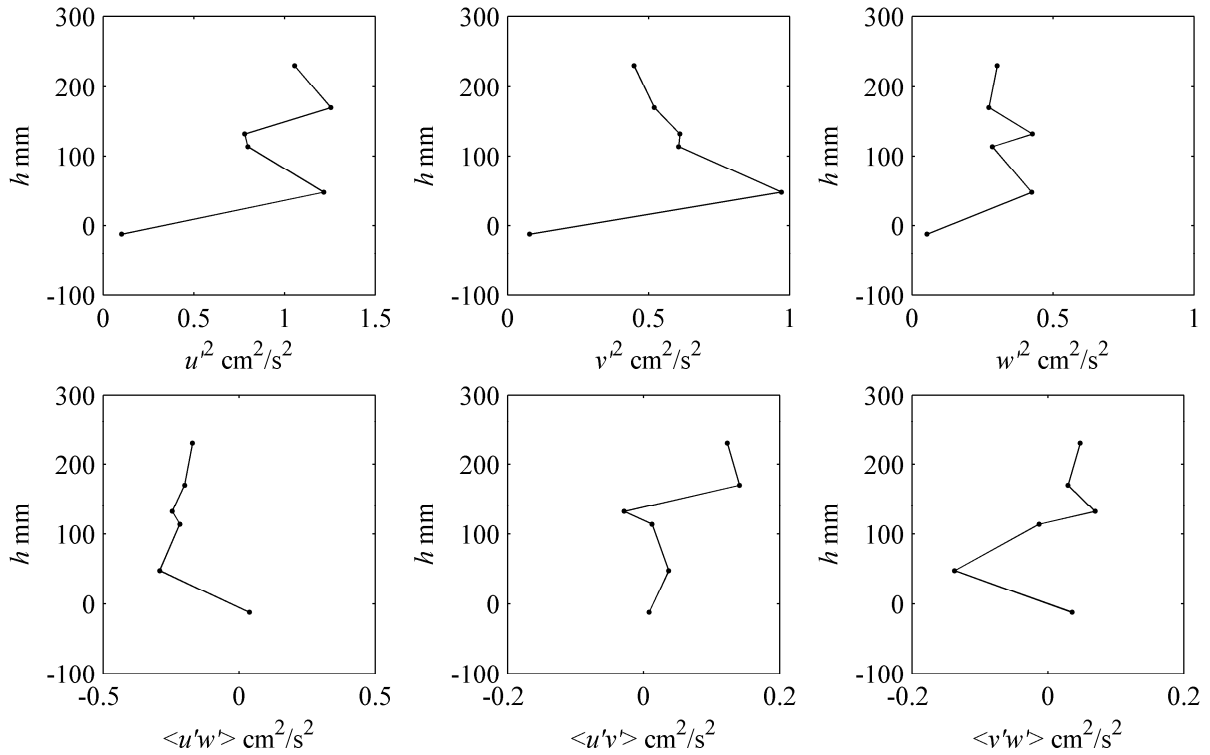


Figure 93 AE sect.3 Reynolds stresses

Sect. 5 (x=-4.5m)

Also in this section, the sheet flow seems to hold the whole section (fig. 32). However, the acoustic characteristics detected by the sonar are similar to that observed for x=-2.5m, with a SONAR amplitude up to 100 counts.

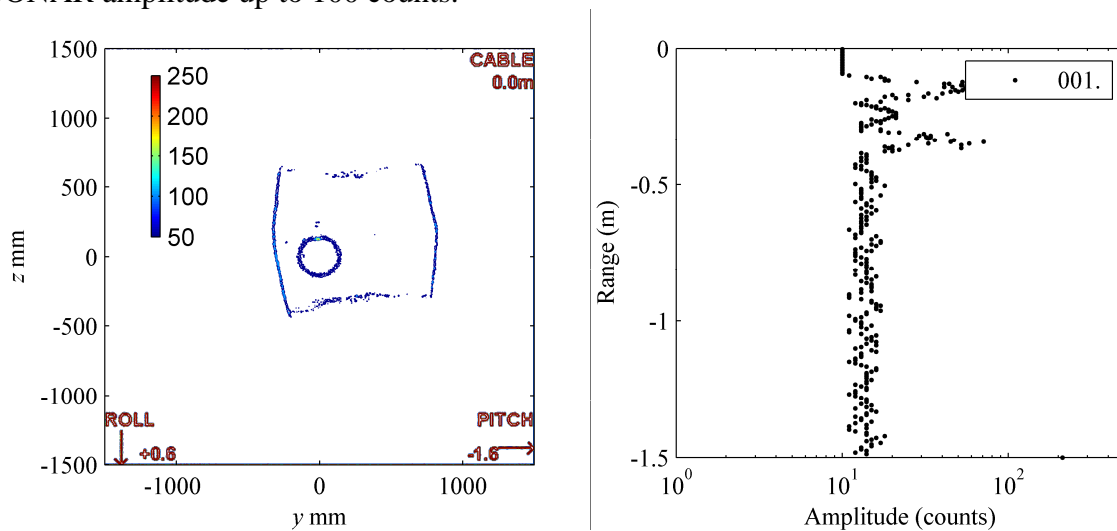


Figure 94 AE transverse profile at section 5 (x=-4.5m), and amplitude profile at x=0 m

The longitudinal velocity profiles (Figure 95) shows a pattern much more similar compared to that observed whit section x=-2.5m rather than section x=-0.5m, most likely linked to the smaller height of the sheet flow in the x=-0.5m. As observed for x=-0.5 m and -2.5 m, correlations are rather good for all the beams. The amplitude again shows a sharp increase toward the bottom of the invert. However, longitudinal velocity shows $u=0$ cm/s for values relatively far from the “interface”. It is worth observing that a certain longitudinal offset occurs between the SONAR gauged section and that measured with the ADV (around 40 cm)

and in zone of high slope the bottom height may not perfectly match between the two sections.

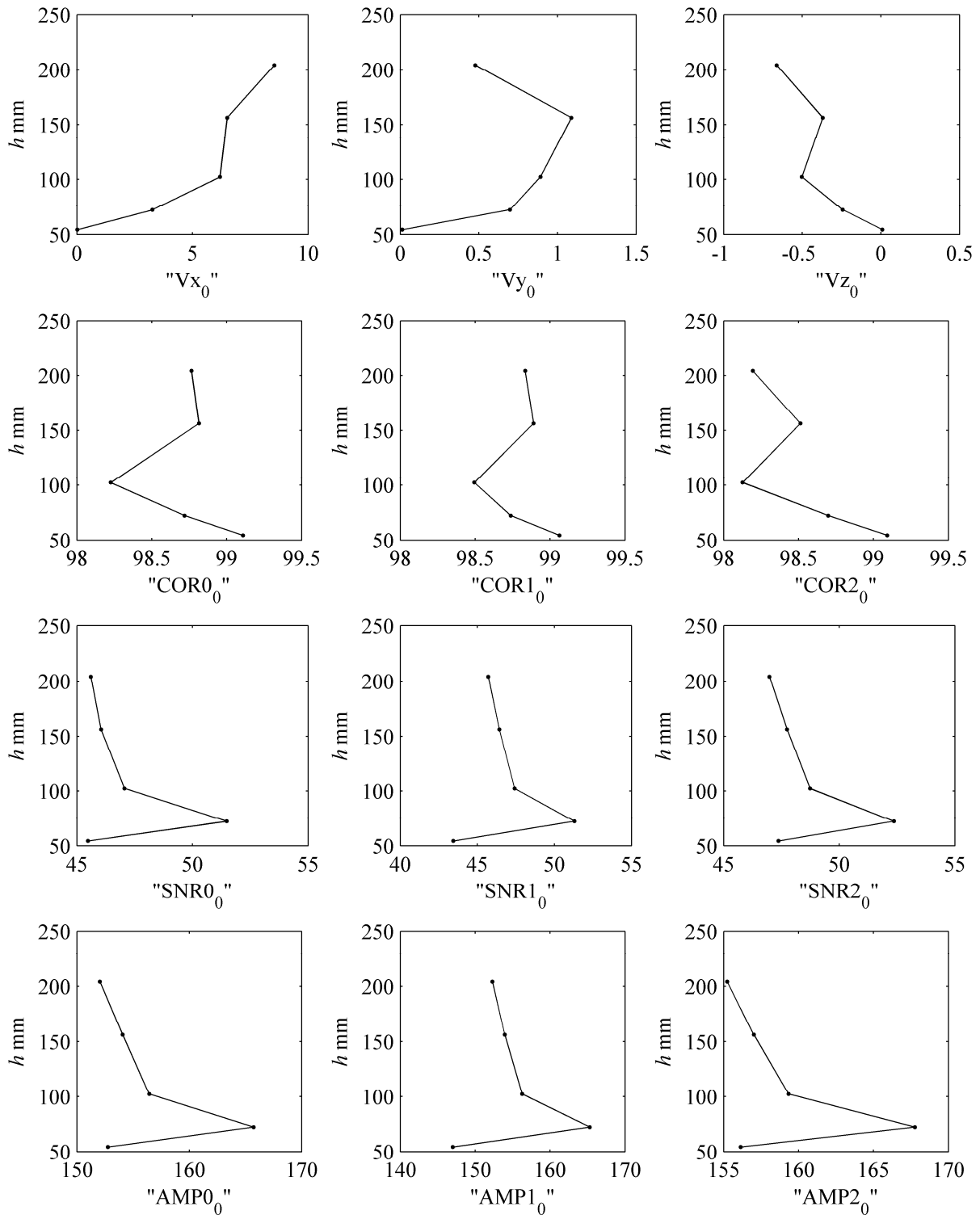


Figure 95 AE sect. 5 averaged ADV data

Again, both longitudinal intensity u' and stress $\langle u'w' \rangle$ shows a pattern which seems affected by the sheet flow in the lower portion (Figure 96). Moreover, the inversion of the Reynolds stress occurs at the same height at which the amplitude profiles suddenly increases. Finally, from the previous plot it is worth observing that a measure of the turbulence characteristics at

the free surface should be carried out to understand the effect of the sheet flow layer on the outer flow region turbulence. The shear velocity observed from the velocity profiles shows values of $u^* = 2.32$ cm/s, whilst from the Reynolds stress a values of $u^* = 0.63$ cm/s

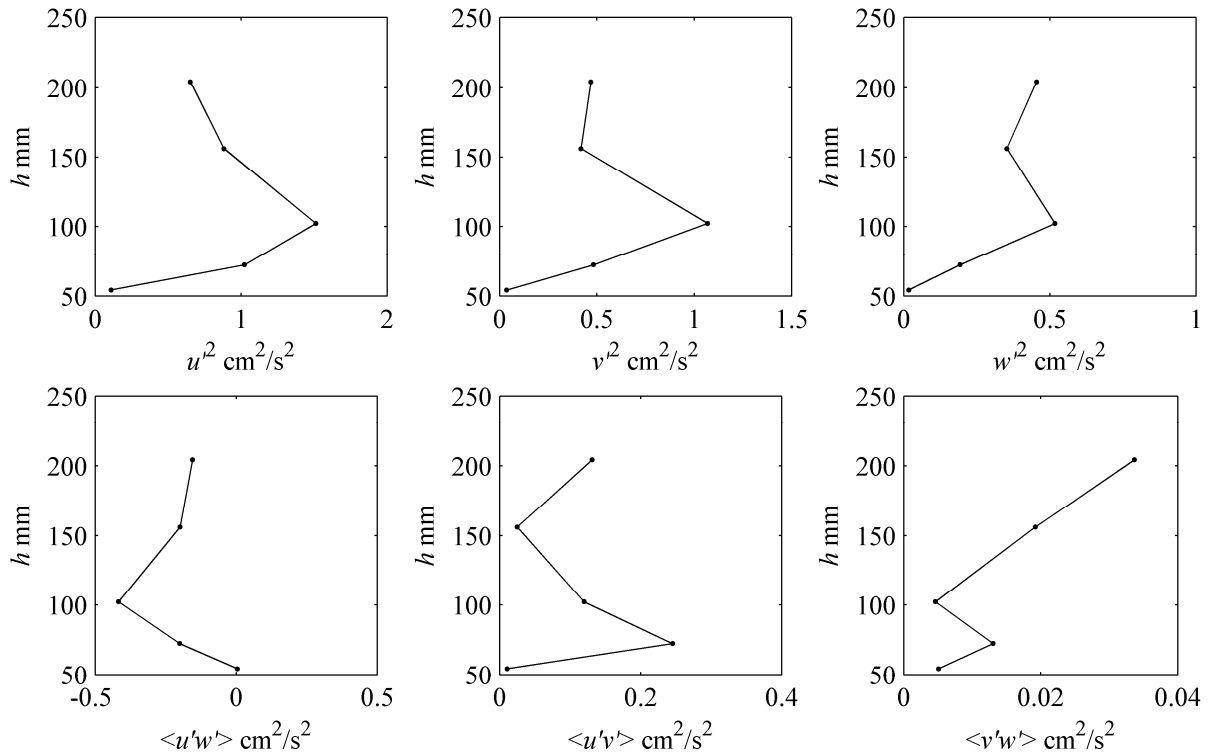
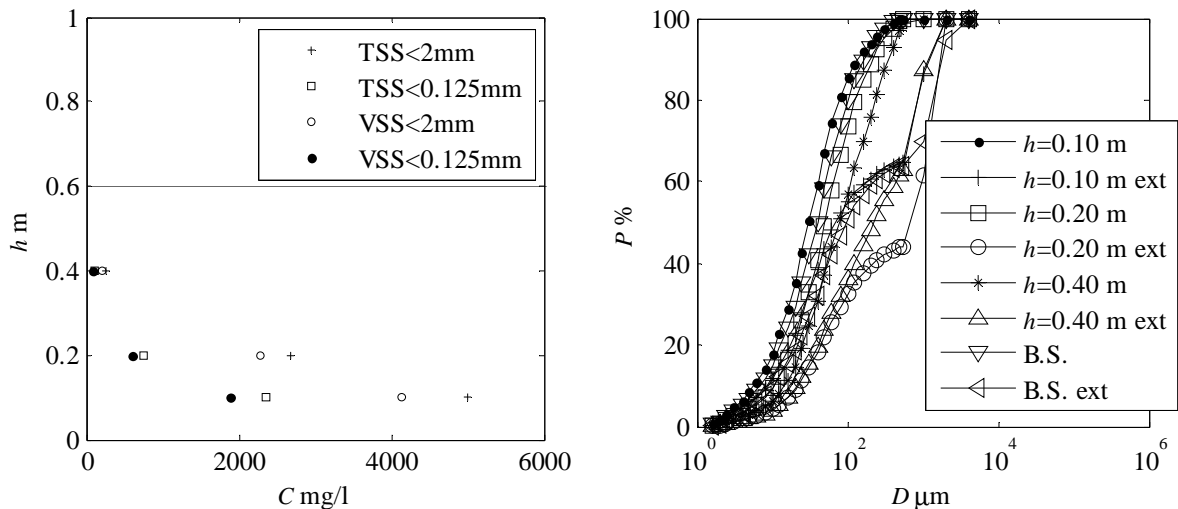


Figure 96 AE sect.5 Reynolds stresses

6.3.8 Flow field Test AE-S4 (2011-02-02)



(a) Suspended solids concentrations at different eight from the interface

(b) bottom sediment particle size distribution and water sediment particle distribution for $D < 0.56$ (B.S.: bottom sediments, ext: extended to $D < 4$ mm).

Figure 97 TSS, VSS and particle size distribution conditions of test AE-S4 (2010-02-02)

The bottom sediment sampler has been used before the SONAR and the ADV. Therefore, the lutocline position has been deeply modified by the latter. However, the concentrations show in Figure 97 values typical of the presence of a mud layer over the tough sediment deposits. Both transverse SONAR outputs are shown in Figure 98, Figure 99, Figure 100. The images show the presence of the mud layer well inside the side bank limits. However, the transverse morphologies differs one from each other, especially for the section $x=-2.5$ m, which shows an almost flat deposit.

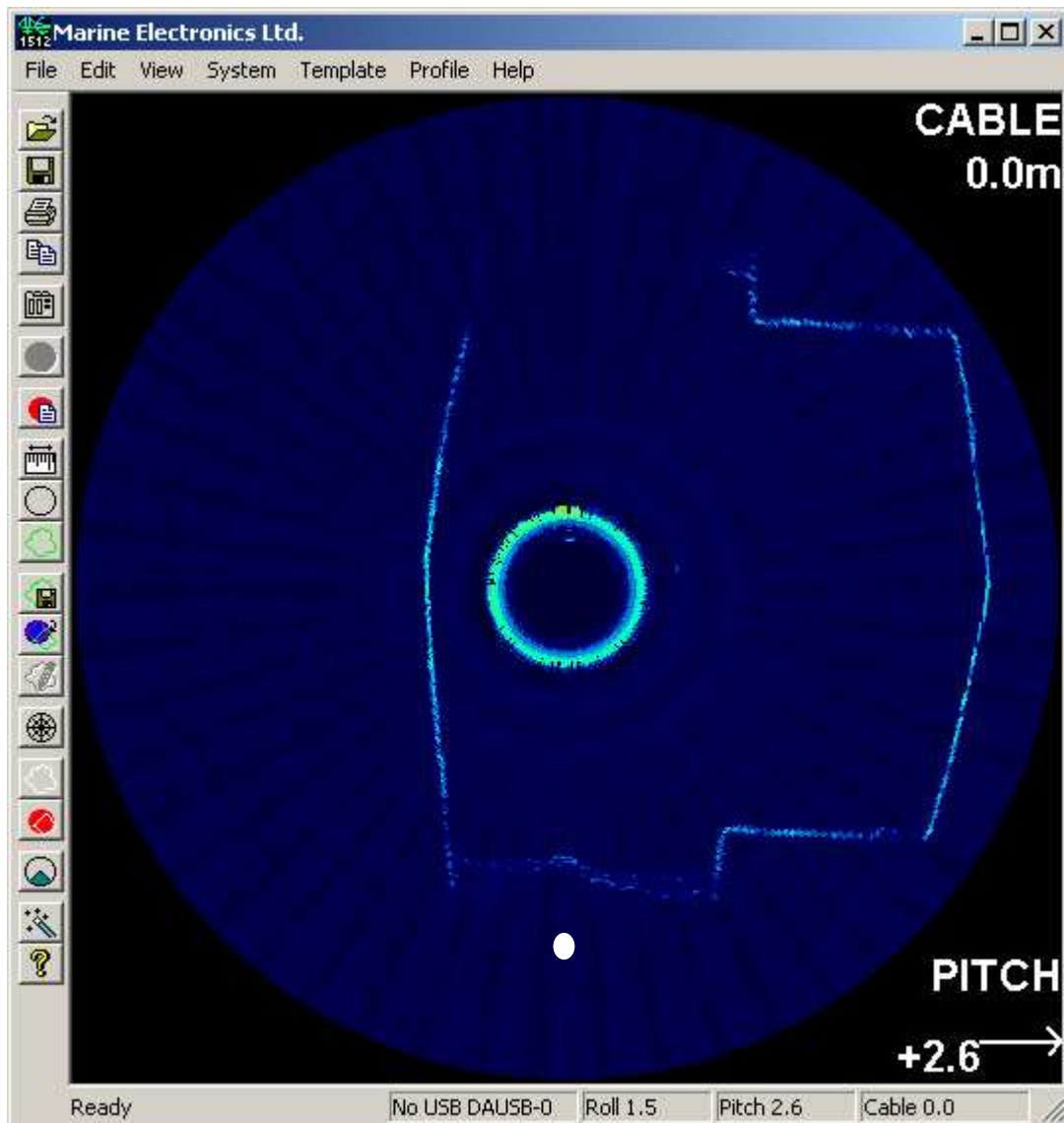


Figure 98 Sonar output for $x=-0.5$ (white spot) sediment interface detected with the gauge

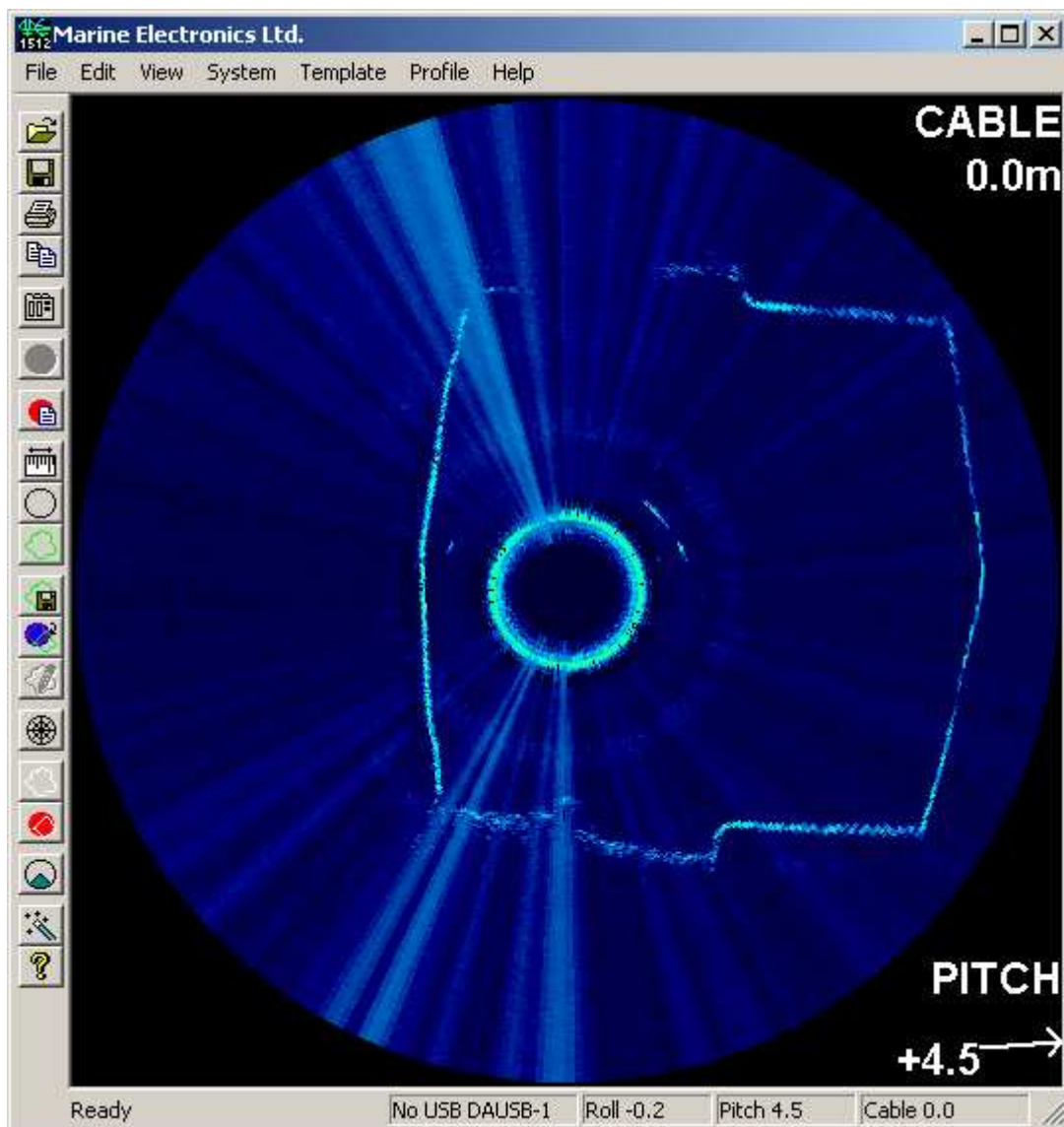


Figure 99 Sonar output for $x=-1.5$, (white spot) sediment interface detected with the gauge

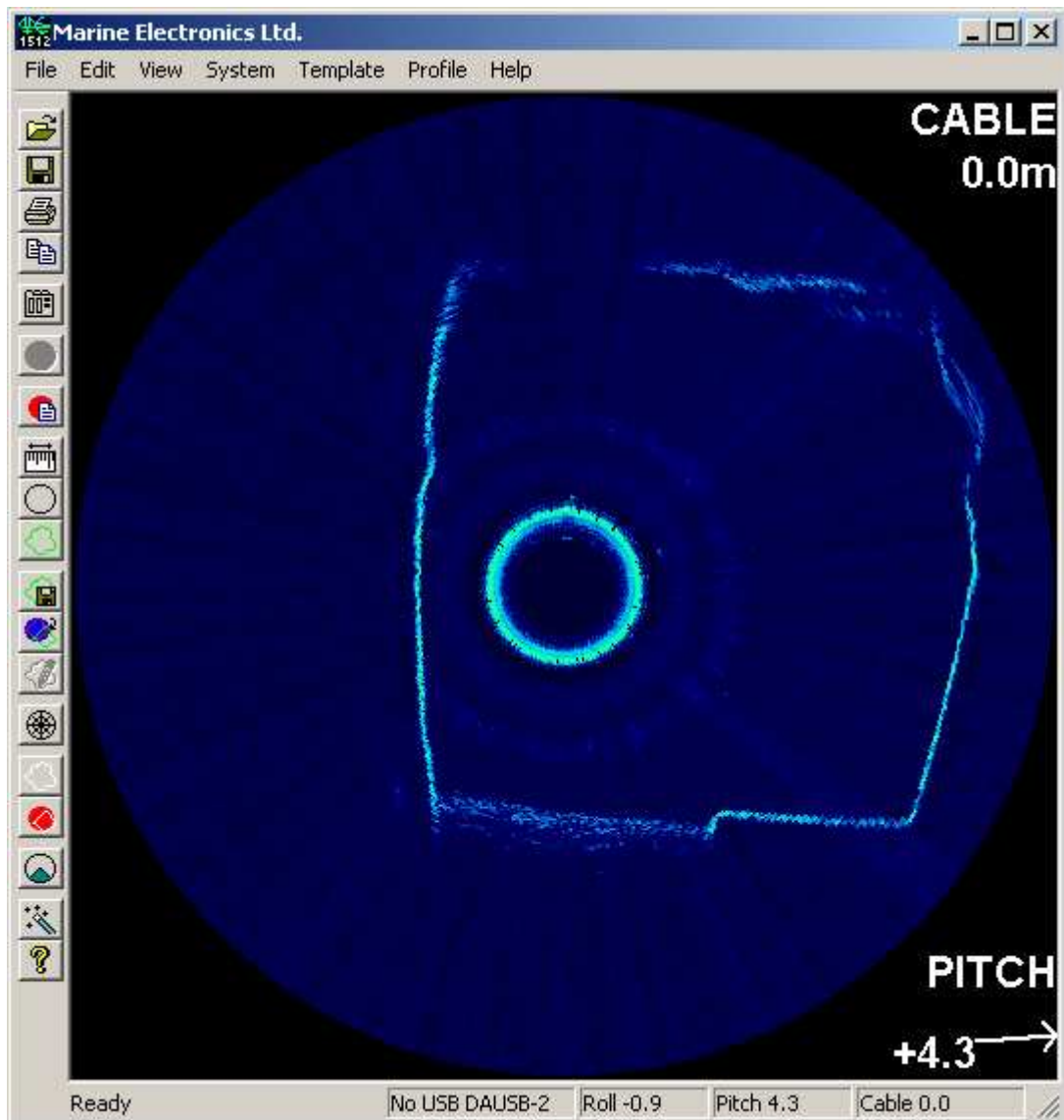


Figure 100 Sonar output for $x=-2.5$ (white spot) sediment interface detected with the gauge

Again, the interface represented by the lutocline and detected by the SONAR does not correspond with the observation made with the sediment gauge.

The surface in Figure 101 shows the presence of a larger deposits at the section $x=-1.5$, indicating the presence of a kind of three dimensional dune. Moreover, the presence of the side bank might generate a larger turbulence, as, in general, lower sediment deposits occurs near the side bank for the section $x=-0.5$ and $x=-1.5$.

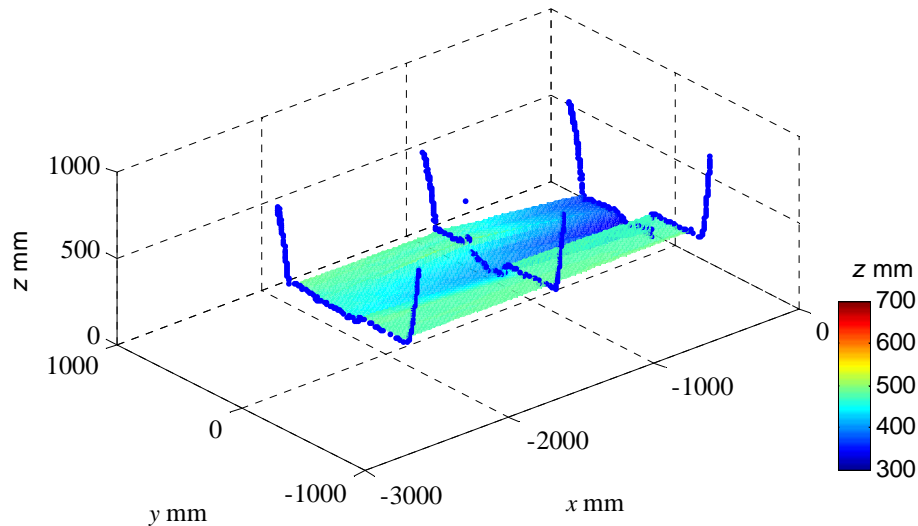


Figure 101 sediment surface referred to the invert test AE-S4

Velocity profiles

This time only two sections have been measured. Longitudinal profiles in both sections shows slow flow velocity with a sort of s-shaped velocity profile, probably affected by the presence of the lutocline (Figure 102). Secondary currents shows values of the order of 5%-10% of the flow velocity, with maximum values of $v=0.6$ cm/s occurring at 200 mm from the bottom, while maximum vertical velocity $w=-1$ cm/s occurred at about 400 mm. However, the position of the probe may disturb the vertical flow, which is directed toward the bottom. Correlation profile shows rather high values, whilst the amplitude profile slightly increased toward the bottom, until the control volume enters in correspondence of the interface detected by the sonar. The amplitude observed in the water column for the preset test generally showed values larger than that observed at DA-S2 test, indicating the presence of a higher sediment concentration.

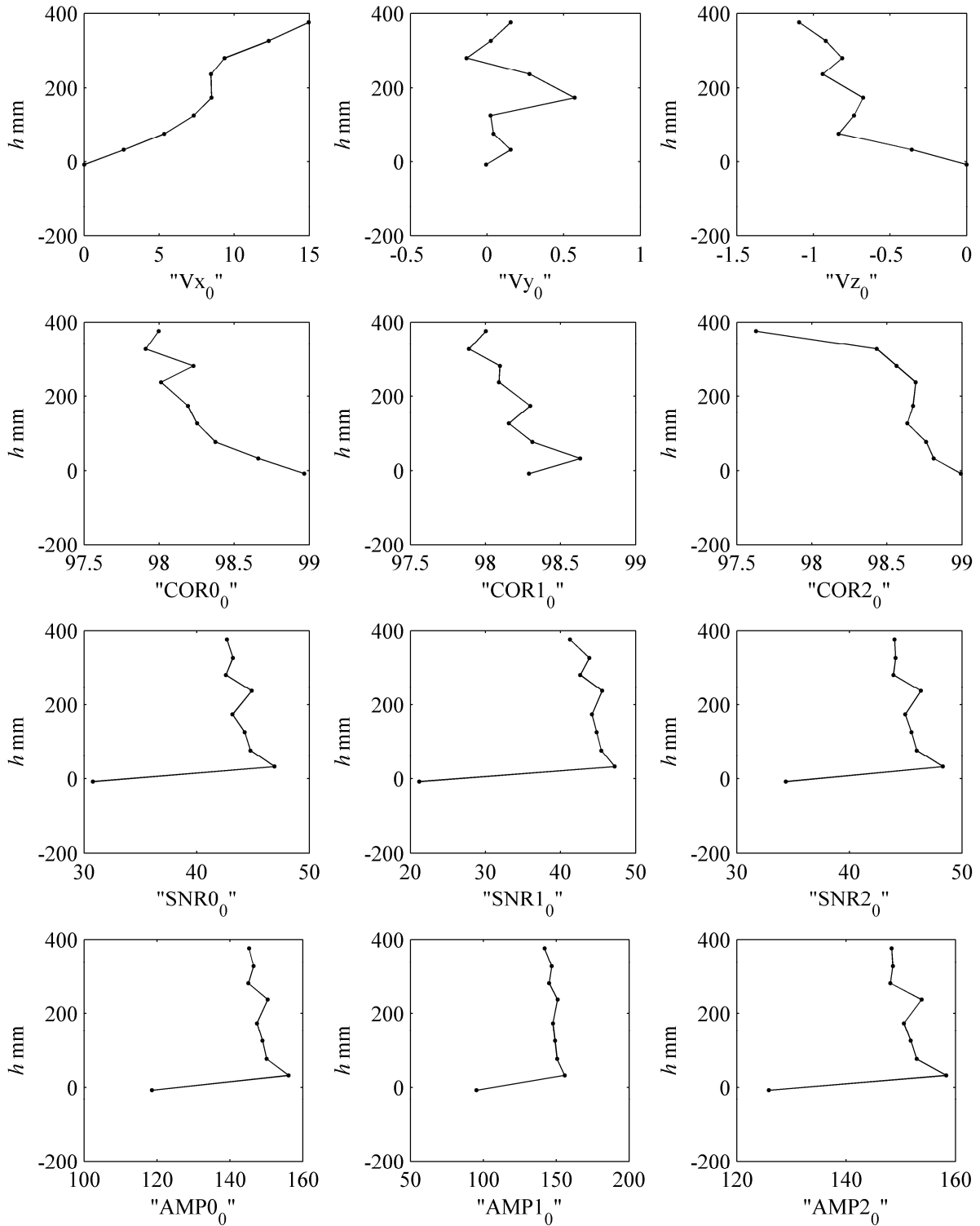


Figure 102 AE-S4 ADV data sect. 1 ($x=-0.5$ m)

Turbulence profiles of figure again shows the typical behaviour of the inner viscous sub-layer (Figure 103) and a reversed behaviour compared to DA results and classical turbulence profile, indicating the presence of a thicker zone in which most likely the viscous effect dominates.

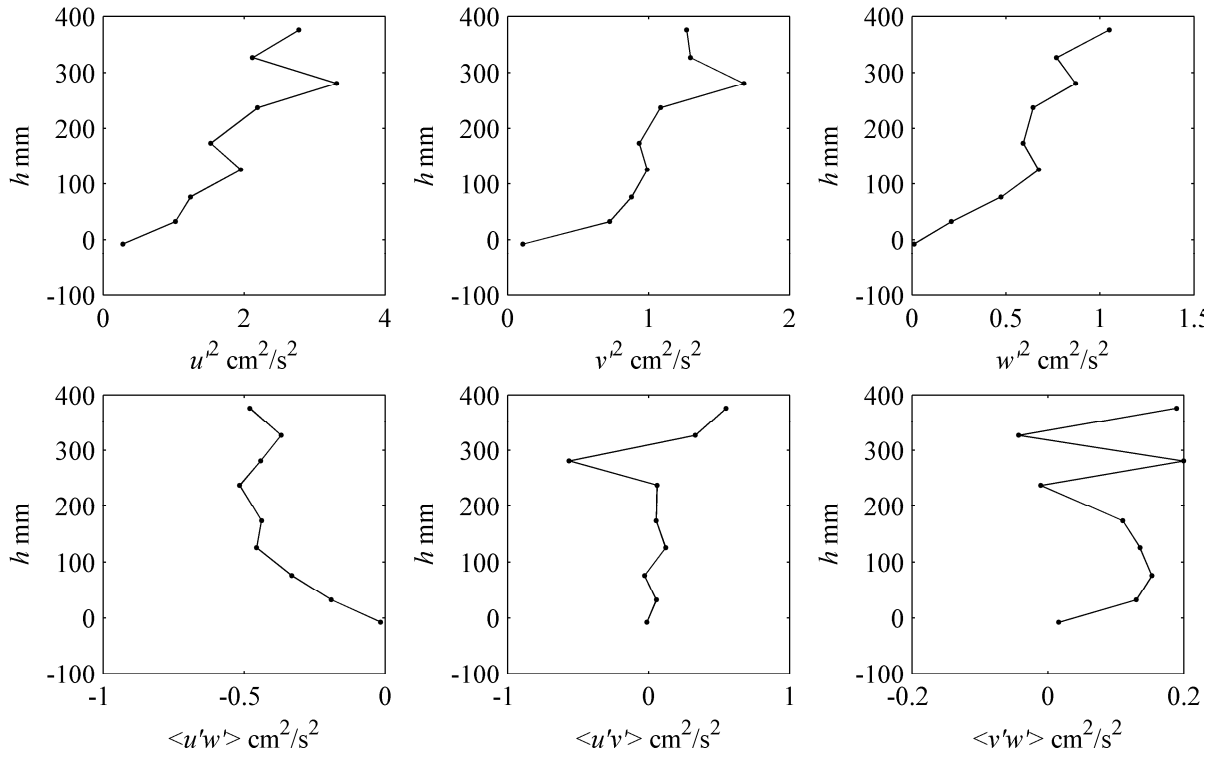


Figure 103 AE-S4 ADV turbulence data sect. 1 ($x=-0.5$ m)

Figure 105 shows longitudinal velocities of maximum 10 cm/s at section $x=-2.5$ m, even smaller if compared to $x=-0.5$ m, whilst secondary current shows similar magnitude. Again, the offset between the two probes might be responsible of the small offset observed between the interface detected by the probe (the drop in the correlation profiles). Similar amplitudes and SNR ADV occurred at the two section.

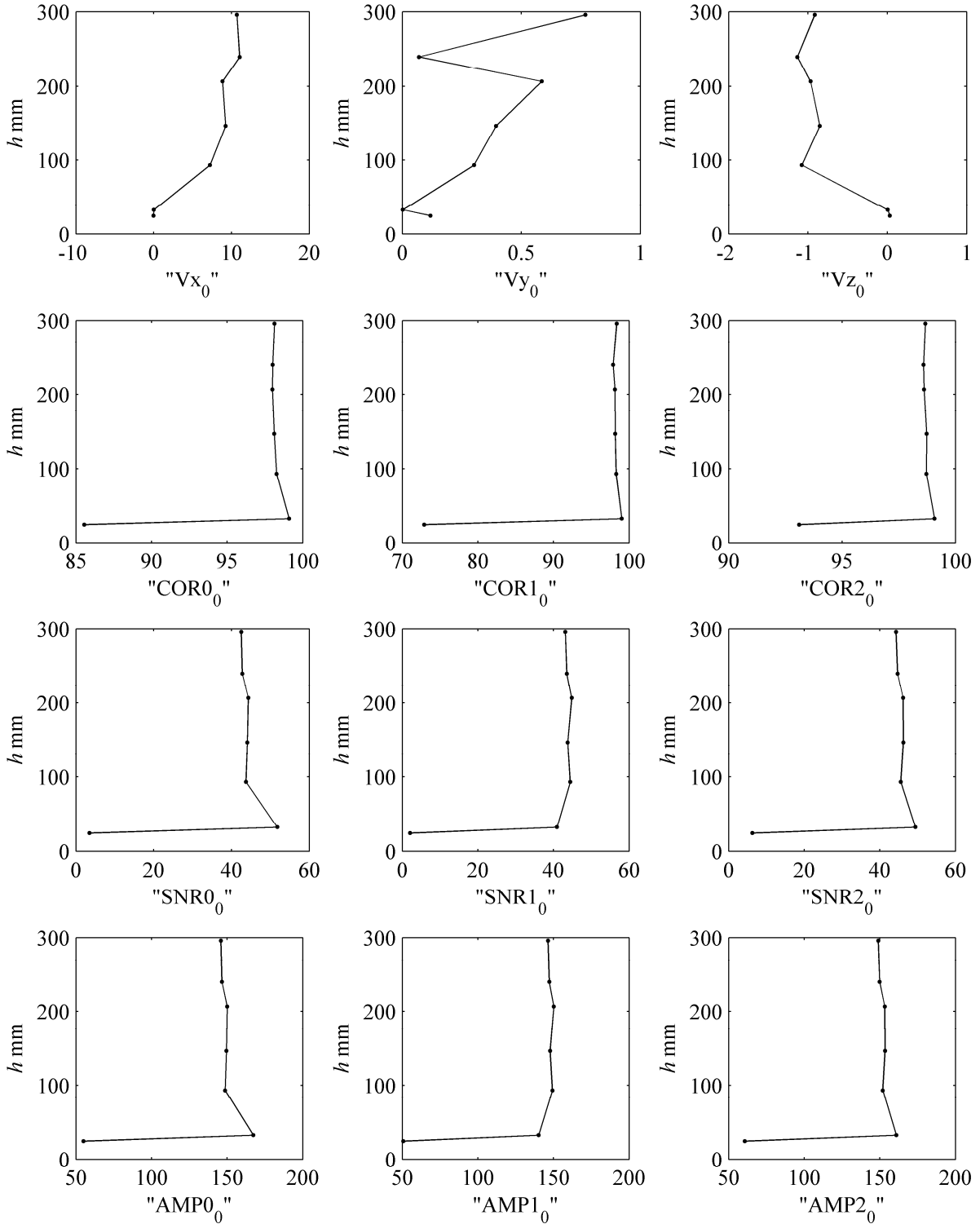
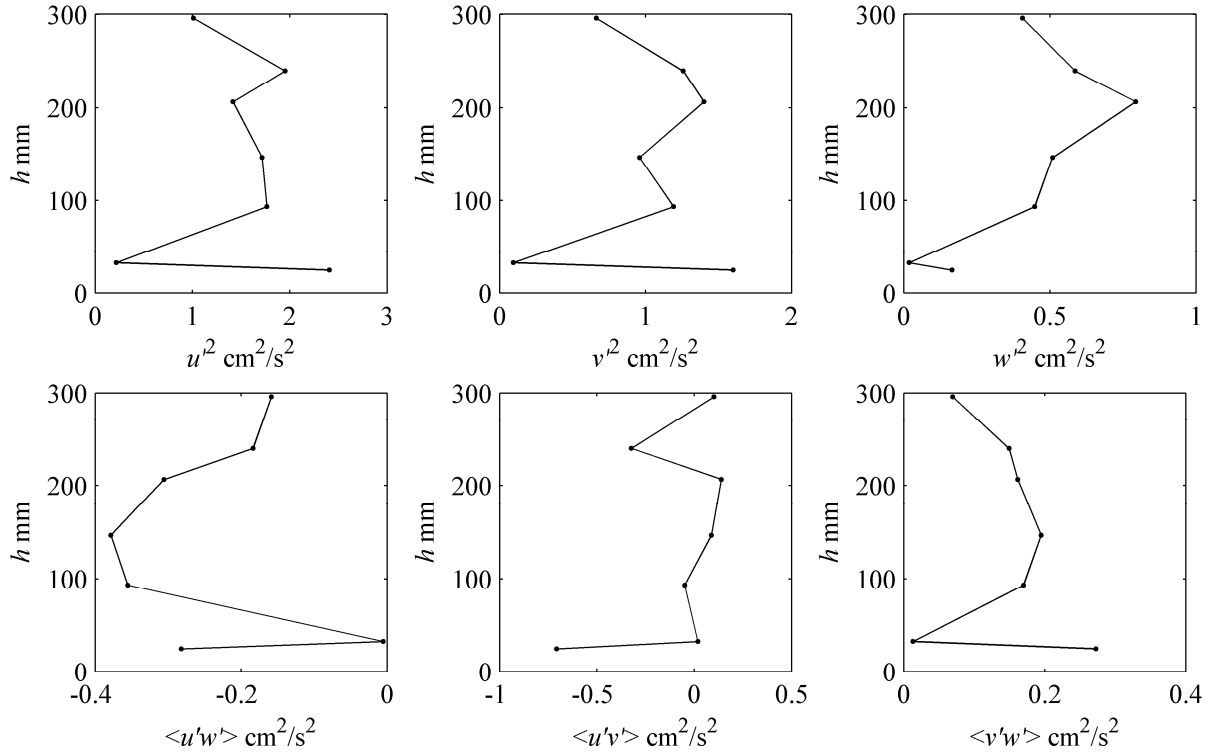


Figure 104 AE-S4 ADV data sect. 3 ($x=-2.5$ m)

The turbulence profiles of Figure 105 (excluding the last point at $h=20$ mm inside the mud layer) still shows the same behaviour as that observed for $x=-0.5$.



6.4 Acoustic backscatter correlation with TSS

According to several Authors (Ha, Hsu, Maa, Shao and Holland, 2009) the ADV acoustic backscatter can be used to evaluate the sediment concentration, once the information is calibrated toward the corrected value of TSS and the right particle size distribution. Thereafter, the plot in Figure 106 shows the correlation existing between the acoustic backscatter for both the SONAR and the ADV and the TSS present at the moment of the survey. It is important to observe that the latter also depends on the sediment particle size and consequently the information gathered has been separated in terms of different particle size and uniformity.

Accordingly, SONAR amplitudes did not reflect the concentration of the suspended solids, most likely due to the automatic gain adjustment. Differently, the ADV backscatter seems to show a larger correlation with the TSS up to 500 mg/l. However, for larger concentration, the signal is saturated and the amplitude values remain constant.

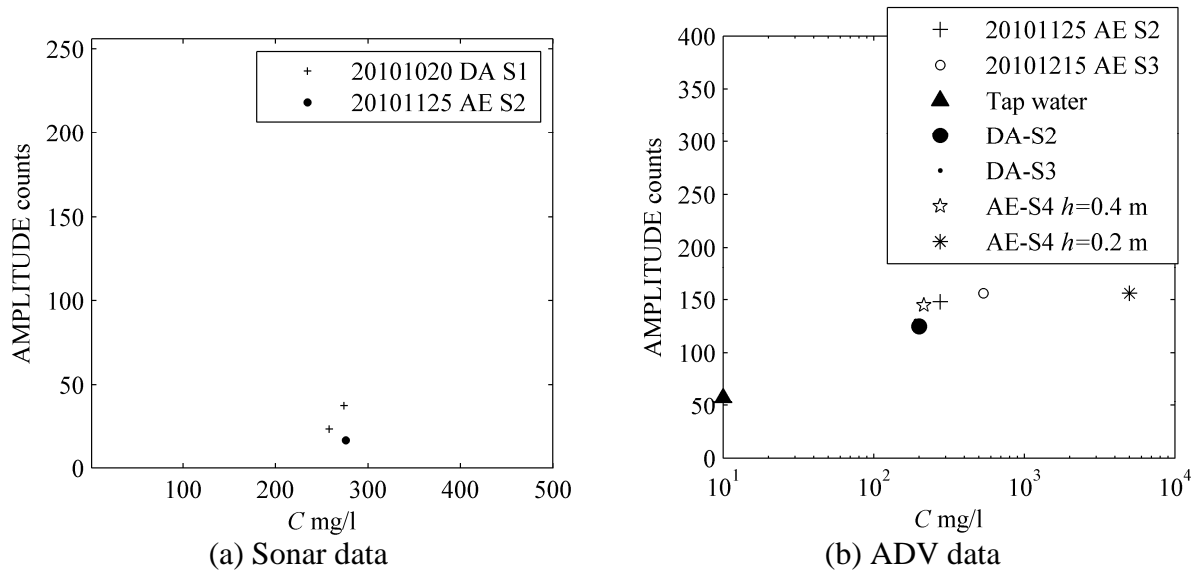


Figure 106 Correlation between TSS<2 mm and amplitude in counts

As can be inferred from the figure, the acoustic backscatter shows

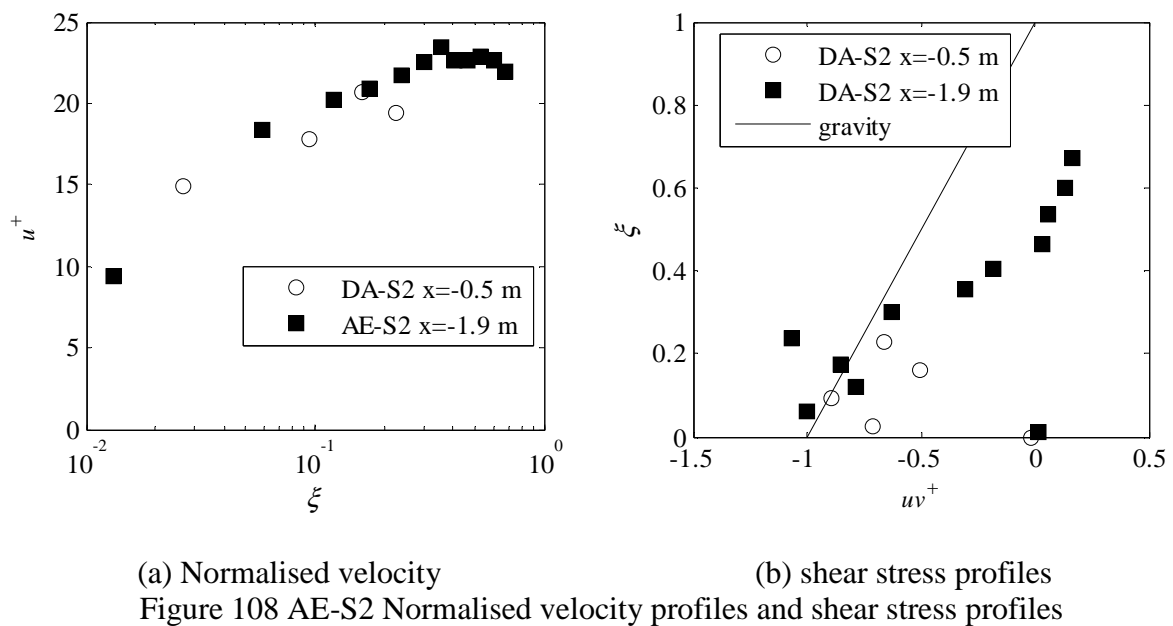
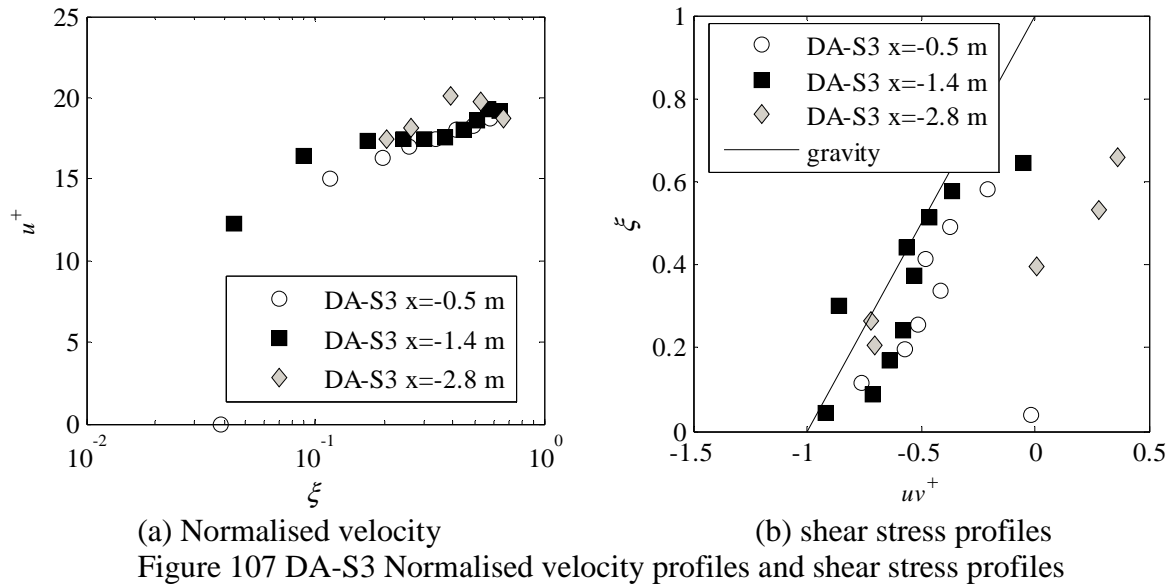
6.5 Comparison between velocity profiles

Velocity profiles and Reynolds stress profiles shows completely different patterns from the two site. Accordingly, the flow in narrow channel is characterised by three dimensional properties which may affect the Reynolds stress, leading to values of the outer layer ($\xi=h/\delta>0.25$) which tends toward $0 \text{ cm}^2/\text{s}^2$ (Nezu and Nakagawa, 1993). Indeed velocity measurements at the site DA shows this particular features starting from $\xi=h/\delta>0.5$ (Figure 107 and Figure 108). In the figure $u^+=u/u_*$ and $uv^+=\langle u'w' \rangle / [u_*^{0.5}]$. The continuous line represents the gravity shear stress for bi-dimensional free surface flows.

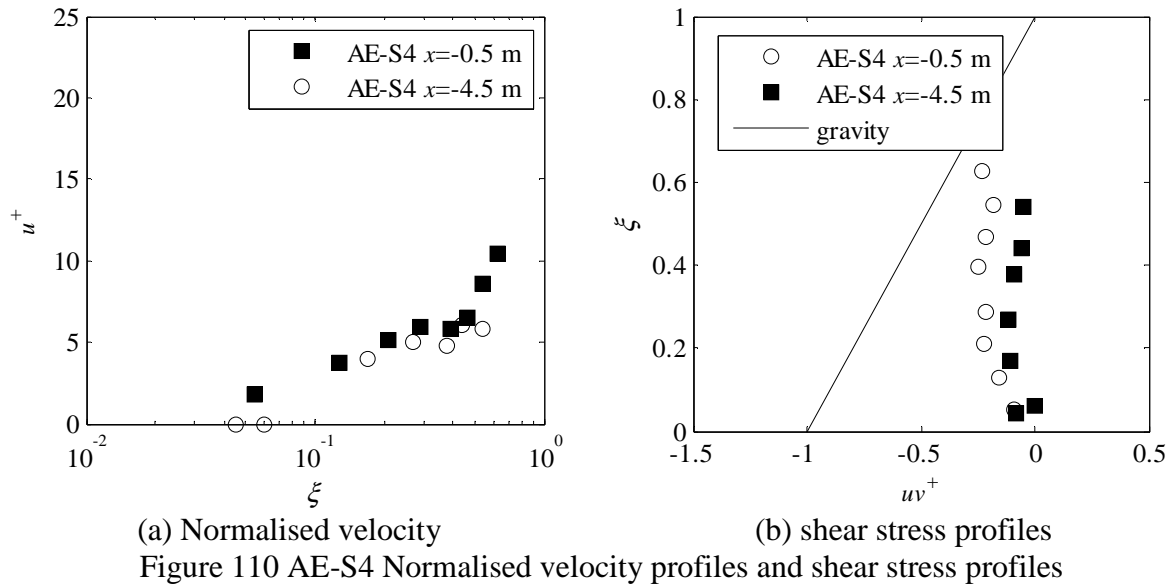
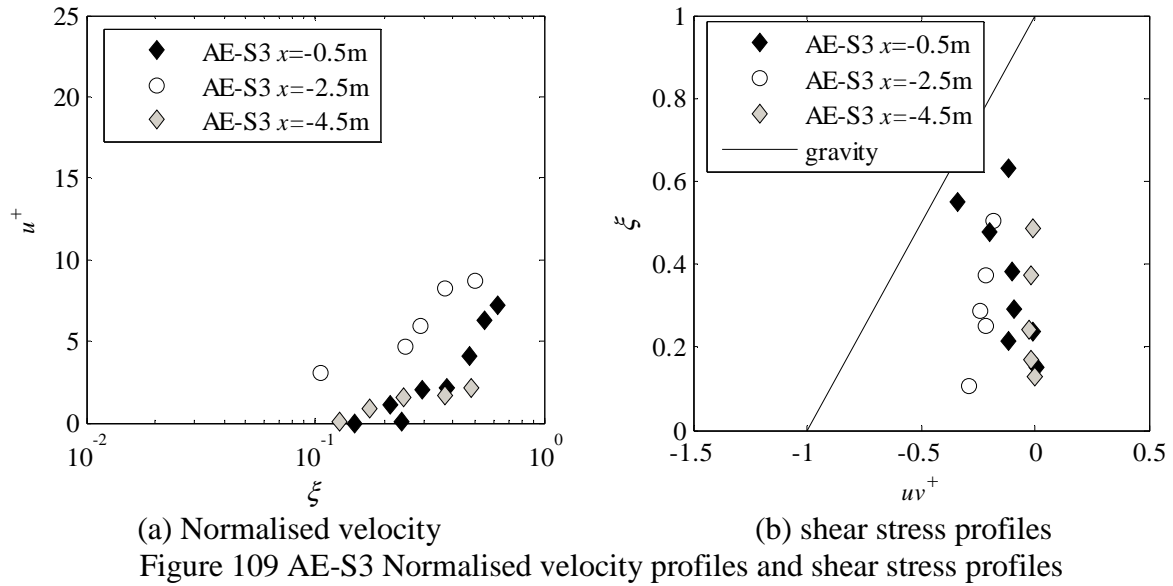
Shear bottom stress u_* have been evaluated following the log law of turbulent rough channel from the data between $0.05<\xi<0.3$, in order to prevent any bias from wrong measurement to close to the interface:

$$u^+ = 1/\kappa \log(\xi) + B_s \quad (24)$$

in which $\kappa=0.41$ is the Von Karman constant, and B_s is a constant (Nezu and Nakagawa, 1993).



Differently, AE surveys shows a completely different behaviour for $\xi=h/\delta < 0.5$. First of all, the value of the Reynolds stress reduced toward the free surface, which is a typical behaviour of the viscous layer. For $\xi=h/\delta > 0.5$, uv^+ increases again to larger values, comparable to that of free surface flow in clear water conditions Figure 109 and Figure 110.



The two sites also shows clear difference from the individuation of the zero velocity flow, which is connected to the non slip condition of the interface. Surprisingly, AE test shows zero velocities for values of $\xi=0.03$. This might be certainly connected to the definition of the interface and hence of the zero level, which has been defined based on the SONAR profiler interpretation using the SONAR software “max” algorithm, rather than using the new algorithm developed. Hence, the control volume of the ADV might have encountered the mud layer for height larger than that observed with the SONAR and the control volume might have been buried into the sediments. This again confirmed the necessity to correctly define the sediment interface.

CONCLUSIONS

The present work shows the results of the bed morphology and flow field measurement for two experimental sites characterised by different sediment deposit properties.

From the results it has been possible to observe that:

- 1) The acoustic signal is reflected and attenuated in different ways according to the nature of the interface, hence a new algorithm has been developed based on the definition of a new interface, i.e., the point where the gradient of the acoustic backscatter strength shows its maximum gradient;
- 2) The nature of the interface deposits is strongly dependent on the flow field velocity observed during the morphological survey; generally at the presence of an average velocity around 0.40 m/s, only sand deposits occur over the invert, while for velocity generally less than 0.10 m/s a mud flow can be observed over the sediment;
- 3) The nature of the interface modifies the capacity of manual gauges to detect the actual mud flow; attention should be paid when using these systems;
- 4) The morphology of the sediment deposits depends on both the nature of the deposits and the flow field. In presence of flow velocity of the order of 0.10 m/s it has been possible to observe dunes characterised by steep upstream slope and mild downstream slope after the crest of the deposit of 3-4 m of wave length and 5- 10 cm of wave height.
- 5) The flow velocity fields are deeply modified by the presence of this mud layer; generally, in presence of sand deposits and despite the strong three-dimensionality of the flow, the turbulence stress well falls into the classical turbulence profiles observed for free surface flows; differently, the presence of the mud layer modifies the nature of the turbulence, thus presenting an inner viscous layer characterised by higher depth compared to classical turbulent free surface flow, even if large Reynolds number is of the order of $6 \cdot 10^4$ (turbulent flow regime) occurs.

REFERENCES

- [1] van Rijn, L. C. (2007). "Unified view of sediment transport by currents and waves. II: Suspended transport." *Journal of Hydraulic Engineering-Asce*, 133(6), 668-689.
- [2] McAnally, W. H., Friedrichs, C., Hamilton, D., Hayter, E., Shrestha, P., Rodriguez, H., Sheremet, A., Teeter, A., and Flu, A. T. C. M. (2007). "Management of fluid mud in estuaries, bays, and lakes. I: Present state of understanding on character and behavior." *Journal of Hydraulic Engineering-Asce*, 133(1), 9-22.
- [3] van Rijn, L. C., and Louisse, C. (1987). "The Effect of Waves on Cohesive Bed Surfaces." *Proc. on Coastal and Port Engineering* Beijing, China, 1518-1532.
- [4] van Rijn, L. C., and Klaassen, G. J. "Experiences with straight flumes for movable bed experiments." *Proc., IAHR Workshop on particle motion*, 1-7.
- [5] Karim, M. F., and J.F., K. (1981). "Computer-based predictors for sediment discharge and friction factors of alluvial streams." Iowa Institute of Hydraulic Research, The University of Iowa, Iowa City, Iowa.
- [6] Karim, M. F., and Kennedy, J. F. (1987). "Velocity and sediment-concentration profiles in river flows." *Journal of Hydraulic Engineering-Asce*, 113(2), 159-178.
- [7] van Rijn, L. C. (1984). "Sediment Transport, Part I: Bed Load Transport." *Journal of Hydraulic Engineering*, 110(10), 1431-1456.
- [8] van Rijn, L. C. (1984). "Sediment Transport, Part III: Bed forms and Alluvial Roughness." *Journal of Hydraulic Engineering*, 110(12), 1733-1754.
- [9] Voogt, L., Vanriijn, L. C., and Vandenberg, J. H. (1991). "SEDIMENT TRANSPORT OF FINE SANDS AT HIGH VELOCITIES." *Journal of Hydraulic Engineering-Asce*, 117(7), 869-890.
- [10] Abouseida, M. M., Muralidhar, M. A., and Lo, J. M. (1992). "Wave-induced sediment concentration in weak current fields." *Journal of Hydraulic Research*, 30(5), 623-638.
- [11] Gallagher, E. L., Boyd, W., Elgar, S., Guza, R. T., and Woodward, B. (1996). "Performance of a sonar altimeter in the nearshore." *Marine Geology*, 133(3-4), 241-248.
- [12] Bell, P. S., and Thorne, P. D. (1997). "Application of a high resolution acoustic scanning system for imaging sea bed microtopography." *7th International conference on electronic engineering in oceanography* Southampton, UK, 128-133.
- [13] Thorne, P. D., and Hanes, D. M. (2002). "A review of acoustic measurement of small-scale sediment processes." *Continental Shelf Research*, 22(4), 603-632.
- [14] Webb, M. P., and Vincent, C. E. (1999). "Comparison of time-averaged acoustic backscatter concentration profile measurements with existing predictive models." *Marine Geology*, 162(1), 71-90.
- [15] Green, M. O., and Black, K. P. (1999). "Suspended-sediment reference concentration under waves: field observations and critical analysis of two predictive models." *Coastal Engineering*, 38(3), 115-141.
- [16] Lee, G. H., Dade, W. B., Friedrichs, C. T., and Vincent, C. E. (2004). "Examination of reference concentration under waves and currents on the inner shelf." *Journal of Geophysical Research-Oceans*, 109(C2).
- [17] Hoitink, A. J. F., and Hoekstra, P. (2005). "Observations of suspended sediment from ADCP and OBS measurements in a mud-dominated environment." *Coastal Engineering*, 52(2), 103-118.
- [18] Ashley, R. M., Bertrand-Krajewski, R. M., Hvitved-Jacobsen, T., and Verbanck, M. (2004). *Solids in Sewers*, IWA Publishing, London, UK.

- [19] Lewis, C. F. M., Mayer, L. A., Mukhopadhyay, P. K., Kruge, M. A., Coakley, J. P., and Smith, M. D. (2000). "Multibeam sonar backscatter lineaments and anthropogenic organic components in lacustrine silty clay, evidence of shipping in western Lake Ontario." *International Journal of Coal Geology*, 43(1-4), 307-324.
- [20] McAnally, W. H., Teeter, A., Schoellhamer, D., Friedrichs, C., Hamilton, D., Hayter, E., Shrestha, P., Rodriguez, H., Sheremet, A., Kirby, R., and Fl, A. T. C. M. (2007). "Management of fluid mud in estuaries, bays, and lakes. II: Measurement, modeling, and management." *Journal of Hydraulic Engineering-Asce*, 133(1), 23-38.
- [21] Alexander, M. P., Teeter, A. M., and Banks, G. E. (1997). "Development and verification of an intrusive hydrographic survey system for fluid mud channels." Department of the Army, U.S. Army Corps of Engineers, Washington, DC.
- [22] Dolphin, T., and Vincent, C. (2009). "The influence of bed forms on reference concentration and suspension under waves and currents." *Continental Shelf Research*, 29(2), 424-432.
- [23] Crabtree, R. W. (1989). "SEDIMENTS IN SEWERS." *Journal of the Institution of Water and Environmental Management*, 3(6), 569-578.
- [24] Laplace, D., Sanchez, Y., Dartus, D., and Bachoc, A. (1990). "SEDIMENT MOVEMENT INTO THE COMBINED TRUNK SEWER NO 13 IN MARSEILLES." *Water Science and Technology*, 22(10-11), 259-266.
- [25] Arthur, S., Ashley, R. M., and Nalluri, C. (1996). "Near bed solids transport in sewers." *Water Science and Technology*, 33(9), 69-76.
- [26] Ahyerre, M., Chebbo, G., and Saad, M. (2001). "Nature and dynamics of water sediment interface in combined sewers." *Journal of Environmental Engineering-Asce*, 127(3), 233-239.
- [27] Oms, C. (2003). "Localization, nature and dynamic of the water-sediment interface in combined sewer network (in French)." Ph.D. Thesis, Ecole Nationale des Ponts et Chaussées, Paris, France.
- [28] Bertrand-Krajewski, J.-L., and Gibello, C. (2008). "A new technique to measure cross-section and longitudinal sediment profiles in sewers." *Proceedings of the 11th International Conference on Urban Drainage* Edinburgh, UK, 31 Aug.-5 Sept., 9 p.
- [29] Le Barbu, E., and Larrarte, F. (2010). "Profileurs acoustiques : un nouveau pas vers la connaissance des flux de polluants en assainissement urbain." *XI Journées Nationales Génie Côtier – Génie Civil* Les Sables d'Olonne, France, 22-25 juin 2010, 513-520.
- [30] Deines, K. L. (1999). "Backscatter estimation using Broadband acoustic Doppler current profilers." *Proceedings of the IEEE Sixth Working Conference on Current Measurement* San Diego, CA , USA 249 - 253.
- [31] Thorne, P., and Meral, R. (2008). "Formulations for the scattering properties of suspended sandy sediments for use in the application of acoustics to sediment transport processes." *Continental Shelf Research*, 28(2), 309-317.
- [32] Larrarte, F., and François, P. (2008). "Suspended solids and attenuation of ultrasonic beam." *11th International Conference on Urban Drainage* Edinburgh, Scotland, UK,, 1-9.
- [33] Wunderlich, J., Wendt, G., and Muller, S. (2005). "High-resolution echo-sounding and detection of embedded archaeological objects with nonlinear sub-bottom profilers." *Marine Geophysical Researches*, 26(2-4), 123-133.
- [34] Apelt, J. R. (1988). *Principles of Oceans Physics*, Academic Press, London UK.
- [35] Wahl, T. L. (2003). *Discussion of ?Despiking Acoustic Doppler Velocimeter Data? by Derek G. Goring and Vladimir I. Nikora*, ASCE.
- [36] Goring, D. G., and Nikora, V. I. (2002). *Despiking Acoustic Doppler Velocimeter Data*, ASCE.

- [37] Strom, K. B., and Papanicolaou, A. N. (2007). "ADV measurements around a cluster microform in a shallow mountain stream." *Journal of Hydraulic Engineering-Asce*, 133, 1379-1389.
- [38] Bonakdari, H., Larrarte, F., Joannis, C., and Levacher, D. (2008). "Champ de vitesses et contraintes de cisaillement dans un collecteur d'assainissement." *La Houille Blanche*(3), 20-25.
- [39] Sarkar, S., and Dey, S. (2010). "Double-averaging turbulence characteristics in flows over a gravel bed." *Journal of Hydraulic Research*, 48(6), 801 - 809.
- [40] Kim, S.-C., Friedrichs, C. T., Maa, J. P.-Y., and Wright, L. D. (2000). "Estimating Bottom Stress in Tidal Boundary Layer from Acoustic Doppler Velocimeter Data." *Journal of Hydraulic Engineering*, 126(6), 399-406.
- [41] Nezu, I., and Nakagawa, H. (1993). *Turbulence in open channel flows*, Balkema, Rotterdam, NL.
- [42] Ha, H. K., Hsu, W. Y., Maa, J. P. Y., Shao, Y. Y., and Holland, C. W. (2009). "Using ADV backscatter strength for measuring suspended cohesive sediment concentration." *Continental Shelf Research*, 29(10), 1310-1316.
- [43] Larrarte, F. (2006). "Velocity fields within sewers: An experimental study." *Flow Measurement and Instrumentation*, 17(5), 282-290.
- [44] Coleman, N. L. (1981). "VELOCITY PROFILES WITH SUSPENDED SEDIMENT." *Journal of Hydraulic Research*, 19(3), 211-229.
- [45] Gaudio, R., Miglio, A., and Dey, S. (2010). "Non-universality of von Karman's kappa in fluvial streams." *Journal of Hydraulic Research*, 48(5), 658-663.

RESUME

Les solides présents dans les réseaux d'assainissement sont répartis en une fraction en suspension dans l'écoulement et une fraction sédimentée. Ces dépôts se trouvent au cœur de deux questions techniques importantes :

- (1) les sédiments grossiers réduisent la section utile des collecteurs visitables, ce qui entraîne des opérations de curage coûteuses impliquant du personnel soumis à des conditions de travail pénibles et dangereuses;
- (2) les sédiments plus fins sont facilement érodés par des augmentations de débits qui les remettent en suspension, ce qui peut surcharger la capacité des ouvrages de traitement et induire des rejets d'effluents pollués dans les milieux récepteurs.

L'appartenance d'une particule à l'une de ces fractions dépend à la fois des caractéristiques de la particule (forme, densité, ..) et de celles de l'écoulement. Or les réseaux d'assainissement sont constitués de collecteurs dans lesquels les écoulements sont tridimensionnels et le cisaillement pariétal présente de fortes variations dans la direction transversale.

Comme une même particule peut ainsi être tour à tour transportée en suspension, par saltation, par charriage/ ou tout simplement déposée, la réalisation de bilan de polluants dans un collecteur s'avère très délicate. Ainsi, différents auteurs montrent l'existence d'une couche fortement organique située à la surface des sédiments plus grossiers, et l'apparition de phénomènes d'arrachage localisés lors d'augmentation du cisaillement pariétal suite à une augmentation de débit. Mais ces phénomènes ne suffisent pas à expliquer les masses observées à l'échelle de bassins versants. C'est pourquoi le projet Sonar a pour objectif d'approfondir les connaissances sur la morphologie des dépôts présents dans les collecteurs de réseau d'assainissement urbain en fonction des caractéristiques de l'écoulement.

Ce rapport comporte

- Un point de bibliographie,
- Un rappel de théorie sur les techniques mises en oeuvre,
- Une présentation des installations expérimentales, des sites de mesures et des procédures d'acquisition des données.
- Les résultats préliminaires des premiers essais effectués en réseaux avec le profileur sonar
- Les résultats des essais effectués en réseaux avec le profileur sonar et un acoustic Doppler Velocimeter (ADV)
- Une discussion des résultats.

Ce travail a permis de montrer que:

- 1) Le signal acoustique est réfléchi et atténué de diverses manières selon la nature de l'interface, et en conséquence un nouvel algorithme a été développé;
- 2) La nature de l'interface est fortement dépendante de la vitesse de l'écoulement,
- 3) La nature de l'interface modifie la capacité des sondes à détecter la « mud flow »,
- 4) La morphologie des dépôts dépend de la nature des dépôts et de la vitesse de l'écoulement,
- 5) En présence de vitesse de l'ordre de 0,10 m par seconde il a été possible d'observer des dunes de 3-4 m de longueur d'onde et de 5- 10 cm crête à crête,
- 6) Le champ des vitesses est modifié par la présence de la "mud flow". Généralement, en présence d'un dépôt sableux et malgré la forte tridimensionnalité de l'écoulement, les contraintes turbulentes décrivent un profil semblable à celui observé en écoulement à surface libre alors qu'en présence de la « mud flow » la sous couche visqueuse est plus épaisse, même pour des nombres de Reynolds de l'ordre de $6 \cdot 10^4$ (régime d'écoulement turbulent).

Suivi par sonar de la dynamique des dépôts en réseau d'assainissement

Les solides présents dans les réseaux d'assainissement sont répartis en une fraction en suspension dans l'écoulement et une fraction sédimentée. Ces dépôts se trouvent au cœur de deux questions techniques importantes :

- (3) les sédiments grossiers réduisent la section utile des collecteurs visitables, ce qui entraîne des opérations de curage coûteuses impliquant du personnel soumis à des conditions de travail pénibles et dangereuses;
- (4) les sédiments plus fins sont facilement érodés par des augmentations de débits qui les remettent en suspension, ce qui peut surcharger la capacité des ouvrages de traitement et induire des rejets d'effluents pollués dans les milieux récepteurs.

L'appartenance d'une particule à l'une de ces fractions dépend à la fois des caractéristiques de la particule (forme, densité, ..) et de celles de l'écoulement. Or les réseaux d'assainissement sont constitués de collecteurs dans lesquels les écoulements sont tridimensionnels et le cisaillement pariétal présente de fortes variations dans la direction transversale.

Comme une même particule peut ainsi être tour à tour transportée en suspension, par saltation, par charriage/ ou tout simplement déposée, la réalisation de bilan de polluants dans un collecteur s'avère très délicate. Ainsi, différents auteurs montrent l'existence d'une couche fortement organique située à la surface des sédiments plus grossiers, et l'apparition de phénomènes d'arrachage localisés lors d'augmentation du cisaillement pariétal suite à une augmentation de débit. Mais ces phénomènes ne suffisent pas à expliquer les masses observées à l'échelle de bassins versants. C'est pourquoi le projet Sonar a pour objectif d'approfondir les connaissances sur la morphologie des dépôts présents dans les collecteurs de réseau d'assainissement urbain en fonction des caractéristiques de l'écoulement.

Ce rapport comporte

- Un point de bibliographie,
- Un rappel de théorie sur les techniques mises en oeuvre,
- Une présentation des installations expérimentales, des sites de mesures et des procédures d'acquisition des données.
- Les résultats préliminaires des premiers essais effectués en réseaux avec le profileur sonar
- Les résultats des essais effectués en réseaux avec le profileur sonar et un acoustic Doppler Velocimeter (ADV)
- Une discussion des résultats.

Ce travail a permis de montrer que:

- 7) Le signal acoustique est réfléchi et atténué de diverses manières selon la nature de l'interface, et en conséquence un nouvel algorithme a été développé;
- 8) La nature de l'interface est fortement dépendante de la vitesse de l'écoulement,
- 9) La nature de l'interface modifie la capacité des sondes à détecter la « mud flow »,
- 10) La morphologie des dépôts dépend de la nature des dépôts et de la vitesse de l'écoulement,
- 11) En présence de vitesse de l'ordre de 0,10 m par seconde il a été possible d'observer des dunes de 3-4 m de longueur d'onde et de 5- 10 cm crête à crête,
- 12) Le champ des vitesses est modifié par la présence de la "mud flow". Généralement, en présence d'un dépôt sableux et malgré la forte tridimensionnalité de l'écoulement, les contraintes turbulentes décrivent un profil semblable à celui observé en écoulement à surface libre alors qu'en présence de la « mud flow » la sous couche visqueuse est plus épaisse, même pour des nombres de Reynolds de l'ordre de $6 \cdot 10^4$ (régime d'écoulement turbulent).